Ingredients Parts by wet weight (g) Skim latex (5.1% DRC) 100 Stabilizers -10% w/v KOH solution 4.0 -25% w/v SDS solution 0.8 Vulcanizing ingredients (50% dispersion) 2.5 -S-ZDEC 2.0 -ZnO 0.5

Table I. Formula used for the preparation of SPVS latex

on a carbon/copper grid at room temperature before investigating under TEM (JEOL, JEM-2010).

#### Preparation and Characterization of CHD-PMA Nanocapsules

PMA was synthesized via the mini-emulsion polymerization process as previously described. The average molecular weight  $(\overline{M}_w)$  of PMA was determined by gel permeation chromatography (Waters/600/2414/600) equipped with refractive index detector.

CHD-PMA nanocapsules were obtained using the modified nanoprecipitation technique. [15,16] PMA (0.15 g) and lecithin (0.1 g) were first dissolved in dichloromethane (12 mL) before the addition of cyclohexane (12 mL), followed by CHD solution (0.5 mL). The mixture was ultrasonicated for 2 min at 90% amplitude (Branson Sonifier, W450 digital) and heated up to 50°C in an open vessel with continuous stirring overnight for the removal of dichloromethane. Cyclohexane was subsequently removed by rotary evaporation at 40°C, and deionized water was finally added to replace the evaporated volume. Size, morphology, and %TSC of CHD-PMA nanocapsules were examined.

For the determination of encapsulation efficiency, the CHD-PMA nanocapsules were separated by centrifugation at 14,000 rpm for 40 min and dried before being dissolved in a mixture of THF and ethanol.  $D_2O$  and known concentration of pyrazine were used as a solvent and a calibration standard in the quantitative analysis by  $^1\text{H-NMR}$  (Bruker, DPX 400). The mass of drug encapsulated in nanocapsules was determined from the area ratio of proton peaks at  $\delta$  7.66–9.07 ppm, corresponding to aromatic protons of CHD and pyrazine, respectively.  $^{[16]}$ 

#### Preparation and Characterization of CHD-PMA/SPVS Composite Latex

In the preparation of CHD-PMA/SPVS composite latex, a known amount of SPVS latex (1% TSC) was mixed with CHD-PMA nanocapsules (1% TSC, 10 g) with continuous stirring for 10 min at room temperature. The weight ratios of CHD-PMA:SPVS were varied from 1:0.98 to 1:0.06. The zeta potential and morphology of CHD-PMA/SPVS composite latex particles were determined.

Raman spectra of the composite particles at weight ratios of 1:0.98 and 1:0.60, as a function of penetration depth, were recorded on a confocal Raman spectroscope

(NT-MDT, NTEGRA Spectra). CHD-PMA/SPVS composite latex particles were dropped onto a cover glass and dried at room temperature. Samples were then illuminated with a He-Ne laser at the excitation wavelength of 632.8 nm. Each spectrum was collected at the frequency range  $80{\text -}5500\,\mathrm{cm}^{-1}$  over 60 s with 10 accumulations and a resolution of  $2\,\mathrm{cm}^{-1}$ . A pinhole diameter of  $50\,\mu\mathrm{m}$  was employed. Spectra were recorded at the surface of samples and at various penetration depths with  $100\,\mathrm{nm}$  intervals.

#### **RESULTS AND DISCUSSION**

#### Characterizations of SPVS Particles and CHD-PMA Nanocapsules

Results from the particle size analyzer indicated that the average sizes of SPVS particles and CHD-PMA nanocapsules in an aqueous phase were 160 and 200 nm, respectively. The morphologies of skim, SPVS particles, and the CHD-PMA nanocapsules under TEM are shown in Figure 2.

The more distinct boundary of SPVS particles in Figure 2(b) compared to the unvulcanized skim particles in Figure 2(a) correlated well with the dense network structure in each SPVS particle. [2] The low swelling ratio of about 200% confirmed full cross-linking of rubber in SPVS latex. The small particle size of skim or the large particle surface area was responsible for the high degree of cross-linking.

For CHD-PMA nanocapsules ( $\overline{M}_w$  of PMA = 250 K, encapsulation efficiency = 86%), spherical and well-dispersed nanocapsules with no aggregation were observed in Figure 2(c). The suspension of CHD-PMA nanocapsules in an aqueous medium resulted from the electrical stabilization of lecithin. Zeta potential values of CHD-PMA nanocapsules and SPVS particles at various pHs are presented in Figure 3.

The amphoteric character of skim and SPVS particles with the isoelectric point (pI) at pH 2.8 was observed. The amphotericity is due to the presence of amino acid moieties derived from the native proteins chemically bound to the surface of the skim particles. These particles bore a negative charge at pH above pI. At pH greater than 3 for the skim and 4 for SPVS, the zeta potential values slightly changed, indicating the complete ionization of the ionogenic groupings. [2,17] Since the pI value did not fall into the normal range of protein's pI (4.0–6.0), it was believed that other compounds, e.g., fatty acids and SDS, were present on the skim particle surface. [5]

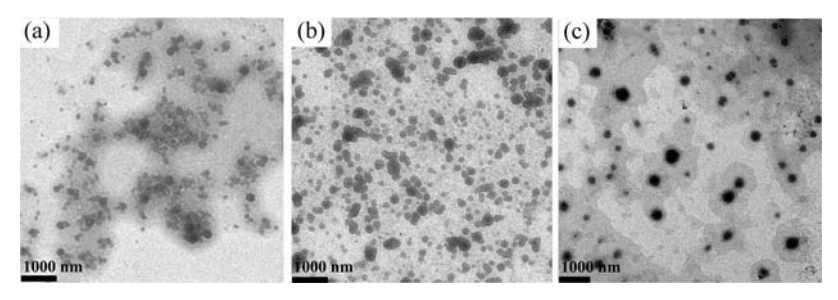


Figure 2. TEM micrographs of (a) skim, (b) SPVS, and (c) CHD-PMA nanocapsules.

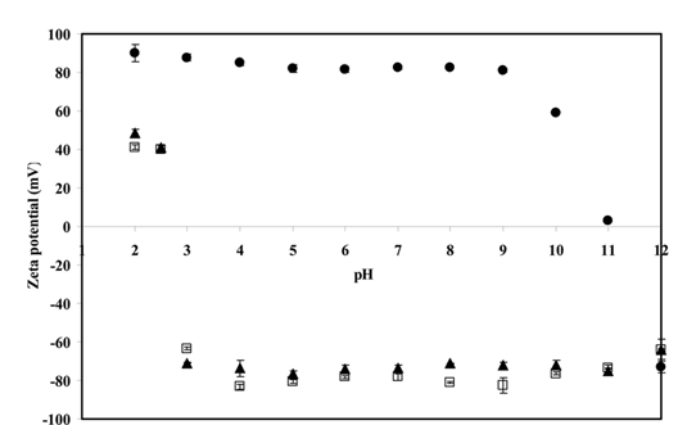


Figure 3. Zeta potential of  $(\bullet)$  CHD-PMA nanocapsules,  $(\spadesuit)$  skim, and  $(\Box)$  SPVS vs. pH.

The results agreed well with the previous work, which reported that the addition of small amounts of carboxylate, sulfonate, and sulfate surfactants whose alkyl chain consisted of approximately 11 carbon atoms effectively enhanced the stability of NR latex by rearranging the indigenous soaps.<sup>[18]</sup>

For CHD-PMA nanocapsules dispersed in an aqueous medium, the zeta potentials over a range of pH 2 to 10 showed a positive value of 85 mV, derived from the protonation of choline moiety [N<sup>+</sup>(CH<sub>3</sub>)<sub>3</sub>] in lecithin.<sup>[15]</sup> The pI value was shown to be 11 due to the zwitterionic character of lecithin, which contains phospholipids, phosphatidyl, and quaternary ammonium moieties. At pH greater than pI, the zeta potential of CHD-PMA nanocapsules was negative. The current result is in good agreement with the pI value (10.8) obtained from TM-40 silica coated with cationic ATRP macroinitiator possessing choline group.<sup>[19]</sup>

## Heterocoagulation of CHD-PMA Nanocapsules and SPVS Latex Particles

At pH 4–10, the difference in the zeta potential values of CHD-PMA nanocapsules and SPVS particles reached the maximum point. The high electrostatic interaction between both particles with opposite charges effectively provoked the heterocoagulation. The pH values of the as-prepared nanocapsules and SPVS were selected for mixing both components at various blending ratios. When the blending ratio was not greater than 1:0.2, the aggregates maintained their stability from the incomplete neutralized ionic surfactants and the repulsion from the hydrophobic part of surfactants. <sup>[20]</sup> To examine the surface charge of aggregates, their zeta potential values at various blending ratios was determined, and the data are shown in Figure 4.

It was believed that the positive value of zeta potentials of composite particles was the result of their surface charges, which were dominated by the  $N^+(CH_3)_3$  moiety in lecithin. The assumption was based on the interaction between SDS on the SPVS and lecithin on the nanocapsule. Several studies argued that SDS is more surface active than lecithin and ready to form micelles, which may be trapped inside the lecithin aggregate or bind to the lecithin film. This could be the result of the absorption onto

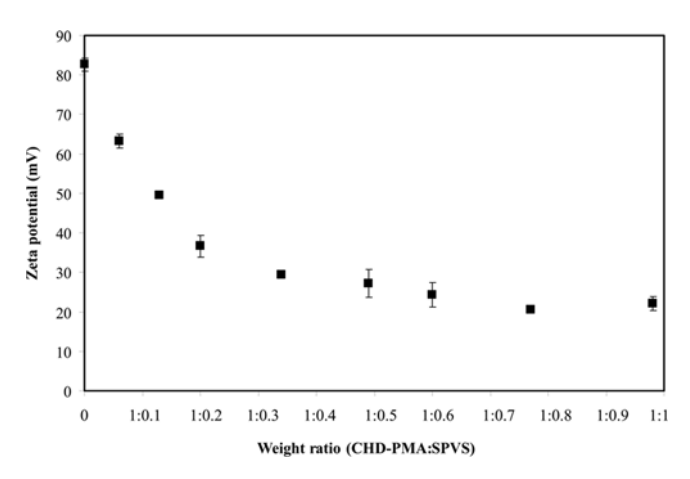


Figure 4. Zeta potential of CHD-PMA/SPVS composite particles prepared with various blending ratios.

the oil droplet surface and the formation of the complex film.  $^{[20,21]}$  The SDS-lecithin complex formation may alter the thickness, viscosity, or density of the stabilized layer surrounding CHD-PMA nanocapsules. Although the interaction between  $SO_4^{2-}$  and  $N^+(CH_3)_3$  may not be strong due to the steric hindrance of lecithin structure, SDS may also cause the lecithin molecule to unfold and change its previous interaction with the PMA or CHD droplet. The binding of SDS onto the surface decreased the electrostatic repulsion between the two components. This explained the fact that zeta potentials of the composite particles significantly decreased from 80 to 30 mV with increase of the weight ratio up to 1:0.3 before reaching to a constant value.

The morphologies of heterocoagulated CHD-PMA/SPVS particles at various blending ratios are shown in Figure 5.

It might be stated that the aggregate consists of CHD-PMA nanocapsules and SPVS particles, as represented in Figure 2 by black and white particles, respectively. Although these particles were similar in size, they were adsorbed in a random manner and formed irregular aggregates of particles. [22,23] This behavior may be due to the simultaneous adhesion of two or three consecutively dissimilar particles by interparticle bridging, which limited the adhesive area on the surface. As a consequence, it saturated more easily than in the regular heterocoagulation. Dispersive Raman spectra of CHD, lecithin, PMA, and CHD-PMA nanocapsules are shown in Figure 6.

All vibrational modes associated with the three components observed in the spectrum of the nanocapsules indicated the presence of these components. Bands due to CHD were observed at 3070, 1600, and 1500 cm<sup>-1</sup> (ring modes); those of lecithin were located at 1658 (C=C stretching) and 1445 (C-O-C) cm<sup>-1</sup>. Bands located at 2955 (C-H stretching), 1730 (C=O stretching), and 1454 (C-O-C) cm<sup>-1</sup> were associated with PMA. The band characteristics of lecithin were very intense despite a low content of the component in the capsules. This confirmed that the molecules were densely located at the surface of the capsules. Figure 6 also shows the spectrum of SPVS, whose characteristic bands were observed at 2932 (C-H stretching), 1665 (C=C stretching), and 1445 (C-O-C) cm<sup>-1</sup>. [24]

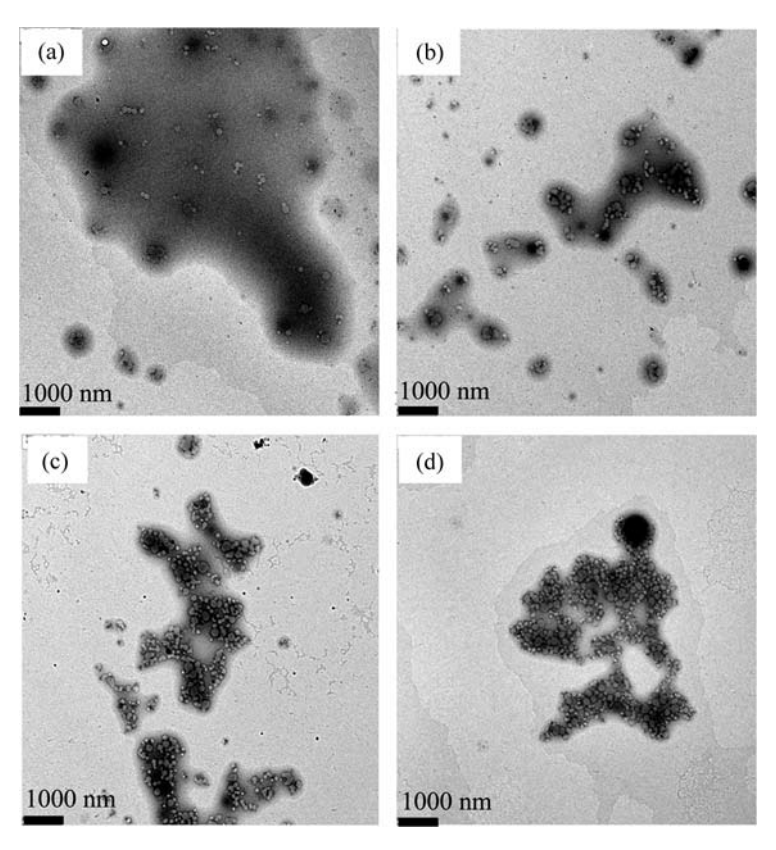


Figure 5. TEM micrographs of CHD-PMA/SPVS composite particles at ratios (a) 1:0.06, (b) 1:0.20 (c) 1:0.60, and (d) 1:0.98.

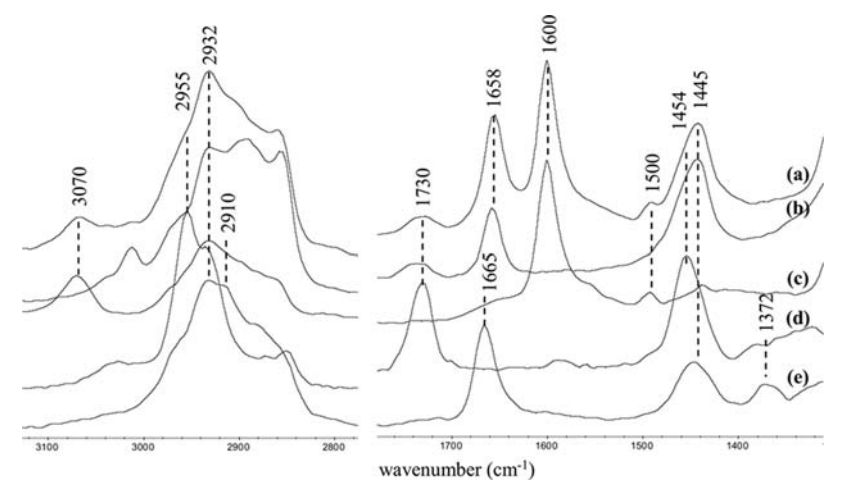


Figure 6. Dispersive Raman spectra of (a) CHD-PMA nanocapsules, (b) lecithin, (c) CHD, (d) PMA, and (e) SPVS.

Depth profile analysis of the CHD-PMA/SPVS aggregates was studied by confocal Raman using the "z-scanning" approach, where the laser was focused on the surface or deeper inside the sample, and the spectrum was recorded at each depth. The depth profiling spectra at 100 nm intervals from the surface of CHD-PMA/SPVS composites with a weight ratio of 1:0.98 are shown in Figure 7.

Bands due to SPVS, as denoted by S, were clearly observed from the spectra recorded at the surface and at penetration depths of up to 200 nm. When the laser was focused at 300 nm from the surface, bands due to SPVS disappeared, and those corresponding to PMA and CHD (denoted by P and C, respectively) were clearly observed. This indicated that in the composite with high content of SPVS, the skim present as shell matrix of roughly 200–300 nm thick, encapsulated the CHD-PMA nanocapsules.

On the other hand, the corresponding spectra of the composite with a weight ratio of 1:0.60, as shown in Figure 8, indicate a combination of band characteristics of SPVS, CHD, and PMA at all penetration depths. Significant differences were observed in relative intensities of the bands. As absorbencies of bands are unaffected by penetration depth, the change in band intensities indicates variations in respective functional group contents.<sup>[26]</sup> This shows that at this blend ratio the relative volume of SPVS to CHD-PMA nanocapsules was not high enough for the skim to form a continuous layer of rubber. The structure of aggregates consisting of random domains of CHD-PMA nanocapsules and SPVS was therefore obtained.

In addition, the depth profiling spectra of the CHD-PMA/SPVS composite particles prepared from both blend ratios clearly showed that the band characteristic of lecithin at 1445 cm<sup>-1</sup> (denoted by L) is strong at the surface and decreases in intensity as penetration depth increases. This confirmed that the surface of

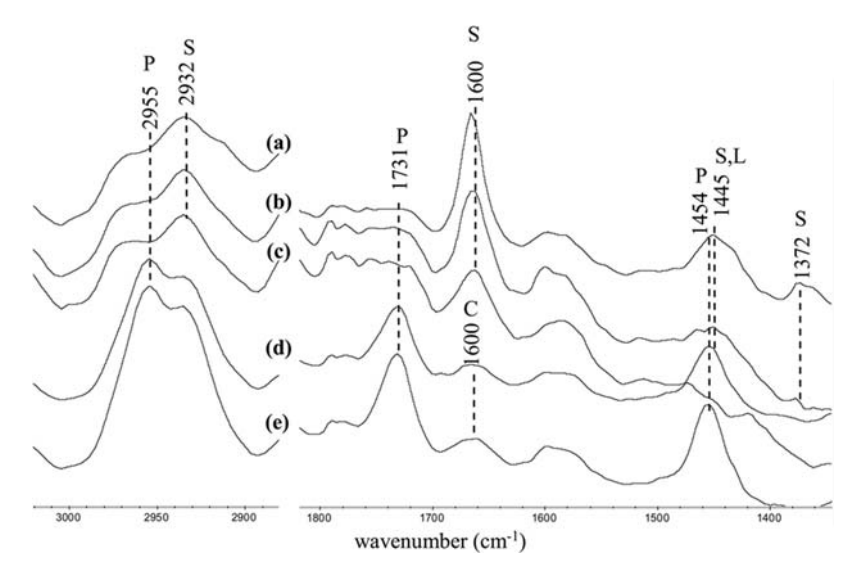


**Figure 7.** Confocal Raman spectra as a function of penetration depth of CHD-PMA/SPVS composites at a blend ratio of 1:0.98 recorded at: (a) surface, and at penetration depths of (b) 100, (c) 200, (d) 300, and (e) 400 nm. (S, P, C, and L denote band characteristics of SPVS, PMA, CHD, and lecithin, respectively).

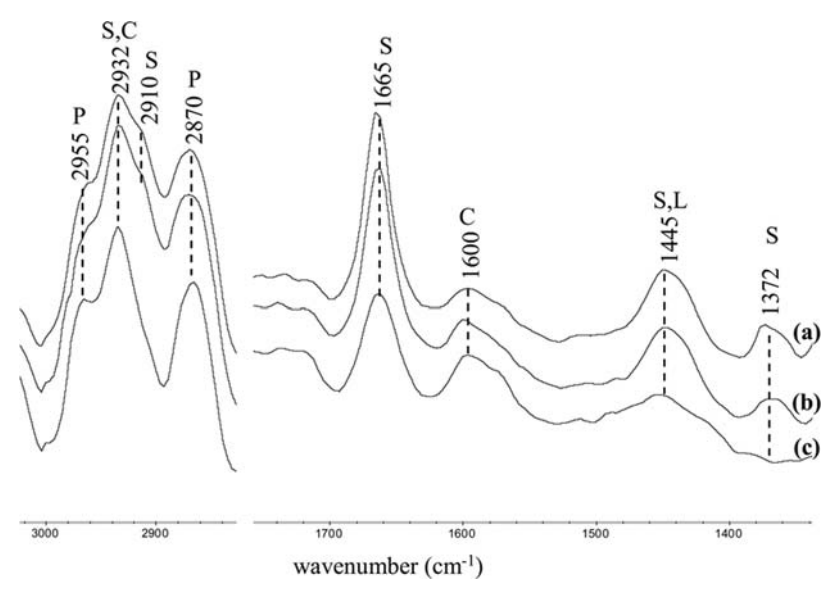


**Figure 8.** Confocal Raman spectra as a function of penetration depth of CHD-PMA/SPVS composites at a blend ratio of 1:0.60 recorded at: (a) surface, and at penetration depths of (b) 100 and (c) 200 nm. (S, P, C, and L denote band characteristics of SPVS, PMA, CHD, and lecithin, respectively).

CHD-PMA/SPVS composite particles was dominated by lecithin molecules. The observation is in agreement with that reported by Belaroui et al. [26] in which confocal Raman spectroscopy was employed to observe the migration of sulfate ions to the film/air interface during the formation of dry latex film.

#### **CONCLUSION**

CHD-PMA nanocapsules were prepared by the controlled nanoprecipitation of PMA onto inverse mini-emulsion droplets containing CHD. After redispersion of nanocapsules in an aqueous medium, the cationic nanocapsules were heterocoagulated with anionic SPVS latex particles. The size, zeta potential, and morphology of composite particles indicated the aggregation in which the surface charge was dominated by the N<sup>+</sup>(CH<sub>3</sub>)<sub>3</sub> moiety in lecithin. Confocal Raman spectra as a function of penetration depth revealed the migration of lecithin to the aggregate surface. The results also indicated that aggregations with different structures were formed, depending on the CHD-PMA/SPVS blend ratios. The corresponding composite particles will be further extended in the preparation of the disinfectant medical glove.

#### **REFERENCES**

1. Rippel, M. M., L. T. Lee, C. A. P. Leite, and F. Galembeck. 2003. Skim and cream natural rubber particles: Colloidal properties, coalescence and film formation. *J. Colloid Interface Sci.* 268: 330–340.

- 2. Paiphansiri, U., and P. Tangboriboonrat. 2005. Prevulcanization of skim latex: Morphology and its use in natural rubber based composite material. *Colloid Polym. Sci.* 284: 251–257.
- 3. Tangboriboonrat, P., T. Tanunchai, and C. Tiyapiboonchiya. 1999. Creaming skim natural rubber latex for encapsulation of urea fertilizer. *Plast. Rubber Compos.* 28: 357–362.
- 4. Gorton, A. D. T. 1979. The production and properties of prevulcanized natural rubber latex. *NR Technol.* 10: 9–20.
- 5. Tangboriboonrat, P., and C. Lerthititrakul. 2002. Morphology of natural rubber latex particles prevulcanised by sulphur and peroxide systems. *Colloid Polym. Sci.* 280: 1097–1103.
- Li, H., and E. Kumacheva. 2003. Core-shell particles with conductive polymer cores. Colloid Polym. Sci. 281: 1–9.
- Maruyama, K., M. Kawaguchi, and T. Kato. 2001. Heterocoagulation behavior of poly(styrene-co-butadiene) and poly(butyl acrylate) at high particle concentrations. Colloids Surf. A 189: 211–223.
- 8. Yamaguchi, K., M. Ito, T. Taniguchi, S. Kawaguchi, and K. Nagai. 2004. Preparation of core-shell composite polymer particles by a novel heterocoagulation based on hydrophobic interaction. *Colloid Polym. Sci.* 282: 366–372.
- 9. Tangboriboonrat, P., and U. Buranabunya. 2001. Composite natural rubber-polychloroprene latex particles produced by the heterocoagulation technique. *Colloid Polym. Sci.* 279: 615–620.
- Sruanganurak, A., and P. Tangboriboonrat. 2007. Surface modification of sulphur prevulcanized natural rubber latex sheet via layer-by-layer assembled PMMA particles. *Colloids Surf. A* 301: 147–152.
- Busnel, R. G., and G. Argy. 1991. Process for preparation a prophylactic device made of rupturable microcapsules and layers of elastomeric material. U.S. Patent 5024852.
- 12. Hajatdoost, S., M. Olsthoorn, and J. Yarwood. 1997. Depth profiling study of effect of annealing temperature on polymer/polymer interfaces in laminates using confocal Raman microspectroscopy. *Appl. Spectrosc.* 51: 1784–1790.
- 13. Tabaksblat, R., R. J. Meier, and B. J. Kip. 1992. Confocal Raman microspectroscopy: Theory and application to thin polymer samples. *Appl. Spectrosc.* 46: 60–68.
- 14. Tangboriboonrat, P., C. Tiyapiboonchaiya, and C. Lerthititrakul. 1998. New evidence of the surface morphology of deproteinized natural rubber particles. *Polym. Bull.* 41: 601–608.
- 15. Paiphansiri, U., and P. Tangboriboonrat. 2009. Deposition of disinfectant poly(methyl acrylate) nanocapsules onto natural rubber film via the layer-by-layer technique. *J. Appl. Polym. Sci.* 112: 769–777.
- 16. Paiphansiri, U., P. Tangboriboonrat, and K. Landfester. 2006. Polymeric nanocapsules containing an antiseptic agent obtained by controlled nanoprecipitation onto water-in-oil miniemulsion droplets. *Macromol. Biosci.* 6: 33–40.
- 17. Gazeley, K. F., A. D. T. Gorton, and T. D. Pendle. 1988. Latex concentrates: Properties and composition. In *Natural Rubber Science and Technology*, ed. A. D. Roberts, Oxford: Oxford Univ. Press, pp. 63–98.
- 18. Blackley, D. C., A. A. N. Aisah, and R. Twaits. 1979. Effect of potassium fatty-acid soaps upon mechanical and chemical stability of natural rubber latex. *Plast. Rubber Mater. Appl.* 4: 77–86.
- 19. Chen, X. Y., S. P. Armes, S. J. Greaves, and J. Watts. 2004. Synthesis of hydrophilic polymer-grafted ultrafine inorganic oxide particles in protic media at ambient temperature via atom transfer radical polymerization: Use of an electrostatically adsorbed polyelectrolytic macroinitiator. *Langmuir* 20: 587–595.

- 20. Deo, N., and P. Somasundaran. 2001. Mechanism of mixed liposome solubilization in the presence of sodium dodecyl sulfate. *Colloid Surf. A* 186: 33–41.
- López, O., M. Cócera, E. Wehrli, J. L. Parra, and A. de la Maza. 1999. Solubilization of liposomes by sodium dodecyl sulfate: New mechanism based on the direct formation of mixed micelles. *Arch. Biochem. Biophys.* 367: 153–160.
- 22. Furusawa, K., and C. Anzai. 1992. Heterocoagulation behaviour of polymer lattices with spherical silica. *Colloids Surf.* 63: 103–111.
- 23. Islam, A. M., B. Z. Chowdhry, and M. J. Snowden. 1995. Heterocoagulation in colloidal dispersions. *Adv. Colloid Interface Sci.* 62: 109–136.
- 24. Colthup, N. B., L. H. Daly, and S. E. Wiberley. 1990. *Introduction to Infrared and Raman Spectroscopy*, 3rd ed. Boston: Academic Press.
- 25. Prakanrat, S., P. Phinyocheep, and P. Daniel. 2009. Spectroscopic investigation of polystyrene surface grafting on natural rubber. *Appl. Spectrosc.* 63: 233–238.
- 26. Belaroui, F., Y. Grohens, H. Boyer, and Y. Holl. 2000. Depth profiling of small molecules in dry latex films by confocal Raman spectroscopy. *Polymer* 41: 7641–7645.



## Polymeric Disinfectant Nanocapsules: Effect of Molecular Weight of Poly(methyl acrylate)

Saovaree Tanpantree<sup>1</sup>, Pakorn Opaprakasit<sup>2</sup>, Duangporn Polpanich<sup>3</sup>, Srung Smanmoo<sup>4</sup>, and Pramuan Tangboriboonrat<sup>1,\*</sup>

<sup>1</sup> Department of Chemistry, Faculty of Science, Mahidol University, Phyathai, Bangkok 10400, Thailand <sup>2</sup> School of Bio-Chemical Engineering and Technology, Sirindhorn International Institute of Technology, Thammasat University, Pathumthani 12121, Thailand

Poly(methyl acrylate) (PMA) of various weight average molecular weights  $(\overline{M}_w)$  were synthesized via the iniferter route and applied for the encapsulation of disinfectant agent (chlorhexidine digluconate; CHD) by using the controlled precipitation technique. The encapsulation efficiency of CHD-PMA nanocapsules suspended in cyclohexane increased from 70 to 100% when the  $\overline{M}_w$  of PMA increased from 40 K to 550 K. After redispersing the capsules into 0.5% w/v of sodium dodecyl sulphate aqueous solution, the maximum content of CHD in the nanocapsules remained >90%. Transmission electron micrographs showed the spherical nanocapsule with continuous intact shell.

**Keywords:** Nanocapsule, Disinfectant Agent, Iniferter, Nanoparticle.

#### 1. INTRODUCTION

Wearing gloves is essential for medical personnel to avoid the infection. However, the gloves, especially those used by surgeons and dentists, are frequently perforated or torn in the case of needle prick or other similar accidents.<sup>1,2</sup> Recently, research attention has been focused on the development of medical gloves in which disinfectant droplets are incorporated as this would neutralize the infectious agents.3-5 Due to the wide spectrum activity against Gram-positive and Gram-negative bacteria, chlorhexidine digluconate (CHD) salt has been widely exploited as an antiseptic agent. Among various methods used for preparation of nanocapsules, the stabilized CHD droplets dispersed in an organic continuous phase (water-in-oil; w/o) were formed by using an inverse miniemulsion process.<sup>6-11</sup> The CHD aqueous solution in the form of nanocapsules with polymer-based shell having different glass transition temperatures  $(T_g)$ , i.e., poly(methyl methacrylate) (PMMA) ( $T_{\rm g} \sim 100~{\rm ^{\circ}C}$ ), poly( $\varepsilon$ -caprolactone) ( $T_{\rm g} \sim 60~{\rm ^{\circ}C}$ ) and poly(methyl acrylate) (PMA) ( $T_{\rm g} \sim 10~{\rm °C}$ ), could be prepared by the controlled precipitation of a polymer onto the w/o or inverse miniemulsion droplets.6

The deposition of polymer from an organic continuous phase onto CHD nanodroplets was achieved by changing the gradient of the solvent/non-solvent mixture of dichloromethane/cyclohexane under mild evaporation. After being redispersed in water, an aqueous dispersion of disinfectant nanocapsules was obtained. It was reported that the remaining amount of CHD in PMMA nanocapsules was significantly decreased with the decrease in shell thickness or molecular weight of PMMA shell.

In order to obtain soft capsule's wall which is strong enough to prevent any premature releases yet delicate enough to break up under required circumstances, PMA having low  $T_{\rm g}$  was investigated. 12 In the previous work, the polymer was synthesized by the miniemulsion process. Since the chain length of polymer shell was considered as an important parameter affecting the strength of the capsule wall, size of capsule and encapsulation efficiency, the effect of weight average molecular weight  $(\overline{M}_{w})$  of this polymer on properties of nanocapsule was herein studied. PMA with various  $\overline{M}_w$  was conveniently synthesized by using the thermal iniferter (initiator-transfer agent-terminator), based on controlled radical polymerization. The method was found to proceed under mild condition.<sup>13</sup> A detail synthesis of PMA and the influences of  $\overline{M}_w$  on size, morphology and encapsulation efficiency

<sup>&</sup>lt;sup>3</sup> National Nanotechnology Center, National Science and Technology Development Agency, Thailand Science Park, Pathumthani 12120. Thailand

<sup>&</sup>lt;sup>4</sup>Bioresources Research Unit, National Center for Genetic Engineering and Biotechnology, National Science and Technology Development Agency, Thailand Science Park, Pathumthani 12120, Thailand

<sup>\*</sup>Author to whom correspondence should be addressed.

of CHD-PMA nanocapsules stabilized by lecithin were presented.

#### 2. EXPERIMENTAL DETAILS

#### 2.1. Materials

Methyl acrylate (MA) (Purum, Fluka, Belgium) was purified by passing through a column packed with neutral and basic aluminium oxide (Purum, Fluka, Switzerland). The iniferter, i.e., *N*-bromosuccinimide (NBS) (99%, Aldrich, China), was recrystallized and dried under vacuum before use. <sup>14</sup> Other reagents, i.e., analytical grade dichloromethane, cyclohexane, methanol and tetrahydrofuran (THF) were purchased from Lab-scan (Thailand). Soybean phosphatidylcholine or lecithin (MP Biochemicals, USA), sodium dodecyl sulfate (SDS) (GC, Fluka, USA), pyrazine (≥98%, Fluka, Japan) and 20% w/v CHD (Sigma, Germany) were used as received.

#### 2.2. Synthesis of PMA

PMA was synthesized via the controlled radical polymerization using NBS as the thermal iniferter. Various  $\overline{M}_{w}$ of PMA were obtained by employing 11.11 M of MA and 0.68, 1.37, 2.74, 11.10 or  $22.23 \times 10^{-2}$  M of NBS using polymerization time of 300 min. The mixture was deoxygenated by three freeze-pump-thaw cycles and then purged with nitrogen for 30 min. When the polymerization was completed at 70 °C, the reaction was terminated by cooling the flask in an ice bath. The product was obtained by precipitating the PMA solution with a large amount of methanol. The monomer conversion was gravimetrically determined.  $\overline{M}_{w}$  and molecular weight distribution (MWD) or  $\overline{M}_{w}/\overline{M}_{n}$ , when  $\overline{M}_{n}$  is number average molecular weight, of PMA were measured by gel permeation chromatography (150-CV, Waters, USA) at 30 °C using THF as an eluent. <sup>1</sup>H-NMR spectra of the PMA samples were recorded on a Bruker (DPX400, USA) using PMA (10 mg) dissolved in CDCl<sub>3</sub> (2 ml). The  $T_g$  of PMA (10 mg) was determined by differential scanning calorimeter (DSC) (DSC7, Perkin-Elmer, USA) with the heating rate of 10 °C/min.

## 2.3. Preparation and Characterizations of CHD-PMA Nanocapsules

In the preparation of CHD-PMA nanocapsules, a known amount of PMA and of lecithin, used as surfactant, were dissolved in dichloromethane (12 ml). Cyclohexane (12 ml) was then slowly added as a non-solvent. After charging CHD (0.5 ml) into the solution, the mixture was ultrasonicated for 2 min at 90% amplitude (W450 digital Branson, USA). The reaction mixture was heated up to 50 °C in an open vessel with continuous stirring for 22 h. During evaporation, cyclohexane was added to

replace dichloromethane and also the evaporated volume. The CHD-PMA nanocapsules suspended in cyclohexane (10 ml) were then redispersed in 0.5% w/v SDS aqueous solution (10 ml). By evaporation of cyclohexane using a rotary evaporator (Rotavapor R200, Buchi, Switzerland) at 40 °C for 15 min, the capsules suspended in SDS aqueous solution were obtained.

The sizes of CHD nanodroplets and CHD-PMA nanocapsules were measured by a particle size analyzer (Zetasizer Nano ZS, Malvern, UK). The zeta potential of nanocapsules redispersed in SDS aqueous solution was determined by a microelectrophoresis apparatus (Zetasizer Nano ZS, Malvern, UK). In the determination of encapsulation efficiency, nanocapsules were centrifuged and dried before dissolving in a mixture of THF and ethanol. Deuterated water and a known amount of pyrazine were, respectively, used as an external solvent and a calibration standard in the quantitative analysis by <sup>1</sup>H-NMR.<sup>6</sup> Mass of drug in nanocapsules was calculated from the integrated areas of peaks at 7.66 to 9.07 ppm corresponding to aromatic-protons of the CHD and pyrazine, respectively. The morphology of the capsules, mounted on copper grid before coating with carbon, was investigated under TEM (JEM-2010, JEOL, Japan).

#### 3. RESULTS AND DISCUSSION

#### 3.1. Characterization of PMA

The polymerization mechanism of PMA by thermal iniferter, NBS, was proposed as shown in Scheme 1.

From Eqs. (1)–(4), the polymerization proceeded *via* the mechanism similar to that of the controlled radical polymerization in a homogeneous system.<sup>13</sup> The successive insertion of monomer (M) molecules into the dissociated bond took place, which produced succinimidyl (R) and bromine (R') as the end groups of PMA chain. However, some propagating chain radicals could be irreversibly terminated according to Eq. (5).<sup>14</sup>

In order to confirm that NBS acted as the thermal iniferter, the end groups of PMA chain were analyzed by <sup>1</sup>H-NMR spectroscopy and the spectrum is presented in Figure 1.

The signals at 3.57 (a), 2.22 (b) and 1.41–1.84 ppm (c), corresponding to the methoxy, methine and methylene protons were observed. Signal of ethylene protons of NBS appeared at 2.68 ppm (d) while that of methylene protons connected to the nitrogen atom of succinimide moiety appeared at 3.69 ppm (e). The peak at 4.12 ppm (f) of the methine protons connected to the bromine atom as the end group of PMA chain was also detected. The presence of the fragment of NBS at the end of PMA chain, therefore, confirmed that the polymerization took place through the thermal iniferter mechanism.

$$R-R' \rightleftharpoons R^{\bullet} + R'^{\bullet} \tag{1}$$

**Initiation** 
$$R^{\bullet} + M \xrightarrow{k_i} R - M^{\bullet}$$
 (2)

**Propagation** 
$$R-M^{\bullet} + nM \xrightarrow{k_p} R-[-M-]_n - M^{\bullet}$$
 (3)

**Reversible termination** 
$$R-[-M-]_n-M^{\bullet}+R'^{\bullet} \Longrightarrow R-[-M-]_n-M-R'$$
 (4)

Irreversible termination 
$$R-[-M-]_n-M^{\bullet}+R-[-M-]_m-M^{\bullet} \xrightarrow{k_t} R-[-M-]_{n+1}-[M-]_{m+1}-R$$
 (5)

Scheme 1. Polymerization mechanism of PMA by using NBS iniferter technique. 13, 14

#### 3.1.1. Effect of Polymerization Time

The effect of polymerization time on conversion,  $\overline{M}_w$  and MWD of PMA was studied. The relationship between monomer conversion and reaction time is presented in Figure 2.

It was observed that percent conversion of MA linearly increased with the increasing of reaction time, indicating that the polymerization proceeded via a mechanism corresponding to controlled radical polymerization. <sup>13, 16</sup> This implied that at the early stage, the iniferter acting as an initiator dissociated into radicals, which then reacted with MA. The long polymer chains were obtained from continuous propagation when polymerization time increased until termination. The successful insertion of monomer unit into polymer chain finally provided the high  $\overline{\rm M}_{\rm w}$  of PMA. However, the conversion did not reach 100% due

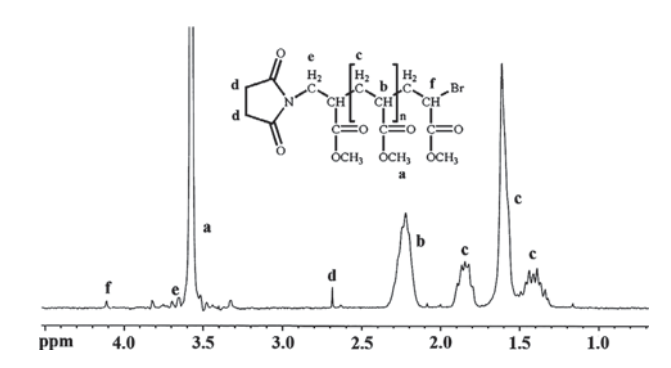


Fig. 1. <sup>1</sup>H-NMR spectrum of PMA polymerized by using NBS.

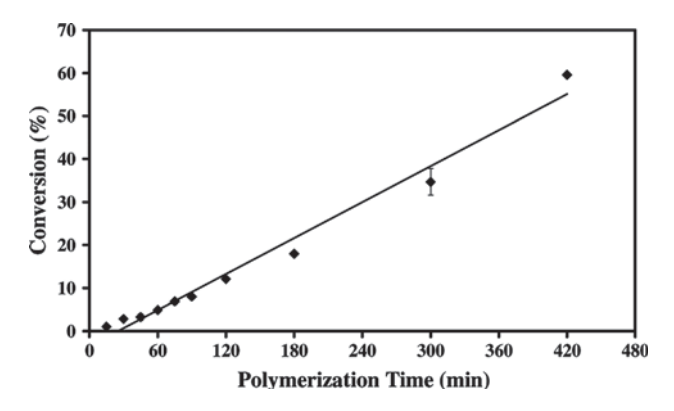


Fig. 2. Percent conversion of MA as a function of polymerization time (Polymerized at 70 °C, [MA] = 11.11 M, [NBS] =  $2.74 \times 10^{-2}$  M).

to the high viscosity imposed by long polymer chains produced in bulk system.

Since the initiator in the controlled polymerization system continuously reacts with monomer in the absence of terminating substance, the linear relationship between  $\overline{M}_w$  and percent conversion should be observed. <sup>13,14</sup> Moreover, in order to confirm the controlled radical characteristic of the bulk thermal polymerization of MA with NBS iniferter, the values of  $\overline{M}_w$  and MWD of PMA determined from GPC were then plotted against the reaction time and the data are presented in Figure 3.

As expected, the results showed that  $\overline{M}_w$  was directly proportional to the increased conversion.  $^{13,\,14}$  The iniferter which acts as an initiator, transfer agent and terminator in polymerization system, would attack the monomer to form the growing chain and finally reach the reversible termination. It was observed that the PMA obtained from using thermal iniferter technique had MWD ranging from 1.65 to 2.05. This agreed well with those (1.6 to 2.0) generally reported in the literature. The MWD values of greater than 1.0 indicated that the reaction system was not a perfect living polymerization as in the case of anionic polymerization. This was probably because the reaction was terminated at different times, resulting in a wide distribution of polymer chain lengths.

#### 3.1.2. Effect of Iniferter Concentration

The effect of iniferter concentration on  $\overline{M}_w$  of PMA was investigated and the results are displayed in Figure 4.

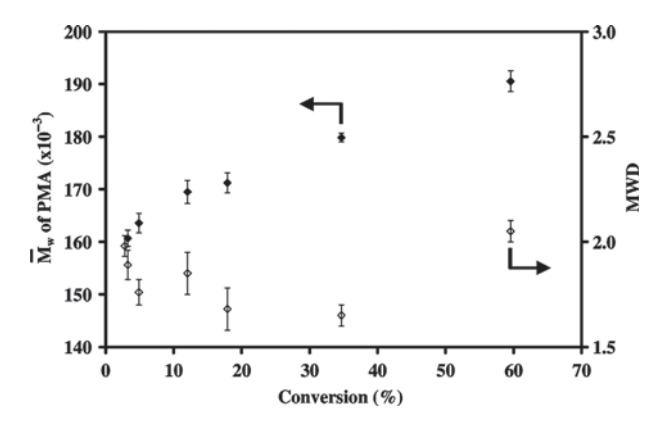


Fig. 3.  $\overline{M}_w$  and MWD of PMA as a function of percent conversion from reaction conducted at 70 °C ([MA] = 11.11 M and [NBS] = 2.74 ×  $10^{-2}$  M).

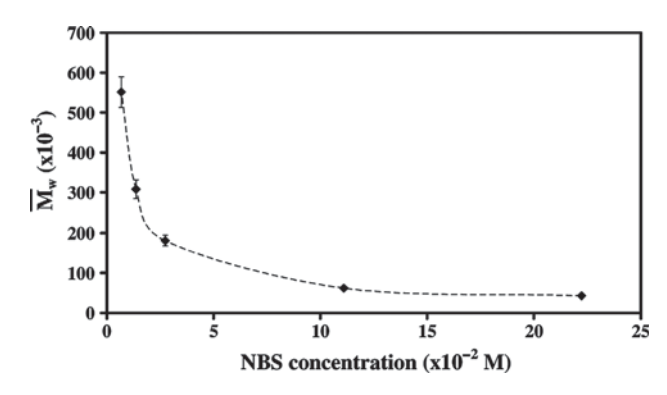


Fig. 4.  $\overline{M}_w$  of PMA as a function of NBS concentration (Polymerization reaction at 70 °C, 5 h).

It was observed that the  $\overline{M}_w$  of PMA increased from 40 K to 550 K with decreasing NBS concentrations from 22.23 to  $0.68 \times 10^{-2}$  M. This could be explained based on the principle of radical polymerization that at the high concentration of NBS, the probability of recombination of propagating chain and the primary radical was high with the low amount of monomer reacted with propagation radical.<sup>19</sup>

The purity of PMA homopolymer could be assumed from the DSC thermograms showing a single  $T_{\rm g}$  in each sample as shown in Figure 5.

Nevertheless, samples with higher  $\overline{M}_w$  showed broader transition state, which was probably resulted from their higher MWD. In addition,  $T_g$  value of PMA shifted to higher temperature with  $\overline{M}_w$  increasing from 40 K to 550 K due to lower movement freedom of longer PMA chains with the higher interchain interaction.

#### 3.2. Analysis of CHD-PMA Nanocapsules

The sizes of CHD droplets, CHD-PMA capsules dispersed in cyclohexane and then redispersed in 0.5% w/v SDS

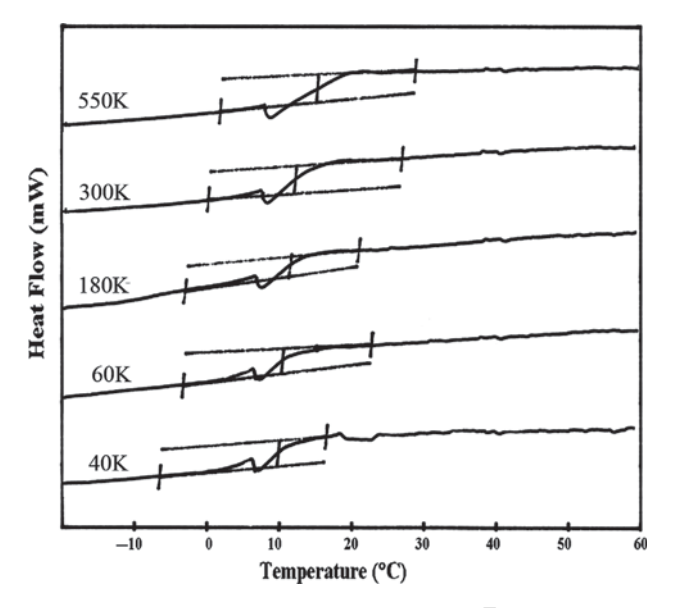


**Fig. 5.** DSC thermograms of PMA having various  $\overline{M}_{w}$ .

aqueous solution, prepared from using various  $\overline{M}_{\rm w}$  of PMA, are shown in Table I.

The data confirmed the monodispersed CHD nanodroplets with sizes ranging from 216 to 251 nm. As previously reported, CHD disinfectant, a lipophobe having low solubility in an oily continuous phase, plays a role in building up the osmotic pressure. As a result, the effective ingredient exchange between the droplets, i.e., Oswald ripening, can be substantially suppressed.<sup>20</sup> When CHD-PMA nanocapsules were formed in cyclohexane, their sizes increased from 251 to 385 nm with an increase in  $\overline{M}_{w}$  of PMA from 40 K to 550 K.<sup>21</sup> This was because the longer PMA chains with higher viscosity would easily precipitate onto the CHD droplets, leading to a thicker shell formation.<sup>22,23</sup> The well-defined tri-layer membrane of lecithin was responsible for steric stabilization in the organic continuous phase.<sup>24</sup> After redispersing in SDS aqueous solution, the zeta potential value of CHD-PMA nanocapsules which remained unchanged at about -95 mV confirmed the electrostatic stabilization of the capsules in the medium. It was noticed that the size of capsules consisting of PMA with  $\overline{M}_{w}$  of lower than 550 K in SDS aqueous solution was smaller than those suspended in cyclohexane. This might be due to the fact that the lower  $\overline{M}_{w}$  of PMA formed a thinner capsule's wall (35–85 nm), which allowed a portion of CHD disinfectant to leak from the aqueous core to the SDS aqueous medium as previously observed in the case of CHD-PMMA.<sup>6</sup> Comparing the samples prepared by using different M<sub>w</sub>, it was found that the size of nanocapsules with PMA of 40 K and 60 K did not increase. This could be explained in term of the large surface area of the nanocapsules. The thickness of the low  $\overline{M}_w$  PMA film over the area was very thin by taking percent ratio of core and polymer shell into account. The nanocapsules prepared from PMA with  $M_{\scriptscriptstyle \rm LM}$ of 40 K showed bimodal size distribution a result of lower  $T_{\sigma}$  of short PMA chains, as shown in Figure 5, in which the soft nature led to the aggregation of capsules. However, the size of redispersed CHD-PMA nanocapsules prepared from PMA of 550 K did not significantly change. This result confirmed that the dense or thick polymeric

**Table I.** Effect of  $\overline{M}_w$  of PMA on the size of CHD nanodroplets, CHD-PMA nanocapsules dispersed in cyclohexane, and those redispersed in SDS aqueous solution.

| $\overline{M}_{w}$ of PMA | Size of CHD<br>nanodroplets<br>(nm) | Size of CHD-PMA<br>nanocapsules in<br>cyclohexane (nm) | Size of CHD-PMA<br>nanocapsules<br>redispersed in SDS<br>aqueous solution (nm) |
|---------------------------|-------------------------------------|--|--|
| 40 K                      | $216 \pm 4$                         | $251 \pm 2$  | $183 \pm 13, 615 \pm 25^a$   |
| 60 K                      | $222 \pm 9$                         | $278 \pm 9$  | $210 \pm 23$   |
| 180 K                     | $236 \pm 5$                         | $308 \pm 9$  | $269 \pm 19$   |
| 300 K                     | $230 \pm 9$                         | $315 \pm 3$  | $286 \pm 23$   |
| 550 K                     | $251 \pm 7$                         | $385 \pm 7$  | $386 \pm 18$   |

<sup>&</sup>lt;sup>a</sup>Bimodal distribution

shell (134 nm) could effectively entrap the CHD core. The thicker shell of nanocapsules provided a higher mass transfer resistance and thus reduced the diffusion of an aqueous continuous phase into the aqueous core.

The encapsulation efficiency of CHD-PMA nanocapsules dispersed in cyclohexane and those redispersed in SDS aqueous solution were determined by <sup>1</sup>H-NMR and the data are displayed in Figure 6.

The encapsulation efficiency of CHD-PMA nanocapsules in cyclohexane increased from 70 to 100% with increasing M<sub>w</sub> of the polymer. The high encapsulation efficiency of the capsules coated with PMA having M<sub>w</sub> of 300 K-550 K was probably due to the entanglement of the long polymer chains which, consequently, provided a high durability of the capsule's wall.<sup>25</sup> In the case of the redispersed nanocapsules, the remaining CHD increased from 55 to 80% when using PMA with  $\overline{M}_{w}$  of 40 K-300 K, whereas the capsules prepared from PMA having  $\overline{M}_{w}$  of 550 K retained >90% of the disinfectant agent. This pointed to the fact that the tight molecular interlocking of long PMA chains formed an effective shell which retarded the water sorption, the penetration across the polymer barrier and, thus, the reduction of diffusion of CHD through the nanocapsules' wall.<sup>26, 27</sup>

#### 3.3. Morphological Study of CHD-PMA Nanocapsules

TEM micrographs of the CHD-PMA nanocapsules using PMA with  $\bar{M}_{\rm w}$  of 40 K and 550 K, redispersed in SDS aqueous solution, are shown in Figures 7(a) and (b), respectively.

The spherical nanocapsules with continuous intact shells, i.e., no shell rupture, was noticed especially in Figure 7(b). This confirmed that the thick shell obtained by using PMA with high  $\overline{M}_w$  was due to the entanglement of long polymer chains as previously described. The soft nanocapsules with low  $\overline{M}_w$  in Figure 7(a) confirmed the bimodal size distribution of nanocapsules. On a contrary, perfect structure of nanocapsules with no leakage of the

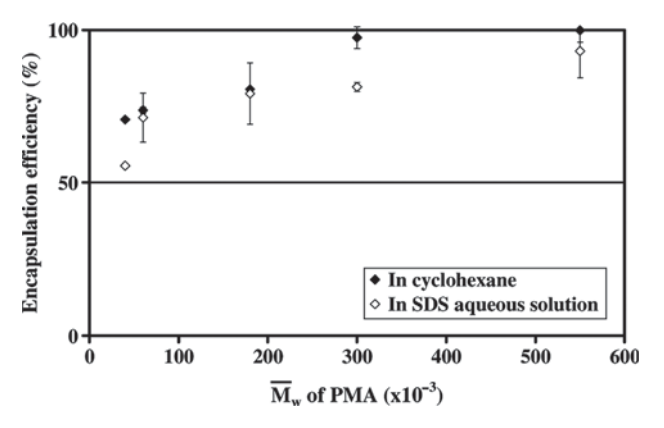


**Fig. 6.** Encapsulation efficiency of CHD-PMA nanocapsules, prepared from PMA with various  $\overline{M}_{\rm w}$ , dispersed in cyclohexane, and those redispersed in SDS aqueous solution.

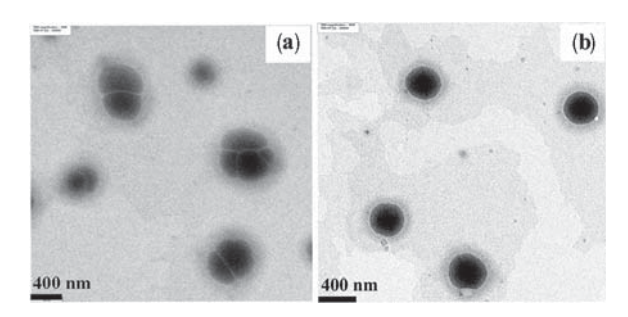


Fig. 7. TEM micrographs of CHD-PMA nanocapsules, prepared from PMA with  $\overline{M}_w$  of (a) 40 K and (b) 550 K, redispersed in SDS aqueous colution

core material was observed in Figure 7(b), when a high  $\overline{M}_w$  PMA was employed. These results, therefore, emphasized the important role of high  $\overline{M}_w$  of polymer shell on the nanocapsules' stability and the encapsulation efficiency. It should be noticed that the size of the dried nanocapsules prepared from PMA with  $\overline{M}_w$  of 550 K (363  $\pm$  10 nm) was slightly smaller than the hydrodynamic volume measured by the particle size analyzer (386  $\pm$  18 nm).

#### 4. CONCLUSIONS

PMA having various  $\overline{M}_w$ , synthesized by varying concentrations of thermal iniferter, were successfully used in the preparation of disinfectant (CHD) nanocapsules. Average size, shell thickness and encapsulation efficiency of the CHD-PMA nanocapsules were significantly improved when PMA with  $\overline{M}_w$  of 550 K was used as shell material, i.e., the encapsulation efficiency of nanocapsules dispersed in 0.5% w/v SDS aqueous solution was greater than 90% and nanocapsules appeared to be intact. This structure is suitable for further development of disinfectant medical glove's preparation.

**Acknowledgments:** Research grant (RTA5180003) from The Thailand Research Fund/Commission on Higher Education to Pramuan Tangboriboonrat and the scholarship under Thailand Graduate Institute of Science and Technology (TGIST), National Science and Technology Development Agency to Saovaree Tanpantree are gratefully acknowledged.

#### **References and Notes**

- A. M. Eklund, J. Ojajärvi, K. Laitinen, M. Valtonen, and K. A. Werkkala, Glove punctures and postoperaive skin flora of hands in cardiac surgery. *Ann. Thorac. Surg.* 74, 149 (2002).
- M. O. Osman and S. L. Jensen, Surgical gloves: Current problems. World J. Surg. 23, 630 (1999).
- **3.** R.-G. Busnel and G. Argy, Process for preparing a prophylactic device made of rupturable microcapsules and layers of elastomeric material. U.S. Patent 5,024,852, June 18 (1991).
- P. Sonntag, P. Hoerner, A. Cheymol, G. Argy, G. Riess, and G. Rieter, Biocide squirting from an elastomeric tri-layer film. *Nat. Mater.* 3, 311 (2004).

- F. Bricout, A. Moraillon, P. Sonntag, P. Hoerner, W. Blackwelder, and S. Plotkin, Virus-inhibiting surgical glove to reduce the risk of infection by enveloped viruses. *J. Med. Virol.* 69, 538 (2003).
- U. Paiphansiri, P. Tangboriboonrat, and K. Landfester, Polymeric nanocapsules containing an antiseptic agent obtained by controlled nanoprecipitation onto water-in-oil miniemulsion droplets. *Macromol. Biosci.* 6, 33 (2006).
- E. Jager, C. G. Venturini, F. S. Poletto, L. M. Colome, J. P. U. Pohlmann, A. Bernardi, A. M. O. Battastini, S. S. Guterres, and A. R. Pohlmann, Sustained release from lipid-core nanocapsules by varying the core viscosity and the particle surface area. *J. Biomed. Nanotechnol.* 5, 130 (2009).
- V. Weiss-Angeli, F. S. Poletto, L. R. Zancan, F. Baldasso, A. R. Pohlmann, and S. S. Guterres, Nanocapsules of octyl methoxycinnamate containing quercetin delayed the photodegradation of both components under ultraviolet A radiation. *J. Biomed. Nanotechnol.* 4, 80 (2008).
- A. Ruebe and K. Mader, Electron spin resonance study on the dynamics of polymeric nanocapsules. J. Biomed. Nanotechnol. 1, 208 (2005).
- M. C. Fontana, K. Coradini, A. R. Pohlmann, S. S. Guterres, and R. C. R. Beck, Nanocapsules prepared from amorphous polyesters: Effect on the physicochemical characteristics, drug release, and photostability. *J. Nanosci. Nanotechnol.* 10, 3091 (2010).
- C. E. Mora-Huertas, H. Fessi, and A. Elaissari, Polymer-based nanocapsules for drug delivery. *Inter. J. Pharmaceut.* 385, 113 (2010).
- U. Paiphansiri and P. Tangboriboonrat, Deposition of disinfectant poly(methyl acrylate) nanocapsules onto natural rubber film via layer-by-layer technique. J. Appl. Polym. Sci. 112, 769 (2009).
- T. Otsu, Iniferter concept and living radical polymerization. J. Polym. Sci. Pol. Chem. 38, 2121 (2000).
- H. Zhou, J. Jiang, and K. Zhang, N-Bromosuccinimide as a thermal iniferter for radical polymerization. J. Polym. Sci. Pol. Chem. 43, 2567 (2005).
- 15. M. J. Fullana, M. J. Miri, S. S. Vadhavkar, N. Kolhatkar, and A. C. Delis, Polymerization of methyl acrylate and as comonomer with ethylene using a bis(imino)pyridine iron(II) chloride/methylaluminoxane catalyst. J. Polym. Sci. Pol. Chem. 46, 5542 (2008).

- 16. A. Kongkaew and J. Wootthikanokkhan, Effects of reaction conditions on poly(methyl methacrylate) polymerized by living radical polymerization with iniferter. J. Appl. Polym. Sci. 75, 938 (2000).
- T. Otsu, M. Yoshida, and A. Kuriyama, Living radical polymerizations in homogeneous solution by using organic sulfides as photoiniferters. *Polym. Bull.* 7, 45 (1982).
- T. Otsu, T. Matsunaga, A. Kuriyama, and M. Yoshioka, Living radical polymerization through the use of iniferters: Controlled polymers. *Eur. Polym. J.* 25, 643 (1989).
- **19.** P. Lambrinos, M. Tardi, A. Polton, and P. Sigwalt, The mechanism of the polymerization of n.butyl acrylate initiated with *N*,*N*-diethyl dithiocarbamate derivatives. *Eur. Polym. J.* 26, 1125 (**1990**).
- K. Landfester, N. Bechthold, F. Tiarks, and M. Antonietti, Formulation and stability mechanisms of polymerizable miniemulsions. *Macromolecules* 32, 5222 (1999).
- **21.** C. Prego, D. Torres, and M. J. Alonso, Chitosan nanocapsules as carriers for oral peptide delivery: Effect of chitosan molecular weight and type of salt on the *in vitro* behaviour and *in vivo* effectiveness. *J. Nanosci. Nanotechnol.* **6**, 2921 **(2006)**.
- 22. G. Mittal, D. K. Sahana, V. Bhardwaj, and M. N. V. Ravi Kumar, Estradiol loaded PLGA nanoparticles for oral administration: Effect of polymer molecular weight and copolymer composition on release behavior in vitro and in vivo. J. Controlled Release 119, 77 (2007).
- 23. R. A. Graves, S. Pamujula, R. Moiseyev, T. Freeman, L. A. Bostanian, and T. K. Mandal, Effect of different ratios of high and low molecular weight PLGA blend on the characteristics of pentamidine microcapsules. *Int. J. Pharm.* 270, 251 (2004).
- 24. A. Yamada, T. Yamanaka, T. Hamada, M. Hase, K. Yoshikawa, and D. Baigl, Spontaneous transfer of phospholipid-coated oil-in-oil and water-in-oil micro- droplets through an oil/water interface. *Langmuir* 22, 9824 (2006).
- C. Yin, S. M. Chia, C. H. Quek, H. Yu, R.-X. Zhuo, K. W. Leong, and H.-Q. Mao, Microcapsules with improved mechanical stability for hepatocyte culture. *Biomaterials* 24, 1771 (2003).
- 26. P. J. Dowding, R. Atkin, B. Vincent, and P. Bouillot, Oil core/polymer shell microcapsules by internal phase separation from emulsion droplets. II: Controlling the release profile of active molecules. *Langmuir* 21, 5278 (2005).
- 27. W. M. Obeidat and J. C. Price, Viscosity of polymer solution phase and other factors controlling the dissolution of theophylline microspheres prepared by the emulsion solvent evaporation method. *J. Microencapsulation* 20, 57 (2003).

Received: 23 March 2010. Revised/Accepted: 7 August 2010.

### DNA detection of chronic myelogenous leukemia by magnetic nanoparticles†

Kulachart Jangpatarapongsa,\*\*a Duangporn Polpanich,\* Vichanan Yamkamon,\* Yuranun Dittharot,\* Jutharat Peng-On,\* Raweewan Thiramanas,\* Suradej Hongeng,\* Saengsuree Jootar,\* Lalida Charoenmak\* and Pramuan Tangboriboonrat\*

Received 4th June 2010, Accepted 19th September 2010 DOI: 10.1039/c0an00374c

A novel tool for the detection of *BCR/ABL* fusion gene in chronic myelogenous leukemia (CML) was developed by a magneto-polymerase chain reaction (PCR)-enzyme linked gene technique. The forward primers covalently bound to the surface of magnetic nanoparticles allowed a convenient separation of PCR products with high sensitivity (0.5 pg ml<sup>-1</sup>) and high specificity using K562 cell line and CML patients. The results were obtained when the biotinylated-reverse primer bound to streptavidin-horseradish peroxidase (HRP) and hydrolysed the substrate. This novel readout system was approximately 1000-fold more sensitive than the conventional agarose gel electrophoresis. The present technique is practical and useful for following up CML patients and for providing appropriate treatment, particularly to patients in remote areas.

#### Introduction

**PAPER** 

Chronic myelogenous leukemia (CML), a common hematologic malignancy worldwide, is defined as a myeloproliferative disorder characterized by uncontrolled proliferation of myeloid lineage. The chimeric oncogene breakpoint cluster region gene and a cellular *ABL* gene (*BCR/ABL*) are traditional genes existing in almost all CML patients. <sup>1-5</sup> Microarray studies of mononuclear cells from CML patients reveal that most of the genes induced by *BCR/ABL* are involved in signaling transduction, cell proliferation, differentiation and apoptosis, thereby, disrupting normal hematopoietic cell regulation. <sup>6</sup> Therefore, the detection of *BCR/ABL* fusion gene is very important in the early diagnosis and monitoring of the disease. Quantitative assay is also necessary to determine the gene level for case follow-up studies.

Currently, several diagnostic tools for CML have been focused on the molecular level. Reverse transcriptase-polymerase chain reaction (RT-PCR) followed by gel electrophoresis is commonly performed in order to detect the specific fusion gene. However, the PCR products often disrupt the interpretation of the electrophoresis band pattern. In addition, this process is laborious and requires the use of ethidium bromide (EB), known as a carcinogenic agent, for visualizing DNA in agarose gel.

Mahidol University, Bangkok, 10700, Thailand. E-mail: mtkjp@mahidol.

Alternative techniques showing comparable sensitivity and specificity to PCR, *e.g.*, southern blot analysis and real-time PCR, are also employed. Nevertheless, these techniques are costly, more laborious, time consuming and not available at the field site or at local hospitals.

To overcome these drawbacks, we developed a novel diagnostic tool which combines the RT-PCR technology with magnetic nanoparticles (MNPs). MNPs are easily magnetized by an external magnetic field and immediately redispersed upon removal of the magnetic field. It has been widely used in various biomedical applications, e.g., cell purification, immunoassay, drug delivery and as a contrast medium for magnetic resonance imaging (MRI).7 Success in the binding of a primer onto the surface of MNPs and its application has been recently reported.8-12 A magneto immuno-PCR (M-IPCR) technique which combined sandwich immunoassay and PCR for detection of recombinant Hepatitis B surface antigen with high sensitivity was also presented. 13,14 Here, we studied an innovative modification of the magneto-PCR-enzyme linked gene technique. It involved forward and reverse primers bound to MNPs and the labeling system (biotin), respectively, for detection of the fusion gene in the CML cell line (K562) and in patients. After RT-PCR amplification, the PCR products attached to MNPs were easily collected by an external magnetic field. By using streptavidin-horseradish peroxidase (SA-HRP), the substrate was allowed to generate the detectable colored product with high sensitivity. The overall system is summarized in Scheme 1. This technique is practical and reliable, with high sensitivity and specificity, and is useful to follow-up patients for an appropriate treatment.

#### **Experimental**

#### Cell culture

L929 (fibroblast cell line), K562 (t(9;22)/BCR/ABL) and NB4 (t(15;17)/PML- $RAR\alpha$ ) fusion genes were cultured in RPMI-1640 supplemented with 10% heat-inactivated fetal calf serum (FCS)

ac.th; Fax: +662-441-4380

<sup>\*</sup>Department of Clinical Microbiology, Faculty of Medical Technology,

<sup>&</sup>lt;sup>b</sup>National Nanotechnology Center, Thailand Science Park, Pathumthani, 12120, Thailand

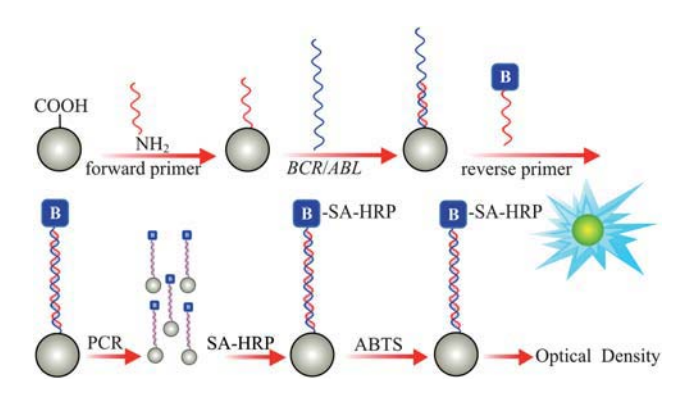
<sup>&</sup>lt;sup>c</sup>Department of Clinical Microscopy, Faculty of Medical Technology, Mahidol University, Bangkok, 10700, Thailand

<sup>&</sup>lt;sup>d</sup>Department of Pediatrics, Faculty of Medicine, Ramathibodi Hospital, Mahidol University, Bangkok, 10400, Thailand

<sup>&</sup>lt;sup>e</sup>Department of Medicine, Faculty of Medicine, Ramathibodi Hospital, Bangkok, 10400, Thailand

Department of Chemistry, Faculty of Science, Mahidol University, Bangkok, 10400, Thailand

<sup>†</sup> Electronic supplementary information (ESI) available: Details of magnetic nanoparticles. See DOI: 10.1039/c0an00374c



Scheme 1 Schematic of the detection of BCR/ABL fusion gene in CML by magneto-PCR-enzyme linked gene technique.

(GIBCO, Carlsbad, USA). Viability and number of cells were determined by tryphan blue exclusion.

#### Sample collection

Blood samples were collected from 5 CML patients registered at Ramathibodi Hospital (Bangkok, Thailand). Diagnosis of patients was based on clinical findings, cytogenetics and RT-PCR performed using a specific primer designed as previously reported.<sup>15</sup> Two healthy adults living in Bangkok were considered as "healthy control" (HC) subjects. This study was approved by the Ethical Approval Committee of Biomedical Institute of Ramathibodi Hospital. Informed consent was obtained from each individual.

#### RNA extraction and cDNA synthesis

Total RNA was extracted from lysed cells by using Trizol® (Invitrogen, USA). Briefly, Trizol® (1 ml) was added to the cells, mixed vigorously for 15 s and then incubated for 5 min. After adding chloroform (1 ml), the mixture was centrifuged (12000 g) for 10 min at 4 °C. RNA in the colorless upper aqueous phase was precipitated by using an equal volume of isopropanol. The RNA was incubated at room temperature for 15 min before being centrifuged (14000 g) for 10 min at 4 °C. The obtained RNA pellet was washed twice with 75% ethanol (in diethyl pyrocarbonate treated distilled water (DW)) and centrifuged (14000 g) for 10 min at 4 °C. The RNA pellet was dried at ambient temperature then treated with RQ1 RNase-free DNase (Promega, USA). Afterwards, RNA (1-5 mg) was employed for cDNA synthesis by using the first strand cDNA synthesis kit including Oligo(dT)<sub>12-18</sub> (Invitrogen, USA) as the primer and reverse transcriptase Superscript™ III (Invitrogen, USA). The experiment was carefully handled to prevent possible contamination.<sup>16</sup> For example, RNA was extracted in the separation areas and the master mix with cDNA was performed before PCR amplification.

#### Immobilization of primers on magnetic nanoparticles

The MNPs were kindly supplied by Chemicell, Germany (see ESI†). Their morphology and size under transmission electron microscopy (JEOL, JEM-2010) are shown in Fig. 1. After washing twice with 25 mM 2-(*N*-morpholino)ethanesulfonic acid

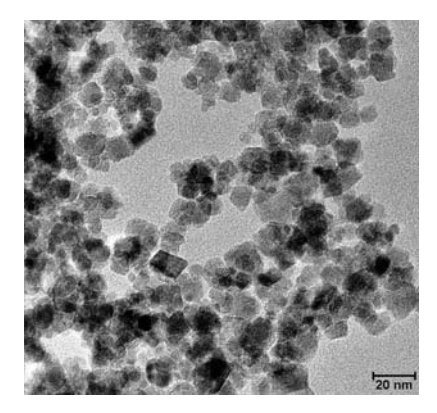


Fig. 1 TEM micrograph of MNPs.

(MES) buffer (500  $\mu$ l, pH 6.0), these carboxylates were immobilized with NH<sub>2</sub>-modified BCR forward primer (5'-NH<sub>2</sub>-C<sub>6</sub>-CTG ACC AAC TCG TGT GTG AAA C-3') by using the carbodiimide method. In brief, the MNPs (1000  $\mu$ g) were mixed with 5.4 nmol NH<sub>2</sub>-modified BCR forward primer and incubated for 30 min at room temperature under gently shaking. 1-ethyl-3-(3-dimethylaminopropyl)carbodiimide (EDC) solution (10  $\mu$ l) (10 mg EDC in 0.25 ml MES buffer) and the MES buffer were, subsequently, added to make a final volume of 100  $\mu$ l. After incubating for 10 min at room temperature, the supernatant was decanted and the immobilized MNPs were mixed with 50 mM Tris buffer (pH 7.4) to quench the unreacted carboxyl groups. The immobilized MNPs were washed twice and then resuspended in Tris-EDTA buffer (10 mM Tris-HCl and 1 mM EDTA, pH 8.0) before storage at 4 °C.

#### RT-PCR

Specific primers for BCR/ABL amplification are shown in Table 1. The NH<sub>2</sub>-modified BCR forward primer and the ABL reverse primer were 5'-labeled with the MNPs and biotin, respectively. Primers for  $\beta$ -actin (a house keeping gene) and DW were used as positive and negative controls, respectively. PCR was carried out in a mixture (20 µl) containing 10 mM Tris-HCl (pH 8.3), 50 mM KCl, 2.0 mM MgCl<sub>2</sub>, 200 μM deoxynucleotide triphosphates (dNTP), synthesized cDNA (100 ng), 1U of Taq DNA polymerase (Intronbiotechnology, USA) and 0.3 µM unbound or MNP bound primers (3 µg MNPs content) using DNA engine PCR system (Bio-Rad Laboratories, USA). Reaction steps were done as follows: denaturation at 95 °C for 5 min, annealing at 57-65 °C for 1 min and at 72 °C for 1 min. The MNPs-bound PCR products were then separated into two parts for: (i) quantitative assay by using an enzyme-substrate system, and (ii) qualitative assay by using agarose gel electrophoresis. The MNPs-PCR products were cleaved by *Baul* enzyme (20 U) (Promega, USA) at 37 °C for 24 h before being subjected to electrophoresis.

#### Quantitative assay by the enzyme-substrate system

To determine the level of gene expression, the MNPs-PCR products were incubated with horseradish peroxidase-conjugated streptavidin (SA-HRP) at room temperature for 30 min. The obtained SA-biotin complexes were washed twice and simply

Table 1 Cell line, target gene, sequence and size of PCR products of fusion transcripts in the present study

| Cell line      | Target<br>gene | Sequence $(5' \rightarrow 3')$                                  | Product<br>size<br>(base pairs) | Ref |
|----------------|----------------|---|---------------------------------|-----|
| K562           | BCR-F          | NH <sub>2</sub> -C <sub>6</sub> -CTGACC<br>AACTCGTG<br>TGTGAAAC | 290                             | 15  |
|                | ABL-R          | Biotin-TGTGATT ATAGCCTA AGACCCGGA                               |                                 |     |
| K562,<br>L929, | β-actin-F      | AGAGGGAAAT<br>CGTGCGTGAC  | 138                             | 17  |
| NB4            | β-actin-R      | CAATAGTG<br>ATGACCT<br>GGCCGT                                   |                                 |     |

separated by applying an external magnetic field. Then, 2,2'-azino-di(3-ethylbenzthiazoline-6-sulfonate) (ABTS) containing  $\rm H_2O_2$  (50%) (Kirkepaard & Perry Laboratories, USA) was sequentially added and the mixture was incubated for 1 h at room temperature. Enzyme activity was measured by a microplate reader (Perkin Elmer, Wallac Victor, Germany) at 405 nm.

#### Statistical analysis

Data were analyzed by SPSS PASW Statistics 17 (SPSS Inc., Chicago, USA) and reported as mean  $\pm$  standard error of mean (sem). The difference between groups in each experiment (annealing temperature, cell line, cDNA template concentration, and CML negative and positive cells) was compared using one way ANOVA followed by Turkey HSD Post-Hoc test. Statistical significance was defined as p < 0.05. The reported bar graphs showed the relative ratio of BCR/ABL expression, calculated from the absorbance of PCR product at 405 nm from K562 cell line divided by DW. Thin lines showed the sem value.

#### Results and discussion

After the immobilization of primers onto the surface of the MNPs, the RT-PCR conditions, *i.e.*, annealing temperature and primer concentration, were optimized. The specificity of the technique was tested by using the K562 cell line as a CML-positive to compare with NB4 and L929 which were used as CML-negative cell lines. In the case of the K562 cell line, sensitivity was obtained by varying the concentration of the cDNA template before PCR amplification. The clinical samples were the peripheral blood collected from 5 CML patients and 2 HC donors.

## Optimization of *BCR/ABL* amplification using MNPs-immobilized primer

The quality of the DNA template from the K562 cell line was investigated by using BCR/ABL primers and  $\beta$ -actin as a positive control. The bands of the PCR products at different sizes, *i.e.*, 290 and 138 base pairs when using BCR/ABL and  $\beta$ -actin as the DNA template, respectively, in Fig. 2A indicated the good quality of the extracted DNA template.

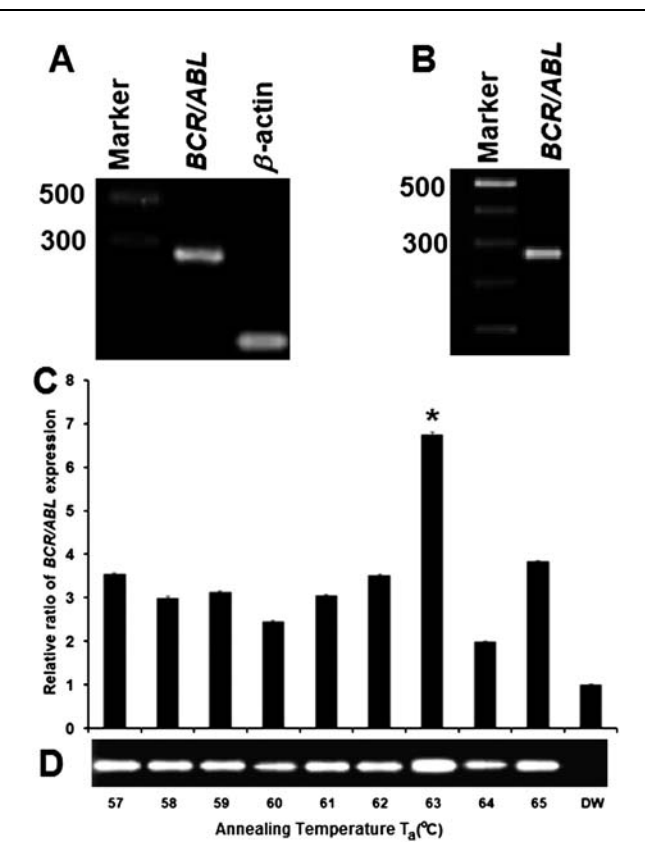


Fig. 2 Optimized conditions for the PCR product. (A) The size of BCR/ABL and  $\beta$ -actin gene product of the DNA template from the K562 cell line at  $T_a$  63 °C. BCR/ABL gene expression using MNPs-bound BCR forward primer at  $T_a$  from 57 to 65 °C determined by the enzyme substrate system (C) and using primer without MNPs determined by gel electrophoresis (D). (B) The gel electrophoresis results of Baul enzyme cleaved products after RT-PCR. Bars show the relative ratio of BCR/ABL expression calculated by the absorbance of PCR product at 405 nm from K562 divided by DW. Thin lines show the value of sem. \*significantly different (p < 0.05) from others.

To obtain a high amount of amplification product, the annealing temperature  $(T_a)$  of BCR/ABL amplification using MNPs-immobilized specific primers was varied from 57 to 65 °C. Fig. 2C shows the highest OD, indicated by the relative ratio of BCR/ABL expression (6.74  $\pm$  0.07), when the reaction was performed at 63 °C. This OD value was significantly different from the others (p < 0.05) (mean  $\pm$  sem at  $T_a$  57 °C = 3.54  $\pm$  0.02, 58 °C = 2.99  $\pm$  0.01, 59 °C = 3.12  $\pm$  0.01, 60 °C = 2.44  $\pm$  0.01, 61 °C = 3.04  $\pm$  0.02, 62 °C = 3.50  $\pm$  0.02, 64 °C = 1.98  $\pm$ 0.02, 65 °C = 3.84  $\pm$  0.02). Since the highest amount of PCR product was obtained at  $T_a$  63 °C, this temperature was used to perform PCR in further steps. Results were correlated well with the band intensities obtained from gel electrophoresis. It should be noticed that the primers without MNPs and biotin tagging were employed in the latter technique as presented in Fig. 2D. The enzyme-substrate system, represented by the BCR/ABL gene expression, could be compared with gel electrophoresis. Moreover, this enzyme substrate assay was safer than the conventional gel electrophoresis because EB, a carcinogenic reagent, was not required.

After amplification, Baul restriction enzyme was used to separate the MNPs from the PCR products. Since Baul enzyme

can cleave the PCR product at 5'-C↓TC GTG-3' located on the 5' terminal of the PCR product, the appearance of the 290 base pairs nucleotide was detected as displayed in Fig. 2B. This confirmed the presence of immobilized primers on the MNPs as previously reported.8

#### Specificity of BCRIABL by the enzyme-substrate system

The specificity of BCR/ABL expression was determined by using a cDNA template extracted from various cell lines, i.e., K562 as CML-positive cell, L929 and NB4 as CML-negative cells, and DW as a negative control. The BCR/ABL gene expression was quantitatively and qualitatively determined by the enzymesubstrate assay and gel electrophoresis, respectively, as presented in Figs. 3A and 3B. The data shows a significant increase in the relative ratio of BCR/ABL gene expression (2.70  $\pm$  0.01) as compared to others (p < 0.05) and specifically detected the BCR/ ABL gene only in the K562 cell line. The values of mean  $\pm$  sem of the relative ratio of BCR/ABL expression from L929, NB4 and DW were  $1.00 \pm 0.01$ ,  $1.06 \pm 0.01$  and  $1.00 \pm 0.01$ , respectively. It can be observed in Fig. 3A that the relative ratio level for K562 was at least 3 fold above the average cut off from CML negative cell lines and DW. This level was also correlated well with the band appeared in the gel electrophoresis shown in Fig. 3B.

#### Sensitivity of the enzyme-substrate system

With the above optimized conditions, the sensitivity of detection was investigated at 63 °C by varying 10 fold dilutions of K562 cDNA template from 1 µg ml<sup>-1</sup> to 0.5 pg ml<sup>-1</sup>. The results in Fig. 4 show the highest relative ratio of BCR/ABL gene expression when using  $0.05 \,\mu \text{g ml}^{-1}$  (7.50  $\pm 0.03$ ) of cDNA. However, this level was not significantly different when cDNA was varied from 1 µg ml<sup>-1</sup> to 0.5 pg ml $^{-1}$  (level of: 1  $\mu$ g ml $^{-1}$  = 4.23  $\pm$  0.01; 0.1  $\mu$ g ml $^{-1}$  =  $4.30 \pm 0.01;\, 0.01 \; \mu g \; m l^{-1} = 3.80 \pm 0.01;\, 0.005 \; \mu g \; m l^{-1} = 4.31 \; \pm$ 0.01; 0.001  $\mu g \ ml^{-1} = 6.53 \pm 0.02$ ; 0.0005  $\mu g \ ml^{-1} = 5.64 \pm 0.02$ ;

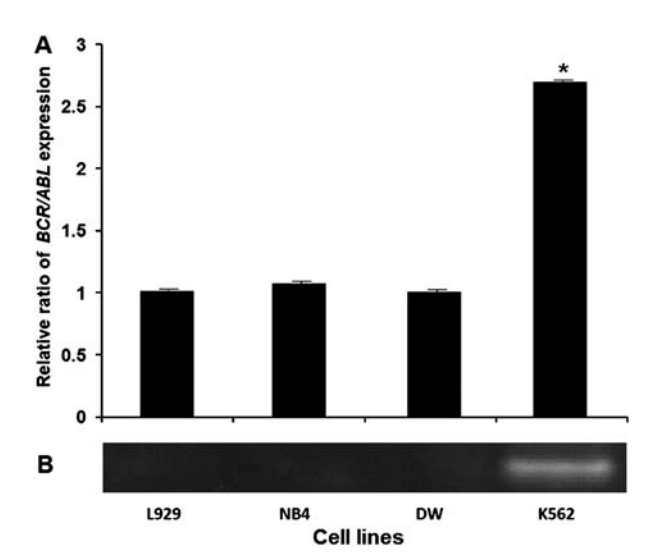


Fig. 3 The relative ratio of BCR/ABL gene expression in various cell lines determined by enzyme substrate system (A) and gel electrophoresis (B). Bar columns represent relative expression comparing to DW. \*significantly different (p < 0.05) from others. Thin lines show the value of sem

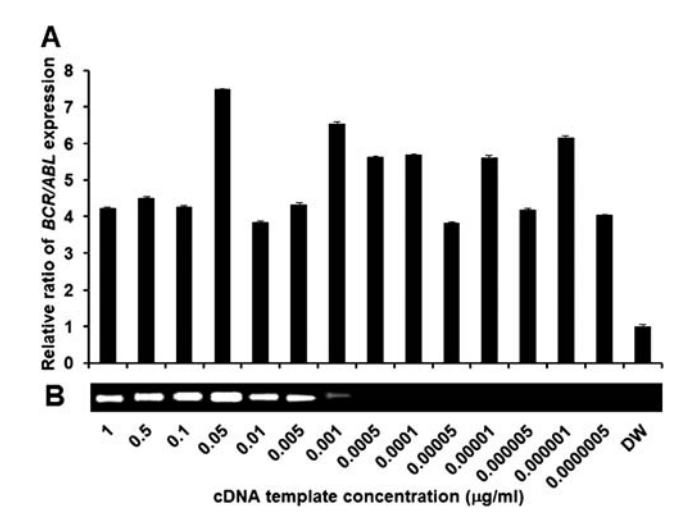


Fig. 4 Relative ratio of BCR/ABL gene expression (A) and gel electrophoresis (B) at various concentrations of cDNA template ranging from 1-0.0000005 µg ml<sup>-1</sup>. Bar columns represent relative expression compared to DW. Thin lines show the value of sem.

 $0.0001~\mu g~ml^{-1} = 5.70~\pm~0.01;~0.00005~\mu g~ml^{-1} = 3.81~\pm~0.01;$  $0.00001~\mu g~ml^{-1} = 5.60 \pm 0.01;~0.000005~\mu g~ml^{-1} = 4.18 \pm 0.01;$  $0.000001~\mu g~ml^{-1} = 6.16~\pm~0.01;~0.0000005~\mu g~ml^{-1} = 4.04~\pm~0.01$ 0.01; DW = 1.00  $\pm$  0.01). On the contrary, the difference between the lowest amount of cDNA template concentration (0.5 pg ml<sup>-1</sup>) and DW was clearly observed (p < 0.05). In addition, at lower than 0.0005 µg ml<sup>-1</sup> of cDNA template concentration, no band appeared on the agarose gel as shown in Fig. 4B. This indicated that the sensitivity of the MNPs-PCR products with the enzymesubstrate system was approximately 1000-fold higher than that of the gel electrophoresis. The detection limit of our assay (in pg) was in the same scale as that of the real-time PCR, both SYBR green and Taqman probe as reported in other systems. 18-21

#### Detection of the BCR/ABL gene in CML patients

The efficiency of the MNPs bound BCR forward primer and the biotinylated ABL reverse primers with SA-HRP system to detect the BCR/ABL fusion gene in clinical samples was evaluated by using blood collected from 5 CML patients and 2 HC donors. The results showed that the assay was able to detect all CML patients compared with HC subjects and the negative control. The BCR/ABL gene expressed by every CML patient was significantly higher than the HC; 20 fold by patient no. 1 (CML1)  $(21.84 \pm 0.04)$  and 7–9 fold by patients no. 2–5 (CML2–5) (the relative ratio of *BCR/ABL* expression from CML2 =  $7.64 \pm$ 0.02, CML3 =  $9.48 \pm 0.03$ , CML4 =  $8.21 \pm 0.03$ , CML5 =  $6.83 \pm 0.03$ , HC1 =  $0.99 \pm 0.01$ , HC2 =  $1.03 \pm 0.01$ , DW =  $1.00 \pm 0.01$ ) (p < 0.05) as presented in Fig. 5. The data correlated well with those results obtained from gel electrophoresis (data not shown). The specificity of our proposed detection system was, therefore, confirmed. Since all patients were diagnosed with the chronic phase of myelogenous leukemia, the correlation between the severity of CML patients with the level of OD could not be determined. As compared to the PCR based-gel electrophoresis, the combination of MNPs and the enzyme-substrate system brought about an enhancement in sensitivity similar to

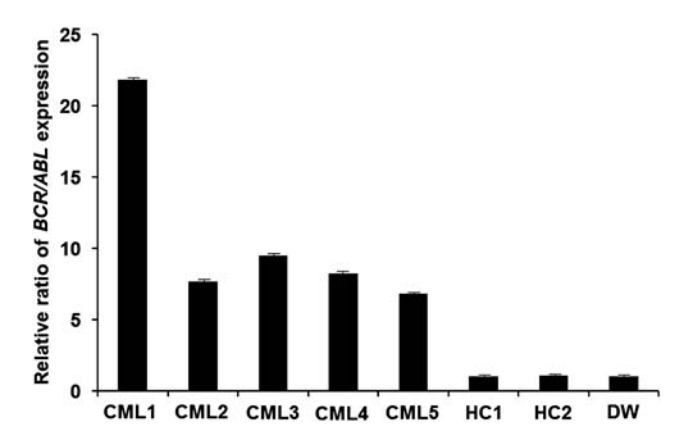


Fig. 5 Relative ratio of BCR/ABL gene expression in the blood from CML patients no. 1-5 (CML1-5) compared to healthy controls (HC1-2) and DW as a control.

the real-time PCR technique. Due to the fact that the proposed assay used the commonly available spectrophotometer to quantitatively determine the level of gene expression, it would be practical, especially in remote areas. Without using EB, this novel method was considered as safer than gel electrophoresis.

#### **Conclusions**

A technique for fusion gene detection of CML by combining MNPs bound to forward primer and biotinylated reverse primer for RT-PCR amplification followed by the use of an enzymesubstrate system for quantitative analysis was developed. The technique could be applied to detect BCR/ABL fusion gene in the CML-positive cell line with high sensitivity (0.5 pg ml<sup>-1</sup> of DNA template). Also, high specificity was obtained when testing with CML-negative cell lines. This assay was successfully used to detect the BCR/ABL gene contained in CML patients. It could also be used as an alternative method for early diagnosis and follow-up treatment leading to a better prognosis for CML patients in clinical trials. Based on this knowledge, the detection of other genetic diseases, infectious diseases and cancers particularly in other leukemic cell types showing high prevalence among the Thai population could be investigated.

#### Acknowledgements

A research grant from the Thailand Research Fund/the Commission on Higher Education (RTA5180003) to PT,

Mahidol University to KJ and the scholarship from National Science and Technology Development Agency under Young Scientist and Technologist Programme (YSTP) to YD and Thailand Graduate Institute of Science and Technology (TGIST) to LC are gratefully acknowledged. We also thank Dr Rachanee Udomsangpetch, Dr Pimpichaya Patamasiriwat and Dr Dalina Tanyong for technical support and Bodeeworrada Jisakul and staffs of Ramathibodi Hospital for sample collection.

#### References

- 1 W. Y. Au, P. B. Caguioa, C. Chuah, S. C. Hsu, S. Jootar, D. W. Kim, I. Y. Kweon, W. M. O'Neil, T. K. Saikia and J. Wang, Int. J. Hematol., 2009, 89, 14-23.
- 2 P. C. Nowell, Exp. Cell Res., 1960, 19, 267-277.
- 3 A. de Klein, A. G. van Kessel, G. Grosveld, C. R. Bartram, A. Hagemeijer, D. Bootsma, N. K. Spurr, N. Heisterkamp, J. Groffen and J. R. Stephenson, Nature, 1982, 300, 765-767.
- 4 H. Pluk, K. Dorey and G. Superti-Furga, Cell, 2002, 108, 247-259.
- 5 C. L. Sawyers, Cancer Cell, 2002, 1, 13-15.
- 6 M. O. Nowicki, P. Pawlowski, T. Fischer, G. Hess, T. Pawlowski and T. Skorski, Oncogene, 2003, 22, 3952-3963.
- 7 T. Osaka, T. Matsunaga, T. Nakanishi, A. Arakaki, D. Niwa and G. Iida, Anal. Bioanal. Chem., 2006, 384, 593-600.
- 8 H. B. Shen, M. Hu, Y. B. Wang and H. Q. Zhou, Biophys. Chem., 2005, 115, 63-66.
- 9 A. Fan, C. Lau and J. Lu, Analyst, 2008, 133, 219-225
- 10 R. Fu, T. Li and H. G. Park, Chem. Commun., 2009, 5838-5840.
- 11 H. Li and Z. He, Analyst, 2009, 134, 800–804.
- 12 H. Liu, S. Li, Z. Wang, M. Ji, L. Nie and N. He, J. Biotechnol., 2007,
- 13 M. Adler, R. Wacker and C. Niemeyer, Analyst, 2008, 133, 702-718.
- 14 R. Wacker, B. Ceyhan, P. Alhorn, D. Schueler, C. Lang and M. Niemeyer, Biochem. Biophys. Res. Commun., 2007, 357, 391-396.
- 15 I. M. Chen, A. Chakerian, D. Combs, K. Garner and D. S. Viswanatha, Am. J. Clin. Pathol., 2004, 122, 783-793.
- 16 T. Hughes, M. Deininger, A. Hochhaus, S. Branford, J. Radich, J. Kaeda, M. Baccarani, J. Cortes, N. C. Cross, B. J. Druker, Gabert, D. Grimwade, R. Hehlmann, S. Kamel-Reid, J. H. Lipton, J. Longtine, G. Martinelli, G. Saglio, S. Soverini, W. Stock and J. M. Goldman, Blood, 2006, 108, 28-37.
- 17 A. Giulietti, L. Overbergh, D. Valckx, B. Decallonne, R. Bouillon and C. Mathieu, *Methods*, 2001, **25**, 386–401.
- 18 P. Deschaght, T. De Baere, L. Van Simaey, S. Van Daele, F. De Baets, D. De Vos, J. P. Pirnay and M. Vaneechoutte, BMC Microbiol., 2009,
- 19 M. M. Lopez, P. Llop, A. Olmos, E. Marco-Noales, M. Cambra and E. Bertolini, Curr. Issues Mol. Bio., 2009, 11, 13-46.
- E. Malinen, A. Kassinen, T. Rinttila and A. Palva, Microbiology, 2003, 149, 269-277.
- 21 S. Yin, Y. Shang, G. Zhou, H. Tian, Y. Liu, X. Cai and X. Liu, J. Biotechnol., 2010, 146, 147-150.

#### ORIGINAL PAPER

# Selective Fluorescence Sensing of Deoxycytidine 5'-Monophosphate (dCMP) Employing a Bis (diphenylphosphate)diimine Ligand

Weerachai Nasomphan • Pramuan Tangboriboonrat • Srung Smanmoo

Received: 25 January 2010 / Accepted: 19 July 2010 / Published online: 12 August 2010 © Springer Science+Business Media, LLC 2010

**Abstract** A new bis(diphenylphosphate)diimine ligand (BP1) was prepared and evaluated for its ability for selective detection of deoxycytidine 5'-monophosphate (dCMP). BP1 exhibited off-type fluorescence in the presence of dCMP. The fluorescence of BP1 was significantly quenched upon the addition of  $2.5 \times 10^{-4}$  M dCMP and the detection limit was  $1.25 \times 10^{-5}$  M in MeCN-H<sub>2</sub>O (1:1, v/v). The binding ratio between BP1 and dCMP was determined to be 1:1 with the binding constant of  $3.98 \pm 0.60 \times 10^{-3}$  M<sup>-1</sup>.

**Keywords** Fluorescence (FL) sensor · Deoxycytidine 5'-monophosphate (dCMP) sensor · Diimine ligand (DLs)

#### Introduction

Analytes are usually present in minute amounts in biological systems. Therefore, sensitive and selective detection of analytes with real-time are highly desired [1–7]. Fluorescence chemosensors have found their applications in various fields, e.g. environmental and biomedical

W. Nasomphan · S. Smanmoo (☒)
Bioresources Research Unit,
National Center for Genetic Engineering and Biotechnology
(BIOTEC) Thailand Science Park,
Phaholyothin Road,
Klong Luang, Pathumthani 12120, Thailand
e-mail: srung.sma@biotec.or.th

W. Nasomphan · P. Tangboriboonrat
 Department of Chemistry, Faculty of Science, Mahidol University,
 Rama 6 Road,
 Phyathai, Bangkok 10400, Thailand

and sensitivity for the detection of biological and chemical analytes [8–15]. In general, the design of chemosensors bases on the incorporation of two functional moieties which are: i) ionophore (the receptor part) and ii) chromophore (the signal generating unit). The binding of the analyte to the ionophore initiates the communication between the receptor and the signaling unit to induce the change of chromophore's physical properties [16–18]. Physical changes of the chromophore can be of various types, e.g. chemiluminescence (CL), redox potentials, absorption and fluorescence (FL) [19–34]. Of these, fluorescence chemosensor receives much research attention since it provides the detection of analytes with low cost sampling and high degree of selectivity and sensitivity [35–37].

sciences since they provide excellent degree of selectivity

Bisphosphonate and its derivatives are well recognized for their applications as diagnostic tools in the cancer treatment [38–42]. Particularly, aminobisphosphonate (NBP) is known as an anti-cancer drug. The mode of action for an anti-cancer activity of NBP is specific for prostate cancers. Apart from its medical roles, NBP is known for its ability as a metal chelator [43–45]. Gummiena and his group demonstrated the ability of  $\beta$ -aminobisphosphonate derivatives as chelating agents for copper (II) ion employing electron paramagnetic spectroscopy (EPR) [46].

It is known that the bisphosphate moiety exhibits the fluorescence quenching via the photon-induced electron transfer (PET) mechanism. Diimine ligands (DLs) are known as metal chelators and also as fluorophores due to their photophysical properties [47]. Based on these facts, the incorporation of these components would emerge a new fluorescence chemosensor. Consequently, we have developed new bisphosphate derivatives based on diimine ligands and evaluated for their FL sensing towards



J Fluoresc (2011) 21:187–194

nucleotides. The introduction of bisphosphate group into DL is aimed to facilitate the optimal hydrogen bonding between the receptor and nucleotide substrates. The detection deoxycytidine 5detection deoxycytidine-monophosphate (dCMP) is normally achieved employing high-performance liquid chromatography (HPLC) [48]. Up to date, the fluorescent (FL) chemosensor for dCMP is not yet reported. To the best of our knowledge, the chemosensor based on diimine bisphosphate has not been reported as a selective receptor for dCMP.

#### **Experiments**

#### Apparatus

Fluorescence measurements were carried out using a FP-6300 spectrofluorometer (JASCO) equipped with a xenon lamp source and a 1.0-cm quartz cell, and the scan speed was 600 nmmin<sup>-1</sup>. <sup>1</sup>H spectrum was recorded on Bruker DPX 400 MHz spectrometer in CDCl<sub>3</sub> using TMS as the internal standard. Mass spectra were recorded on Bruker Esquire and Finnigan MAT INCOS 50 mass spectrometers.

#### Reagents

All reagents for the synthesis of diimine ligand phosphates obtained commercially were used without further purification. The stock solution of diimine ligand phosphates was prepared in acetonitrile with the concentration of 10 mM. The corresponding nucleotide monophosphates [deoxycytidine 5'-monophosphate (dCMP); deoxyadenosine 5'-monophosphate (dAMP); deoxycyclicadenosine 5'-monophosphate (dcAMP); deoxythymidine 5'-monophosphate (dTMP); deoxyguanosine 5'-monophosphate (dGMP); uridine 5'-monophosphate (UMP); adenosine 5'-monophosphate (AMP); guanosine 5'-monophosphate (GMP); cytidine 5'-monophosphate (CMP); thymidine 5'-monophosphate (TMP)] used in this study were purchased from Sigma Aldrich (USA) and used without further purification. Methanol was used as a HPLC grade. All other chemicals used were supplied from Sigma Aldrich (USA) as analytical grade and used without further purification. MilliQ water was used throughout this study. The concentration of stock solution of metal ions was 1 mM.

#### General Synthesis of Diimine Ligands

DL was synthesized from the condensation between a corresponding benzaldehyde (1 mmol) and *o*-phenylenediamine (1 mmol) in the presence of distilled water (10 mL). After the reaction mixture was left stirring for 6 h, the crude

solid was collected by filtration and crystallized from methanol to obtain the final product in good yields.

3,3'-[1,2-Phenylenebis(nitrilomethylidene)]bis-phenol (DL1)

DL1 was obtained as white crystals (2.16 g, 74 %).  $^{1}$ H NMR (DMSO-d6)  $\delta_{\rm H}$  7.65 (d, 1H), 7.60 (m, 2H), 7.41 (q, 1H), 7.19 (m, 1H), 6.89 (d, 2H), 6.64 (d, 2H), 5.41 (s, 2H). MS (ESI) [M+H] $^{+}$  317.13.

4,4'-[1,2-Phenylenebis(nitrilomethylidene)]bis-phenol (DL2)

DL2 was obtained as white crystals (2.40 g, 82 %).  $^{1}$ H NMR (DMSO-d6)  $\delta_{\rm H}$  8.94 (s, 2H), 7.67 (d, 2H), 7.46 (m, 4H), 7.41 (m, 4H), 6.97 (m, 4H).  $^{13}$ C NMR  $\delta$  117.6, 119.1, 119.4, 119.8, 127.9, 132.5, 133.5, 142.6, 161.5, 163.8. MS (ESI)  $[M+H]^{+}$  317.35.

Synthesis of *N,N'*-Phenylenebis[2-hydroxybenzylidene-2-benzylidenealdimine] (MP)

In a flame dried round bottom flask, DL1 (0.5 g, 1.58 mmol) was added followed by addition of dry THF (5 mL). The reaction mixture was stirred until the disappearance of DL1 and the solution was brought to -80 °C followed by addition of potassium tert-butoxide (0.19 g, 1.74 mmol). The reaction mixture was left stirring at room temperature for 3 h before the reaction solution was cooled down to -80 °C followed by the addition of diphenyl chlorophosphate (0.33 mL, 1.58 mmol). The reaction mixture was left stirring at room temperature overnight before the addition of saturated aqueous NH<sub>4</sub>Cl solution followed by extraction with EtOAc (3×10 mL). The organic phase was washed with brine and dried over MgSO<sub>4</sub>. The solvent was removed under a vacuum and the crude product was chromatographed on a silica gel column. Elution of the column with a mixture of EtOAc and hexane (2:8) afforded the desired product as clear oil (0.54 g, 62 %). <sup>1</sup>H NMR (DMSO-d6)  $\delta_{\rm H}$  8.40 (s, 1H), 7.70 (d, 2H, J=8.51), 7.39 (d, 1H, J=8.50), 7.30 (t, 2H, J= 15.77), 7.22 (m, 2H), 7.08 (t, 2H, J=7.81 and 15.53), 6.92 (d, 1H, 7.49), 6.61 (d, 1H, J=7.74), 6.48 (d, 1H, J=7.49), 6.38 (s, 1H), 5.45 (s, 2H). <sup>13</sup>C NMR δ 111.13 (ArCH), 117.47 (ArCH), 119.57 (ArCH), 119.74 (ArCH), 119.79 (ArCH), 119.88 (ArCH), 119.92 (ArCH), 120.54 (ArCH), 121.38 (ArCH), 121.70 (ArCH), 122.61 (ArCH), 123.22 (ArCH), 123.66 (ArCH), 125.54 (ArCH), 125.94 (ArCH), 126.04 (ArCH), 126.36 (ArCH), 128.77 (ArCH), 129.35 (ArCH), 130.04 (ArCH), 130.19 (ArCH), 130.28 (ArCH), 130.76 (ArCH), 130.89 (ArCH), 131.90 (ArC), 135.91 (ArC), 139.37 (ArC), 142.53 (ArC), 149.64 (ArC), 149.71 (ArC), 150.17 (C=NH), 151.69 (C=NH). HRMS (ESI+)  $[M+Na]^+$  found 571.1392  $[M+H]^+$ , calcd for  $C_{32}H_{25}N_2O_5P$ 



Fig. 1 Chemical structures of BP1, BP2 and MP. Conditions and Reagents; (a) (i) 2.2 equiv *tert*-BuOK, THF, room temperature, 2 hrs (ii) 2 equiv ClP(O) (OPh)<sub>2</sub>, -80 °C, overnight. (b) (i) 1.1 equiv *tert*-BuOK, THF, room temperature, 2 hrs (ii) 1 equiv ClP(O)(OPh)<sub>2</sub>, -80 °C, overnight

548.1501. IR (KBr, cm<sup>-1</sup>) 3417, 3071, 2615, 1941, 1788, 1606, 1416, 1389, 1025, 964, 849, 777.

Synthesis of *N,N'*-Phenylenebis[2-benzylidenealdimine] phosphate (BP1)

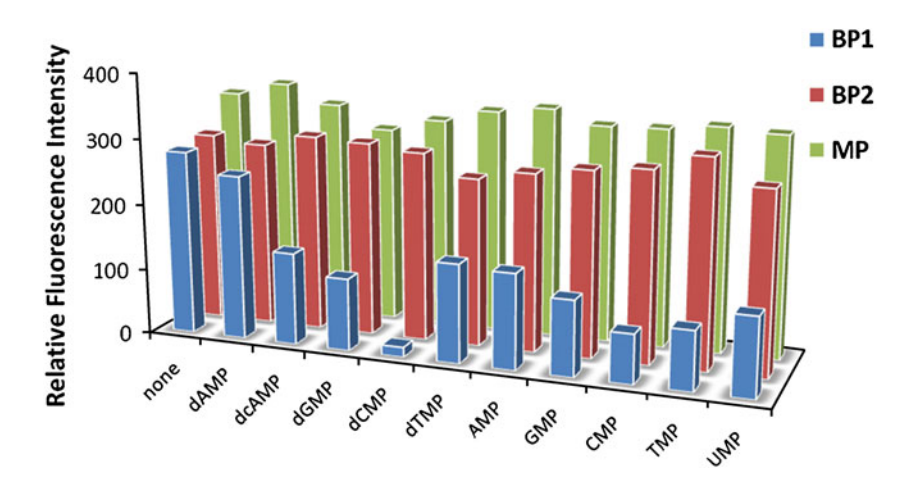
BP1 was synthesized according to the procedure described for the synthesis of MP except 2 molar equiv of diphenyl chlorophosphate was used.  $^{1}$ H NMR (DMSO-d6)  $\delta_{\rm H}$  8.40 (s, 1H), 7.80 (d, 2H, J=8.67), 7.72 (d, 1H, J=8.96), 7.42 (m, 13H), 7.26 (m, 19H), 7.06 (d, 2H, J=8.61), 5.59 (s, 2H).  $^{13}$ C NMR δ 111.14 (ArCH), 115.26 (ArCH), 119.36 (ArCH), 119.91 (ArCH), 119.97 (ArCH), 120.30 (ArCH), 120.35 (ArCH), 120.41 (ArCH), 121.76 (ArCH), 122.42 (ArCH), 122.94 (ArCH), 125.97 (ArCH), 126.08 (ArCH), 128.10 (ArCH), 128.79 (ArCH), 130.24 (ArCH), 130.32 (ArCH), 130.49 (ArCH), 131.16 (ArC), 134.53 (ArC),

135.81 (Ar*C*), 142.61 (Ar*C*), 149.77 (Ar*C*), 152.13 (*C*=NH). HRMS (ESI+) [M+Na]<sup>+</sup> found 803.1687 [M+H]<sup>+</sup>, calcd for  $C_{44}H_{34}N_2O_8P_2$  780.1790. IR (KBr, cm<sup>-1</sup>) 3064, 2929, 2870, 2611, 1942, 1867, 1783, 1730, 1588, 1487, 1449, 1389, 1298, 1186, 1161, 1090, 1072.

Synthesis of *N,N'*-Phenylenebis[3-benzylidenealdimine] phosphate (BP2)

BP2 was similarly prepared according to the procedure for BP1 except DL2 was used as a starting material.  $^{1}$ H NMR (DMSO-d6)  $δ_{\rm H}$  7.82 (d, 2H, J=8.65), 7.44–7.39 (m, 15H), 7.31–7.20 (m, 14H), 7.15 (d, 2H, J=7.15), 5.60 (s, 2H).  $^{13}$ C NMR δ 111.14 (ArCH), 115.26 (ArCH), 119.37 (ArCH), 119.87 (ArCH), 120.36 (ArCH), 121.80 (ArCH), 122.41 (ArCH), 125.61 (ArCH), 126.02 (ArCH), 128.10 (ArCH), 130.14 (ArCH), 131.16 (ArCH), 135.83 (ArCH), 142.64

Fig. 2 The effect of various nucleotides on the FL intensities of MP, BP1 and BP2 in MeCN:  $H_2O$  (1:1; v/v). [receptor] =  $2.5 \times 10^{-6}$  M. [nucleotides] =  $2.5 \times 10^{-4}$  M.  $\lambda_{ex} = 280$  nm





J Fluoresc (2011) 21:187–194

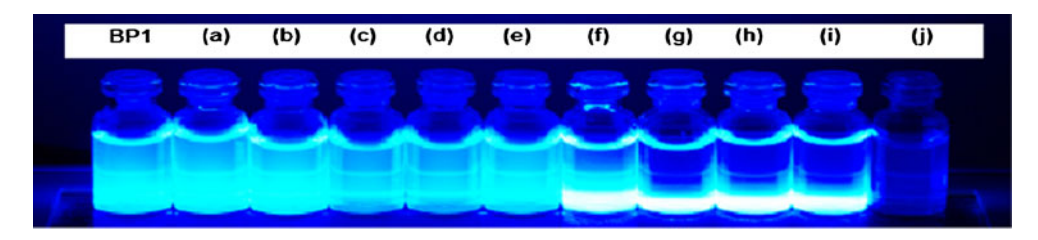


Fig. 3 FL changes of BP1  $(2.5 \times 10^{-6} \text{ M})$  in the presence and absence of nucleotides (a) BP1 + dAMP (b) BP1 + dcAMP (c) BP1 + dTMP (d) BP1 + dGMP (e) BP1 + AMP (f) BP1 + GMP (g) BP1 + CMP (h) BP1 + TMP (i) BP1 + UMP and (j) BP1 + dCMP. [nucleotides] =  $5 \times 10^{-4} \text{ M}$ 

(ArCH), 142.77 (ArCH), 149.08 (ArCH), 149.83 (ArCH), 150.88 (ArCH), 151.51 (ArCH), 152.14 (ArC), 153.67 (ArC), 153.95 (ArC), 157.07 (ArC), 159.07 (ArC), 161 (C=NH). HRMS (ESI+)  $[M+Na]^+$  found 803.1681  $[M+H]^+$ , calcd for  $C_{44}H_{34}N_2O_8P_2$  780.1790. IR (KBr, cm<sup>-1</sup>) 3451, 3268, 3070, 3007, 2881, 2512, 2249, 2123, 1996, 1828, 1768, 1621, 1374, 1223, 1056, 882, 759.

#### **Results and Discussion**

Syntheses of MP, BP1 and BP2

BP1 was synthesized in two steps from the reaction between DL1 with 2 equiv of diphenylchlorophosphate in the presence of potassium *tert*-butoxide as base. BP2 was also synthesized in order to investigate the positional effect of bisphosphate group. The synthesis of BP2 was similar to the procedure described for the synthesis of BP1 except DL2 was used as the starting material. After purification, BP1 and BP2 were obtained in good isolated yields (BP1=72% and BP2=77%) (Fig. 1). Monodiphenylchlorophosphate diimine ligand (MP) was also synthesized as the control ligand for the investigation of the effect of bisphosphate group due to the fact that the presence of bisphosphate group is important for facilitating the hydro-

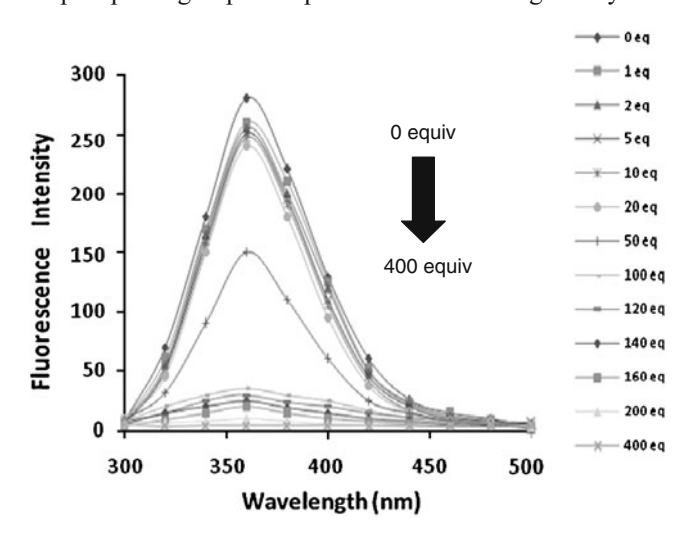


**Fig. 4** FL emission spectra of BP1 (2.5×10<sup>-6</sup> M) in the presence of various concentrations of dCMP

gen bonding between the receptor and analytes. The synthesis of MP was achieved by reacting DL1 with 1 equiv of diphenylchlorophosphate. BP1 was prepared in moderate yield (62%).

Fluorescence Screening of MP, BP1 and BP2 with Various Nucleotide Substrates

Obtaining BP1, BP2 and MP, FL quenching experiments of these receptors in the presence of various nucleotides were investigated. With reference to the screened nucleotides, the FL property of BP1 exhibited a significant quenching in the presence of deoxycytidine 5'-monophosphate (dCMP) (Fig. 2). It was shown that after the addition of 2.5×  $10^{-4}$  M dCMP, the FL intensity of BP1 was significantly inhibited. The presence of other nucleotides did not significantly quench the FL of BP1. BP2 and MP showed no degree of FL quenching upon treating with any nucleotides. It was shown that the presence of bisphosphate group at the *meta* position on the aromatic ring of BP1 is necessary for proper chelation between BP1 and dCMP.

In the case of MP, it lacks a phosphate group which resulted in an improper interaction between MP and dCMP. This was evident that the presence of bisphosphate group was important since no FL quenching of MP was observed in the presence of any nucleotides. BP2 possesses the

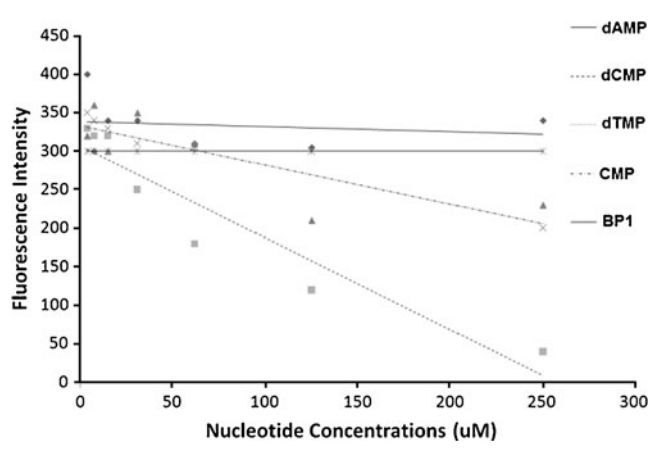
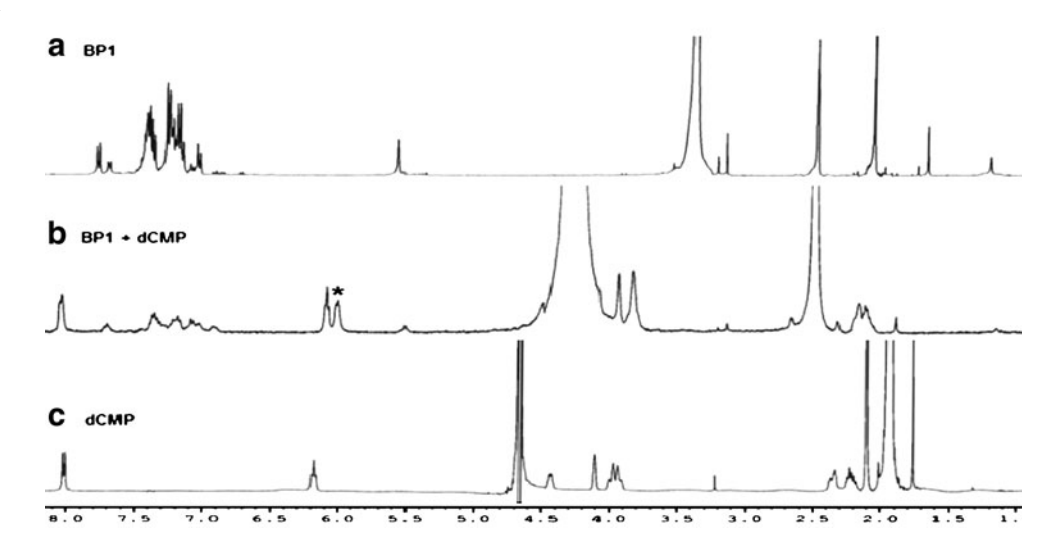


Fig. 5 FL quenching of BP1 by various concentrations of dAMP, dCMP, dTMP, and CMP



**Fig. 6** <sup>1</sup>H NMR spectra (400 MHz) of (a) free BP1 (10 mM) in DMSO (top); (b) BP1 + 1 equiv of dCMP in DMSO:D<sub>2</sub>O (1:1; v/v); (c) dCMP in D<sub>2</sub>O



bisphosphate group which meets the requirement described above for the optimal interaction between the receptor and dCMP. The position of the bisphosphate group on the BP2 aromatic ring is too remote for the good binding between the receptor and dCMP. It was obvious that BP1 exhibited high degree of selectivity towards dCMP. The presence of the bisphosphate group at the *meta* position on the aromatic ring of BP1 is a prerequisite for the good recognition between the receptor and dCMP. Therefore, BP1 was used as the optimal receptor for subsequent experiments.

BP1 was shown to exhibit strong FL emission in acetonitrile. The excitation wavelength (*Ex*) of BP1 was 280 nm while the emission wavelength (*Em*) was 360 nm.

Figure 3 shows the FL changes of BP1 upon the addition of various nucleotides. The presence of various nucleotides slightly to moderately affected the FL intensity of BP1. It was clearly observed that  $2.5 \times 10^{-4}$  M of dCMP dramatically quenched the FL of BP1.

FL emission of BP1 was measured at different concentrations of dCMP while fixed the concentration of BP1 at  $2.5 \times 10^{-6}$  M (Fig. 4). Increasing concentration of dCMP resulted in the decrease of the FL emission of BP1. When the concentration of dCMP reached  $2.5 \times 10^{-4}$  M, the FL intensity of BP1 was significantly quenched. To investigate more precisely, the quenching effect of BP1 with dCMP and other representing nucleotides at different concentrations was studied. The FL intensity of BP1 was measured in the presence of various concentrations of four nucleotides, dAMP, dCMP, dTMP and CMP. At all concentrations of dAMP, there was a little FL quenching of BP1 (Fig. 5).

Addition of dTMP and CMP resulted in slight decrease of BP1's FL intensity. The FL intensity of BP1 was significantly inhibited in the presence of dCMP even at low concentration. Further increasing concentrations of dCMP resulted in a gradual FL quenching of BP1. When the concentration of dCMP reached 400

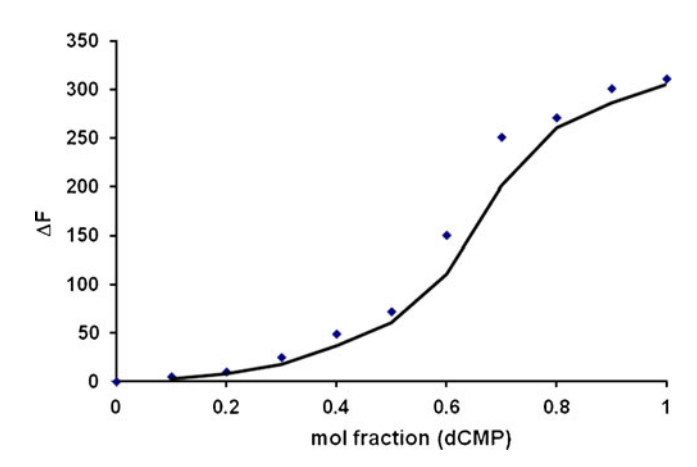
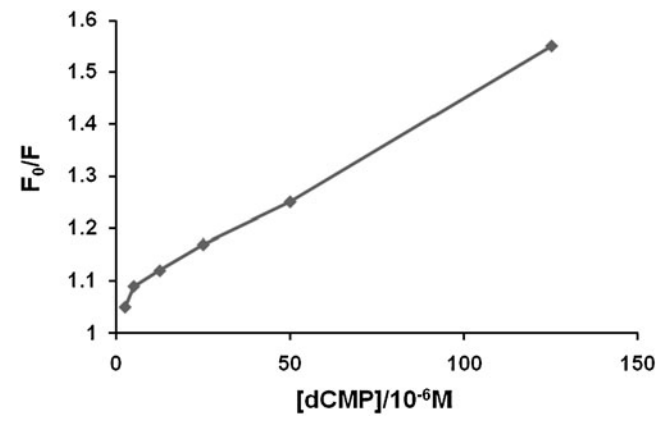


Fig. 7 Job's plot for BP1·dCMP. Y axis is fluorescence changes of BP1



**Fig. 8** Stern-Volmer plot of BP1 with increasing concentrations of dCMP. [BP1] =  $2.5 \times 10^{-6}$  M. [dCMP]/ $10^{-6}$  M=2.5, 5, 12.5, 25, 50, 300 (T=298 K)



J Fluoresc (2011) 21:187–194

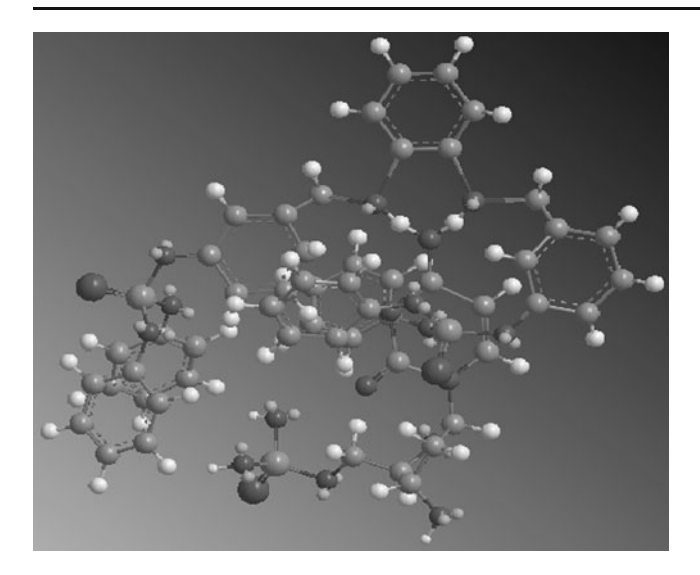


Fig. 9 Energy minimized structure of the complex between BP1 and dCMP

molar equiv of BP1, the FL intensity of BP1 was significantly quenched.

#### <sup>1</sup>H NMR Titration of BP1 with dCMP

Of the mechanistic detail concerning interaction between BP1 and dCMP,  $^1H$  NMR experiments were used for the investigation (Fig. 6). It was clearly shown that the addition of 1 equiv dCMP into BP1 solution caused a slight downfield shift of aromatic protons in BP1 indicating the disturbance of the electron density within this area. Apart from the downfield shift of protons in the aromatic region, the solution contained both BP1 and dCMP exhibited the change of the multiplicity for the designated cytosine proton. This effect was evident with the appearance of the new peak at  $\delta$  6.15 ppm (indicating as an asterisk in Fig. 6b). This new peak was the result from the perturbation for the electronic environment of the cytosine proton in dCMP due to the interaction with BP1.

## Determination of the Binding Ratio and Constant for BP1 and dCMP

Attempting to obtain the binding ratio between BP1 and dCMP by mass spectrometry was unsuccessful. Therefore, Job's plot analysis was used to determine the binding ratio [49]. Job's plot analysis indicated a breaking point at 0.6 mol fraction of dCMP indicating the formation of a 1:1 complex of BP1·dCMP (Fig. 7). The binding constant between BP1 and dCMP was determined using the Stern-Volmer plot ( $K_{sv}$ ). The  $K_{sv}$  was obtained from the Stern-Volmer Eq. (1) [50]

$$F_0/F = 1 + K_{SV}[Q]$$
 (1)

Where [Q] is the concentration of the quencher (dCMP),  $K_{sv}$  is the Stern-Volmer constant. The Stern-Volmer

constant indicates the constant equilibrium of BP1·dCMP complex in the static quenching process. It was shown in Fig. 8 that the Stern-Volmer plot of BP1·dCMP complex exhibited a linear relationship. The  $(F_0/F)$  was directly proportional to the increased concentration of dCMP with the correlation coefficient of 0.9953. From the plot, BP1 had a weak binding affinity to dCMP (3.98±0.60×  $10^{-3}$  M<sup>-1</sup>) and upon the binding between BP1 and dCMP it formed the non-fluorescent complex.

#### Proposed Mechanism for BP1 Binding with dCMP

The mechanistic detail for the binding between BP1 and dCMP is believed to involve the hydrogen bonding between the bisphosphate group of BP1 and the cytosine NH<sub>2</sub> of dCMP. The good alignment for the binding between BP1 and dCMP optimizes the interaction of these two species. Upon binding between BP1 and dCMP, the PET mechanism plays a significant role which resulted in the FL quenching of the system. The steric hindrance is also thought to play a role on the binding between BP1 and dCMP. The steric hindrance could be used to explain why the FL intensity of BP1 was not quenched upon the addition with CMP. In the case of CMP, the presence of the 2'-hydroxyl group causes the structure more bulky to fit into the receptor's pocket. Therefore, the presence of the 2'-hydroxyl group in CMP hindered proper binding between BP1 and CMP. This explained the fact that CMP is not a good substrate for BP1 due to the steric effect. The absence of the 2'hydroxyl group in dCMP facilitates the good binding between BP1 and dCMP (Fig. 9).

#### **Conclusions**

In conclusion, we have discovered the selective FL quenching of BP1 by dCMP. The FL quenching of BP1 exhibited excellent degree of selectivity towards dCMP among various nucleotide substrates. FL and <sup>1</sup>H NMR experiments indicated the interaction between BP1 and dCMP. Job's plot analysis indicated the binding ratio between BP1 and dCMP at 1:1 with the Stern-Volmer constant of  $3.98\pm0.60\times10^{-3}~\text{M}^{-1}$ . It was suggested that the FL quenching of BP1 by dCMP took place via the PET mechanism. The recognition of dCMP by BP1 may be due to the extended hydrogen bonding with the proper alignment. The steric effect of the substrate also plays a determining role for good binding between BP1 and dCMP. Since BP1 shows high degree of selectivity and sensitivity to dCMP over other nucleotides it could be regarded as a new FL chemosensor for dCMP.



**Acknowledgements** The Thailand Research Fund (TRF)/Commission on Higher Education (CHE)'s research grant to S.S. and P.T. The Development and Promotion of Science and Technology Talents Project's scholarship to W.N. are gratefully acknowledged. We are also grateful to the partial support from National Center for Genetic Engineering and Biotechnology (BIOTEC).

#### References

- Lu C, Xu Z, Cui J, Zhang R, Qian X (2007) Ratiometric and highly selective fluorescent sensor for cadmium under physiological pH range: a new strategy to discriminate cadmium from zinc. J Org Chem 72:3554
- Tang B, Yin L, Wang X, Chen Z, Tong L, Xu K (2009) A fastresponse, highly sensitive and specific organoselenium fluorescent probe for thiols and its application in bioimaging. Chem Commun 5293
- Xue X, Wang F, Liu X (2008) One-step, room temperature, colorimetric detection of mercury (Hg<sup>2+</sup>) using DNA/nanoparticle conjugates. J Am Chem Soc 130:3244
- Kim HJ, Kim SH, Kim JH, Anh LN, Lee JH, Lee CH, Kim JS (2009) ICT-based Cu(II)-sensing 9, 10-anthraquinonecalix[4] crown. Tetrahedron Lett 50:2782
- Maiti J, Pokhrel B, Boruah R, Dolui SK (2009) Polythiophene based fluorescence sensors for acids and metal ions. Sensors Actuat B Chem 141:447
- Zeng X, Dong L, Wu C, Mu L, Sai-Feng X, Tao Z (2009) Highly sensitive chemosensor for Cu(II) and Hg(II) based on the tripodal rhodamine receptor. Sensors Actuat B Chem 141:506
- Lee SJ, Lee SS, Jeong IY, Lee JY, Jung JH (2007) Azobenzene coupled chromogenic receptors for the selective detection of copper(II) and its application as a chemosensor kit. Tetrahedron Lett 48:393
- Wu JS, Kim HJ, Lee MH, Yoon JH, Lee JH, Kim JS (2007) Anion-induced ring-opening of fluorescein spirolactam: fluorescent OFF-ON. Tetrahedron Lett 48:3159
- 9. Rieth T, Sasamoto K (1998) Detection of nitric oxide and nitrite by using a Rhodamine-type fluorescent indicator. Anal Commun 35:195
- Soh JH, Swamy KMK, Kim SK, Sim S, Lee SH, Yoon J (2007) Rhodamine urea derivatives as fluorescent chemosensors for Hg<sup>2</sup>
   Tetrahedron Lett 48:5966
- Kikuchi K, Hashimoto S, Mizukami S, Nagano T (2009) Anion sensor-based ratiometric peptide probe for protein kinase activity. Org Lett 11:2732
- Xue L, Liu Q, Jiang H (2009) Ratiometric Zn<sup>2+</sup> fluorescent sensor and new approach for sensing Cd<sup>2+</sup> by ratiometric displacement. Org Lett 11:3454
- Wang HH, Gan Q, Wang XJ, Xue L, Liu SH, Jiang H (2007) A water soluble, small molecular fluorescent sensor with femtomolar sensitivity for zinc ion. Org Lett 9:4995
- 14. Xu Z, Xiao Y, Qian X, Cui J, Cui D (2005) Ratiometric and selective fluorescent sensor for Cu<sup>II</sup> based on internal charge transfer (ICT). Org Lett 7:889
- Rhee HW, Lee CR, Cho SH, Song MR, Cashel M, Choy HE, Seok YJ, Hong JI (2008) Selective fluorescent chemosensor for the bacterial alarmone (p)ppGpp. J Am Chem Soc 130:784
- 16. Kim NY, Chang SK (1998) Calix[4]arenes bearing two distal azophenol moieties: highly selective chromogenic ionophores for the recognition of Ca<sup>2+</sup> ion. J Org Chem 63:2362
- 17. He X, Hu S, Liu K, Guo Y, Xu J, Shao S (2006) Oxidized bis (indolyl)methane: a simple and efficient chromogenic-sensing molecule based on the proton transfer signaling mode. Org Lett 8:333

 Jiménez D, Martínez-Máñez R, Sancenón F, Ros-Lis JV, Benito A, Soto J (2003) A new chromo-chemodosimeter selective for sulfide anion. J Am Chem Soc 125:9000

- 19. Matsumoto M, Kasai D, Yamada K, Fukuda N, Watanabe N, Ijuin HK (2004) Color modulation for chemiluminescence of a dioxetane bearing a 3-(anthracen-9-yl)-5-hydroxyphenyl moiety induced by a complex of crown ether with potassium *tert*-butoxide. Tetrahedron Lett 45:8079
- Zhu Y, Shi J, Zhang Z, Zhang C, Zhang X (2002) Development of a gas sensor utilizing chemiluminescence on nanosized titanium dioxide. Anal Chem 74:120
- Hu X, Takenaka N, Takasuna S, Kitano M, Bandow H, Maeda Y, Hattori M (1993) Determination of ammonium ion in rainwater and fogwater by flow injection analysis with chemiluminescence detection. Anal Chem 65:3489
- Corrales T, Abrusci C, Peinado C, Catalina F, Fluorescent sensor as physical amplifier of chemiluminescence: application to the study of poly(ethylene terephthalate). Macromolecules 37:6596
- Kang D, Zuo X, Yang R, Xia F, Plaxco KW, White RJ (2009) Comparing the properties of electrochemical-based DNA sensors employing different redox tags. Anal Chem 81:9109
- Cai Q, Zeng K, Ruan C, Desai TA, Grimes CA (2004) A wireless, remote query glucose biosensor based on a pH-sensitive polymer. Anal Chem 76:4038
- Xiao Y, Qu X, Plaxco KW, Heeger AJ (2007) Label-free electrochemical detection of DNA in blood serum via targetinduced resolution of an electrode-bound DNA pseudoknot. J Am Chem Soc 129:11896
- 26. Xiao Y, Lou X, Uzawa T, Plakos KJI, Plaxco KW, Soh HT (2009) An electrochemical sensor for single nucleotide polymorphism detection in serum based on a triple-stem DNA probe. J Am Chem Soc 131:15311
- Watanabe S, Seguchi H, Yoshida K, Kifune K, Tadaki T, Shiozaki H (2005) Colorimetric detection of fluoride ion in an aqueous solution using a thioglucose-capped gold nanoparticle. Tetrahedron Lett 46:8827
- Zhang C, Suslick KS (2005) A colorimetric sensor array for organics in water. J Am Chem Soc 127:11548
- Liu J, Lu Y (2003) A colorimetric lead biosensor using DNAzymedirected assembly of gold nanoparticles. J Am Chem Soc 125:6642
- Zhang D, Zhang M, Liu Z, Yu M, Li F, Yi T, Huang C (2006) Highly selective colorimetric sensor for cysteine and homocysteine based on azo derivatives. Tetrahedron Lett 47:7093
- Scrafton DK, Taylor JE, Mahon MF, Fossey JS, James TD (2008)
   Click-fluors: modular fluorescent saccharide sensors based on a 1,
   3-triazole ring. J Org Chem 73:2871
- 32. Yang RH, Chan WH, Lee AWM, Xia PF, Zhang HK, Li K (2003) A ratiometric fluorescent sensor for Ag<sup>I</sup> with high selectivity and sensitivity. J Am Chem Soc 125:2884
- Yao Z, Feng X, Li C, Shi G (2009) Conjugated polyelectrolyte as a colorimetric and fluorescent probe for the detection of glutathione. Chem Commun 5886
- 34. Mu H, Gong R, Ma Q, Sun Y, Fu E (2007) A novel colorimetric and fluorescent chemosensor: synthesis and selective detection for Cu<sup>2+</sup> and Hg<sup>2+</sup>. Tetrahedron Lett 48:5525
- Hong SY, Czarnik AW (1993) A metal ion-insensitive polyanion chemosensor. J Am Chem Soc 115:3330
- Namkung W, Padmawar P, Mills AD, Verkman AS (2008) Cell-based fluorescence screen for K<sup>+</sup> channels and transporters using an extracellular triazacryptand-based K<sup>+</sup> sensor. J Am Chem Soc 130:7794
- Zhao J, Davidson MG, Mahon MF, Kociok-Köhn G, James TD (2004) An enantioselective fluorescent sensor for sugar acids. J Am Chem Soc 126:16179
- 38. Merrell MA, Wakchoure S, Ilvesaro JM, Zinn K, Gehrs B, Lehenkari PP, Harris KW, Selander KS (2007) Differential effects



J Fluoresc (2011) 21:187–194

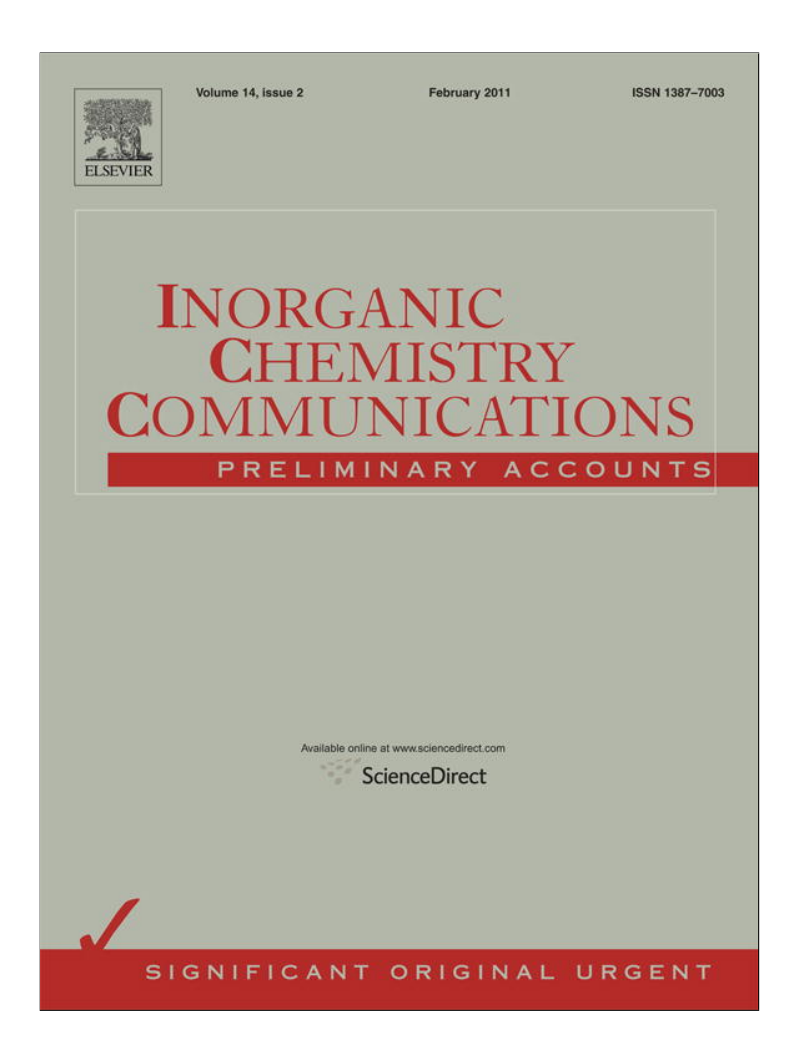
of Ca<sup>2+</sup> on bisphosphonate-induced growth inhibition in breast cancer and mesothelioma cells. Eur J Pharm 559:21

- Segawa H, Kimura S, Kuroda J, Sato K, Nogawa M, Yuasa T, Yokota A, Hodohara K, Fujiyama Y, Maekawa T (2005) The antileukemic efficacy of the third generation bisphosphonate ONO5920/YM529. Leukemia Res 29:451
- 40. Cramer JA, Lynch NO, Gaudin AF, Walker M, Cowell W (2006) The effect of dosing frequency on compliance and persistence with bisphosphonate therapy in postmenopausal women: a comparison of studies in the united states, the united kingdom, and france. Clin Ther 28:1686
- Sillero MAG, de Diego A, Silles E, Pérez-Zúñiga F, Sillero A (2006) Synthesis of bisphosphonate derivatives of ATP by T4 RNA ligase. FEBS Lett 580:5723
- Takahashi R, Shimazaki C, Inaba T, Okano A, Hatsuse M, Okamoto A, Hirai H, Ashihara E, Nakagawa M (2001) A newly developed bisphosphonate, YM529, is a potent apoptosis inducer of human myeloma cells. Leukemia Res 25:77
- 43. Kamila S, Callan JF, Mulrooney RC, Middleton M (2007) A novel fluorescent chemosensor for Cu(II) in aqueous solution based on a β-aminobisphosphonate receptor. Tetrahedron Lett 48:7756
- Matczak-Jon E, Kurzak B, Sawka-Doborwolska W, Lejczak B, Kafarski P (1998) Zinc(II) complexes of phosphonic acid

- analogues of aspartic acid and asparagine. J Chem Soc Dalton Trans 161
- 45. Gumienna-Kontecka E, Jezierska J, Lecouvey M, Leroux Y, Kozlowski HJ (2002) Bisphosphonate chelating agents: Coordination ability of 1-phenyl-1-hydroxymethylene bisphosphonate towards Cu<sup>2+</sup> ions. J Inorg Biochem 89:13
- 46. Gumienna-Kontecka E, Galezowska J, Drag M, Latajka R, Kafarski P, Kozlowski H (2004) Coordination abilities of substituted  $\beta$ -aminophosphonates towards  $Cu^{2+}$  and  $Zn^{2+}$  ions. Inorg Chim Acta 357:1632
- Jung HJ, Singh N, Jang DO (2008) Highly Fe<sup>3+</sup> selective ratiometric fluorescent probe based on imine-linked benzimidazole. Tetrahedron Lett 49:2960
- 48. Havlis J, Madden JE, Revilla AL, Havel J (2001) Highperformance liquid chromatographic determination of deoxycytidine monophosphate and methyldeoxycytidine monophosphate for DNA demethylation monitoring: experimental design and artificial neural networks optimization. J Chromatogr B 755:185
- 49. Schneider HJ, Yatsimirsky A (2000) Principles and methods in supramolecular chemistry. Wiley, Chichester, p 151
- Mei X, Wolf C (2004) Enantioselective sensing of chiral carboxylic acids. J Am Chem Soc 126:14736



Provided for non-commercial research and education use. Not for reproduction, distribution or commercial use.



This article appeared in a journal published by Elsevier. The attached copy is furnished to the author for internal non-commercial research and education use, including for instruction at the authors institution and sharing with colleagues.

Other uses, including reproduction and distribution, or selling or licensing copies, or posting to personal, institutional or third party websites are prohibited.

In most cases authors are permitted to post their version of the article (e.g. in Word or Tex form) to their personal website or institutional repository. Authors requiring further information regarding Elsevier's archiving and manuscript policies are encouraged to visit:

http://www.elsevier.com/copyright

#### Author's personal copy

Inorganic Chemistry Communications 14 (2011) 351-354



Contents lists available at ScienceDirect

#### **Inorganic Chemistry Communications**

journal homepage: www.elsevier.com/locate/inoche



## Highly selective fluorescent chemosensor for Fe<sup>3+</sup> imaging in living cells

Srung Smanmoo <sup>a,\*</sup>, Weerachai Nasomphan <sup>b</sup>, Pramuan Tangboriboonrat <sup>b</sup>

- <sup>a</sup> Bioresources Research Unit, National Center for Genetic Engineering and Biotechnology (BIOTEC), 113 Thailand Science Park, Phaholyothin Road, Klong Luang, Pathumthani 12120. Thailand
- <sup>b</sup> Department of Chemistry, Faculty of Science, Mahidol University, Rama 6 Road, Phyathai, Bangkok 10400, Thailand

#### ARTICLE INFO

Article history: Received 24 August 2010 Accepted 18 November 2010 Available online 25 November 2010

Keywords: Fluorescent chemosensor Fe<sup>3+</sup> sensor Dansyl cadaverine Fluorescence quenching Bioimaging

#### ABSTRACT

2-Hydroxybenzyl dansyl cadaverine (DNSCH) was designed as a fluorescent chemosensor for Fe $^{3+}$ . DNSCH exhibited significant FL quenching with increasing concentrations of Fe $^{3+}$ . The presence of 15 M equiv of Fe $^{3+}$  significantly quenched the FL intensity of DNSCH. The binding constant of DNSCH towards Fe $^{3+}$  was determined and found to be  $1.5 \pm 0.4 \times 10^{-4}$  M $^{-1}$ . DNSCH was employed as an intracellular chemosensor for Fe $^{3+}$ 

© 2010 Elsevier B.V. All rights reserved.

Molecular recognition of metal ions is one of active areas in supramolecular chemistry. Based on de Silva et al., the design of fluorescent (FL) chemosensor is simply achieved by the incorporation of metal-binding receptor and fluorophore via the spacer [1]. FL chemosensor receives much research attention in the field of bioanalytical science due to its high selectivity, real-time detection and simplicity [2–6]. The recognition of metals at the receptor is achieved through various modes of interactions, e.g., hydrogen bonding, van der Waals and electrostatic forces [7–9]. The binding of metal ions at the receptor initiates the communicating event with the fluorophore in which the signal obtained can be expressed as an energy transfer. Particularly, in the FL quenching type chemosensor, the quenching process involves the formation of an exciplex with charge transfer or photo-induced electron transfer.

The design of FL chemosensors exhibiting selective recognizing of  ${\rm Fe}^{3+}$  receives much research attention due to  ${\rm Fe}^{3+}$  is the most abundant ion in intracellular compartments. Recently, several FL chemosensors have been designed for the recognition of  ${\rm Fe}^{3+}$ . Jang et al. designed a benzimidazole-based FL sensor in which the imidazole moiety presents in the sensor serves as the binding part for  ${\rm Fe}^{3+}$  [10]. The sensor exhibits good binding constant with  ${\rm Fe}^{3+}$ . Zheng and Huang reported an on/off chemosensor for  ${\rm Fe}^{3+}$  controlled by protonation–deprotonation processes [11]. The sensor is designed based on calix[4]arene with two 3-alkoxy-2-naphthoic acids pending on the upper rim. The binding of  ${\rm Fe}^{3+}$  is controlled by the deprotonation of phenolic moieties of calix

[4]arene and dicarboxylic group of napthoic acid. On the contrary, the unbound state of calix[4]arene towards  $Fe^{3+}$  is driven by the protonation of calix[4]arene's phenol. Noh and his co-workers have designed an excellent chemosensor for  $Fe^{3+}$ . The sensor is based on a ferrocenyl chalcone structure which is capable in discriminating  $Fe^{3+}$  and  $Fe^{2+}$  via the selective oxidation [12]. Up to date,  $Fe^{3+}$  chemosensors for cell applications are scarcely reported and challenging for the design.

We have designed a new FL chemosensor, DNSCH, based on dansyl cadaverine. DNSCH adopts the fluorophore–spacer–receptor format. The dansyl fluorophore was attached via a pentylene spacer to the 2-hydroxybenzaldehyde receptor. DNSCH was evaluated against various metal ions and found to exhibit selective FL quenching in the presence of Fe<sup>3+</sup>. DNSCH was employed as an intracellular chemosensor for Fe<sup>3+</sup>.

Dansyl derivatives were extensively used as chromophores to construct a chemosensor platform [13–15]. The incorporation of 2-hydroxybenzaldehyde is expected to serve as the metal ion binding moiety and to affect the intramolecular charge transfer which induces the emission change of the sensor. 2-Hydroxybenzyl dansyl cadaverine (DNSCH) was synthesized in one step from the condensation reaction between dansyl cadaverine and 2-hydroxybenzaldehydes (Scheme 1). After reaction mixture was left stirring under nitrogen atmosphere for 24 h, DNSCH was isolated and crystallized from ethyl acetate/hexane to afford DNSCH in 81% (the spectroscopic identification for DNSCH is accomplished and can be found in Supplementary Material). The C = N group formed is aimed to provide the chelation to metal ions since it is known that C = N exhibits good degree of affinity towards transition and post-transition metal cations due to its electronic structure [16.17].

The selectivity of DNSCH towards metal ions was investigated (Fig. 1). Of all metal ions, DNSCH exhibited a significant degree of FL quenching in the presence of Fe<sup>3+</sup>. In the presence of 15 M equiv of

<sup>\*</sup> Corresponding author. Tel.: +66 2 564 6700x3560; fax: +66 2 564 6632. E-mail address: srung.sma@biotec.or.th (S. Smanmoo).

S. Smanmoo et al. / Inorganic Chemistry Communications 14 (2011) 351-354

Scheme 1. Synthesis of DNSCH.

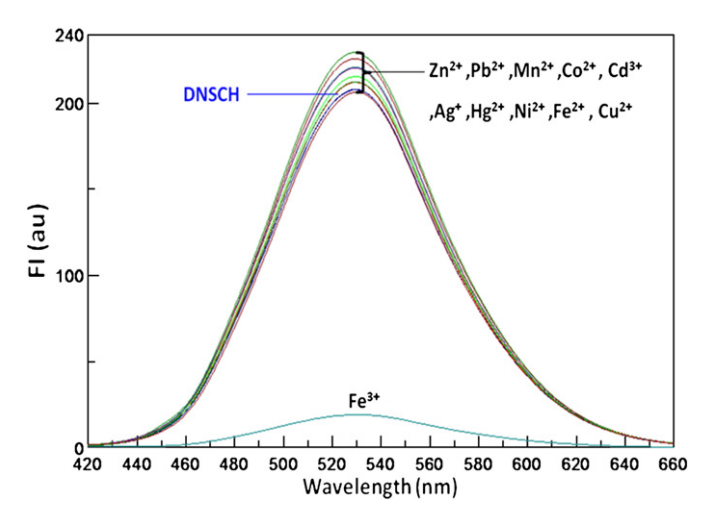


**Fig. 1.** Emission spectra of DNSCH  $(2.5\times10^{-6}~M)$  upon the addition of different metal ions  $(3.75\times10^{-5}~M)$  in CH<sub>3</sub>CN-H<sub>2</sub>O (50:50, v/v);  $\lambda_{ex}=342~nm$ .

Fe<sup>3+</sup>, the FL intensity of DNSCH was significantly quenched. The design of Fe<sup>3+</sup> chemosensor with good discrimination between the iron valence states (Fe<sup>2+</sup> and Fe<sup>3+</sup>) is necessary for better understanding of various biological processes and Fenton reaction [18]. It was clearly shown that DNSCH is a selective Fe<sup>3+</sup> chemosensor with the good discrimination for iron valence states. The presence of the 2-hydroxyl group in DNSCH is thought to facilitate the binding of Fe<sup>3+</sup> near to the dansyl fluorophore prior to initiate the quenching process.

Fig. 2 represented the color and FL images of DNSCH in the presence of various metal ions. In the absence of metal ions, DNSCH exhibited strong yellow ( $\lambda_{em} = 525 \text{ nm}$ ) FL when excited at 342 nm. The emission of DNSCH at 525 nm is the characteristic emission of dansyl fluorophore ( $\lambda_{em} = 520 \text{ nm}$ ) [19]. In the addition of other metal ions except Fe³+, DNSCH exhibited no color and FL changes. However, the addition of Fe³+ induced a slight change in color from clear to pale yellow [Fig. 2(a)], associated with the strong FL quenching [Fig. 2(b)].

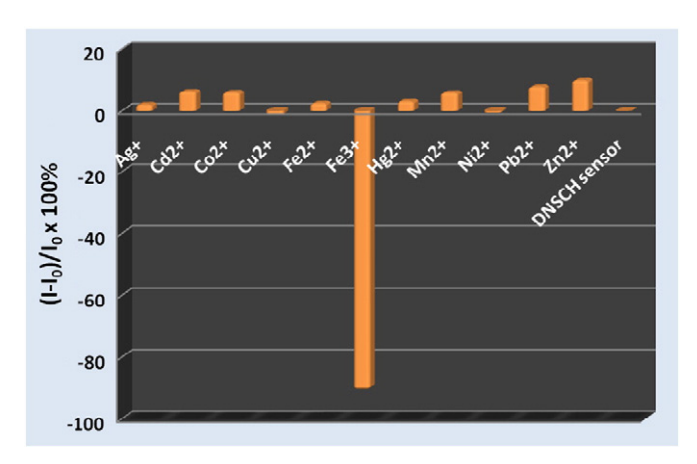


**Fig. 3.** FL ratio ( $I_0$ - $I/I_0$ ) of DNSCH ( $2.5 \times 10^{-6}$  M) upon the addition of 15 M equiv ( $3.75 \times 10^{-5}$  M) of metal guests in CH<sub>3</sub>CN-H<sub>2</sub>O (50:50, v/v);  $\lambda_{ex} = 342$  nm.

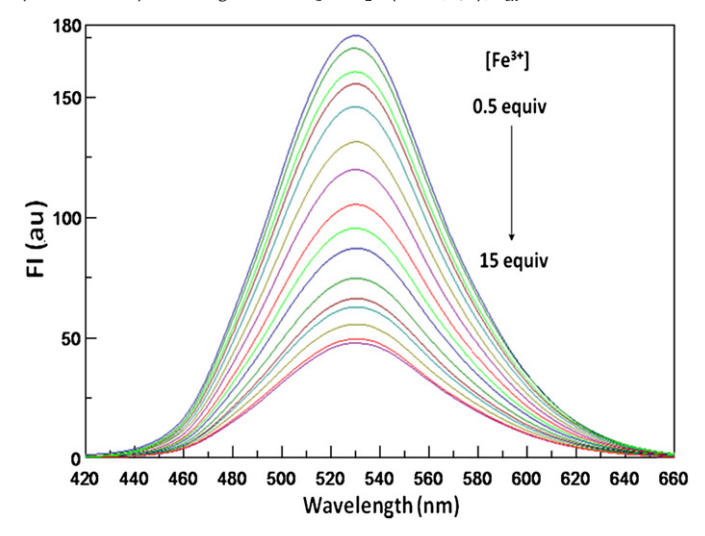
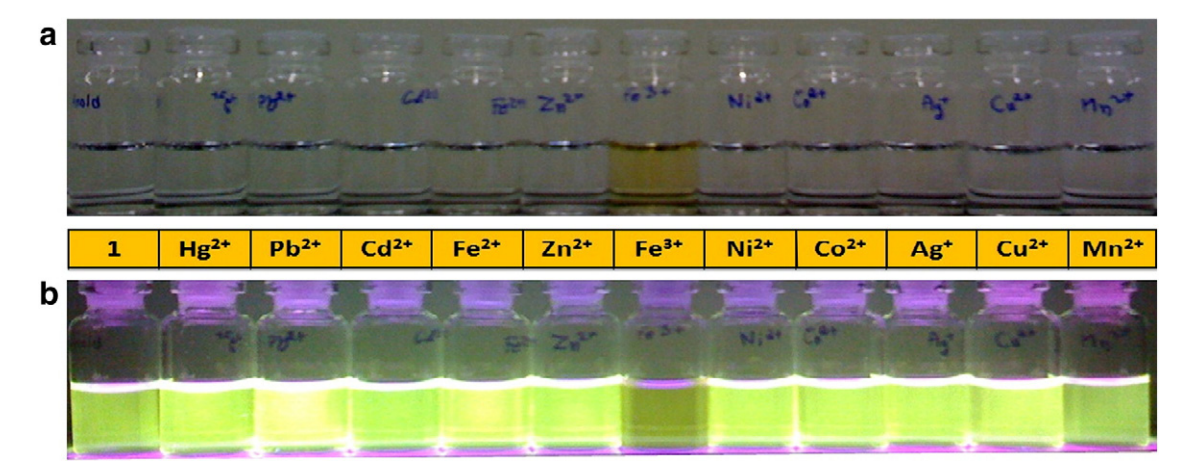


**Fig. 4.** FL spectra of DNSCH  $(2.5\times10^{-6}$  M) titrated with (a) 0.5–15 M equiv of Fe<sup>3+</sup>, in CH<sub>3</sub>CN-H<sub>2</sub>O (50:50, v/v);  $\lambda_{ex}$  = 342 nm.



 $\textbf{Fig. 2.} \ (a) \ lmages \ and \ (b) \ FL \ images \ of \ DNSCH \ (2.5\times10^{-6} \ M) \ in \ the \ presence \ of \ various \ metal \ ions \ (3.75\times10^{-5} \ M) \ in \ CH_3CN-H_2O \ (50:50, \ v/v); \ \lambda_{ex} = 342 \ nm.$ 

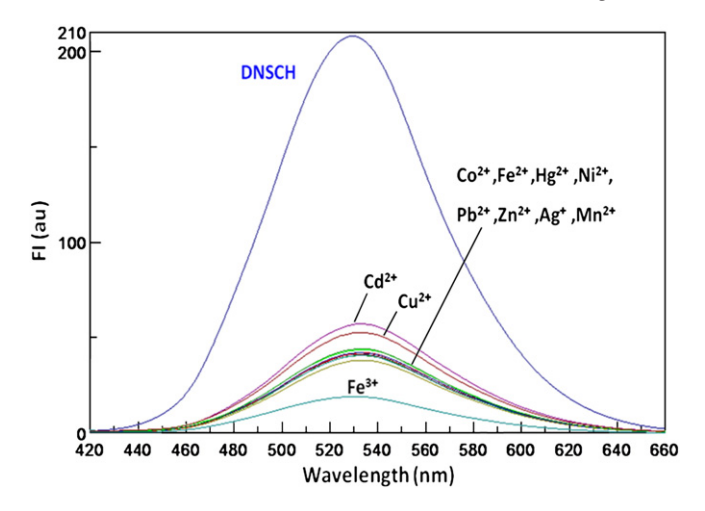


**Fig. 5.** FL responses of DNSCH  $(2.5\times10^{-6} \text{ M})$  containing Fe<sup>3+</sup> (15 M equiv) and other co-existing metal ions (15 M equiv) in CH<sub>3</sub>CN-H<sub>2</sub>O (50:50, v/v);  $\lambda_{\text{ex}} = 342 \text{ nm}$ .

In order to determine the degree of FL quenching of DNSCH by Fe $^{3+}$ , the FL ratio was employed for this investigation. It was clearly shown in Fig. 3 that the degree of FL quenching for DNSCH was mostly pronounced in the presence of Fe $^{3+}$ . There were also slight changes in FL of DNSCH in the presence of Cd $^{2+}$ , Co $^{2+}$ , Mn $^{2+}$ , Pb $^{2+}$  and Zn $^{2+}$  ions. Comparing to other metal ions, DNSCH is highly selective in its response to Fe $^{3+}$ .

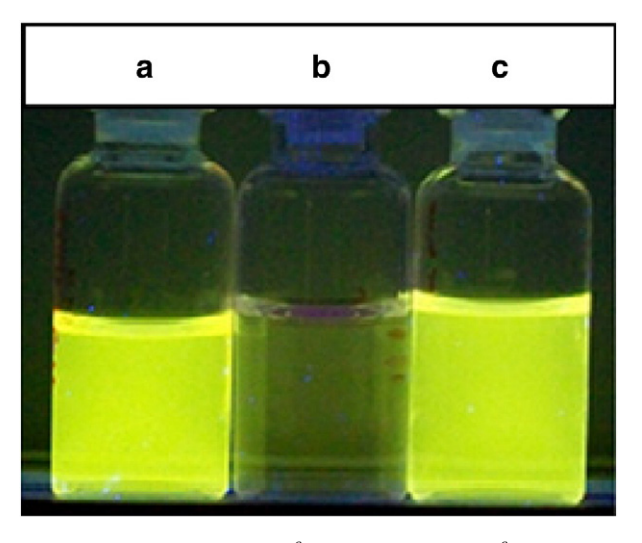


**Fig. 7.** FL images of (a) DNSCH  $(2.5\times10^{-6}~\text{M})$ . (b) DNSCH  $(2.5\times10^{-6}~\text{M})$  in the presence of 15 M equiv of Fe<sup>3+</sup>  $(3.75\times10^{-5}~\text{M})$ . (c) DNSCH  $(2.5\times10^{-6}~\text{M})$  in the presence of 15 M equiv Fe<sup>3+</sup> with the addition of excess EDTA.

To determine the selectivity range of DNSCH towards  $Fe^{3+}$ , the titration experiment was conducted. The FL quenching of DNSCH was investigated in the presence of various concentrations of  $Fe^{3+}$ . Fig. 4 shows that with increasing concentrations of  $Fe^{3+}$ , the FL emission intensity of DNSCH at  $\lambda_{max}$  525 nm was gradually decreased. The FL

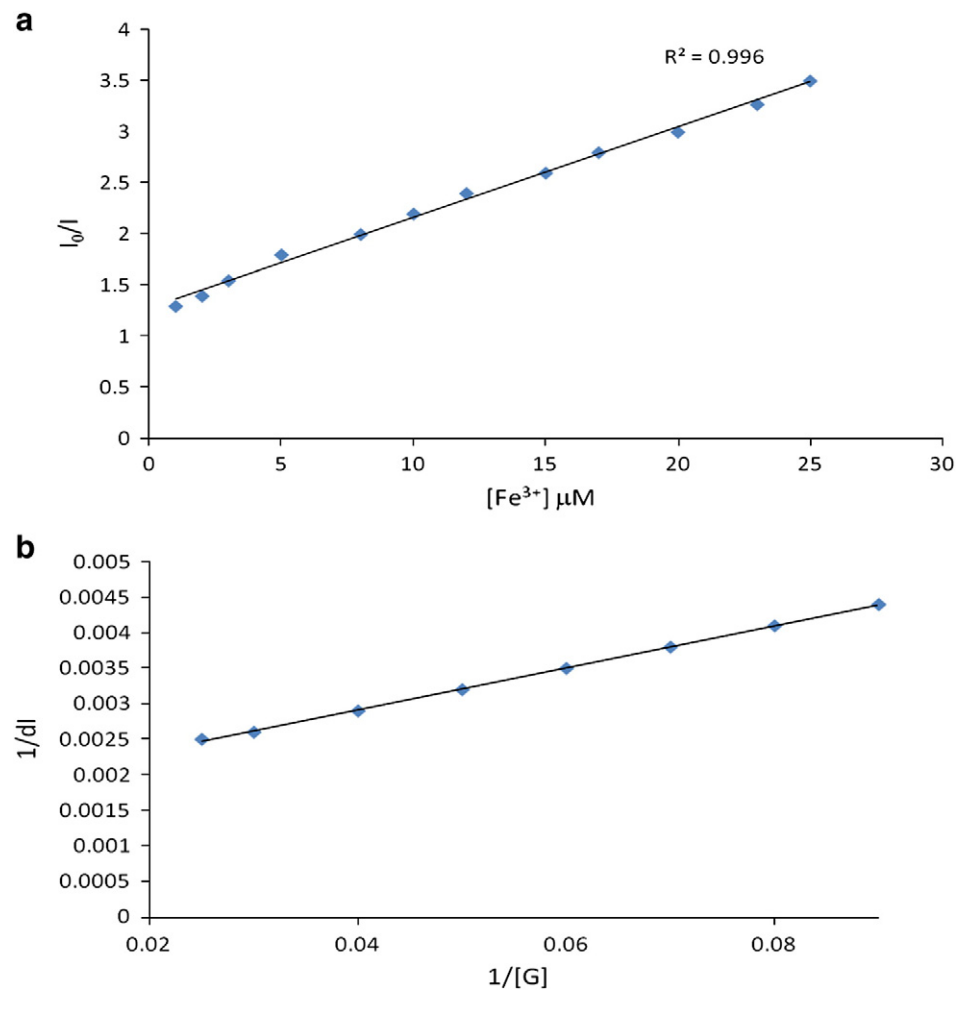


**Fig. 6.** (a) Stern–Volmer plot for DNSCH in the presence of various Fe<sup>3+</sup> concentrations indicating 1:1 stoichiometry. (b) Benesi–Hilderbrand to determine the binding constant between DNSCH and Fe<sup>3+</sup>.

S. Smanmoo et al. / Inorganic Chemistry Communications 14 (2011) 351-354

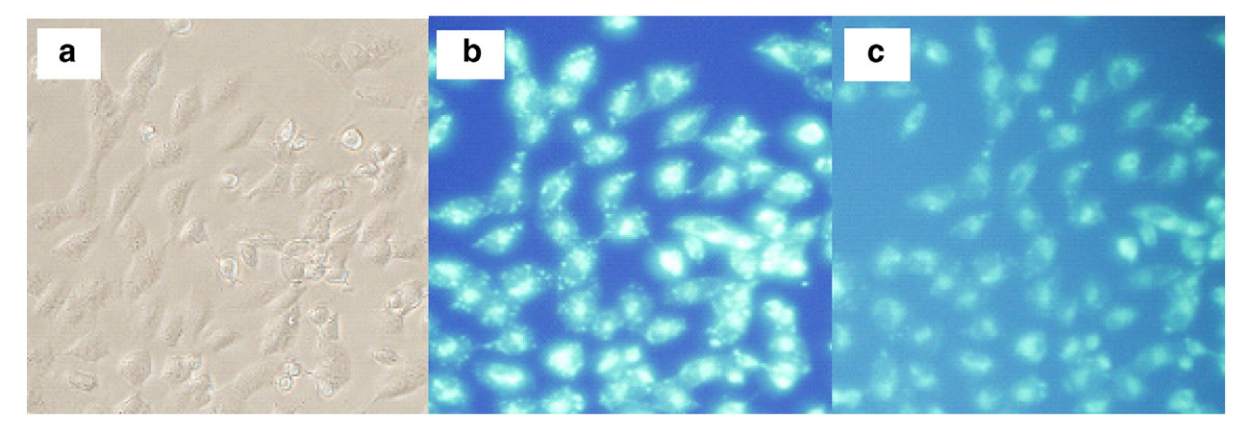


Fig. 8. Living-cell imaging of intracellular Fe<sup>3+</sup> by FL microscopy: (a) Bright field transmission image of Vero cells incubated with 50 μM of DNSCH. (b) FL image of Vero cells supplemented with 50 µM of DNSCH in the growth media for 15 min at 25 °C. (c) Vero cells incubated with 50 µM of DNSCH in the growth media for 15 min at 25 °C, washed three times, and then further incubated with  $100\,\mu M$  FeCl<sub>3</sub> for 5 min at 25 °C.

quenching of DNSCH was mostly pronounced after the addition of Fe<sup>3+</sup> at 15 M equiv  $(3.75 \times 10^{-5} \,\mathrm{M})$ . The addition of Fe<sup>3+</sup> at 15 M equiv significantly quenched the FL of DNSCH.

FL responses of DNSCH towards Fe<sup>3+</sup> were investigated in the presence of co-existing metal ions, e.g., Co<sup>2+</sup>, Fe<sup>2+</sup>, Hg<sup>2+</sup>, Ni<sup>2+</sup>, Pb<sup>2+</sup>, Zn<sup>2+</sup>, Ag<sup>+</sup>, Mn<sup>2+</sup>, Cd<sup>2+</sup> and Cu<sup>2+</sup>. It was shown in Fig. 5 that the presence of other metals did not interfere the FL quenching of DNSCH by Fe<sup>3+</sup> and the FL changes caused by the addition of Fe<sup>3+</sup> were not affected by the co-existing metal ions.

In order to determine the binding ratio between DNSCH and Fe<sup>3+</sup>, the Stern-Volmer plot was used and found the good fit in the concentration range between 1 and 25 µM which indicated the binding ratio between DNSCH and Fe<sup>3+</sup> at 1:1 stoichiometry [Fig. 6(a)]. On the basis of this binding ratio, the binding constant for DNSCH and Fe<sup>3+</sup> was then calculated using the Benesi-Hilderbrand equation and found to be  $1.5\pm0.4\times10^{-4}\,\text{M}^{-1}$  [Fig. 6(b)] [20]. The reversible binding mode of DNSCH towards Fe<sup>3+</sup> was investigated. It was clear that DNSCH was a reversible FL chemosensor (Fig. 7). In the presence of 15 M equiv Fe<sup>3-</sup>  $(3.75 \times 10^{-5} \text{ M})$ , DNSCH  $(2.5 \times 10^{-6} \text{ M})$  exhibited strong FL quenching. However, the FL of DNSCH was recovered after the addition of excess EDTA. This demonstrated the potential application of DNSCH as a reversible FL chemosensor.

The mechanism for FL quenching of DNSCH by Fe<sup>3+</sup> is proposed from ligand metal charge transfer (LMCT) in which the transition of the charge transfer is initiated by the binding of Fe<sup>3+</sup> to the ligand (DNSCH). The chelation between DNSCH and Fe<sup>3+</sup> is facilitated by the extra coordination from i) C = N group which is known for the strong binding affinity to transition and post-transition metals [16,17] and ii) the 2-hydroxyl group. These functional groups are in the positions where Fe<sup>3+</sup> is held close enough to the dansyl fluorophore. The electronic charge of DNSCH transfers to Fe<sup>3+</sup> (d-orbital) results in the distribution of charge at the excited state. This finally causes the FL quenching of DNSCH.

For the practical application of DNSCH, it was employed as a selective intracellular chemosensor for Fe<sup>3+</sup> (Fig. 8). DNSCH's ability was assessed as an intracellular FL chemosensor for Fe3+ by FL microscopy. As seen from the bright field image, Vero cells incubated with 50 µM of DNSCH for 15 min at 25 °C show cell viability [Fig. 8(a)] with strong intracellular background FL [Fig. 8 (b)]. After, Vero cells which pre-incubated with DNSCH were supplemented with 100  $\mu M$  of  $Fe^{3+}$  in the growth medium for 5 min at 25 °C, and intracellular background FL was significantly reduced in its FL intensity [Fig. 8(c)]. Apart from its high selectivity of DNSCH towards Fe3+ in CH3CN-H2O, DNSCH was as an intracellular chemosensor for Fe<sup>3+</sup>. According to this fact, DNSCH was a membrane-permeable FL chemosensor exhibiting selective FL quenching towards Fe<sup>3+</sup>.

In summary, a novel FL chemosensor based on dansyl cadaverine, DNSCH, was synthesized and evaluated for its sensing ability towards metal ions. DNSCH exhibited high selectivity towards Fe<sup>3+</sup> among other screened metal ions with good discrimination between different iron oxidation state ( $Fe^{2+}$  and  $Fe^{3+}$ ). The 2-hydroxyl group in DNSCH facilitates the binding of Fe<sup>3+</sup> prior to LMCT mechanism, which was initiated to induce the FL quenching. DNSCH exhibited a selective recognizing mode with high selectivity towards Fe<sup>3+</sup>. DNSCH shows no interference from other metal ions. DNSCH was evaluated as a cell-permeable chemosensor for intracellular detection of Fe<sup>3+</sup>.

#### Acknowledgments

The Thailand Research Fund/Commission on Higher Education's research grant to S.S. (DIG5180025) and P.T. (RTA5180003) and the Development and Promotion of Science and Technology Talents Project's scholarship to W.N. are gratefully acknowledged. We are also grateful to the partial support from National Center for Genetic Engineering and Biotechnology (BIOTEC).

#### Appendix A. Supplementary Material

Supplementary data to this article can be found online at doi:10.1016/j.inoche.2010.11.025.

#### References

- [1] A.P. de Silva, H.Q.N. Gunaratne, T. Gunnlaugsson, A.J.M. Huxley, C.P. McCoy, J.T. Rademacher, T.E. Rice, Chem. Rev. 97 (1997) 1515-1566.
- F.-Y. Wu, S.W. Bae, J.-I. Hong, Tetrahedron Lett. 47 (2006) 8851–8854. F.-Y. Wu, Y.-Q. Zhao, Z.-J. Ji, Y.-M. Wu, J. Fluoresc. 17 (2007) 460–465. L.J. Ma, Y.-F. Liu, Y. Wu, Chem. Commun. (2006) 2702–2704.
- L. Ma, H. Li, Y. Wu, Sens. Actuators B Chem. 143 (2009) 25-29.
- H. Li, J. Xu, H. Yan, Sens. Actuators B Chem. 139 (2009) 483-487.
- M.H. Keefe, K.H. Benkstein, J.T. Hupp, Coord. Chem. Rev. 205 (2000) 201–228.
- $F.\,Wang,\,Y.\,Xu,\,B.X.\,Ye,\,M.P.\,Song,\,Y.\,J.\,Wu,\,Inorg.\,Chem.\,Commun.\,9\,(2006)\,797-801.$
- L.A. Baumes, M.B. Sogo, P. Montes-Navajas, A. Corma, H. Garcia, Tetrahedron Lett. 50 (2009) 7001-7004
- [10] D.Y. Lee, N. Singh, D.O. Jang, Tetrahedron Lett. 51 (2010) 1103-1106.
- J.-M. Liu, Q.-Y. Zheng, J.-L. Yang, C.-F. Chen, Z.-T. Huang, Tetrahedron Lett. 43 (2002) 9209-9212.
- S.-K. Lee, Y.-S. Noh, K.-I. Son, D.-Y. Noh, Inorg. Chem. Commun. 13 (2010) 1343-1346.
- C.R. Lohani, K.-H. Lee, Sens. Actuators B Chem. 143 (2010) 649-654.
- O.-Y. Chen, C.-F. Chen, Tetrahedron Lett. 46 (2005) 165-168.
- A. Azam, H.M. Chawla, S. Pandey, Tetrahedron Lett. 51 (2010) 4710-4711.
- V.K. Bhardwaj, A.P.S. Pannu, N. Singh, M.S. Hundal, G. Hundal, Tetrahedron 64 (2008) 5384-5391.
- S.I. Pascu, G. Balazs, J.C. Green, M.L.H. Green, I.C. Vei, J.E. Warren, C. Windsor, Inorg. Chim. Acta 363 (2010) 1157-1172
- P. Wu, Y. Li, X.P. Yan, Anal. Chem. 81 (2009) 6252-6257.
- [19] H. Sulowska, W. Wiczk, J. Modzianowski, M. Przyborowska, T. Ossowski, J. Photochem. Photobiol. 150 (2002) 249-255.
- [20] H.A. Benesi, J.H. Hilderbrand, J. Am. Chem. Soc. 71 (1949) 2703–2707.

#### Journal of Applied Polymer Science Journal

Copy of e-mail Notification

Journal of Applied Polymer Science Published by John Wiley & Sons, Inc.

Dear Author.

YOUR PAGE PROOFS ARE AVAILABLE IN PDF FORMAT; please refer to this URL address:

http://115.111.50.156/jw/retrieval.aspx?pwd=acbf6c41ee86

Login: your e-mail address Password: acbf6c41ee86

The site contains 1 file. You will need to have Adobe Acrobat Reader software to read these files. This is free software and is available for user downloading at http://www.adobe.com/products/acrobat/readstep.html.

Alternatively, if you would prefer to receive a paper proof by regular mail, please contact Prashant/Sankar/Balaji (e-mail: wileysupport@kwglobal.com, phone: +91 (44) 4205-8888 (ext.217)). Be sure to include your article number.

This file contains:

Author Instructions Checklist

Adobe Acrobat Users - NOTES tool sheet

Reprint Order Information

A copy of your page proofs for your article

Please read the page proofs carefully and:

- 1) indicate changes or corrections in the margin of the page proofs;
- 2) answer all queries (footnotes AQ1, AQ2, etc.) on the last page of the PDF proof;
- 3) proofread any tables and equations carefully;
- 4) check that any Greek symbols, especially "mu", have translated correctly.

Special Notes:

Please return corrections to Wiley via REPLY E-MAIL as soon as possible.

Your article will be published online via our EarlyView service after correction receipt. Your prompt attention to and return of page proofs is crucial to faster publication of your work. Thank you for your cooperation.

NEW! Return corrections via reply e-mail to:

APP Journal Team
APPproofuser@wiley.com

#### Journal of Applied Polymer Science Journal

Copy of e-mail Notification

If you experience technical problems, please contact Prashant/Sankar/Balaji (e-mail: wileysupport@kwglobal.com, phone: +91 (44) 4205-8888 (ext.217)).

PLEASE NOTE: This e-proof is to be used ONLY for the purpose of returning corrections to the publisher. The APPproofuser@wiley.com address is to be used ONLY for the submission of proof corrections, the reprint order form, and the copyright transfer agreement (if you have not already signed one). PLEASE ALWAYS INCLUDE YOUR FIVE-DIGIT ARTICLE NO. (35088) WITH ALL CORRESPONDENCE.

Thank you.

Sincerely,

**APP Journal Team** 

E-mail: APPproofuser@wiley.com

#### Softproofing for advanced Adobe Acrobat Users - NOTES tool

NOTE: ACROBAT READER FROM THE INTERNET DOES NOT CONTAIN THE NOTES TOOL USED IN THIS PROCEDURE.

Acrobat annotation tools can be very useful for indicating changes to the PDF proof of your article. By using Acrobat annotation tools, a full digital pathway can be maintained for your page proofs.

The NOTES annotation tool can be used with either Adobe Acrobat 6.0 or Adobe Acrobat 7.0. Other annotation tools are also available in Acrobat 6.0, but this instruction sheet will concentrate on how to use the NOTES tool. Acrobat Reader, the free Internet download software from Adobe, DOES NOT contain the NOTES tool. In order to softproof using the NOTES tool you must have the full software suite Adobe Acrobat Exchange 6.0 or Adobe Acrobat 7.0 installed on your computer.

#### Steps for Softproofing using Adobe Acrobat NOTES tool:

- 1. Open the PDF page proof of your article using either Adobe Acrobat Exchange 6.0 or Adobe Acrobat 7.0. Proof your article on-screen or print a copy for markup of changes.
- 2. Go to Edit/Preferences/Commenting (in Acrobat 6.0) or Edit/Preferences/Commenting (in Acrobat 7.0) check "Always use login name for author name" option. Also, set the font size at 9 or 10 point.
- 3. When you have decided on the corrections to your article, select the NOTES tool from the Acrobat toolbox (Acrobat 6.0) and click to display note text to be changed, or Comments/Add Note (in Acrobat 7.0).
- 4. Enter your corrections into the NOTES text box window. Be sure to clearly indicate where the correction is to be placed and what text it will effect. If necessary to avoid confusion, you can use your TEXT SELECTION tool to copy the text to be corrected and paste it into the NOTES text box window. At this point, you can type the corrections directly into the NOTES text box window. **DO NOT correct the text by typing directly on the PDF page.**
- 5. Go through your entire article using the NOTES tool as described in Step 4.
- 6. When you have completed the corrections to your article, go to Document/Export Comments (in Acrobat 6.0) or Comments/Export Comments (in Acrobat 7.0). Save your NOTES file to a place on your harddrive where you can easily locate it. Name your NOTES file with the article number assigned to your article in the original softproofing e-mail message.
- 7. When closing your article PDF be sure NOT to save changes to original file.
- 8. To make changes to a NOTES file you have exported, simply re-open the original PDF proof file, go to Document/Import Comments and import the NOTES file you saved. Make changes and reexport NOTES file keeping the same file name.
- 9. When complete, attach your NOTES file to a reply e-mail message. Be sure to include your name, the date, and the title of the journal your article will be printed in.



## Additional reprint purchases

Should you wish to purchase additional copies of your article, please click on the link and follow the instructions provided:

https://caesar.sheridan.com/reprints/redir.php?pub=10089&acro=APP

Corresponding authors are invited to inform their co-authors of the reprint options available.

Please note that regardless of the form in which they are acquired, reprints should not be resold, nor further disseminated in electronic form, nor deployed in part or in whole in any marketing, promotional or educational contexts without authorization from Wiley. Permissions requests should be directed to mail to: <a href="mailto:permissionsus@wiley.com">permissionsus@wiley.com</a>

For information about 'Pay-Per-View and Article Select' click on the following link: wileyonlinelibrary.com/aboutus/ppy-articleselect.html

# Polylactic Acid/Ethylene Glycol Triblock Copolymers as Novel Crosslinkers for Epoxidized Natural Rubber

T.-H. Nguyen, P. Tangboriboonrat, N. Rattanasom, A. Petchsuk, M. Opaprakasit, C. Thammawong, P. Opaprakasit

<sup>1</sup>School of Bio-Chemical Engineering and Technology, Sirindhorn International Institute of Technology (SIIT), Thammasat University, Pathum Thani 12121, Thailand

Thammasat University, Pathum Thani 12121, Thailand <sup>2</sup>Department of Chemistry, Faculty of Science, Mahidol University, Phyathai, Bangkok 10400, Thailand

<sup>3</sup>Institute of Molecular Biosciences, Mahidol University, Salaya, Nakhon Pathom 73170, Thailand

AQ2 <sup>4</sup>National Metal and Materials Technology Center (MTEC), Pathum Thani 12120, Thailand <sup>5</sup>Department of Materials Science, Faculty of Science, Center for Petroleum, Petrochemicals and Advanced Materials, Chulalongkorn University, Bangkok 10330, Thailand

Received 24 September 2010; accepted 13 June 2011 DOI 10.1002/app.35088

Published online 00 Month 2011 in Wiley Online Library (wileyonlinelibrary.com).

**ABSTRACT:** Polylactic acid/ethylene glycol triblock copolymer (LLA<sub>46</sub>EG<sub>46</sub>LLA<sub>46</sub>) was prepared and used in a crosslink process of epoxidized natural rubber (ENR) by employing a ring-opening reaction using Sn(Oct)<sub>2</sub> as a catalyst. The OH-capped copolymer acts as a macromolecular crosslinking agent in the formation of ENR networks, leading to drastic enhancement in tensile properties. Crosslink efficiency and chemical structures of the cured materials are examined by solvent fractionation, swelling experiments, XRD, <sup>1</sup>H-NMR, and ATR-

FTIR spectroscopy. The efficiency of the curing process is dependent on the ENR/copolymer feed ratios. The degree of property improvement and gas permeability/selectivity behaviors of the cured materials are strongly dependent on the copolymer content and the efficiency of the curing process. © 2011 Wiley Periodicals, Inc. J Appl Polym Sci 000: 000–000, 2011

**Key words:** rubber; crosslinking; gas permeation; biodegradable; block copolymers

#### **INTRODUCTION**

Natural rubber (NR) is known as a "green," sustainable, renewable, and biodegradable material. However, NR latex film cannot be used without vulcanization because it is not very strong and lacks elasticity. Vulcanization is required to introduce chemical network junctures between rubber or polyisoprene chains to form crosslinked networks, which enhances their mechanical properties suitable for applications. Vulcanization is mainly classified as sulfur and nonsulfur processes. The crosslink junctures from sulfur vulcanization are derived from either single sulfur atoms or short-chain sulfur compounds with accelerators such as 2-benzothiazole disulfide. In contrast, organic peroxides for example dicumyl peroxide are commonly used in non-

sulfur vulcanization. In addition, NR latex can be vulcanized by employing chemical-free processes, such as using electron beams,  $^9$   $\gamma$  rays,  $^{10,11}$  UV radiation, and ultrasonic waves.  $^{12}$ 

Vulcanization by crosslinking of specially functionalized rubbers has attracted great interest in the research community. Epoxide groups are introduced and used as crosslink sites instead of allylic groups in sulfur vulcanization. <sup>12–14</sup> The double bonds of NR are well known to react with peracids to produce epoxide groups in the conversion of NR to epoxidized NR (ENR). This process leads to an enhancement in certain properties, such as higher hysteresis and oil resistance, and lower air permeability compared with its native NR counterpart. 13,15 Moreover, epoxide groups can readily react with many nucleophilic reagents for further modification of the material properties, such as amines, 14,16,17 phosphorus, 18 and carboxylic acids. 19 The interest of reacting hydroxyl groups with ENR has been initiated and reported by Derouet et al., where alcohols were grafted onto ENR backbone through ring-opening reaction of its epoxide. 20,21

Polylactic acid (PLA) is a biodegradable/biocompatible polymer that is particularly attractive for use in various applications, especially in biomedical fields.<sup>22</sup> However, its low hydrophilicity limits its use in certain applications. Therefore, poly(ethylene

Correspondence to: P. Opaprakasit (pakorn@siit.tu.ac.th). Contract grant sponsor: The Thailand Research Fund/Thailand Office of Higher Education Commission; contract grant number: RTA5180003.

Contract grant sponsors: National Research University Project of Thailand Office of Higher Education Commission, Thailand Toray Science Foundation, Siam Cement Foundation and SIIT, Thammasat University.

Journal of Applied Polymer Science, Vol. 000, 000–000 (2011)  $\ @$  2011 Wiley Periodicals, Inc.

2 NGUYEN ET AL.

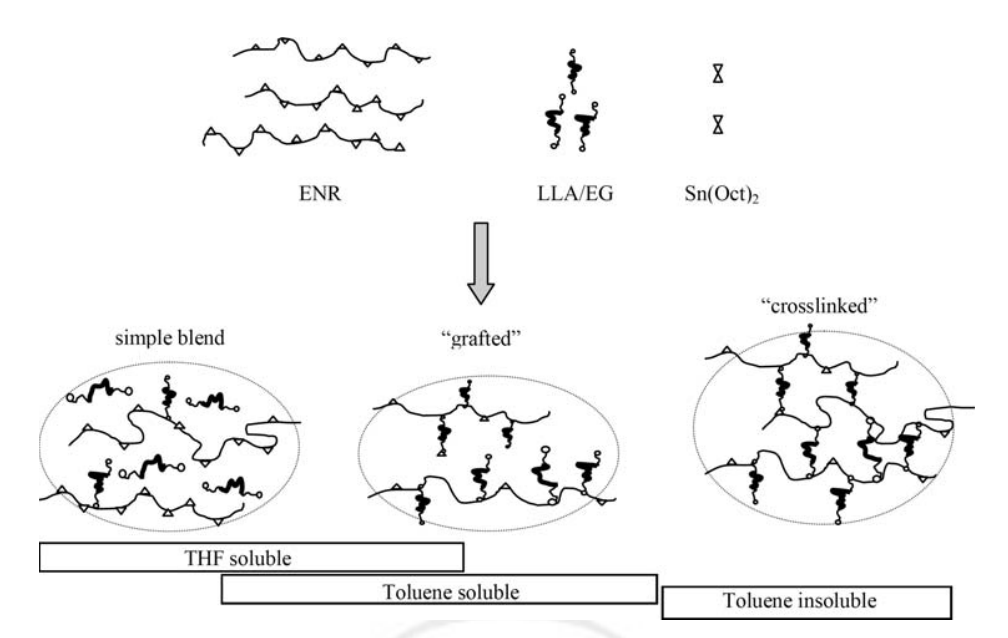


Figure 1 Proposed curing reaction of ENR by OH-capped LLA/EG/LLA block copolymers, and the possible structures of the "cured" products and their solvent solubility.

glycol) (PEG), a hydrophilic polymer with outstanding properties, i.e., nontoxicity and biocompatible characteristics, is introduced. Copolymerization of PLA and PEG at various compositions offers an opportunity to combine the advantages of these polymers to obtain biocompatible/degradable materials with tailored hydrophilicity.<sup>23–25</sup> Incorporation of NR with PLA has been conducted to improve its mechanical properties, especially the impact strength. It was reported that miscibility enhancement of ENR/PLA blend was achieved by a reactive mixing process at high temperature. The reaction of epoxides of ENR and ester groups of PLA was proposed as the origin of this enhancement.<sup>26,27</sup>

In our previous work,<sup>28</sup> OH-capped triblock copolymers of L-lactide (LLA) and ethylene glycol (EG) were synthesized by ring-opening polymerization of LLA using PEG as a macroinitiator. The LLA/EG/LLA copolymers with various block lengths and hence different properties were prepared by varying LLA/PEG molar ratios. In this study, the block copolymer is used as macromolecular crosslinker for ENR by utilizing the reaction of its two hydroxyl groups at the chain-ends with epoxides of ENR.<sup>20,21</sup> Properties of the resulting cured ENR products are then characterized. The materials are not only biocompatible and biodegradable, but also exhibit good mechanical properties comparable to conventionally cured rubber materials. Gas permeability behaviors of the cured ENR are also characterized for potential use in high-value and specific applications: membranes or medical applications such as breathable gloves or patches. Most importantly, the properties of these materials can be further modified by varying block lengths of the copolymer, epoxide content of ENR, and the copolymer/ENR feed ratios for specific applications.

#### **EXPERIMENTAL**

#### Materials

OH-capped LLA<sub>46</sub>EG<sub>46</sub>LLA<sub>46</sub> triblock copolymer was synthesized by the method reported in our previous work.<sup>28</sup> ENR with 20% epoxidation (ENR20) was synthesized from commercial high ammonia (HA)-preserved NR latex concentrate (Rayong Bangkok Rubber, Thailand) based on the methodology reported by Saendee et al.<sup>29</sup> Sn(Oct)<sub>2</sub> (Wako) and dried tetrahydrofuran (THF) was respectively, used as a catalyst and solvent.

## Crosslinking of ENR by LLA/EG copolymer

The crosslink reaction was conducted by mixing ENR20 and the OH-capped LLA $_{46}$ EG $_{46}$ LLA $_{46}$  copolymer at three weight compositions (4/1, 2/1, 1/1) in dried THF (20% w/v) at 50°C. The samples are referred to as R41, R21, and R11, respectively. The mixture solution was first dried under vacuum for 1 h before purging with nitrogen gas. Sn(Oct) $_2$  catalyst (1 wt % of copolymer) was then added. The crosslink reaction was performed in a round-bottom flask equipped with magnetic stirrer at 70°C for 24 h.

The proposed chemical structures of the cured ENR products obtained from the reaction with the OH-capped copolymer are illustrated in Figure 1. When both OH end groups of the copolymer

F1

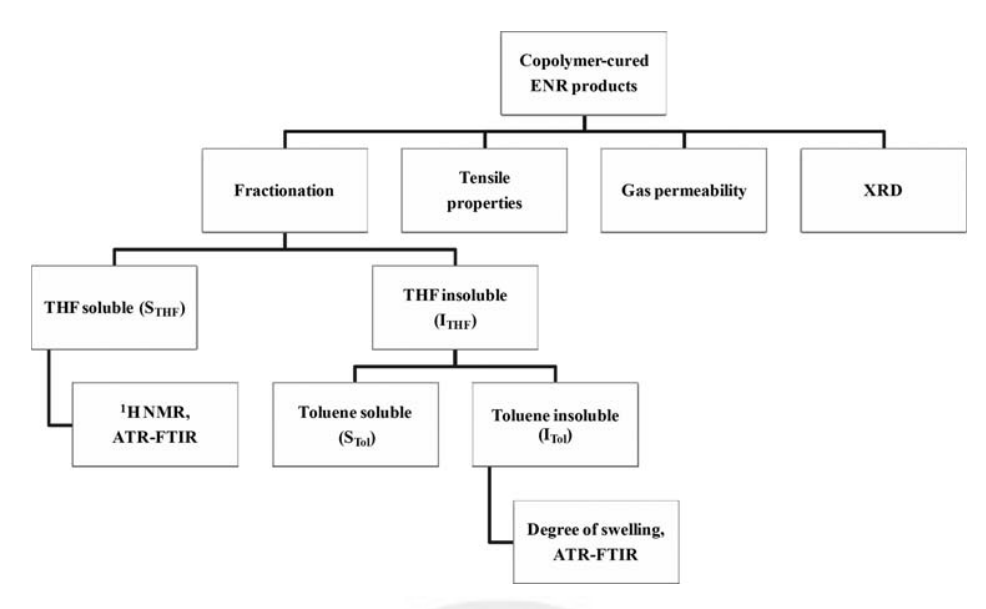


Figure 2 Overview of characterizations of the copolymer-cured ENR products.

undergo ring-opening reaction with epoxides of ENR, crosslink junctions are generated. In contrast, grafting of copolymer onto ENR backbone is achieved when only one hydroxyl per copolymer chain reacts. As ENR20 has 20% epoxide content, grafted ENR products with varied degree of grafting are generated. Additionally, unreacted copolymer chains may be present in the ENR matrix as a blended mixture, due to an excess amount of copolymer, when ENR20/copolymer ratios are varied. These possibilities will be referred to as "crosslinked," "grafted," and "free" or simple blend fractions. These fractions of products exhibit different solubility behaviors (discussed later), as summarized in Figure 1.

#### Characterizations

The cured ENR product, suspended in THF solvent after the crosslink reaction, was cast on a Teflon plate at room temperature. After completion of solvent evaporation, film samples (~ 0.1 mm thick) were obtained. The samples were then characterized F2 as summarized in Figure 2. First, efficiency of the curing process in terms of weight fraction of "crosslinked," "grafted," and "free" copolymers in ENR matrix, was examined by sequential solvent fractionation, employing THF and toluene solvents. Given that ENR and the copolymer are completely dissolved in THF at 50°C, Soxhlet extraction by THF was first employed for 24 h to determine the weight content of remaining uncured ENR and "free" or unreacted copolymers in the soluble fraction (denoted by  $S_{\text{THF}}$ ), which was recovered by complete evaporation of the solvent. The THF-insoluble fraction ( $I_{THF}$ ) was then further extracted by toluene at room temperature for ssven days. The soluble and

insoluble fractions (denoted by  $S_{\rm Tol}$  and  $I_{\rm Tol}$ ), corresponding to "grafted" and fully "crosslinked" ENR domains, respectively, were recovered. The remaining weight of each fraction was then recorded and the weight percentage was calculated based on mass of the original sample. Chemical structures and chain compositions of each fraction were characterized by  $^{1}$ H-NMR spectroscopy on a Bruker DRX400 using CDCl<sub>3</sub> as a solvent. ATR-FTIR spectra of each fraction were recorded on a ThermoNicolet 6700 model spectrometer. The spectra were recorded at 2 cm<sup>-1</sup> resolution with 32 scans. ATR accessory equipped with ZnSe with a face angle of  $45^{\circ}$  was employed.

The crosslink density of the toluene insoluble ( $I_{\rm Tol}$ ) samples was examined by using the solvent swelling method. A piece of sample was accurately weighed and then immersed in toluene (40 mL) at room temperature in a dark cabinet. At equilibrium swelling time, where a constant solvent weight uptake was reached (about seven days), the test piece was removed, wiped with filter paper, and its weight was recorded. The swelling percentage was calculated, as follows:

% swelling = 
$$\frac{W_{\text{eq}} - W_o}{W_o} \times 100$$
 (1)

where  $W_o$  = original weight of dried sample (g)

 $W_{\rm eq}=$  weight of swollen sample at equilibrium swelling time (g)

Tensile tests were carried out using dumbbell specimens cut from the cured rubber films (prepared from solution cast technique) with a thickness of  $\sim 0.1$  mm by using the Type II die, in accordance with ISO 37. At the onset of testing, two extensometer clamps were set and attached to the sample 20-mm apart within the gauge region. The cross-head

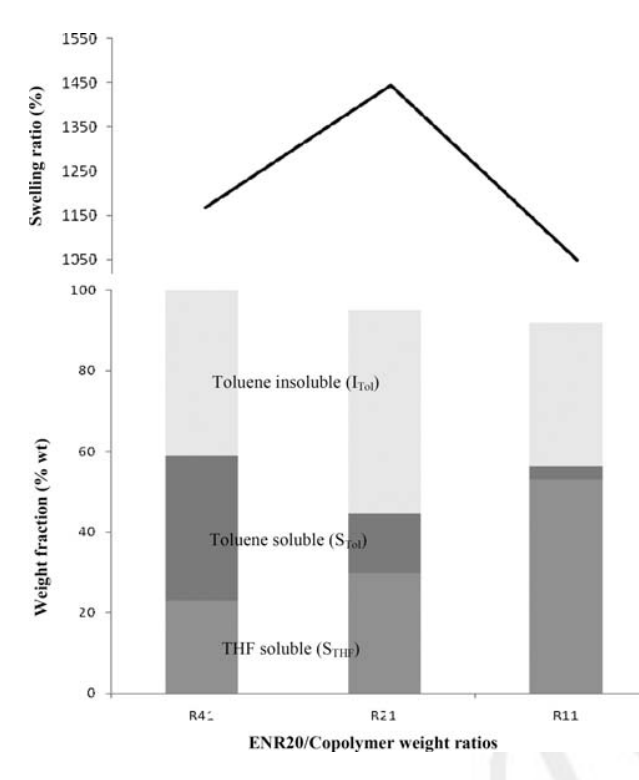


**Figure 3** Solvent extraction results and swelling behaviors of cured products as a function of ENR20/copolymer feed content.

speed and full scale force used were 100 mm/min and 1 kN, respectively. The specimens were pulled in tension until rupture. The values of 100 and 300% modulus, tensile strength, and elongation at break were recorded, and the average value from three to four specimens was reported. Crystalline characteristics of the cured samples were examined by XRD on a JEOL JDX-3530 Diffractometer, using CuK $_{\alpha 1}$  radiation. The sample films were scanned from  $2\theta$  of 5– $40^\circ$  with 0.02 step size.

Permeability tests were also conducted on cast film samples with thickness of  $\sim 0.1$  mm. Water vapor permeability was measured on an Illinois instrument (Model 7200), using ASTM F1249-01 at 38°C, 90% relative humidity and 1 atm pressure. Oxygen permeability was recorded on a Mocon instrument (Ox-Tran Model 2/21), following ASTM D3985 at 23°C, 0% relative humidity. Carbon dioxide permeability was measured on a Mocon instrument (Permatran-C Model 4/41) at 23°C, 0% relative humidity.

#### **RESULTS AND DISCUSSION**

## Solvent fractionation

Results on weight percentage of products obtained from sequential solvent fractionation are summar-F3 ized in Figure 3. As ENR20, LLA/EG copolymer, and a simple mixture of the two materials are completely dissolved in THF at  $50^{\circ}$ C, the content of  $S_{\rm THF}$ , therefore, indicates the amount of the "free" or simple blend fraction. It is noted that slightly grafted ENR chains (copolymer-grafted ENR with low degree grafting) are also extractable by THF.  $^{30,31}$  This is confirmed by NMR spectrum of the soluble material, where peaks due to copolymer dominate, with weak signals associated with ENR, as shown in Figure 4.

The content of the insoluble extracted sample ( $I_{\rm THF}$ ) represents the amount of newly formed "crosslinked" structure and "grafted" ENR domains, which are not soluble in THF solvent. These two fractions are then further separated by toluene extraction. The "grafted" portions are soluble in toluene, while the "crosslinked" network remains insoluble. Unlike its slightly grafted counterpart, solubility behavior of the "grafted" ENR in toluene (but not THF) may be explained in terms of a decrease in epoxide content of ENR as a result of conversion to grafting points, and a large increase in the molecular weight of the "grafted" products. These two effects lead to a decrease in polarity and hence lower solubility in THF.

In the sample with low copolymer content in feed (R41), "crosslinked" and "grafted" fractions of ~ 40 and 36 wt % are observed. Unreacted "simple blend" of  $\sim$  20 wt % is obtained. These indicate that the majority of hydroxyl groups in the copolymer chains effectively react with ENR20. When the copolymer content in feed is increased, the weight content of the "crosslinked" fraction is significantly comparable in all samples at  $\sim 40$  wt %. In contrast, those of the "grafted" and the "simple blend" portions vary with the copolymer content. The "simple blend" ( $S_{THF}$ ) content increases with an increase in the copolymer content in feed, while that of the "grafted" ( $S_{Tol}$ ) fraction shows the opposite trend. Therefore, the feed ratio of ENR20/copolymer can be optimized to control the reaction efficiency. It is noted that the ENR: copolymer weight ratios of 4: 1, 2:1, and 1:1 are equivalent to epoxide: OH molar ratios of 50: 1, 25: 1, and 12: 1, respectively. The variation in the feed ratio leads to changes in two factors, i.e., the probability of copolymer's hydroxyls reacting with ENR (grafting efficiency), and the crosslinking efficiency (two hydroxyls from the same copolymer chain react with ENR to form crosslink junctions).

The increase in hydroxyls content leads to an increase in the grafting efficiency, which may reach a constant value when the limiting reagent (hydroxyl) is completely consumed. It was expected that hydroxyl groups are completely consumed in all three compositions. However, it is observed that unreacted copolymer remain in all samples even in

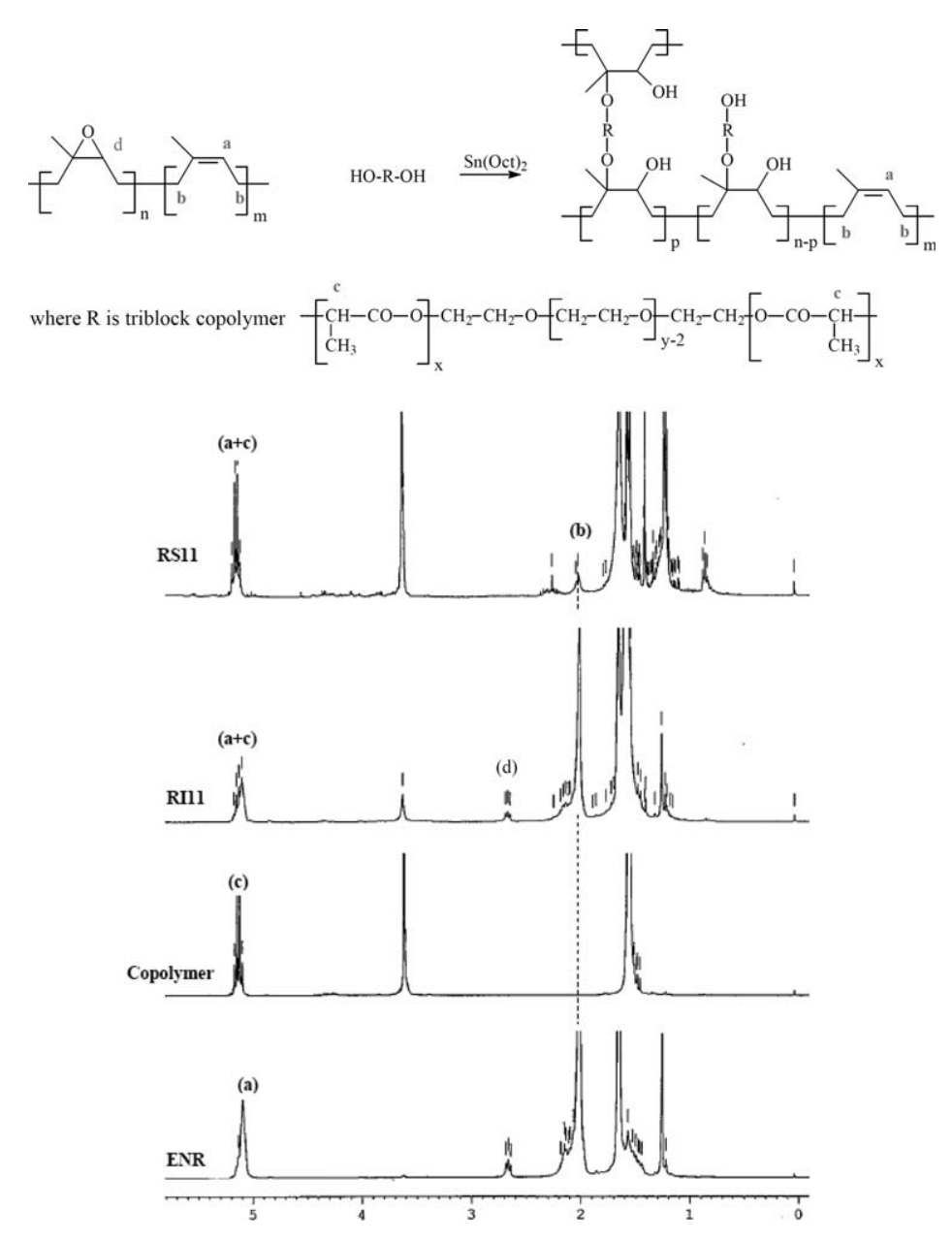


**Figure 4**  $^{1}$ H-NMR spectra and signal assignments of ENR20, LLA<sub>46</sub>EG<sub>46</sub>LLA<sub>46</sub> triblock copolymer, insoluble ( $I_{THF}11$ ) and soluble ( $S_{THF}11$ ) fractions of the cured products after THF Soxhlet extraction.

the sample with the epoxide: hydroxyl molar ratio as high as 50: 1. This is probably due to restriction in accessibility of the hydroxyls to epoxides, i.e., epoxide groups are spaced apart in ENR chains (20% epoxidation). In addition, steric factors and chain stiffness also play a role, as the hydroxyls are terminal groups of long copolymer chains and ENR contains double bonds in its backbone. Nonetheless, improvement of the grafting efficiency can be achieved by employing a reactive blend process, where catalyst and mechanical force are applied to aid the reaction. This will be reported in a separate communication.

In contrast, the increase in the feed hydroxyl content leads to a lower probability for two hydroxyl end-groups from the same copolymer chain, to react and form crosslink junctions, compared with that of forming grafted points. This results in a decrease in the crosslink efficiency. Figure 3 clearly indicates that the content of "grafted" fraction decreases upon increasing the feed ratio from 4:1 to 1:1. This reflects that the former effect is a dominant factor in this curing process. It is noted that solubility behavior of copolymer-grafted ENR chains varies with the degree of grafting. This may cause some uncertainties in the results obtained from the sequential

6 NGUYEN ET AL.

solvent extraction, as "grafted" ENR with certain range of degree of grafting is likely to dissolve in both THF and toluene solvents, as indicated by an overlap area of solubility in Figure 1.

#### Degree of crosslinking

Degree of crosslinking of the insoluble fraction after solvent fractionation ( $I_{Tol}$ ) is examined in terms of the swelling percentage in toluene. The results are also summarized in Figure 3. All samples exhibit a swelling ability, higher than 10 times their original dimensions, where the lowest swelling ratio of 1050% is observed in the sample derived from a 1: 1 ENR20/copolymer feed ratio, indicating the highest crosslink density. This value is clearly higher ( $\sim$  2-fold) than those reported for typical sulfurvulcanized NR samples,<sup>32</sup> where short sequences of sulfur bridges are employed as crosslink junctions. These results firmly support our proposed crosslink mechanism and structures that the copolymers act as long-chain junctions, which provide higher flexibility for the rubber network swelling.

## <sup>1</sup>H-NMR spectra

Chemical structure of the cured ENR products is illustrated in Figure 4. Formation of "crosslinked" or "grafted" structures is obtained, as a result from the variation in ENR20/copolymer feed ratio. <sup>1</sup>H-NMR and signal assignments of ENR20, spectra LLA<sub>46</sub>EG<sub>46</sub>LLA<sub>46</sub> OH-capped triblock copolymer are also compared in Figure 4, where THF soluble and insoluble fractions of the R11 cured sample are also shown. Signals located near 5.10 ppm consist of a singlet of methine proton (a) of cis-1,4-isoprene repeat units and a quartet of methine proton (c) of lactate units. Signals located at 2.10 (b) and 2.65 (d) ppm are assigned to methylene proton of NR units and methine proton of ENR, respectively. The strong (b) signal and a combination of signals at 5.10 ppm (a+c) in the spectrum of the THF-insoluble fraction strongly indicate that the sample consists of ENR20 matrix with the presence of the copolymer as crosslinked junctions. In contrast, a weak (b) signal in the spectrum of the soluble fraction demonstrates that the sample mainly consists of "uncrosslinked" copolymers and some copolymer-grafted ENR. 26,33

Content of the copolymer in the THF soluble fraction of the cured products is calculated from <sup>1</sup>H-NMR spectra, as follows:

$$S_{c} = S_{(a+c)} - S_{a} \tag{2}$$

 $S_a = \text{peak}$  integration of methine proton (5.10 ppm) of ENR

Journal of Applied Polymer Science DOI 10.1002/app

TABLE I Weight Fractions and Copolymer Content of the Extracted Products After THF Soxhlet Extraction

| Samples            | ENR20/copolymer | Weight                | Copolymer            |
|--------------------|-----------------|-----------------------|----------------------|
|                    | feed content    | fraction <sup>a</sup> | content <sup>b</sup> |
|                    | (wt %)          | (wt %)                | (wt %)               |
| $S_{\text{THF}}41$ | 75 : 25         | 23                    | 63                   |
| $S_{\text{THF}}21$ | 66 : 33         | 30                    | 84                   |
| $S_{\text{THF}}11$ | 50 : 50         | 53                    | 90                   |

<sup>&</sup>lt;sup>a</sup> Result from Soxhlet extraction.

 $S_c$  = peak integration of methine proton (5.10 ppm) of copolymer

 $S_{a+c}$  = peak integration of methine protons of ENR and copolymer

 $S_b$  = peak integration methylene proton (2.10 ppm) of *cis*-1,4-polyisoprene unit

The weight content of the copolymer in the samples is calculated, as follows:

$$C(\%) = \frac{M_P}{M_P + \left(S_b \times \frac{U_{LA}}{S_c} \times M_{NR}\right) \times \left(\frac{100}{100 - X_{\text{epoxy}}}\right)} \times 100$$
(3)

where C(%) = weight content of the copolymer,  $M_P$  = molar mass of copolymer (8600 g/mol),

 $U_{LA}$  = average number of LLA repeat units in the copolymer chain (92 units),

 $M_{\rm NR} = {\rm molar\ mass\ of\ } {\it cis}$ -1,4-polyisoprene repeat unit (68 g/mol),

 $X_{\rm epoxy} = {\rm epoxide} \ {\rm content} \ {\rm of} \ {\rm ENR20} \ (20\%).$ 

Results on the weight fraction and copolymer content of THF-soluble samples ( $S_{\rm THF}$ ), as summarized in Table I and Figure 3, show an increasing trend, as a function of increasing copolymer content in the feed. The increase in weight fraction of  $S_{\rm THF}$  from the Soxhlet extraction reflects an increase in (excess) unreacted copolymers, present as simple blend component or small amount of "grafted" fraction with low degree of grafting. In addition, the increase in copolymer content of  $S_{\rm THF}$  samples, calculated from NMR spectra, with the copolymer content in the feed also reflects that the  $S_{\rm THF}$  sample consists of a certain amount of slightly grafted ENR and an increasing quantity of unreacted copolymers.

## ATR-FTIR spectra

ATR-FTIR spectra of ENR20, LLA/EG copolymer, and R41 cured sample are shown in Figure 5. Characteristic bands of ENR20 are observed at 3030 (C—H stretching of epoxide), 1655 (C=C stretching of rubber unit), 1375 (C—H symmetric deformation of rubber's —CH<sub>3</sub>), and 1250 cm<sup>-1</sup> (C—O stretching

F5

T1

<sup>&</sup>lt;sup>b</sup> Calculated from <sup>1</sup>H-NMR spectra.

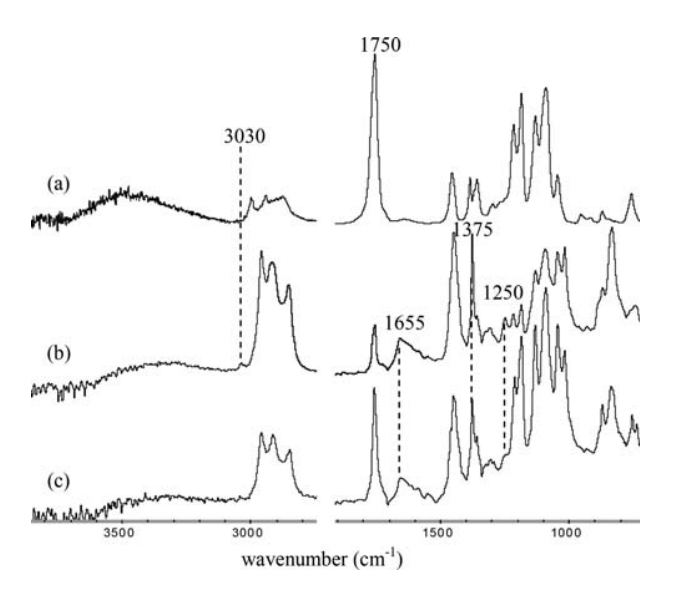


**Figure 5** ATR-FTIR spectra of  $LLA_{46}EG_{46}LLA_{46}$  triblock copolymer (a), ENR20 (b), and R41-cured sample (c).

of epoxide).<sup>34</sup> The characteristic absorption bands of LLA/EG triblock copolymer are observed at 1750 (C=O stretching), and 1375 and 1360 cm<sup>-1</sup> (C-H symmetric deformation of -CH<sub>3</sub> of lactate).<sup>34</sup> The spectrum of R41 cured ENR sample, also shown in Figure 5, exhibits band characteristics of the two components. It is clearly observed that the epoxide bands located at 3030 and 1250 cm<sup>-1</sup> decrease in band intensity upon reacting with the copolymers, indicating a reduction in epoxide content as a result from the ring-opening reaction with hydroxyl groups.

The infrared spectra of cured ENR samples prepared from different ENR20/copolymer feed ratios F6 are compared in Figure 6. Changes in relative intensities of the band characteristics of the two components as a function of feed content are clearly observed. The relative quantity of the two components can be measured by examining the intensity ratio of the 1750/1655 or 1375/1360 cm<sup>-1</sup> bands. The spectra indicate the intensity ratios that are in

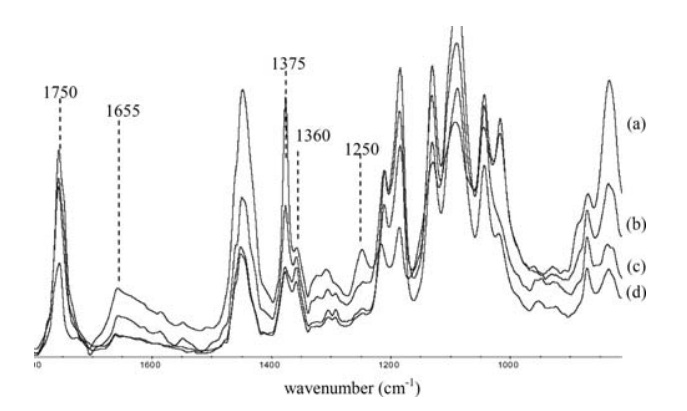


**Figure 6** ATR-FTIR spectra of ENR20 (a), R41 (b), R21 (c), and R11 cured samples (d).

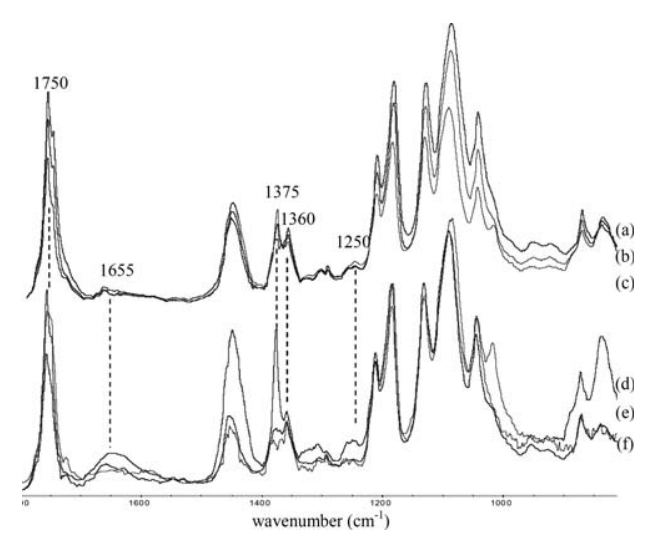


**Figure 7** ATR-FTIR spectra of extracted products after THF Soxhlet extraction:  $S_{\rm THF}41$  (a),  $S_{\rm THF}21$  (b), and  $S_{\rm THF}11$  (c) soluble fractions; and  $I_{\rm THF}41$  (d),  $I_{\rm THF}21$  (e), and  $I_{\rm THF}11$  (f) insoluble fractions.

accord with the feed compositions. The efficiency of the curing process can be determined from the ATR-FTIR spectra by following the change in intensity of the 1250 cm $^{-1}$  band, i.e., the epoxide content. The band intensity clearly decreases as the feed copolymer content increases, reflecting the conversion of epoxide groups after reaction with the hydroxyl groups. The corresponding spectra of THF extraction products,  $S_{\rm THF}$  and  $I_{\rm THF}$ , as a function of feed ENR20/copolymer content are compared in Figure 7. The change in relative intensity of band characteristics of the ENR and copolymer components is clearly observed, and the results are in accord with those observed from  $^{1}$ H-NMR spectra.

## XRD spectra

XRD traces of LLA/EG copolymer, ENR20 and the cured samples are compared in Figure 8. The spectrum of ENR20 shows a broad diffraction pattern due to its highly amorphous nature. In contrast, the spectrum of LLA<sub>46</sub>EG<sub>46</sub>LLA<sub>46</sub> copolymer show diffraction peaks at  $2\theta$  of 16.8, 19.1, and  $22.4^{\circ}$ , which correspond to crystalline domains of the LLA blocks. The diffraction patterns of EG blocks are not observed, probably because of its significantly short sequences and chain restriction imposed by the LLA terminal blocks that retards its crystallization. XRD traces of cured ENR products show diffraction peaks of the copolymer, whose intensity and sharpness increase with an increase in the copolymer in the feed. This reflects an increase in the copolymer content in the cured products, and an enhancement in crystallize ability of the copolymer, due to excess amount of copolymer chains in the ENR matrix.

Journal of Applied Polymer Science DOI 10.1002/app

F8

F7

8 NGUYEN ET AL.

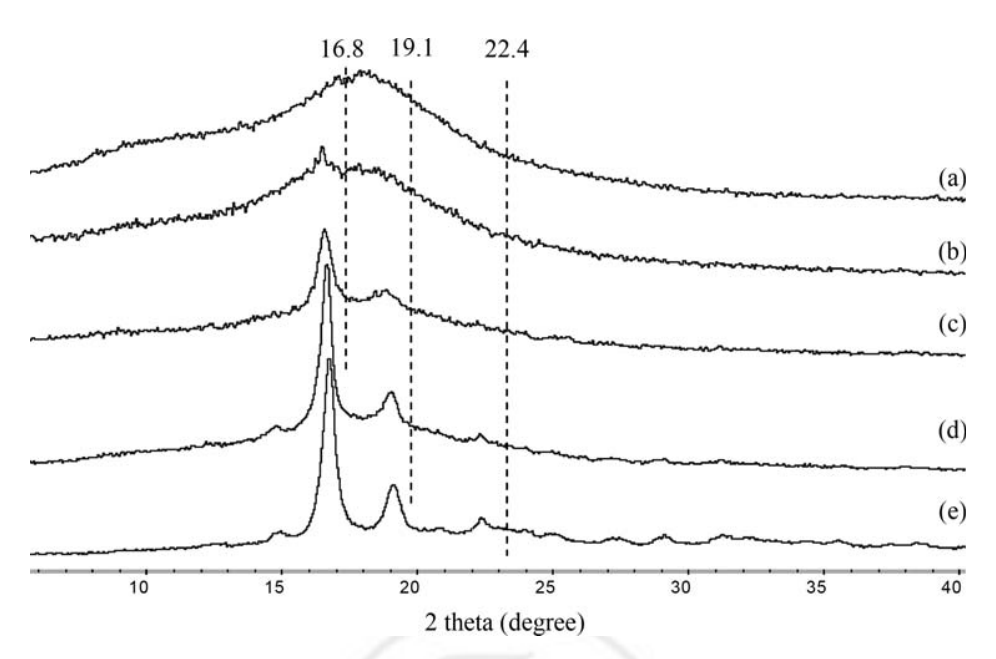


Figure 8 XRD traces of ENR20 (a), R41 (b), R21 (c), R11 (d) cured samples, and LLA<sub>46</sub>EG<sub>46</sub>LLA<sub>46</sub> triblock copolymer (e).

This is in good agreement with our previous discussion. It should also be noted that the peak position of the diffraction peaks, especially at 16.8°, shifts to lower angle along with the decrease in the peak intensity and sharpness as the feed ENR20/copolymer ratio increases from 1:1 to 4:1. This is probably due to lower degree of order arrangement of the copolymer domains, as the chains effectively react with the ENR and are present as "grafted" or "crosslink junctions." This results in mobility restriction, and hence a retardation of crystal formation.

#### Tensile properties

Tensile properties of R11 cured sample, a 1:1 ENR20/copolymer simple blended mixture without the use of catalyst (N11), and pristine ENR20 are T2 examined and compared in Table II. It is noted that these samples do not contain ENR chains linked by conventional crosslinking junctions, i.e., reaction with double bonds. R11 and N11 show drastic improvement in 100% Modulus (M100), 300% Modulus (M300), and tensile strength, compared with those of the original ENR20. This indicates that the incorporation of LLA/EG copolymer, either by simple blending (N11) or as grafted chains and crosslink junctions (R11), leads to an enhancement in tensile

properties of the samples. Given that the NMR spectrum of N11 and its extraction result (100% soluble in THF) indicate no significant chemical change in the simple blended mixture, the property improvement observed in this sample is probably attributed to interfacial adhesion of copolymer and ENR20 chains in the blend.<sup>35</sup> With the application of Sn(Oct)<sub>2</sub> catalyst, formation of "grafted" and "crosslinked" ENR networks by copolymer junctions is obtained in R11. This leads to further improvement in the tensile properties.

The elongation at break of R11 and N11 clearly decreases, compared to that of the original (uncured) ENR, because the incorporation of plastic materials, i.e., copolymers, into the rubber matrix leads to a decrease in elastic properties of the mixture, hence a drop in elongation at breaks. A mismatch in solubility parameter of the two components, which affects the mixture's miscibility, and the presence of excess copolymers may also play a role in the drop in the elongation at break of N11. The results also show that elongation at break of R11 is higher than that of N11. This is probably due to the existent of "grafted" ENR, which generate higher degree of chain entanglements and a closer match in solubility of the components, leading to an increase in elongation at break. In addition, the present of "crosslinked"

TABLE II

Tensile Properties of R11-Cured Sample, a 1 : 1 ENR20/Copolymer Blend (N11), and ENR20

| Samples | M100 (MPa)   | M300 (MPa)      | Tensile strength (MPa) | Elongation at break (%) |
|---------|--|-----------------|------------------------|-------------------------|
| R11     | $\begin{array}{c} 2.11  \pm  0.10 \\ 1.88  \pm  0.03 \\ 0.41  \pm  0.02 \end{array}$ | $3.98 \pm 0.22$ | $5.97 \pm 0.31$        | $407 \pm 30$            |
| N11     |  | $2.68 \pm 0.04$ | $3.14 \pm 0.13$        | $345 \pm 25$            |
| ENR20   |  | $0.42 \pm 0.02$ | $0.52 \pm 0.04$        | $650 \pm 20$            |

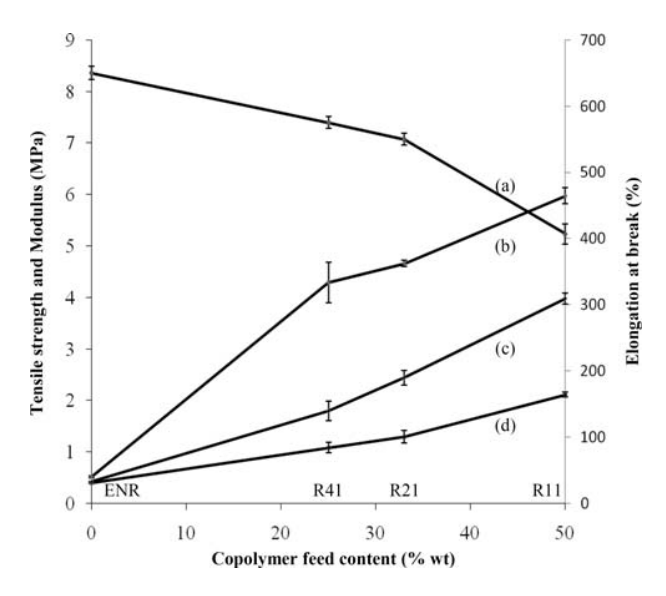


**Figure 9** Elongation at break (a), Tensile strength (b), 100% Modulus, M100 (c), 300% Modulus, M300 (d) of ENR cured samples as a function of ENR20/copolymer feed content.

ENR in R11 also results in an enhancement of elongation at break.

Tensile properties of the cured samples as a function of ENR20/copolymer feed content are shown in Figure 9. The degree of improvement in tensile strength, M100, and M300 is dependent on the copolymer feed content, where R11 shows an improvement of more than 10 times of those of neat ENR20. This is due to the presence of network structure and "grafted" ENR chains, leading to a mobility restriction of the cured ENR products, as previously discussed. Additionally, the increase in the content of excess copolymers in the samples is also responsible for the increase in modulus and tensile strength. It is also clearly observed that elongation at break decreases with the increase in the copolymer content in the feed, mainly due to the increase in the content of excess copolymers. As the degree of improvement of tensile properties is strongly dependent on the ENR20/copolymer ratio in the feed, cured ENR products with specific properties can be obtained by adjusting this value. Given these excellent mechanical properties and their biocompatibility, the materials can be applied in various applications, especially in biomedical fields.

## Permeability behaviors

Permeability characteristics of the cured samples are examined to elucidate their potential use in membrane applications. Theoretically, the permeability of a polymer for a gas penetrant is defined as a product of solubility coefficient and diffusion coefficient, where the former is derived from the relative size of

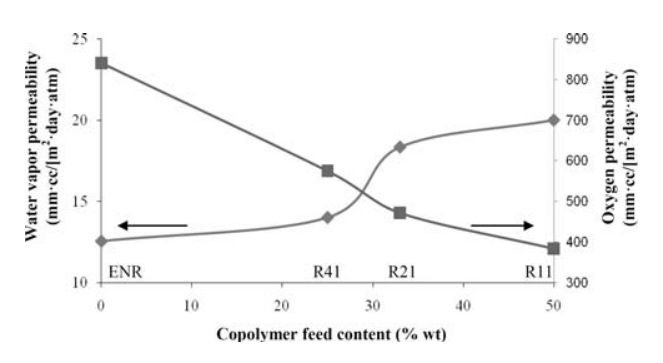


**Figure 10** Water vapor and oxygen permeabilities of cured ENR samples as a function of ENR20/copolymer feed content.

penetrant and the inter/intrachain spacing of the polymer. The latter term is associated with sorption ability of the penetrant on the polymer.<sup>36</sup> Results of water vapor permeability of the cured samples, as summarized in Figure 10, show an increasing trend with increasing feed copolymer content, compared to that of neat ENR20, at 13 mm cc/(m<sup>2</sup>·day atm). This is mainly because the cured products contain long-chain crosslink junctions that disrupt chain arrangement of the ENR matrix (See Fig. 1), leading to an enlargement of chain spacing and hence ease of water vapor permeation. EG sequences in the block copolymer also play a key role in the enhancement of the solubility coefficient term, as its strong hydrophilic nature provides high sorption ability to the vapor. This agrees with those observed by Zenkiewicz et al.37 that the presence of 20% of PEG in the PLLA matrix doubly increased the water permeability of the mixture.

Results on oxygen permeability, as shown in Figure 11, indicate that an increase in copolymer content in the cured materials leads to a drastic reduction in the oxygen permeability. Oxygen permeability of pristine ENR25, PEG and PLLA was

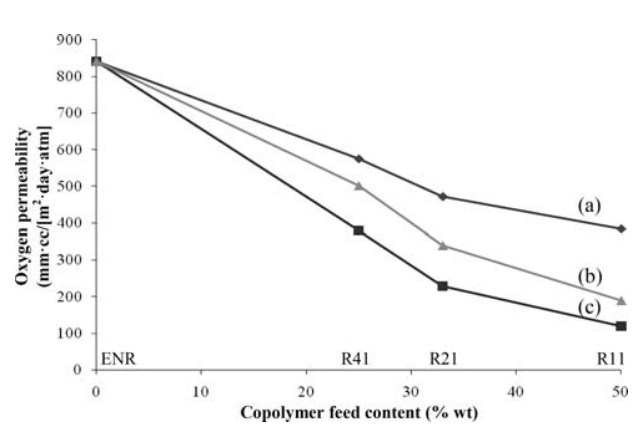


Figure 11 Experimental (a) and theoretical oxygen permeability: the free volume theory (b) and the empirical model (c), of cured samples as a function of ENR20/copolymer feed content.

Journal of Applied Polymer Science DOI 10.1002/app

F10

F11

10 NGUYEN ET AL.

reported as 328, 17, and 17 mm cc/(m² day atm), respectively. 36,38,39 Given the much lower values for PEG and PLA compared with that of ENR, a decrease in the permeability of the cured ENR samples is expected as a result from the incorporation of the copolymer. The reduction in the oxygen permeability can be explained in terms of a decrease in both diffusion and solubility coefficients, due to the relatively larger size of oxygen molecule and its non-polar nature.

The variation in the oxygen permeability as a function of ENR20/copolymer content can be explained by the following empirical model, which was modified from that proposed by Paul et al. in the explanation of polymer blend characteristics.<sup>40</sup>

$$log P_{cured} = \phi_{co} log P_{co} + \phi_{ENR} log P_{ENR}$$
 (4

where  $P_{\rm cured}$  is gas permeability of the cured samples.

 $\phi_{co}$  and  $\phi_{ENR}$  are volume fractions of copolymer and ENR20 in the cured samples.

 $P_{\rm co}$  and  $P_{\rm ENR}$  are oxygen permeabilities of pure copolymer and ENR components.

Alternatively, the free volume model,<sup>40</sup> which is used to explain the transport behavior of gas in a polymer matrix, can be adopted, as described below:

$$\ln \frac{P_{\text{cured}}}{A} = \left[ \frac{\phi_{\text{ENR}}}{\ln \left( \frac{P_{\text{ENR}}}{\ln A} \right)} + \frac{\phi_{\text{co}}}{\ln \left( \frac{P_{\text{co}}}{A} \right)} \right]^{-1}$$
(5)

where A is parameter for free volume model at 25°C,  $7.9 \times 10^{-7}$  (cm<sup>3</sup>(STP)·cm/[cm<sup>2</sup> sec cmHg])

Figure 11 summarizes oxygen permeability of the cured samples obtained from experiments, compared with those calculated from the empirical model and the free volume theory. Data obtained from the two models are significantly lower than the experimental results, probably because the models were designed for polymer blend systems. However, these cured ENR materials consist of full/partial crosslinked networks and blend mixtures. The free volume theory is a closer match to the experimental values, and perhaps more suitable to describe the gas permeability behavior of these materials. The higher experimental values compared to the predicted values by the free volume theory is probably due to the long-chain crosslink junctions derived from the block copolymers, which leads to formation of excess free volume in the cured network and hence, higher gas permeability.

Carbon dioxide permeability characteristics of T3 ENR20 and R11 are compared in Table III. The values of 6142, 531, and 72 mm cc/(m $^2$  day atm) were reported for ENR25, PEG, and PLA, respectively.  $^{38,39,41}$  Given the empirical model (log $P_{\rm cured}$  =

TABLE III
Carbon Dioxide, Oxygen Permeability, and CO<sub>2</sub>/O<sub>2</sub>
Selectivity of ENR20 and Cured R11 Sample

| Samples | CO <sub>2</sub> permeability<br>(mm·cc/<br>[m²·day·atm]) | O <sub>2</sub> permeability<br>(mm·cc/<br>[m²·day·atm]) | CO <sub>2</sub> /O <sub>2</sub><br>selectivity |  |
|---------|--|---|--|--|
| ENR20   | 6 117  | 841   | 7.3  |  |
| R11     | 12 840   | 384   | 33.4   |  |

 $\phi_{\text{co}} \log P_{\text{co}} + \phi_{\text{ENR}} \log P_{\text{ENR}}$ , the CO<sub>2</sub> permeability of the cured samples is expected to decrease with increasing copolymer content. The experimental data, however, shows the reverse trend, where the cured R11 sample shows higher CO<sub>2</sub> permeability of more than two times, compared to that of the original ENR20. This intriguing behavior is mainly due to EG segments in the copolymer chains. It was reported that PEG can dissolve a substantial amount of sour gas. 42 Ether groups in PEG as polar moiety groups have affinity to  $CO_2$  gas due to dipole-quadrupole interaction.<sup>38</sup>  $CO_2$  is present as a strong sorbing penetrant for PEG, resulting in large solubility coefficient. The polymer matrix is subsequently plasticized by high concentration of this strong sorbing penetrant, resulting in an increase in local segment motion. Therefore, an enhancement in diffusion coefficients and permeability is achieved. 36,38,43 In addition, the presence of hydroxyl end-groups from "grafted" or "free" copolymers in the ENR matrix, and the newly formed hydroxyls from ring-opening reaction of epoxide (See Fig. 4), also favor the transport of CO<sub>2</sub> through the membrane because of its acidity.

Results on CO<sub>2</sub>/O<sub>2</sub> selectivity are also summarized in Table III. An enhancement in the CO<sub>2</sub>/O<sub>2</sub> selectivity of more than four times is observed in R11 sample, compared with that of the neat ENR20. The ideal selectivity of penetrant is defined as the product of diffusivity selectivity and solubility selectivity. For rubbery polymer, it is commonly found that the selectivity is dominated by the solubility term.<sup>36</sup> This is firmly supported, as the solubility selectivity of the system strongly favors the transport of CO<sub>2</sub>, as previously discussed. In addition, the permeability and selectivity of these materials may be further adjusted by varying the block length of EG sequence in the copolymer chains. Therefore, these copolymer-cured ENR samples are excellent choice for use as selective materials in membrane applications.

#### **CONCLUSIONS**

OH-capped LLA/EG/LLA triblock copolymer is used as a macromolecular crosslink agent for the ENR matrix by utilizing ring-opening reaction of epoxides and hydroxyl groups, using Sn(Oct)<sub>2</sub> as a

catalyst. <sup>1</sup>H-NMR and ATR-FTIR spectra indicate the formation of chemical bonds between copolymer chains and ENR. Efficiency of the crosslinked reaction is varied as a function of ENR/copolymer feed ratios, which is reflected by the content of "crosslinked," "grafted," and "free" simple blend fractions of the copolymer-cured ENR samples. These are examined by <sup>1</sup>H-NMR, ATR-FTIR, XRD, solvent fractionation, and swelling experiments. The cured ENR products exhibit drastic improvement in tensile properties, suitable for use as crosslinked rubber materials for specific and high-value applications. The use of a rather high content of the biocompatible/biodegradable copolymer as a curing agent is, therefore, not a major concern. Improvement in permeability and selectivity behaviors of the materials is also achieved, where water vapor and carbon dioxide permeability increase with an increase in copolymer feed content. The opposite trend is observed for oxygen permeability. These cured materials with excellent properties show high potential for use in biomedical and membrane applications. In addition, the properties of these cured materials can be fine tuned for specific applications by varying the ENR20/copolymer ratios, the epoxide content of ENR, and the relative block lengths of the copolymer.

#### References

- Bhowmick, A. K.; Stephens, H. L. Handbook of Elastomers; Marcel Dekker: New York,2001.
- 2. Morgan, B.; McGill, W. J. J Appl Polym Sci 2000, 76, 1413.
- 3. Porter, M. J Appl Polym Sci 1967, 11, 2255.
- Craig, D.; Davidson, W. L.; Juve, A. E.; Geib, I. G. J Polym Sci 1951, 6, 1.
- 5. Bristow, G. M.; Moore, C. G.; Russell, R. M. J Polym Sci Part A: General Papers 1965, 3, 3893.
- 6. Bristow, G. M. J Appl Polym Sci 1965, 9, 3255.
- 7. Moore, C. G.; Scanlan, J. J Polym Sci 1960, 43, 23.
- 8. Dunn, J. R. J Appl Polym Sci 1963, 7, 1543.
- 9. Chowdhury, R. J Appl Polym Sci 2007, 103, 1206.
- 10. Minoura, Y.; Asao, M. J Appl Polym Sci 1961, 5, 233.
- Minoura, Y.; Asao, M. J Appl Polym Sci 1961, 5, 401.
   Akiba, M.; Hashim, A. S. Prog Polym Sci 1997, 22, 475.

- 13. Gelling, I. R. J Natural Rubber Res 1991, 6, 184.
- Hashim, A. S.; Kohjiya, S. J Polym Sci Part A: Polym Chem 1994, 32, 1149.
- 15. Gelling, I. R. Rubber Chem Technol 1985, 58, 86.
- 16. Perera, M. C. S. J Appl Polym Sci 1990, 39, 749.
- 17. Jayawardena, S.; Reyx, D.; Durand, D.; Pinazzi, C. P. Die Makromolekulare Chemie 1984, 185, 2089.
- Derouet, D.; Radhakrishnan, N.; Brosse, J.-C. Boccaccio, G. J Appl Polym Sci 1994, 52, 1309.
- Mohanty, S.; Nando, G. B.; Vijayan, K.; Neelakanthan, N. R. Polymer 1996, 37, 5387.
- Derouet, D.; Brosse, J.-C.; Challioui, A. Eur Polym J 2001, 37, 1315.
- Derouet, D.; Brosse, J.-C.; Challioui, A. Eur Polym J 2001, 37, 1327.
- 22. Gupta, A. P.; Kumar, V. Eur Polym J 2007, 43, 4053.
- 23. Cohn, D.; Younes, H. J Biomed Mater Res 1988, 22, 993.
- Deng, X. M.; Xiong, C. D.; Cheng, L. M.; Xu, R. P. J Polym Sci Part C, Polym Lett 1990, 28, 411.
- Kulkarni, R. K.; Moore, E. G.; Hegyeli, A. F.; Leonard, F. J Biomed Mater Res 1971, 5, 169.
- 26. Saito, T.; Klinklai, W.; Yamamoto, Y.; Kawahara, S.; Isono, Y.; Ohtake, Y. J Appl Polym Sci 2009, 115, 3598.
- Nghia, P. T.; Siripitakchai, N.; Klinklai, W.; Saito, T.; Yamamoto, Y.; Kawahara, S. J Appl Polym Sci 2008, 108, 393.
- Nguyen, T.-H.; Petchsuk, A.; Tangboriboonrat, P.; Opaprakasit, M.; Sharp, A.; Opaprakasit, P. Adv Mater Res 93 2010, 94, 198.
- 29. Saendee, P.; Tangboriboonrat, P. Colloid Polym Sci 2006, 284, 634.
- Derouet, D.; Tran, Q. N.; Thuc, H. H. J Appl Polym Sci 2009, 114, 2149.
- 31. Phinyocheep, P.; Phetphaisit, C. W.; Derouet, D.; Campistron, I.; Brosse, J. C. J Appl Polym Sci 2005, 95, 6.
- Aprem, A. S.; Joseph, K.; Mathew, T.; Altstaedt, V.; Thomas, S. Eur Polym J 2003, 39, 1451.
- 33. Saito, T.; Klinklai, W.; Kawahara, S. Polymer 2007, 48, 750.
- 34. Mathew, V.; Sinturel, C.; George, S.; Thomas, S. J Mater Sci
- 35. Yong, M. K.; Ismail, H.; Ariff, Z. M. Polym-Plast Technol Eng 2007, 46, 1001.
- 36. Johnson, T.; Thomas, S. Polymer 1999, 40, 3223.
- 37. Zenkiewicz, M.; Richert, J. Polym Test 2008, 27, 835.
- 38. Lin, H.; Freeman, B. D. J Membr Sci 2004, 239, 105.
- Bao, L.; Dorgan, J. R.; Knauss, D.; Hait, S.; Oliveira, N. S.; Maruccho, I. M. J Membr Sci 2006, 285, 166.
- 40. Paul, D. R. J Membr Sci 1984, 18, 75.
- 41. Barrie, J. A.; Becht, M.; Campbell, D. S. Polymer 1992, 33, 2450.
- 42. Kuehne, D. L.; Friedlander, S. K. Indust Eng Chem Proc Des Dev 1980, 19, 609.
- 43. Koros, W. J.; Hellums, M. W. Fluid Phase Equilibria 1989, 53, 339.

AQ1: Kindly check whether the short title is OK as given.

AQ2: Please provide the department and university names for Affiliation 4.



## **Communications**

# Selective Sensing of L-Arginine Employing Luminol Dextran Conjugate

Weerachai Nasomphan<sup>a,b</sup>, Pramuan Tangboriboonrat<sup>b</sup>, Srung Smanmoo<sup>a\*</sup>

<sup>a</sup>Bioresources Research Unit, National Center for Genetic Engineering and Biotechnology (BIOTEC), 113 Thailand Science Park, Phaholyothin Road, Klong Luang, Pathumthani 12120, Thailand <sup>b</sup>Department of Chemistry, Faculty of Science, Mahidol University, Rama 6 Road, Phyathai, Bangkok 10400, Thailand

#### Abstract

Luminol dextran conjugate (LD) was synthesized by incorporating luminol into the oxidized dextran template followed by reduction with sodium borohydride. The fluorescence (FL) response of LD towards various amino acids was investigated by FL spectroscopy. The FL intensity of LD significantly quenches upon the addition of L-arginine and goes to completion after the addition of  $50\times10^{-5}~\text{mol}~\text{L}^{-1}$  L-arginine. Since LD is highly soluble in water, LD could be potentially used as a FL polymeric sensor for the determination of L-arginine in aqueous environment.

#### Introduction

Chemosensors have found their standing position in environmental and biomedical applications. <sup>1-3</sup> Due to the limited signal generated by molecular chemosensors, polymeric chemosensors have therefore gained their popularity due to the amplified signal output. <sup>4-7</sup> The effect could be due to a large number of chromophores incorporated into the macromolecular template. <sup>8</sup> Recently, polymeric chemosensors have been widely used for detection of explosives, volatile organic compounds, biological and chemical molecules. <sup>9-12</sup>

Amino acids (AAs) are important analytes present in biological fluids. It is known that many diseases are directly correlated to the deficiency of AAs. 11 Among these AAs, Larginine is of research focus due to its various biological roles. L-arginine is a precursor for biosynthesis of a signaltransduction molecule, nitric oxide, via the enzymatic process assisted by nitric oxide synthase (NOS). 13-14 Over the past decades, AA chemosensor for L-arginine is scarcely reported. However, the specific recognition between adenosine triphosphate (ATP) and L-arginine has been recently exemplified.15 The recognition of L-arginine by ATP proceeds via the hydrogen bonding and the charge-charge interaction between the guanidinium residue of L-arginine and the triphosphate moiety of ATP. A chemosensor based on the calix[4]pyrrole-TCBQ assembly has been carefully designed and used for the detection of AAs and amines. 16 The photophysical response of the calix[4]pyrrole-TCBQ assembly towards AAs is driven by the n- $\pi$  charge-transfer.

Herein, we have designed a polymeric chemosensor for L-arginine based on luminol dextran conjugate (LD). Dextran, a polysaccharide consisting of a number of glucose subunits, is chosen as a polymeric template due to the fact that it exhibits strong affinity towards L-arginine via a charge-charge interaction. Luminol (Lu) is selected as a chromophore because its fluorescence (FL) could be quenched in the presence of analytes via the internal charge transfer (ICT) pathway. Upon binding of L-arginine to LD, ICT process is operated which quenches the FL of Lu moiety. Since LD is highly soluble in water and highly selective towards L-arginine, this offers LD as a potential chemosensor for an intracellular detection of L-arginine.

#### **Experimental**

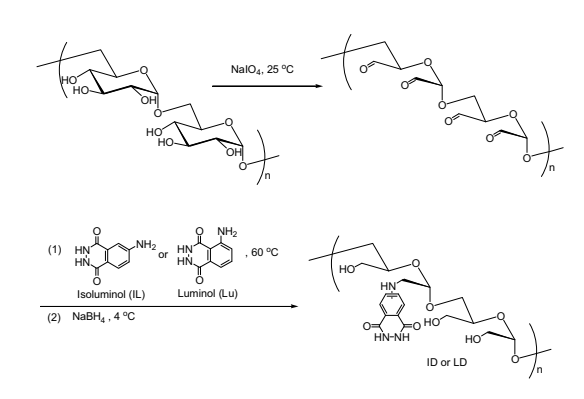
**Materials.** Luminol and isoluminol were purchased from Tokyo Chemical Industry (TCI), Japan. Dextran and other chemicals were supplied from Aldrich. All reagents were used without further purification.

**General.** <sup>1</sup>H NMR spectrum was recorded on Bruker DPX 400 MHz spectrometer in D<sub>2</sub>O using TMS as the internal standard. Elemental analysis for the synthesized compound was analyzed by Tokyo Chemical Industry (Japan).

**Luminol dextran conjugated (LD):** LD was prepared according to a literature. HNMR (400 MHz,  $D_2O$ ) [ppm]: 8.33 (s), 7.55-7.41 (m), 7.28-7.23 (m), 6.95 (d, J = 8.38 Hz), 4.85 (br, dextran), 4.08-3.23 (m, dextran).

## **Results and Discussion**

Isoluminol dextran conjugate (ID) and LD were prepared according to Kai's procedure with slight modification. <sup>8</sup> Briefly, dextran (Mr approx.  $2 \times 10^6$  g/mol) was oxidized with sodium periodate (NaIO<sub>4</sub>) to provide the oxidized dextran which was then reacted with either isoluminol (IL) or Lu, followed by reduction with sodium borohydride (NaBH<sub>4</sub>) to furnish ID and LD as yellow powder (Scheme 1).



Scheme 1. The synthesis of ID and LD.

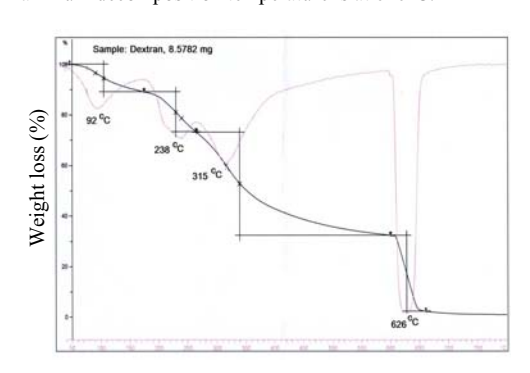
ID and LD were dried in *vacuo* before subjecting to elemental analyses performed by Tokyo Chemical Industry

Table 1. Elemental Analysis and Molecular Weight Determination of ID and LD

|    |       |      |      |  | Molecular weight        | Polydispersity index |
|----|-------|------|------|--|-------------------------|----------------------|
|    | %C    | %Н   | %N   | Composition of compound                      | (GPC)                   | $(M_w/M_n)$          |
| ID | 43.76 | 5.65 | 5.95 | (IL) <sub>3262</sub> -(Glc) <sub>12346</sub> | $2.5 \times 10^6$ g/mol | 1.59                 |
| LD | 43.96 | 5.62 | 5.50 | (Lu) <sub>2726</sub> -(Glc) <sub>12375</sub> | $2.6 \times 10^6$ g/mol | 1.56                 |

IL = isoluminol unit; Lu = luminol unit; Glc= glucose unit.

(Japan). Table 1 shows %C, %H and %N of ID and LD. From the data obtained, the composition of IL, Lu and glucose (Glc) units in ID and LD were deduced. According to the data, a large number of IL (3,262 units) or Lu (2,726 units) has been incorporated into a macromolecular dextran template. This could improves the sensitivity of the polymeric sensor.<sup>19</sup> The molecular weight of ID and LD, determined by Gel Permeation Chromatography (GPC), were found to be  $2.5 \times 10^{-6}$  and  $2.6 \times 10^{-6}$  g/mol, respectively. Their polydispersity indexes (M<sub>w</sub>/M<sub>n</sub>) were 1.59 and 1.56. FL emission of ID and LD appeared at 425 nm in water which is the characteristic FL emission of IL and Lu. The thermogram obtained from thermogravimetric analysis (TGA) of LD is displayed in Figure 1. The weight loss of LD is found over three regions (0-238, 238-315 and 315-626°C) where the maximum decomposition temperature is at 626°C.



Temperature (°C)

Figure 1. TGA thermogram of LD.

The selectivity of LD ( $25 \times 10^{-5}$  mol L<sup>-1</sup>) towards different concentrations of AAs was investigated. In the presence of AAs, various degrees of FL enhancement and quenching of LD were observed. However, only L-arginine significantly quenched the FL of LD. The FL quenching effect was clearly observed when  $50 \times 10^{-5}$  mol L<sup>-1</sup> of L-arginine was added into the LD solution. FL of LD gradually decreases upon increasing concentrations of L-arginine and nearly undergoes to completion after the concentration of L-arginine reached  $25 \times 10^{-5}$  mol L<sup>-1</sup> (Figure 2). Figure 3 shows FL quenching of ID, used here as a control, in the presence of AAs. It was clearly shown that FL enhancement and quenching of ID were also observed with different AAs. L-arginine, although,

exhibited some degrees of FL quenching of ID. However, the quenching effect was less pronounced when compared to LD. This indicates that the Lu moiety in LD serves as a specific chromophore interacting with L-arginine and the interaction initiates the FL quenching of LD via the ICT process. Since IL is an isomer of Lu, it would expect to display some degrees of FL quenching.<sup>20</sup> The more quenching effect of LD compared to ID is presumably due to the orientation of Lu moiety in the present conformation of polymeric dextran in which the Lu moiety and L-arginine achieves the maximal interaction.

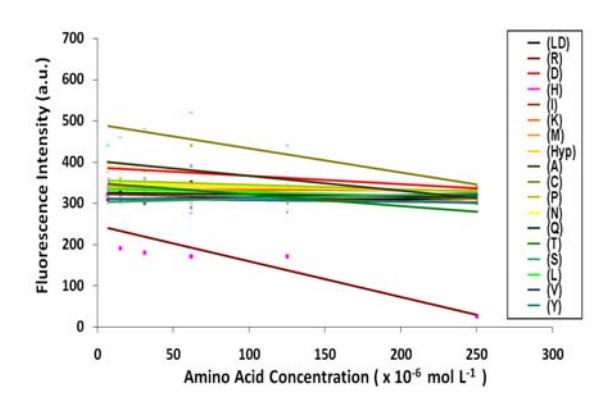


**Figure 2.** FL emission of LD  $(25 \times 10^{-5} \text{ mol L}^{-1})$  in the presence of various concentrations of AAs in water. Excitation wavelength  $(\lambda_{Ex}) = 275$  nm. Where LD = luminol dextran conjugate; R = L-Arginine; D = L-Aspartic acid; H = L-Histidine; I = L-Isoleucine; K = L-Lysine; M = L-Methionine; Hyp = L-Hydroxyproline; A = L-Alanine; C = L-Cysteine; P = L-Proline; N = L-Asparagine; Q = L-Glutamine; T = L-Threonine; S = L-Serine; L = L-Leucine; V = L-Valine; Y = L-Tyrosine.

Since the ICT process highly depends on the choice of donor and acceptor, the FL quenching of LD in the presence of L-arginine is presumably due to the ICT channel in which Lu and guanidinium groups are good electron donor/acceptor in this process.<sup>21</sup>

A curve equation is linearly obtained in the range of L-arginine concentrations from 0 to  $0.1 \times 10^{-5}$  mol L<sup>-1</sup>, R = -0.982, N = 3. According to the equation, the FL detection of LD was determined to be as low as  $1.0 \times 10^{-5}$  mol L<sup>-1</sup>.

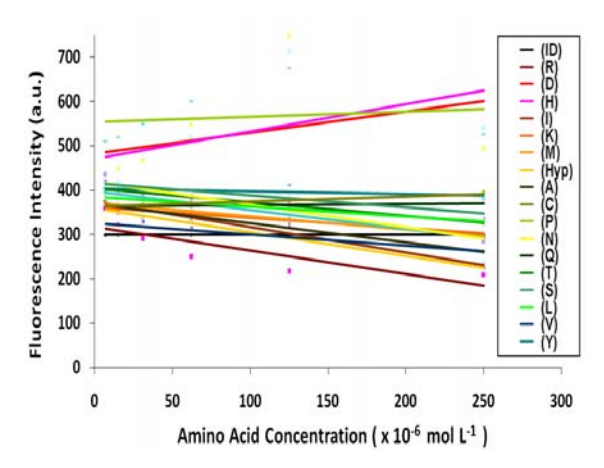


**Figure 3.** FL emission of ID  $(25 \times 10^{-5} \text{ mol L}^{-1})$  in the presence of various concentrations of AAs in water. Excitation wavelength  $(\lambda_{Ex}) = 275$  nm. Where ID = isoluminol dextran conjugate; R = L-Arginine; D = L-Aspartic acid; H = L-Histidine; I = L-Isoleucine; K = L-Lysine; M = L-Methionine; Hyp = L-Hydroxyproline; A = L-Alanine; C = L-Cysteine; P = L-Proline; N = L-Asparagine; Q = L-Glutamine; T = L-Threonine; S = L-Serine; L = L-Leucine; V = L-Valine; Y = L-Tyrosine.

The FL change of LD in the presence of AAs was clearly observed under UV light. When LD ( $1.0 \times 10^{-5} \text{ mol L}^{-1}$ ) was added with various AAs ( $50 \times 10^{-5} \text{ mol L}^{-1}$ ), only L-arginine exhibited significant FL quenching. The presence of other AAs displayed no noticeable FL change of LD (Figure 4). Increasing concentrations of L-arginine resulted in gradually FL quenching of LD and the significant FL quenching of LD was clearly observed after the addition of  $50 \times 10^{-5} \text{ mol L}^{-1}$  of L-arginine [Figure 5(h)].





**Figure 4.** FL change of LD  $(1.0 \times 10^{-5} \text{ mol L}^{-1})$  in the presence of different AAs  $(50 \times 10^{-5} \text{ mol L}^{-1})$  in water. LD with (a) water (blank) (b) L-Methionine (c) L-Isoleucine (d) L-Histidine (e) L-Lysine (f) L-Hydroxyproline (g) L-Alanine (h) L-Cysteine (i) L-Glutamine (j) L-Tyrosine (k) L-Aspartic acid (l) L-Proline (m) L-Serine (n) L-Asparagine (o) L-Leucine (p) L-Valine (q) L-Threonine (r) L-Glutamic acid (s) L-Arginine. Excitation wavelength ( $λ_{Ex}$ ) = 275 nm.

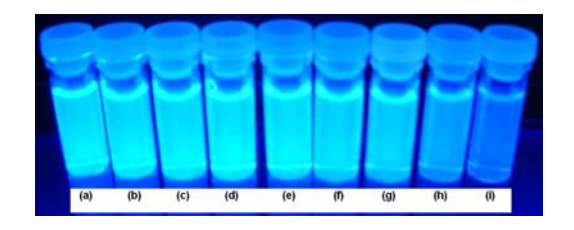


**Figure 5.** FL change of LD ( $10 \times 10^{-5}$  mol L<sup>-1</sup>) in the presence of various concentrations of (a) 0 (b) 0.38 (c) 0.75 (d) 1.5 (e) 3 (f) 6 (g) 12 (h) 25 (i)  $50 \times 10^{-5}$  mol L<sup>-1</sup> of Larginine. Excitation wavelength ( $\lambda_{EX}$ ) = 275 nm.

#### Conclusions

In summary, LD was prepared as a selective polymeric chemosensor for AAs. Among screened AAs, LD displayed high selectivity towards L-arginine. In the presence of  $50 \times 10^{-5}$  mol L<sup>-1</sup> of L-arginine, the FL of LD undergoes to completion. Since LD is highly soluble in water, LD serves as a potential intracellular chemosensor for detection of L-arginine.

Acknowledgements The Thailand Research Fund/Commission on Higher Education's research grants to P.T. (RTA5180003) and S.S. (TRG5380029), and the Development and Promotion of Science and Technology Talents Project's scholarship to W.N. are gratefully acknowledged. We are also grateful to the partial support from National Center for Genetic Engineering and Biotechnology (BIOTEC).

#### References

- (1) A. P. de Silva, H. Q. N. Gunaratne, T. Gunnalaugsson, A. J. M. Huxley, C. P. McCoy, and J. T. Rademacher, Chem. Rev., **97**, 1515 (1997).
- (2) B. Valeur, and L. Leray, Coord. Chem. Rev., **205**, 3 (2000).
- (3) M. H. Keefe, K. D. Benkstein, and J. T. Hupp, Coord. Chem. Rev., **205**, 201 (2000).
- (4) B. Adhikari, and S. Majumdar, Prog. Polym. Sci., **29**, 699 (2004).
- (5) Y. Xu, L. Zheng, X. Huang, Y. Cheng, and C. Zhu, Polymer, **51**, 994 (2010).
- (6) J. Meng, G. Wei, X. Huang, Y. Dong, Y. Cheng, and C. Zhu, Polymer, **52**, 363 (2011).
- (7) X. Huang, J. Meng, Y. Dong, Y. Cheng, and C. Zhu, Polymer, **51**, 3064 (2010).
- (8) H. Zhang, C. Smanmoo, T. Kabashima, J. Lu, and M. Kai, Angew. Chem. Int. Ed., **46**, 8226 (2007).
- (9) Z. Wang, Z. Y. Wang, J. Ma, W. J. Bock, and D. Ma, Polymer, **51**, 842 (2010).
- (10) J. Li, C. E. Kendig, and E. E. Nesterov, J. Am. Chem. Soc., **129**, 15911 (2007).
- (11) H. O. Yoo, S. K. Chae, J. M. Kim, and D. J. Ahn, Macromol. Res., **15**, 478 (2007).

- (12) E. L. Dane, S. B. King, and T. M. Swager, J. Am. Chem. Soc., **132**, 7758 (2010).
- (13) G. Wu, and S. M. Morris Jr., Biochem. J., 336, 1 (1998).
- (14) R. M. Palmer, D. S. Ashton, and S. Moncada, Nature, **333**, 664 (1988).
- (15) L. Xian, S. Liu, Y. Maa, and G. Lua, Spectrochim. Acta A., **67**, 368 (2007).
- (16) K. Liu, L. He, X. He, Y. Guo, S. Shao, and S. Jiang, Tetrahedron Lett., **48**, 4275 (2007).
- (17) K. Ohtake, H. Natsume, H. Ueda, and Y. Morimoto, J. Control. Release, **82**, 263 (2002).
- (18) M. Voicescu, M. Vasilescu, T. Constantinescu, and A. Meghea, J. Luminesc., 13, 315 (2003).
- (19) J. S. A. Simpson, A. K. Campbell, M. E. T. Ryall, and J. S. Woodhead, Nature, 279, 646 (1979).
- (20) T. Burdo, and W. R. Seltz, Anal. Chem., 47, 1639 (1975).
- (21) Z. C. Wen, and Y-B. Jiang, Tetrahedron, **60**, 11109 (2004).

Subject: 7068P accepted by PPC

From: "liuvic" <vctrliu@hotmail.com> **Date:** Fri, June 10, 2011 8:44 pm

To: scptb@mahidol.ac.th

**Priority:** Normal

View Full Header | View Printable Version | Download this as a file

Options: Block Sender

Block Sender's Domain

#### Dear authors:

Congratulations. Your article (7068P, N. Kanjanathaworn, C. Kaewsaneha, D. Polpanich, K. Jangpatarapongsa and P. Tangboriboonrat Composite Nanoparticles on the Natural Rubber Latex Glove for Reduction of Surface Friction and Cytotoxicity) submitted to AM2011 is now accepted by PPC.

The editor will send your proof later this year before they send it for publication.
Best wishes,
Sincerely yours,

## Prof. Dr. Shiquan LIU

School of Materials Science and Engineering University of Jinan (West Campus)
Jiwei Road 106
Jinan 250022, Shandong
China
tel:0086-(0)15953169792
fax:0086-531-87974453

## Composite Nanoparticles on the Natural Rubber Latex Glove for Reduction of Surface Friction and Cytotoxicity

N. Kanjanathaworn<sup>1,a</sup>, C. Kaewsaneha<sup>1,a</sup>, D. Polpanich<sup>2,b</sup>, K. Jangpatarapongsa<sup>3,c</sup> and P.Tangboriboonrat<sup>\*1,a</sup>

<sup>1</sup>Department of Chemistry, Faculty of Science, Mahidol University, Phyathai, Bangkok, Thailand <sup>2</sup>National Nanotechnology Center (NANOTEC), Thailand Science Park, Klong Luang, Pathumthani, Thailand

<sup>3</sup>Department of Clinical Microbiology, Faculty of Medical Technology, Mahidol University, Bangkok, Thailand

<sup>a</sup>scptb@mahidol.ac.th, <sup>b</sup>duangporn@nanotec.or.th, <sup>c</sup>mtkjp@mahidol.ac.th

Keywords: Composite, Surface modification, Rubber, Nanoparticle, Cytotoxicity

Abstract. Poly(methyl methacrylate) (PMMA) particles were deposited *via* the Layer-by-Layer technique onto sulphur prevulcanized natural rubber latex film grafted with polyacrylamide (SPNR-g-PAAm). Besides an increase in surface hardness and roughness, hence, decrease of the surface friction of SPNR glove, a direct contact between skin and rubber film was reduced. Consequently, it was expected that the allergic problem to certain sensitive individuals and cytotoxic potential caused by the leachable non-rubbers (proteins) and lubricant powder sprinkled onto SPNR glove would be lowered. The SPNR and SPNR-g-PAAm coated with PMMA particles were extracted by using the culture medium and subjected to the *in vitro* cytotoxicity evaluation on L-929 fibroblasts. Results showed that the cytotoxicity was effectively reduced by coating PMMA particles onto the grafted rubber film. In order to improve both the binding ability with SPNR and antimicrobial activity, the PMMA-chitosan core-shell particles were prepared for further depositing onto the non-grafted SPNR film. Moreover, the nanocapsules containing an aqueous core of disinfectant agent (chlorhexidine digluconate) and poly(methyl acrylate) or sulphur prevulcanized skim rubber shell were prepared for being embedded in SPNR glove.

## Introduction

Sulphur prevulcanized natural rubber (SPNR) latex is generally used as raw material for the gloves' production due to the good physical properties of thin film. However, the high surface friction between skin and glove still causes the drawback and powder talc or cornstarch is traditionally applied to solve this problem. Unfortunately, the lubricant powder is not appropriate for the gloves used in certain applications, e.g., in electronic and biomedical fields. Therefore, the mimetic system, i.e., the deposition of hard poly(methyl methacrylate) (PMMA) particles onto SPNR film grafted with poly(acrylamide) (SPNR-g-PAAm) *via* the Layer-by-Layer (LbL) technique, was investigated [1-4]. Besides effectively roughening the film surface, the presence of PMMA particles reduced the direct contact area between SPNR film and skin. Therefore, the allergic and cytotoxic potential caused by non-rubbers or additives would effectively decrease. However, the penetration from needle or sharp objects through the glove might lead to infection for the medical personnel who contact to blood or body fluids from patients [5]. The three-layer glove consisting of disinfectant or

antiseptic agent, i.e., aqueous chlorhexidine digluconate (CHD), incorporating between two elastomeric layers is, therefore, desired [6].

In this present work, the soap-free PMMA latexes and the PMMA latex particles stabilized by chitosan (PMMA-CS) were prepared and then deposited *via* the LbL technique onto the SPNR-g-PAAm and non-grafted SPNR sheets, respectively. The modified rubber was characterized by scanning electron microscope (SEM) and atomic force microscope (AFM). An *in vitro* test on L-929 fibroblast cells was used for investigation of the cytotoxicity of rubber film coated with PMMA particles. In addition, the nanocapsules of poly(methyl acrylate) (PMA) containing an aqueous solution of CHD were synthesized [6-8]. The aggregate of CHD-PMA nanocapsules was, subsequently, used as a core for the preparation of composite particle having sulphur prevulcanized skim latex (SPVS) particles as shell *via* the heterocoagulation technique. The coherent film of SPVS is expected to be miscible with the SPNR substrate when coating with these core-shell particles for further preparation of medical gloves.

## **Experimental**

**Latexes.** SPNR latex (Dr.Boo Co. Ltd., Thailand) was used for preparation of SPNR-g-PAAm [3,4]. SPVS was prepared from skim latex (5% dry rubber content) as described elsewhere [9].

**Preparation of PMMA and PMMA-CS latexes.** PMMA latexes with different sizes were prepared at 80°C for 2 h by the soap-free emulsion polymerization using potassium persulphate (0.18 g) dissolved in deionized water (137 g) and various MMA contents (0.18-3.28 M) [3]. The PMMA-CS particles were synthesized *via* the miniemulsion polymerization process at 80°C for 2 h by using 2,2' azobisisobutyronitrile as initiator, hexadecane as hydrophobe and oligochitosan (1% w/v in 0.1 M acetic acid) as stabilizer. The size and zeta potential of particle were measured by a Zetasizer (Malvern) while its morphology was observed under TEM (Phillips, EM 400).

**Preparation of CHD-PMA/SPVS composite particle.** CHD-PMA nanocapsules in cyclohexane, prepared *via* the modified nanoprecipitation technique, were redispersed in deionized water and 0.5% w/v sodium dodecyl sulphate (SDS) aqueous solution (1:1) to produce cationic and anionic nanocapsules, respectively [8]. The homocoagulated CHD-PMA at the weight ratio of cationic to anionic nanocapsules of 40:60 was used as a core of CHD-PMA/SPVS composite particle. Nonidet, a nonionic surfactant (10% w/w of dried nanocapsules) was adsorbed onto the aggregate and a known amount of 1% CHD-PMA(Nonidet) was mixed with 1% SPVS latex at pH 2 in an Erlenmeyer flask at room temperature. The blending ratio was calculated from the theoretical number (N<sub>max</sub>) [8,9]. The zeta potential and morphology of the CHD-PMA/SPVS composite latex particle under TEM were examined.

**Deposition of PMMA or PMMA-CS particles on rubber.** A piece of SPNR-g-PAAm or SPNR sheet, was dipped into PMMA or PMMA-CS latex. The sample was washed with Milli-Q water three times and dried at room temperature before being characterized. The surface coverage, a ratio of the area of deposited PMMA particles to selected area, was determined under SEM (Hitachi, S-2500). The surface morphology and roughness of the modified rubber were examined by using AFM. The SPNR and SPNR-g-PAAm coated with PMMA particles were extracted by the culture medium and subjected to the *in vitro* cytotoxicity evaluation on L-929 fibroblasts as previously explained [4].

## Results and discussion

**Effect of PMMA particles.** SEM and AFM techniques confirmed the adsorption of monodispersed PMMA particles onto the SPNR-g-PAAm surface in the form of monolayer [3]. With increasing average size of PMMA from 162, 364, 480 and 626 nm (at surface coverage of 12%), the

AFM in tapping mode indicated the increase in surface mean roughness from 50, 60, 80 and 89 nm and the decrease of friction coefficient from 2.0, 1.9, 1.6 and 1.4, respectively. Due to the decrease of contact area of the top surface of the sample, the presence of PMMA particles on the rubber surface would also cause the change in surface chemical compositions.

*In vitro* cytotoxicity test on L-929 fibroblasts. The SPNR and SPNR-g-PAAm coated with PMMA particles were extracted at 37°C for 24 h by using the culture medium. After mixing the extracts or the culture medium (negative control) with L-929 fibroblast cells for 6 days, the number of cell colonies when cells proliferated and theirs morphologies are shown in Fig. 1.

As compared to the negative control,  $\leq$  12.5% diluted sample slightly affected the growth inhibition of cells. When compared with the positive control (unmodified SPNR) at the extract concentrations  $\leq$  25%, the significant decrease of growth inhibition indicated that the cytoxicity was effectively reduced by the coating PMMA particles onto the SPNR-g-PAAm.

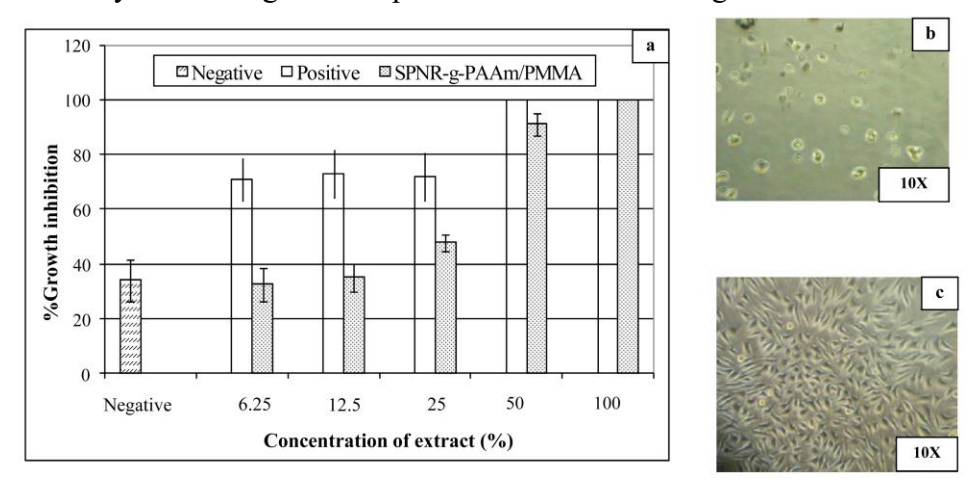


**Fig. 1** Growth inhibitions of L-929 fibroblasts as a function of concentrations of the extract of SPNR-g-PAAm/PMMA films compared with that of SPNR (positive control) (extraction time 24 h, 37°C) and of the medium without extract (negative control) (a), morphology of L-929 cells incubated with the extract of SPNR (b) and with that of SPNR-g-PAAm/PMMA (c) [4].

Surface modification of SPNR film by PMMA-CS particles. TEM image of monodisperse and spherical PMMA-CS particles (average size = 380 nm) is shown in Fig. 2(a). Theirs positive zeta potentials at pH ranging from 2 to 7 in Fig. 2(b) confirmed the presence of CS as the outer layer. These cationic particles could electrostatically attract the negative charges derived from non-rubbers (protein-lipid) at the surface of SPNR sheet as observed under SEM in Fig. 2(c). The formation of aggregates was possibly caused from the attractive capillary force between these particles during drying step [3]. In order to increase particle repulsion, various CS concentrations were added into the PMMA-CS latex. The increase in hydrodynamic volume of PMMA-CS after adding different CS concentrations was observed.

**Preparation of CHD-PMA/SPVS composite particles.** Before preparation of CHD-PMA/SPVS core-shell particle, the size of core was increased by homocoagulation of CHD-PMA nanocapsules having oppositely charges. When the weight ratio of cationic:anionic nanocapsules was 40:60, the largest size of homocoagulated CHD-PMA or aggregate of 415 nm with their zeta potential of -54 mV were obtained. The aggregate covered with Nonidet molecules having PEO moieties could form complex *via* hydrogen bonding at pH 2 with protein-lipid and/or SDS molecules on the SPVS shell particles. The zeta potentials of all blends at various ratios (N<sub>max</sub>, N<sub>max</sub>/2, N<sub>max</sub>/4 and N<sub>max</sub>/8) were

positive and reached the maximum value of +25.7 mV at  $N_{max}$ . This value which was vastly different from that of the CHD-PMA(Nonidet) (-19.6 mV) but approached that of SPVS particles (+40.8 mV) confirmed the presence of SPVS as the outer layer of the composite particles. The TEM micrographs of aggregate CHD-PMA(Nonidet) and CHD-PMA/SPVS composite particles at  $N_{max}$  before and after being heated at 40°C for 3 h are shown in Fig. 3.

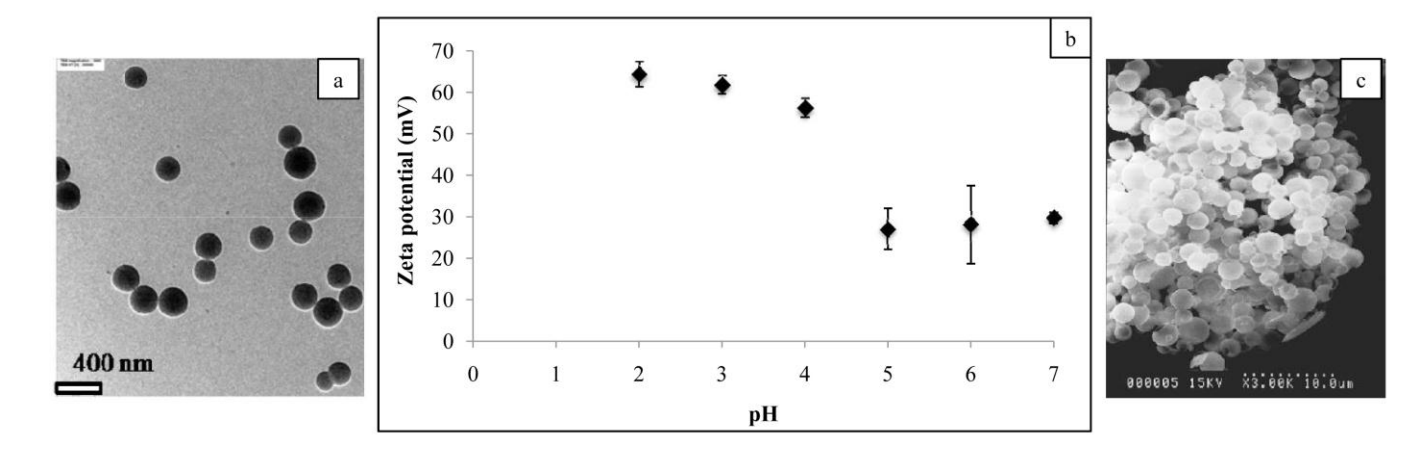


**Fig. 2** TEM micrograph (a), zeta potentials of PMMA-CS particles at different pH (b) and SEM micrograph of SPNR surface coated with PMMA-CS particles (c).

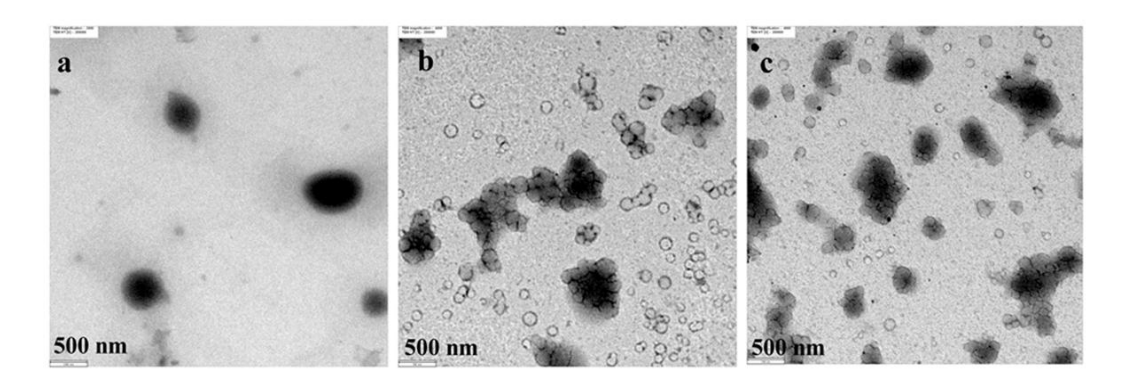


**Fig. 3** TEM micrographs of aggregate CHD-PMA(Nonidet) (a), CHD-PMA/SPVS composite particles before (b) and after being heated at 40°C for 3 h (c).

In Fig. 3(b), the CHD-PMA/SPVS composite particles consisted of the SPVS particles (light) surrounding an aggregate CHD-PMA(Nonidet) core (dark) as shown in Fig. 3(a). After raising the temperature to 40°C for 3 h, the SPVS particles were partially fused to provide the composite CHD-PMA/SPVS core-shell particle as shown in Fig. 3(c). The coherent film of the outer SPVS shell would be miscible with the SPNR film used as the substrate for further gloves' preparation.

## **Summary**

The cytotoxicity to L-929 fibroblast cells and surface friction of SPNR film were effectively reduced by coating with PMMA latex particles. With the aim to improve the binding ability with SPNR, antimicrobial and antiseptic activity, the PMMA-CS and the CHD-PMA/SPVS core-shell particles were successfully prepared. The deposition of these particles onto the non-grafted SPNR film for further gloves' preparation was under investigation.

## Acknowledgement

Research grant (RTA5180003) from The Thailand Research Fund (TRF)/the Commission on Higher Education (CHE) is gratefully acknowledged.

## References

- [1] A. Sruanganurak, K. Sanguansap, P. Tangboriboonrat: Colloid Surf. A Vol. 289 (2006), p. 110
- [2] A. Sruanganurak, P. Tangboriboonrat: Colloid Surf. A Vol. 301 (2007), p. 147
- [3] W. Anancharungsuk, W. Taweepreda, S. Wirasate, R. Thonggoom, P. Tangboriboonrat: J. Appl. Polym. Sci. Vol. 115 (2010), p. 3680
- [4] W. Anancharungsuk, D. Polpanich, K. Jangpatarapongsa, P. Tangboriboonrat: Colloid Surf. B Vol. 78 (2010), p. 328
- [5] R.G. Busnel, G. Argy: U.S. Patent 5,024,852. (1991)
- [6] S. Tanpantree, P. Opaprakasit, S. Loykulnant, W. Kangwansupamonkon,P. Tangboriboonrat: J. Appl. Polym. Sci. Vol. 117 (2010), p. 1798
- [7] U. Paiphansiri, P. Tangboriboonrat, K. Landfester: Macromol. Biosci. Vol. 6 (2006), p. 33
- [8] C. Kaewsaneha, P.Tangboriboonrat, D. Polpanich, S. Smanmoo: Macromol. Res. Vol. 18 (2010), p. 876
- [9] U. Paiphansiri, P. Tangboriboonrat: Colloid. Polym. Sci. Vol. 284 (2006), p. 251

# Preparation of Superparamagnetic Polystyrene-based Nanoparticles Functionalised by Acrylic Acid

Lalida Charoenmark<sup>1</sup>, Duangporn Polpanich<sup>2,\*</sup>, Raweewan Thiramanas<sup>2</sup> and Pramuan Tangboriboonrat<sup>1</sup>

<sup>1</sup>Department of Chemistry, Faculty of Science, Mahidol University, Bangkok 10400,

Thailand

<sup>2</sup>National Nanotechnology Center, National Science and Technology Development

Agency, Thailand Science Park, Pathumthani 12120, Thailand

\*Corresponding Author: Dr. Duangporn Polpanich

E-mail: duangporn@nanotec.or.th

Tel: +66 2564 7100 ext. 6564

Fax: +66 2564 6981

Running head: Superparamagnetic Polystyrene-based Nanoparticles Functionalised by Acrylic Acid

**Abstract:** 

This work aimed to reduce the steps used for preparing homogeneous and

functionalised magnetic polymeric nanoparticle (MPNP) under mild condition. Fe<sub>3</sub>O<sub>4</sub>

magnetic nanoparticle (MNP) was synthesised by the chemical co-precipitation of an

aqueous  $Fe^{3+}/Fe^{2+}$  solution with  $NH_4OH$  at room temperature under  $N_2$  atmosphere.

After dispersing MNP coated with oleic acid into a mixture of styrene (St) and acrylic

acid (AA) monomers, the MPNP functionalised with AA was directly produced via

the miniemulsion polymerisation without using magneto-template. When mixing a

crosslinking agent (divinyl benzene; DVB) with St and AA in the polymerisation

recipe, we obtained the homogeneous distribution of MNP (53%) in the PS/DVB

without the appearance of non-magnetic polymer particle. The

superparamagnetic MPNP was, therefore, fulfilled criteria for further use in bio-

related applications.

Keywords: Functionalisation, Magnetic nanoparticle, Miniemulsion polymerisation,

Polystyrene.

2

## Introduction

Magnetic nanoparticle (MNP) has attracted more and more scientific and technological interest because of its unique properties under applied magnetic field. In most applications, e.g., magnetically guided drug delivery, cell separation, protein purification and molecular diagnostics, monodisperse MNP is required in order to have uniform chemical and physical properties which depend strongly on particle size and size distribution. <sup>1,2</sup> To date, a range of techniques, e.g., the thermal decomposition and hydrothermal synthesis, have been developed for the preparation of MNP.<sup>3,4</sup> Among these techniques, the chemical co-precipitation is a cost-effective and simple method to produce the high yield of MNP. 5,6 Iron oxide MNP, i.e., magnetite (Fe<sub>3</sub>O<sub>4</sub>) or maghemite ( $\gamma$ -Fe<sub>2</sub>O<sub>3</sub>), is obtained from precipitating an aqueous Fe<sup>3+</sup>/Fe<sup>2+</sup> salt solution under base condition. The size, shape and composition of MNP can be controlled by the type of salt used, Fe<sup>3+</sup>/Fe<sup>2+</sup> ratio, reaction temperature, pH and ionic strength of the media. 1,6,7 The fraction of superparamagnetic components of cobalt ferrite (CoFe<sub>2</sub>O<sub>4</sub>) MNP decreased as the precipitation temperature increased with the increased particle size.<sup>8</sup> In addition, the selection of a proper surfactant is the key in the production of monodisperse iron oxide nanoparticle. It was reported that oleic acid (OA) is an effective surfactant to stabilise Fe<sub>3</sub>O<sub>4</sub> MNP. The co-precipitation method is conventional for grafting MNP with oleate or OA and for preventing the agglomeration of the ferrofluid or OA-MNP dispersed in organic solvent and nonpolar monomer. 9 When a monomer, e.g., styrene (St), containing OA-MNP is polymerised, magnetic polymeric nanoparticle (MPNP), a polymer encapsulating MNP, is obtained. The stability of MPNP in an aqueous solution derived from the added ionic surfactant or hydrophilic polymer and functionalised monomer can be the conjugation site for attachment MPNP with biomolecules. 10 The MNP functionalised

by glucuronic acid was covalently attached to specific primer for detection of *BCR/ABL* fusion gene in chronic myelogenous leukemia with high sensitivity and high specificity.<sup>11</sup>

In order to obtain monodisperse MPNP with high magnetic content, miniemulsion polymerisation is one of the most effective methods used for encapsulating MNP.<sup>12</sup> By using this polymerisation technique, the stable monomer droplets with 50-500 nm in diameter are generated when applying ultrasonic. Since the particle nucleation occurs primarily within the droplets, the size of MPNP is controlled via the size of the initial emulsion. Moreover, the hydrophobic inorganic particles can be directly dispersed in the monomer phase. The MPNP with the magnetic content of 20-40%wt was obtained by polymerisation of St miniemulsion containing OA/sodium dodecyl sulphate (SDS) bilayer stabilised magnetite. 13 The magnetic content was increased when a two-step preparation route including ferrofluid droplet preparation and swelling of the droplets with monomer were applied. 10 Recently, the less complicated process using minidroplet of Fe<sub>3</sub>O<sub>4</sub> dispersed in octane as the magneto-template miniemulsion polymerisation of St-divinyl benzene (DVB) has been applied for producing uniform-sized MPNP with high magnetic content. 12 However, the presence of octane in the Fe<sub>3</sub>O<sub>4</sub> minidroplet induced the phase separation of polystyrene (PS) from the magneto-template due to the low viscosity of the polymerisation medium. The use of monomer as a dispersed phase of the MNP was found to be an effective way to solve this problem. 12,14

With the aim of reducing the steps used for preparing homogeneous and functionalised MPNP under mild condition, we synthesised Fe<sub>3</sub>O<sub>4</sub> MNP *via* the coprecipitation method at room temperature using OA as stabiliser. Then, the prepared MNP was mixed with St/AA or St/DVB/AA monomer which was subsequently

polymerised *via* the miniemulsion process without using magneto-template. The effects of OA and DVB on the final morphology of the prepared MPNP were considered. Their crystallographic structure, composition and magnetisation were determined. Distribution of the MNP into PS/AA or PS/DVB/AA was investigated under Transmission Electron Microscope (TEM). The amount of AA presented in PS/DVB/AA-MNP was also examined *via* the conductometric back titration technique.

## **Experimental**

Materials. St (Fluka, Purum) and AA (Fluka, Purum) monomers were purified by passing through aluminium oxide column and distilled under reduced pressure. The purified monomers were stored in a refrigerator at 4°C until use. Anhydrous FeCl<sub>3</sub> (Riedle-de Haen), FeCl<sub>2</sub>·4H<sub>2</sub>O (Fluka, Purum), NH<sub>4</sub>OH solution (25%v/v) (Merck, AR), OA (Fluka, Natural from suet), SDS (Fluka, GC), potassium persulphate (KPS; Fluka, Puriss), hexadecane (HD; Fluka, Purum), DVB (Merck), NaOH (Lab-scan, AR), HCl (Merck, GR) and methanol (Merck, AR) were used without further purification. Deionised water was used throughout this work.

Preparation of MNP and MPNP. FeCl<sub>3</sub> (2.92 g) and FeCl<sub>2</sub>.4 H<sub>2</sub>O (1.76 g) were dissolved in milli-Q water (80 ml) under nitrogen atmosphere while stirring at 400 rpm. After adding NH<sub>4</sub>OH solution (40 ml), the mixture immediately turned to black. The reaction was allowed to continue under centrifugation (Beckman; JA 20) at 5,000 rpm for 15 min. The precipitate MNP was mixed with St (15 ml) and OA (10 %v/v based on St) with stirring for 10 min. The ferrofluid (OA-MNP-St) was centrifuged at 5,000 rpm for 15 min to remove large aggregate. Then the upper phase

containing stable MNP was separated into 2 portions. The first portion of OA-MNP-St (7.0 g) was mixed with St monomer (3.0 g) whereas the second one was repeatedly washed with methanol to remove excess OA before redispersing in St (1.5 g)/DVB (1.0 g). In both cases, AA (3% wt based on St) and HD (0.3 g) were added. After sonication for 2 min, each mixture was poured into an aqueous solution of SDS (0.072 g of SDS in 24.0 g of deionised water) under continuous stirring for 1 h for preemulsification. It was then ultrasonicated for 10 min at 60% amplitude (Vibracell, VCX 700) in an ice bath. After raising temperature to 72°C, an aqueous solution of KPS (0.1 g KPS in 2 g of deionised water) was introduced into the reaction mixture to start the polymerisation. The reaction was left for 22 h under nitrogen atmosphere. The obtained PS/AA-MNP and PS/DVB/AA-MNP were purified by dialysis method (pore size of dialysis membrane = 25.5 mm, MWCO = 6,000-8,000 Da) before being characterised.

Characterisations of MNP and MPNP. X-ray powder diffraction (XRD; Rigaku TTRAX III, 18kW) with a high power  $CuKa_{\alpha}$  X-ray source was used to investigate the crystallographic structure of the prepared MNP and MPNP. The phases of sample were identified through the Power Diffraction File (PDF) database (JCPDS, International Centre for Diffraction Data). The average crystallite size of MNP was calculated from the Debye-Sherrer equation, <sup>15</sup>

$$D = \frac{0.9\lambda}{\beta\cos\theta} \tag{1}$$

where D is average crystallite size (Å),  $\lambda$  is X-ray wavelength (CuKa $_{\alpha}$ :  $\lambda$ =1.5418 Å),  $\beta$  is the full width at half maximum (FWHM) (in radians) and  $\theta$  is the Bragg diffraction angle.

Thermogravimetric analysis (TGA; Mettler Toledo, SDTA851), Fourier transform infrared spectroscopy (FTIR; Perkin Elmer, Spectrum GX) and Zetasizer (Malvern, Nano ZS) were applied to determine the magnetic content, composition and zeta potential of the prepared MNP and/or MPNP, respectively. Vibrating sample magnetometer (VSM; Lakechore, 7403) was used for recording the magnetisation curve. The magnetic moment of each sample was examined over a range of applied magnetic field from -10 to 10 kOe. Particle morphology and selected area electron diffraction (SAED) pattern of the MNPs were observed under TEM (JEOL, JEM-2010).

For determination of surface charge density (σ) representing the amount of ionised groups existing on the surface of MPNP, the conductimetric back titration was applied. The PS/DVB/AA-MNP (500 μl) was dispersed in deionised water (25 ml) under stirring. Excess amount of 1 M NaOH (50 μl) solution was added into the sample before being titrated with 1 M HCl aqueous solution. The conductivity was measured by using conductimeter (ORION, 180) equipped with a glass conductivity cell (K=1). The number of microequivalent of acid groups per gram ([Acid]) were calculated by using the following equation, <sup>17</sup>

$$\left[Acid\right] = \frac{V_{HCI} \cdot M_{HCI} \cdot 10^{3}}{V_{part} \left(ml\right) \cdot \frac{SC_{part}}{100}} \quad \left(\mu eq/g\right)$$
(2)

where  $V_{HCl}$  is volume of HCl at equivalent point (ml),  $V_{part}$  is sample volume (ml),  $M_{HCl}$  is concentration of HCl (M) and  $SC_{part}$  is solid content of the magnetic latex. The  $\sigma$  value of latex was calculated from equation (3),

$$\sigma = \frac{\rho_{\text{part}}}{6} \cdot D_{\text{h}} \cdot [\text{Acid}] \cdot N_{\text{A}} \cdot e \qquad (\mu \text{C/cm}^2)$$
 (3)

where  $\rho_{part}$  is density of MPNP,  $D_h$  is particle diameter (cm),  $N_A$  is Avogadro's number  $(6.022 \times 10^{23} \text{mol}^{-1})$  and e is electronic charge in coulombs  $(1.602 \times 10^{-19} \, \text{C})$ .

## **Results and Discussion**

MPNP functionalised by PAA was prepared in two stages: i) synthesis of initial ferrofluid or OA-MNP-St and ii) polymerisation of St/AA-MNP or St/DVB/AA-MNP. Each step was followed by characterisation of the product including crystallographic structure, morphology, chemical composition and magnetisation.

Preparation and Characterisations of MNP. Fe<sub>3</sub>O<sub>4</sub> was synthesised at room temperature through the chemical co-precipitation of the mixture of Fe<sup>3+</sup>/Fe<sup>2+</sup> at stoichiometric ratio of 2:1 in order to avoid the formation of nonmagnetic hydroxides (Fe(OH)<sub>2</sub> and Fe(OH)<sub>3</sub>).<sup>14,18</sup> The MNP obtained from using NH<sub>4</sub>OH as the precipitator should have better crystallinity, smaller size and higher magnetisation than that using NaOH due to the gradual change of the reaction conditions.<sup>2</sup> It was observed that the resulted MNP was dense, black in colour and strongly attracted by a magnet. The critical oxidation of magnetite to maghemite was prevented by bubbling nitrogen gas through the solution. Since the as-prepared MNP could be flocculated mainly due to the Van der Waals force, its surface was subsequently modified by using OA through esterification with the hydroxyl group on the particle. After adding into OA mixed with St monomer, the brownish ferrofluid was stable due to the steric stabilisation generated from the hydrophobic tail of OA turned to the St phase while its carboxylated groups anchored on the surface of iron oxide nanoparticle.<sup>14,19</sup>

The crystallinity of OA-MNP was indicated in the XRD pattern shown in Figure 1(A). The position and relative intensity of the peaks at 220, 311, 400, 422,

511 and 440 matched well with the standard patterns of the magnetite Fe<sub>3</sub>O<sub>4</sub> with inverse cubic spinel structure.<sup>2,9</sup> The results, therefore, confirmed the successful synthesis of Fe<sub>3</sub>O<sub>4</sub>. By using the Debye-Scherrer equation, equation (1), the calculated size of the OA-MNP was 8.9 nm which was similar to that determined by TEM (9 nm) as shown in Figure 1(B). This revealed that each individual particle was a single crystal.<sup>20</sup> It could be assumed from the square form of the particle that the inhibition factor for the crystal growth of the particle was absent.<sup>21</sup> The good dispersion of the particle resulted from the OA coated on the particle surface. In addition, the distinct rings which are the characteristics of polycrystalline sample of the SAED pattern are observed in Figure. 1(C). This indicated that the structure of the prepared MNPs composed of domains whose crystallograghic axes randomly oriented.<sup>22</sup> The pattern correlated well with that of XRD pattern in Figure 1(A).

\_\_\_\_\_\_

Figure 1.

------

The chemical composition of the OA-MNP was analysed by FT-IR and the spectrum of OA-MNP compared to that of MNP is presented in Figure 2.

-----

## Figure 2.

-----

In Figure 2(A), the characteristic absorption peaks at 437 and 582 cm<sup>-1</sup> relating to the stretching vibration of Fe-O bond of Fe<sub>3</sub>O<sub>4</sub> before coating with OA were observed. Whereas, the new absorption peaks at 1708 cm<sup>-1</sup> corresponding to the C=O stretching vibration of ester bond appeared in Figure 2(B). This indicated that the carboxylic group of OA was esterified with the hydroxyl group on the surface of the MNP. The peaks at 2852 and 2923 cm<sup>-1</sup> can be attributed to the stretching of saturated C-H bond of OA. From this analysis, it was evident that the as-prepared MNP was Fe<sub>3</sub>O<sub>4</sub> which chemically bound to OA.

The magnetic and OA contents of the OA-MNP were determined by TGA and the thermograms are shown in Figure 3.

-----

## Figure 3.

-----

In Figure 3(A), one-step decay at temperature less than 120°C was ascribed to water evaporation from the MNP. In the case of OA-MNP, the detection of two-step decay in Figure 3(B) indicated the presence of two types of OA. The first weight loss of 11.1% at less than 400°C corresponded to the physically adsorbed OA in the outer layer. The second one of 8.4% at 400-500°C was resulted from the inner layer of OA that covalently bound to the MNP surface. Thus, the residual weight loss of 80.5% was owed to the magnetic content. Based on the mean diameter (9 nm) and magnetite density (5.16 g/cm³) of the MNP, the calculated area occupied by an OA molecule

was  $0.31 \text{ nm}^2/\text{molecule}$  which was slightly less than the mean molecular area occupied by a single OA molecule ( $\sim 0.42 \text{ nm}^2/\text{molecule}$ ).<sup>23</sup>

Preparation and Characterisations of MPNP. The PS/AA-MNP was prepared by polymerisation of St/AA containing OA-MNP (without removing excess OA) and HD. On contrary, the excess OA was removed by repetitive washing with methanol before preparation of PS/DVB/AA-MNP. In both cases, HD acted as hydrophobe to suppress the Oswald ripening in the miniemulsion system while DVB was used as crosslinker only in the latter case. TEM micrographs of the prepared PS/AA-MNP and PS/DVB/AA-MNP are shown in Figures 4(A) and (B), respectively.

-----

## Figure 4.

\_\_\_\_\_

In both micrographs, the PS/AA-MNP and PS/DVB/AA-MNP were spherical in shape with an average size of 148±38 and 117±28 nm and polydispersity index (PDI) of 1.2 and 1.1, respectively. The phase separation between magnetite and PS matrix, previously observed when using the conventional OA/octane-based ferrofluid, was suppressed. However, the non-magnetic PS/AA particles (light phase), i.e., free from magnetic material (dark spot), and the inhomogeneous distribution of MNPs within each PS/AA-MNP particle are noticed in Figure 4(A). The formation of non-magnetic particle might be due to the immiscibility between the excess OA in the OA-MNP-St and PS. It was reported that the large amount of OA in the ferrofluid droplets could act as poor solvent for PS chains and the low viscosity of polymer matrix enhanced the possibility of non-magnetic PS/AA particle formation. Therefore,

the abundant OA was removed before polymerisation of St/DVB/AA. Since DVB is a crosslinking agent of PS, the internal viscosity of the magnetic St/DVB/AA-MNP particles would increase during polymerisation. The homogeneous distribution of MNP in the PS/DVB/AA matrix without non-magnetic polymer particle was obtained accordingly. The previous work showed that the optimum concentration of DVB to produce the uniform distribution of MNP and to eliminate the non-magnetic polymer particle was about 20-40 wt% relative to total amount of monomer. 12 Hence, 40% of DVB based on St monomer was used in this present work. As expected, Figure 4(B) displays that MNPs were completely incorporated into the PS/DVB/AA, i.e., neither free magnetite nor the non-magnetic polymer particle appeared. The high viscosity caused from the presence of DVB inside the particle kept the Fe<sub>3</sub>O<sub>4</sub> nanoparticle from moving outward. It was reported that, even the St monomer was replaced with methyl methacrylate, the well-dispersed MNP into polymer matrix containing DVB was still obtained. 12 The results confirmed that combination of the removal of the excess OA and the addition of DVB was the key role to produce the homogeneous distribution of MNP in the polymer matrix without pure polymer particle formation. Additionally, AA tended to be on the particle surface due to its hydrophilic nature. Consequently, poly(acrylic acid) (PAA) chain and/or oligomer that formed during the polymerisation was imparted electrosteric stabilisation. Since the AA monomer was added into the reaction at the initial period before pre-emulsification, the polymerisation step in our study was reduced when compared to the previous work. Although, some carboxyl groups might be buried in the polymer matrix, most of them possibly remained on the particle surface and provided the colloidal stability of the PS/AA-MNP and PS/DVB/AA-MNP particles. This was supported by the zeta potential values of the particles which were -63.3±1.8 and -49.8±1.1 mV for PS/AA-MNP and PS/DVB/AA-

MNP, respectively. With increasing the amount of AA more than 3% based on monomer content, the MPNP was not stable possibly due to the bridging effect originated from long PAA chains.

Owing to its satisfied morphology, the PS/DVB/AA-MNP was systematically characterised. Figure 5(A) illustrates its XRD pattern which revealed that the crystallographic structure of MNP contained in the PS/DVB/AA matrix after polymerisation did not change compared to that in Figure 1(A). The low intensity peak at  $2\theta$  less than 25 degree, which related to the amorphous polymer matrix, was additionally observed. <sup>18,26</sup>

------

## Figure 5.

-----

The magnetic content which is a very important factor to alter the respond speed of the MPNP to an external magnetic field was determined from TGA and its thermogram is shown in Figure 6(A).

## Figure 6.

------

In Figure 6(A), the two-step weight loss was observed. The first peak of 8.4% between 150 and 300°C was attributed to the dehydration and decomposition of residual surfactant and HD. The weight loss of 38.8% between 300 and 500°C was mainly due to the decomposition of polymer matrix.<sup>24</sup> Therefore, the magnetic content

deduced from the residual weight percentage of PS/DVB/AA-MNP was 53%. Due to the high magnetic content, the MPNP (10%v/v) could be completely separated from the aqueous phase under an externally applied magnetic field within only 3 min, as shown in Figure 6(B).

The magnetic properties of the PS/DVB/AA-MNP compared to those of the MNP and OA-MNP were investigated by VSM at room temperature and the magnetisation curves are displayed in Figure 7.

-----

#### Figure 7.

-----

From Figures. 7(A)-(C), the magnetisation versus magnetic field of the MNP, OA-MNP and PS/DVB/AA-MNP exhibited no hysteresis with undetectable remanence and coercivity at room temperature. This confirmed that all samples had superparamagnetic behaviour at room temperature. The superparamagnetism enables the nanoparticles to respond to an applied magnetic field without any permanent magnetisation and rapidly redisperse after removal of the magnetic field. Under applying a large external magnetic field, the magnetisation of the particle aligns with the field direction and reaches its saturation value. The saturation magnetisation (M<sub>s</sub>) values of the MNP, OA-MNP and PS/DVB/AA-MNP were 47.4, 36.5 and 17.4 emu/g, respectively. The presence of OA and PS/DVB/AA matrix reduced the M<sub>s</sub> value possibly because the surfactant and polymer substances changed the surface anisotropy of MNP, which led to the increase in surface spin disorientation resulting in the reduction of the magnetic moment.<sup>27</sup>

With the objective of further use of the prepared MPNP as a solid support for immobilisation of biomolecules, the amount of –COOH functional group originated from AA onto the PS/DVB/AA-MNP surface were quantified. Therefore, the surface charge density ( $\sigma$ ) of the MPNP was determined by the conductimetric back titration technique. The titration result of the PS/DVB/AA-MNP is presented in Figure 8.

-----

#### Figure 8.

\_\_\_\_\_

In Figure 8, the three different intervals in the conductimetric back titration curve were observed. The rapid descending curve appeared in the first interval I corresponded to the neutralisation of excess  $OH^-$ ions of NaOH previously added causing a decrease in conductivity of the system to the first minimum point. Then, the increase in the volume of HCl to the second minimum point in interval II related to the titration of acidic groups ( $COO^-$  from AA and  $SO_4^-$  from KPS initiator) at the particle surface. Finally, the ascending back titration curve in the last interval III corresponded to the excess of HCl added. The difference of HCl volume between the two minimum points of the back titration curve (about 1.1 ml) was used to calculate the [Acid] and the  $\sigma$  value of PS/DVB/AA-MNP which were 919±97  $\mu$ eq/g and 832±87  $\mu$ C/cm², respectively. Our previous work revealed that the  $\sigma$  value of poly(styrene-co-acrylic acid) (St/AA) increased with increasing the amount of AA added in the reaction. Due to the presence of the surface carboxyl group, the prepared PS/DVB/AA-MNP would potentially coupled with biomolecules for further applying in a wide variety of biological applications.

#### **Conclusions**

MNP coated with OA (OA-MNP) having an average size of 9 nm and 80.5% of the magnetic content was simply prepared by adding NH<sub>4</sub>OH into an aqueous Fe<sup>3+</sup>/Fe<sup>2+</sup> (2:1) solution at room temperature. Through ultrasonication, the OA-MNP dispersed in St/AA or St/DVB/AA was directly emulsified for the synthesis of MPNP *via* the miniemulsion polymerisation. The use of DVB to crosslink the PS matrix enhanced the integrity of the MPNP and, hence, provided more uniform distribution of MNP without any non-magnetic polymer particle. The MPNP (53% of magnetic content) was superparamagnetic and, thus, appropriate for biomedical applications after suitable surface modification.

# Acknowledgements.

Research grant (RTA5180003) from The Thailand Research Fund/Commission on Higher Education to P.T. and the scholarship from Thailand Graduate Institute of Science and Technology (TGIST)/National Science and Technology Development Agency to L.C. are gratefully acknowledged. The authors also thank Dr. Metha Rutnakornpituk for helpful comments and suggestions.

#### References

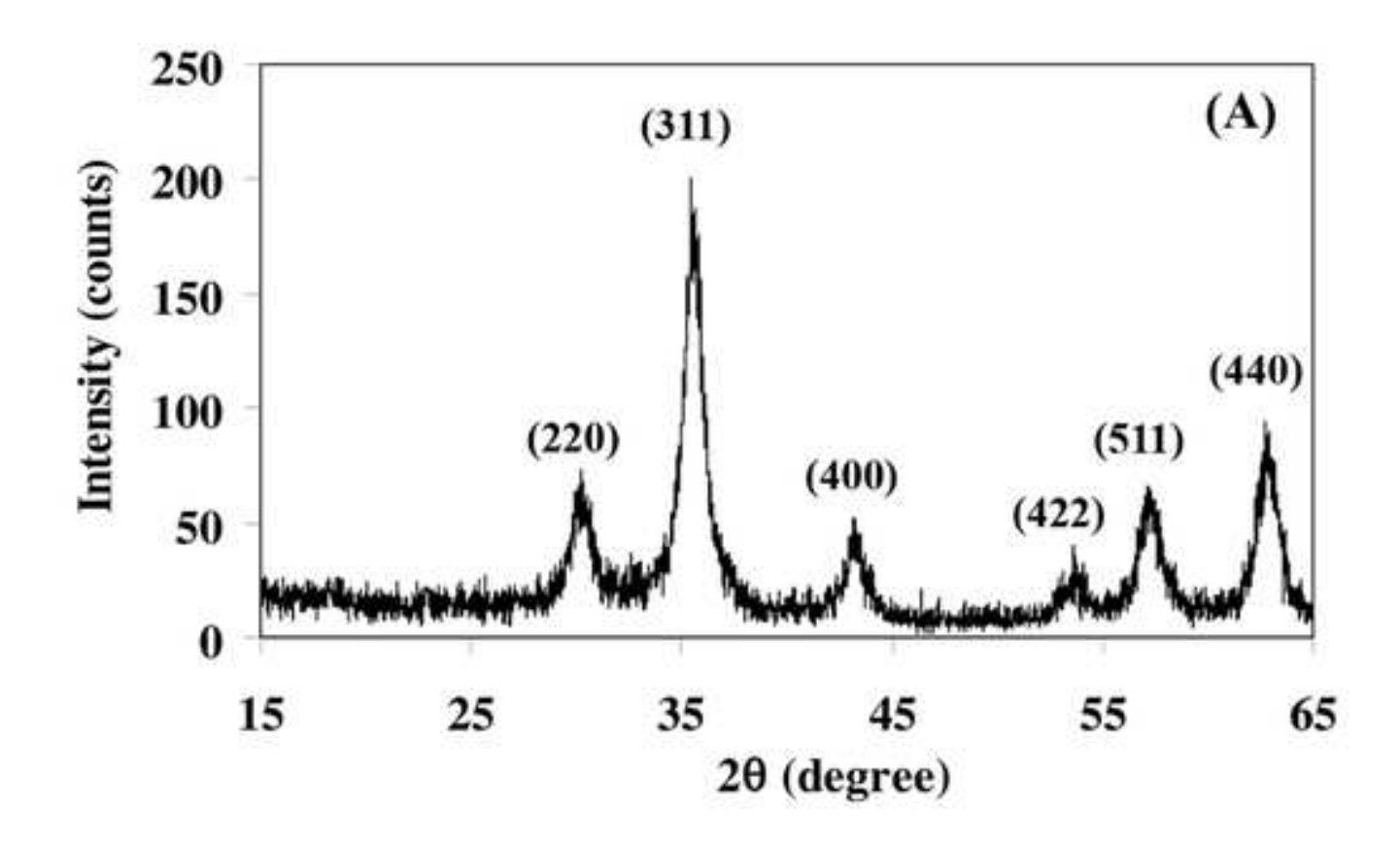
- (1) S. Laurent, D. Forge, M. Port, A. Roch, C. Robic, L.V. Elst, and R.N. Muller, *Chem. Rev.*, **108**, 2064 (2008).
- (2) R.Y. Hong, J.H. Li, H.Z. Li, J. Ding, Y. Zheng, and D.G. Wei, *J. Magn. Magn. Mater.*, **320**, 1605 (2008).
- (3) Z.P. Chen, Y. Zhang, S. Zhang, J.G. Xia, J.W. Liu, K. Xu, and N. Gu, *Colloids Surf. A: Physicochem. Eng. Aspects*, **316**, 210 (2008).
- (4) S. Xuan, L. Hao, W. Jiang, X. Gong, Y. Hu, and Z. Chen, *J. Magn. Magn. Mater.*, **308**, 210 (2007).
- (5) J.H. Wu, S.P. Ko, H.L. Liu, M.-H. Jung, J.H. Lee, J.-S. Ju, and Y.K. Kim, Colloids Surf. A: Physicochem. Eng. Aspects, 313-314, 268 (2008).
- (6) A.-H. Lu, E.L. Salabas, and F. Schüth, *Angew. Chem. Int. Ed.*, **46**, 1222 (2007).
- (7) A.K. Gupta, and M. Gupta, *Biomaterials*, **26**, 3995 (2005).
- (8) Y.I. Kim, D. Kim, and C.S. Lee, *Physica B*, **337**, 42 (2003).
- (9) W. Jiang, Y. Wu, B. He, X. Zeng, K. Lai, and Z. Gu, *J. Colloid Interface Sci.*, **347**, 1 (2010).
- (10) F. Montagne, O. Mondain-Monval, C. Pichot, and A. Elaissari, *J. Polym. Sci. Part A: Polym. Chem.*, **44**, 2642 (2006).
- (11) K. Jangpatarapongsa, D. Polpanich, V. Yamkamon, Y. Dittharot, J. Peng-On, R. Thiramanas, S. Hongeng, S. Jootar, L. Charoenmak, and P. Tangboriboonrat, *Analyst*, **136**, 354 (2011).
- (12) T. Gong, D. Yang, J. Hu, W. Yang, C. Wang, and J.Q. Lu, *Colloids Surf. A: Physicochem. Eng. Aspects*, **339**, 232 (2009).
- (13) L.P. Ramírez, and K. Landfester, Macromol. Chem. Phys., 204, 22 (2003).

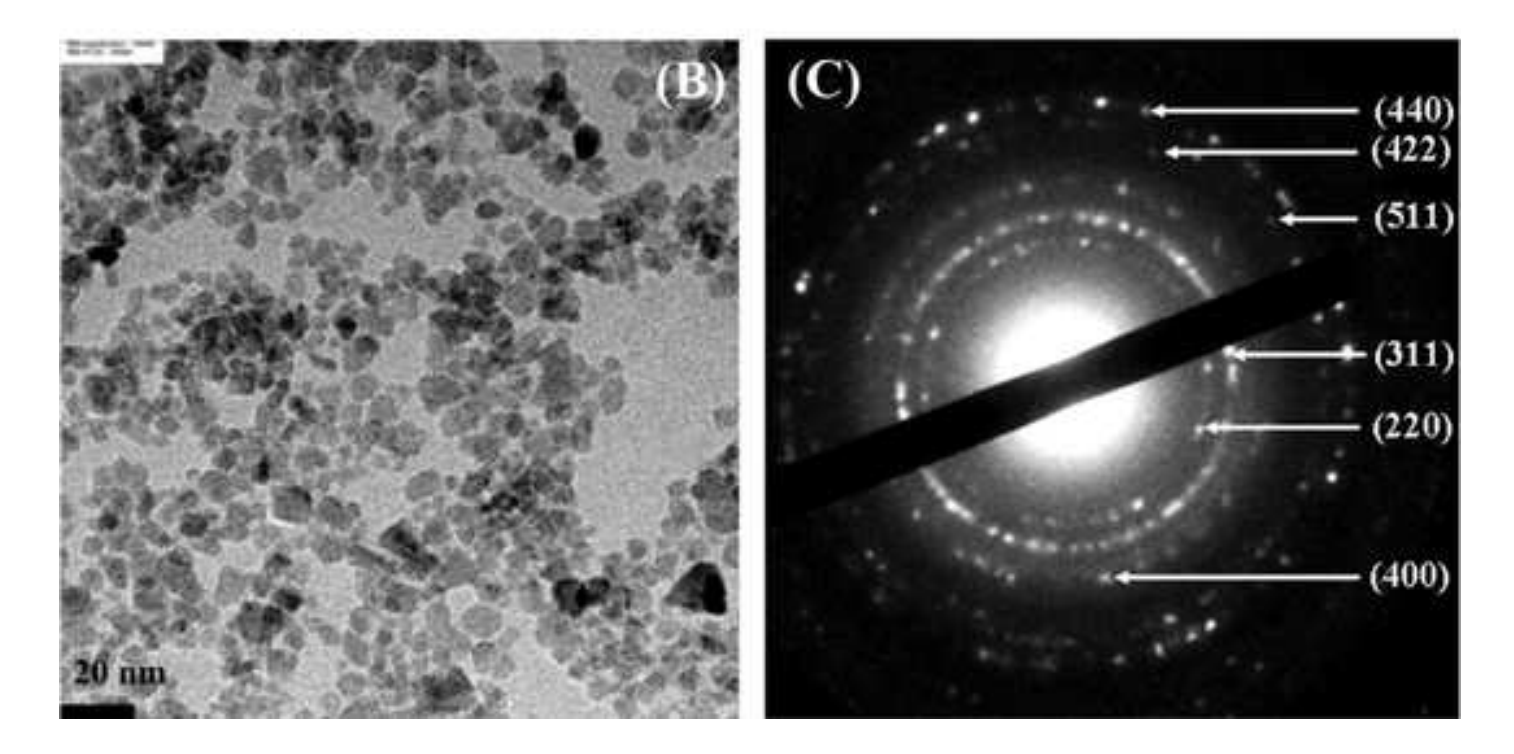
- (14) N. Joumaa, P. Toussay, M. Lansalot, and A. Elaissari, *J. Polym. Sci. Part A: Polym. Chem.*, **46**, 327 (2008).
- (15) Y.-D. Luo, C.-A. Dai, and W.-Y. Chiu, J. Appl. Polym. Sci., 112, 975 (2009).
- (16) D. Polpanich, P. Tangboriboonrat, and A. Elaissari, *Colloid Polym. Sci.*, **284**, 183 (2005).
- (17) S. Braconnot, C. Hoang, H. Fessi, and A. Elaissari, *Mater. Sci. Eng. C*, **29**, 624 (2009).
- (18) C.-L. Lin, C.-F. Lee, and W.-Y. Chiu, J. Colloid Interface Sci., 291, 411 (2005).
- (19) S. Meerod, G. Tumcharern, U. Wichai, and M. Rutnakornpituk, *Polymer*, **49**, 3950 (2008).
- (20) S. Sun, H. Zeng, D.B. Robinson, S. Raoux, P.M. Rice, S.X. Wang, and G. Li, *J. Am. Chem. Soc.*, **126**, 273 (2004).
- (21) L. Babes, B. Denizot, G. Tanguy, J.J. Le Jeune, and P. Jallet, *J. Colloid Interface Sci.*, **212**, 474 (1999).
- (22) H. Yan, J. Zhang, C. You, Z. Song, B. Yu, and Y. Shen, *Mater. Chem. Phy.*, **113**, 46 (2009).
- (23) L. Bromberg, L. Chen, E.P. Chang, S. Wang, and T.A. Hatton, *Chem. Mater.*, **22**, 5383 (2010).
- (24) Z. Qian, Z. Zhang, and Y. Chen, J. Colloid Interface Sci., 327, 354 (2008).
- (25) K. Landfester, and L.P. Ramírez, J. Phys.: Condens. Matter, 15, S1345 (2003).
- (26) C. Yang, Q. Shao, J. He, and B. Jiang, *Langmuir*, **26**, 5179 (2010).
- (27) S. Wang, Y. Zhou, S. Yang, and B. Ding, *Colloids Surfaces B: Biointerfaces*, **67**, 122 (2008).

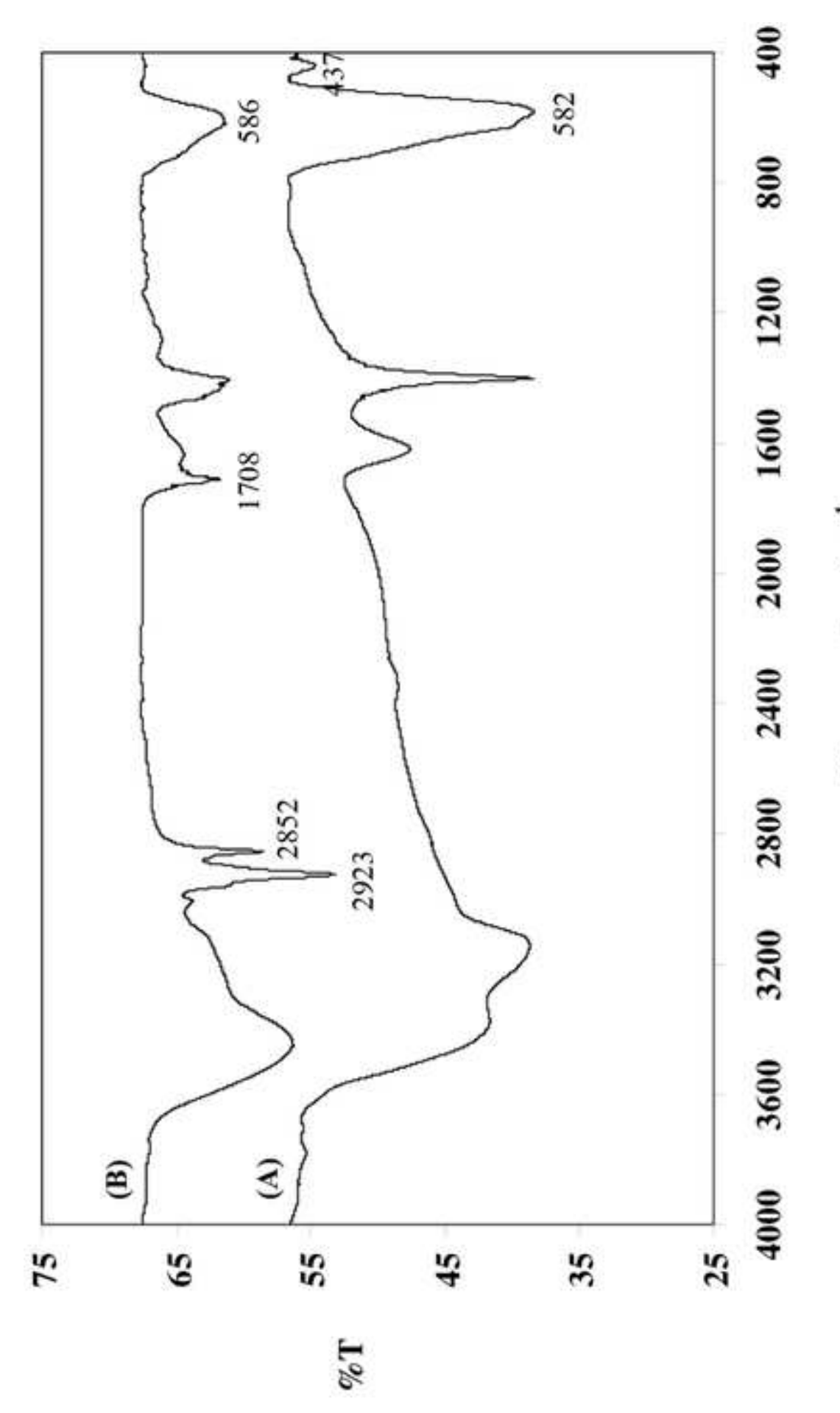
#### **FIGURE CAPTIONS**

- Figure 1. (A) XRD pattern, (B) TEM micrograph and (C) SAED of the OA-MNP.
- Figure 2. FT-IR spectra of (A) MNP and (B) OA-MNP.
- Figure 3. TGA thermograms of (A) MNP and (B) OA-MNP.
- Figure 4. TEM micrographs of (A) PS/AA-MNP and (B) PS/DVB/AA-MNP.
- Figure 5. XRD pattern of PS/DVB/AA-MNP.
- **Figure 6.** (A) TGA thermogram of PS/DVB/AA-MNP and (B) photographic images of the PS/DVB/AA-MNP before and after applying magnetic field.
- **Figure 7.** Magnetisation curves of (A) MNP, (B) OA-MNP and (C) PS/DVB/AA-MNP measured by VSM at room temperature.
- Figure 8. Conductimetric back titration curve of PS/DVB/AA-MNP.

Figure 1
Click here to download high resolution image







Wavenumber (cm<sup>-1</sup>)

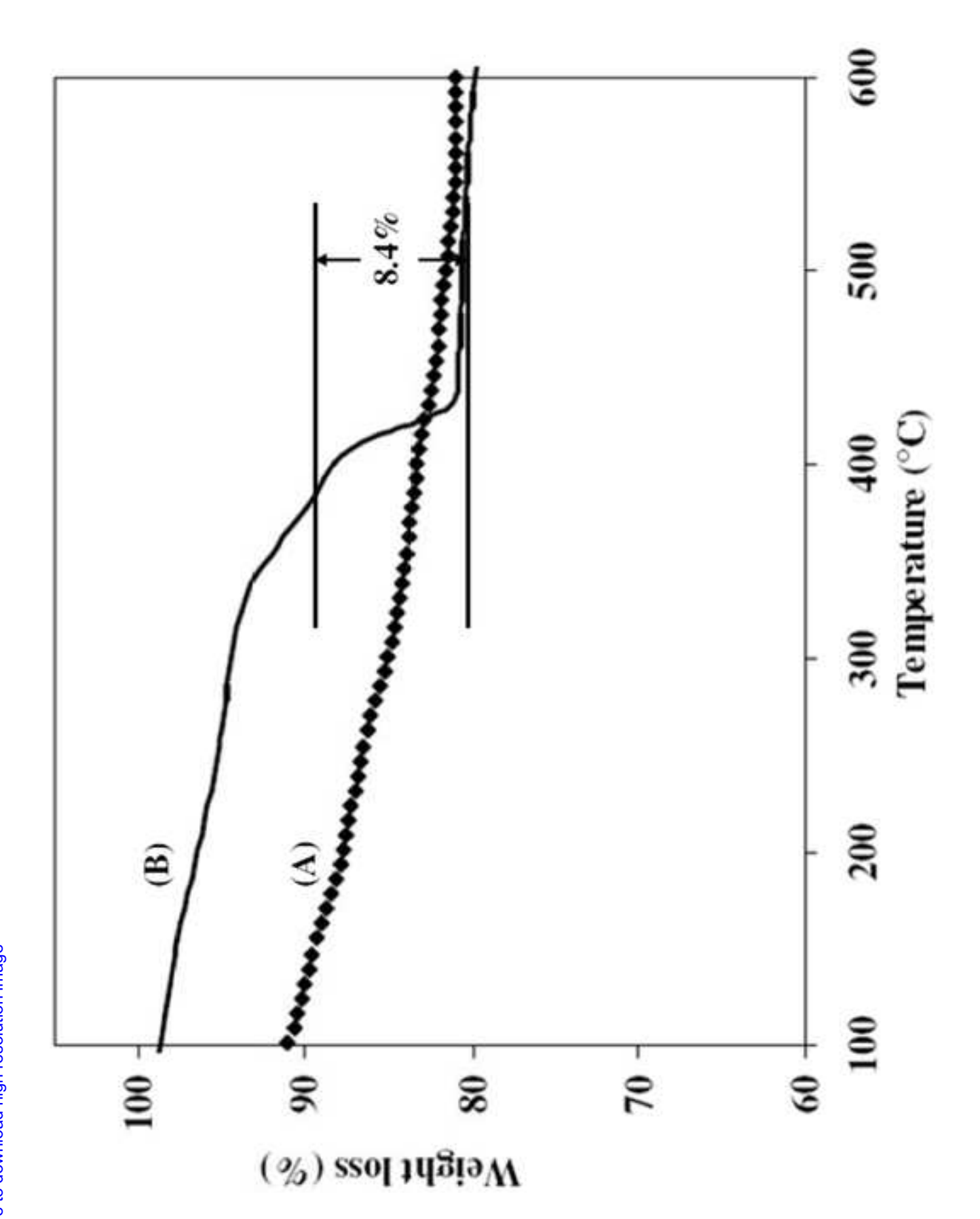
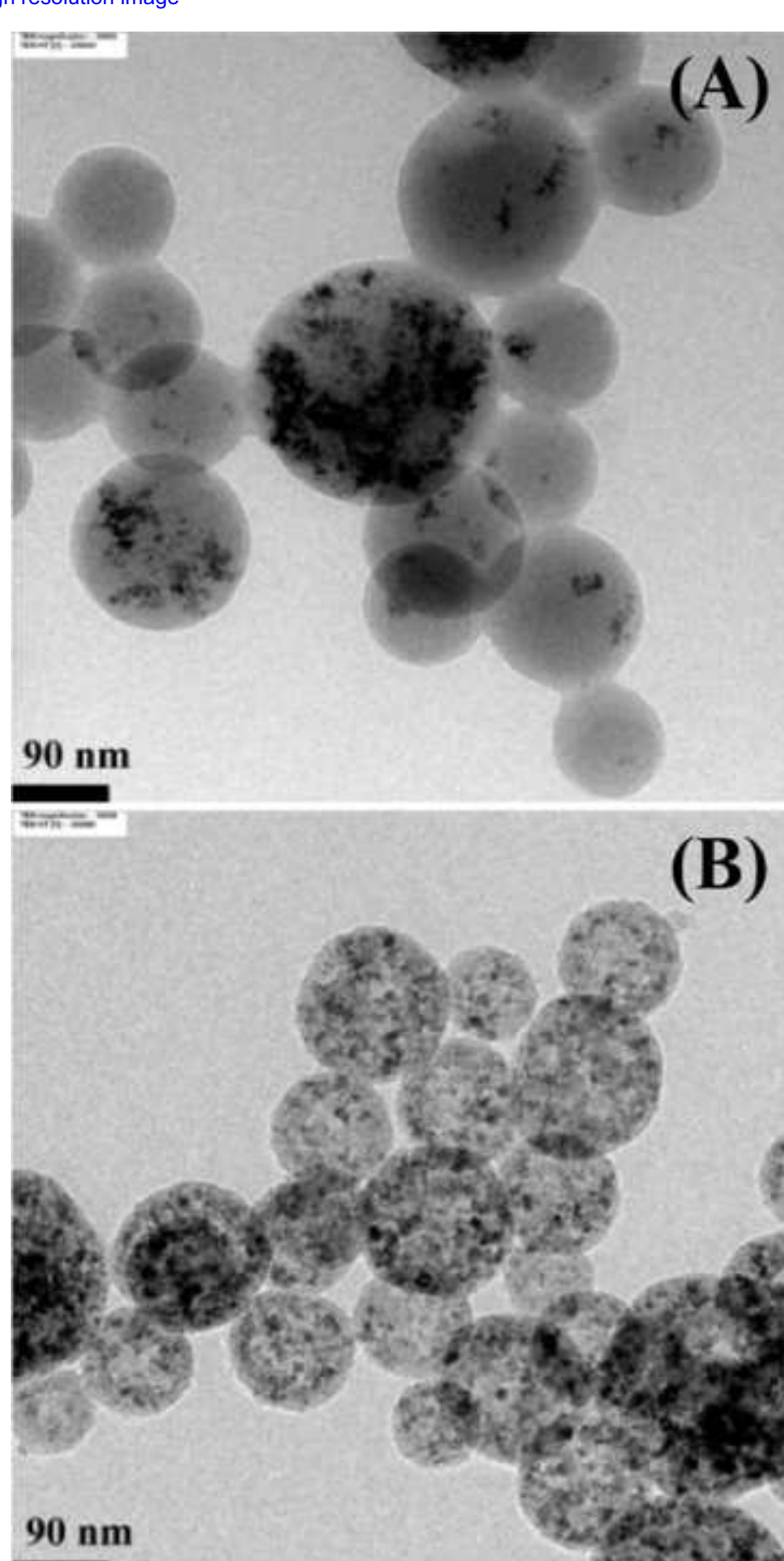


Figure 4
Click here to download high resolution image



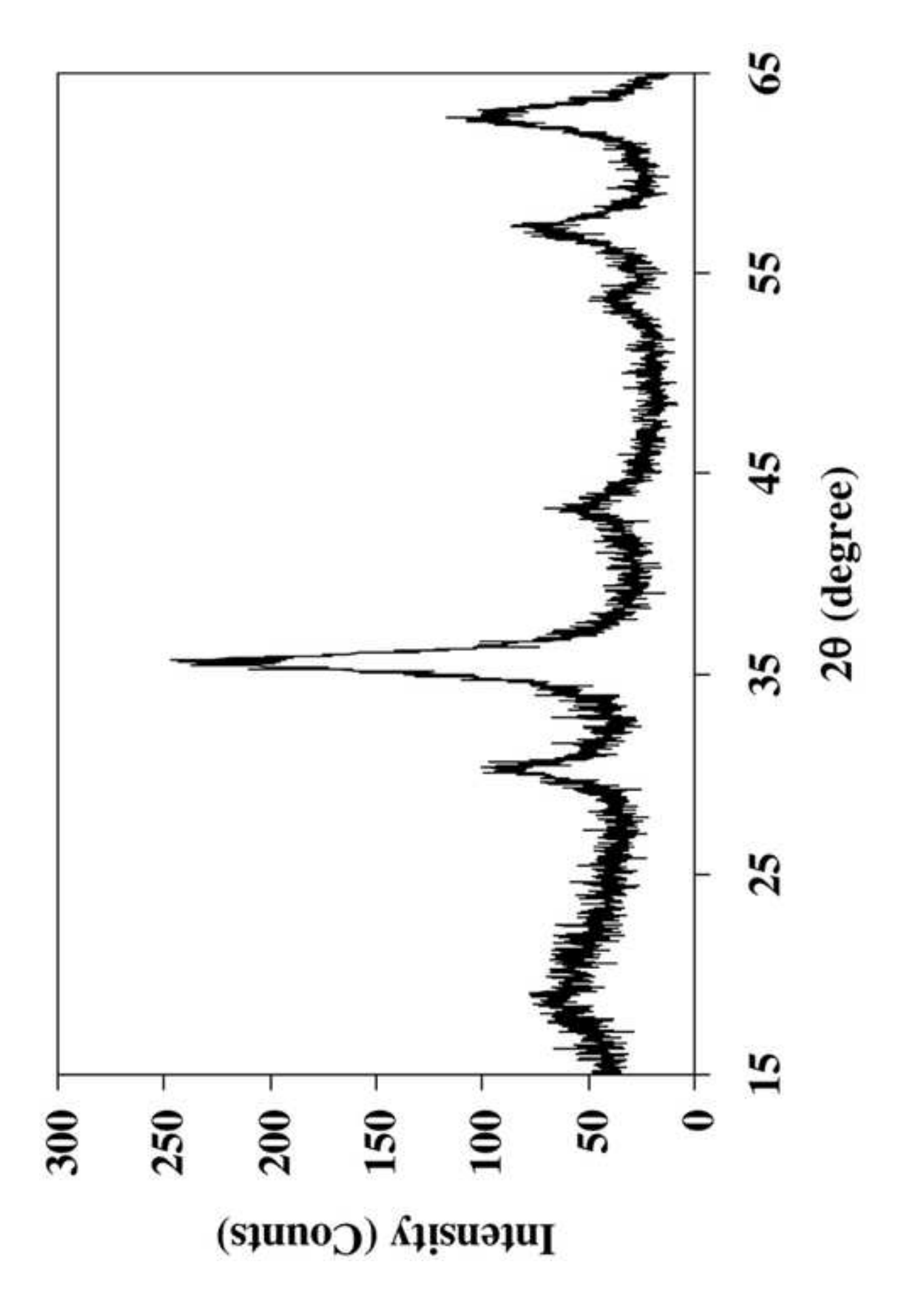
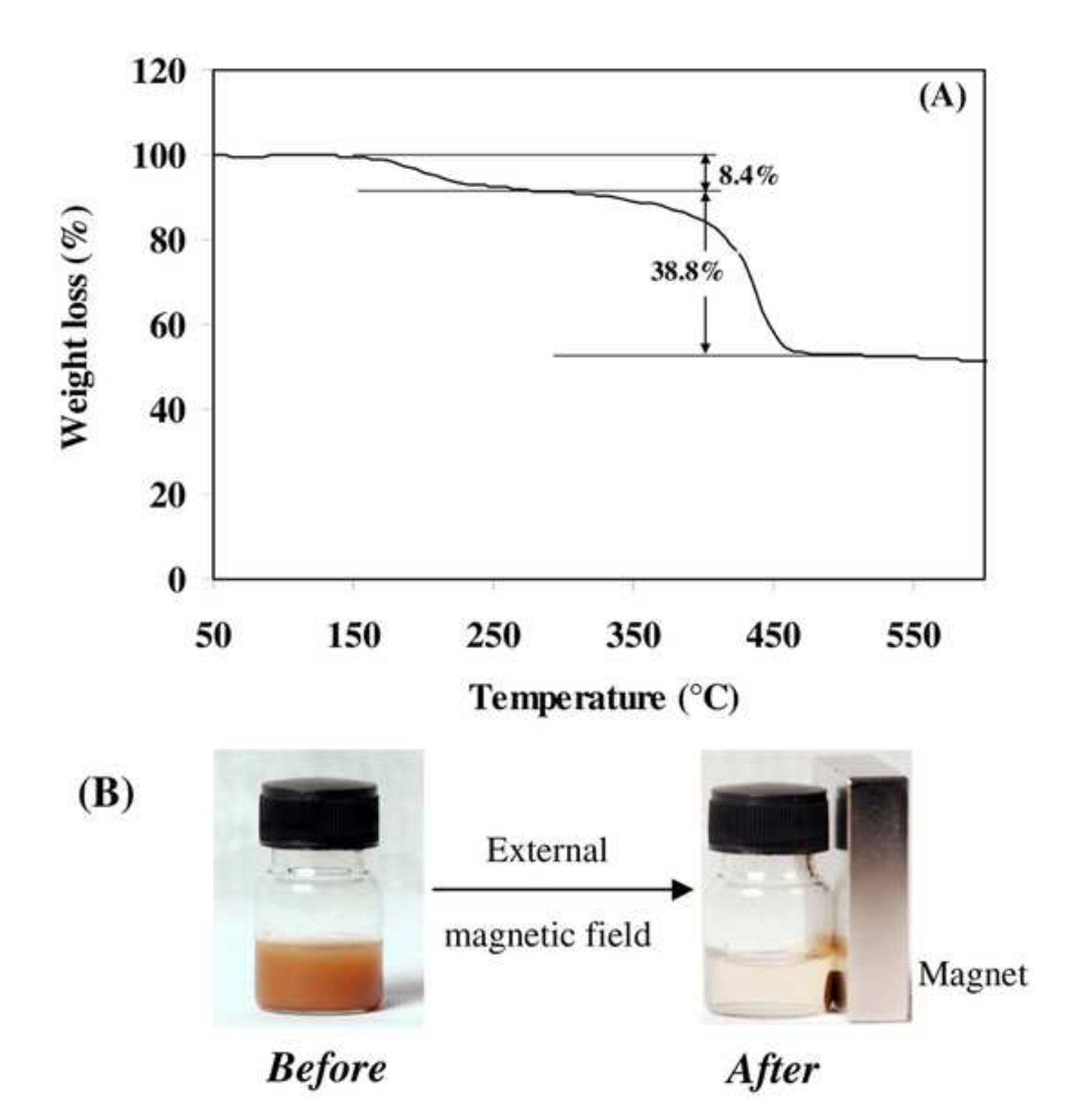
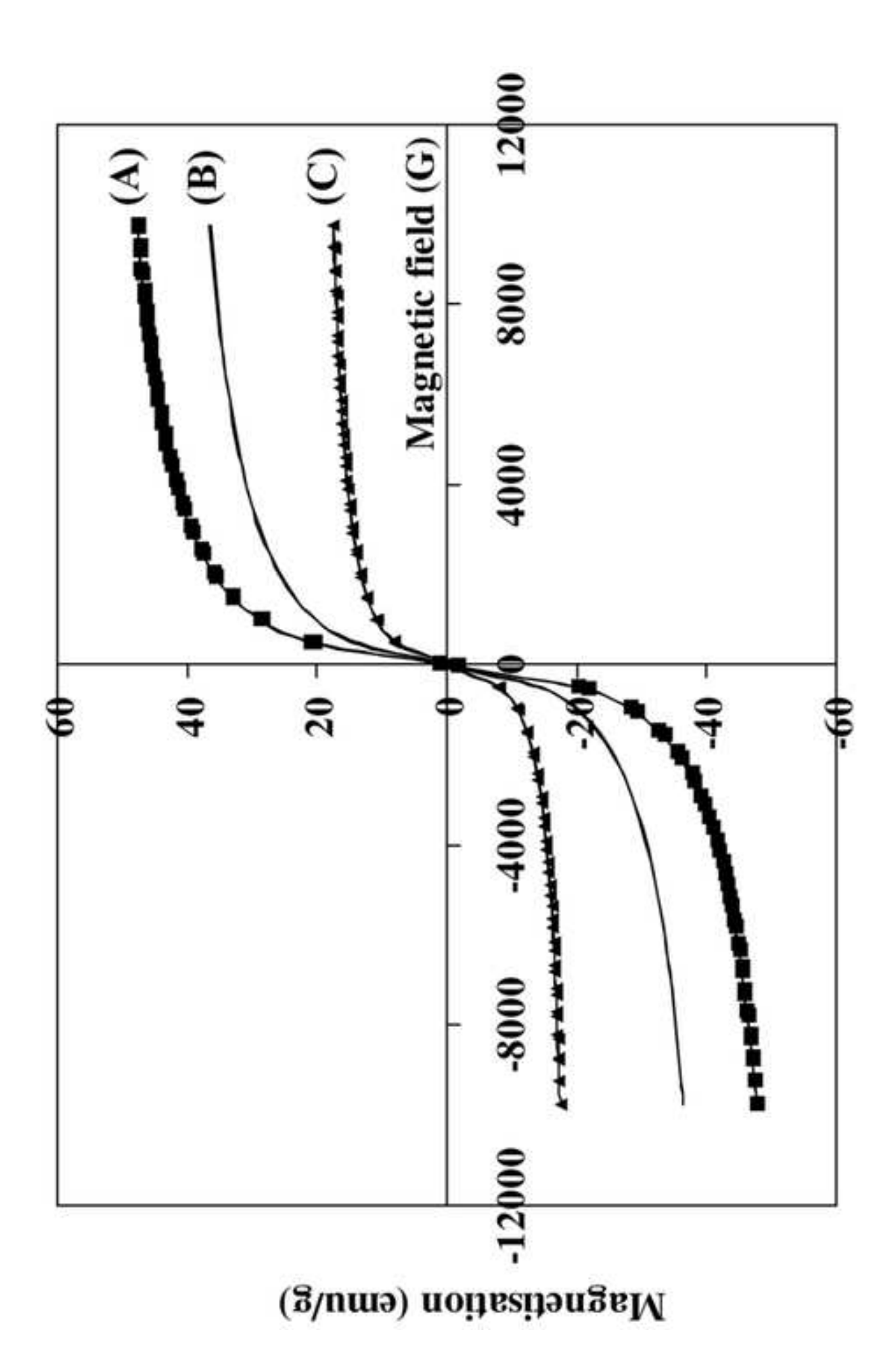
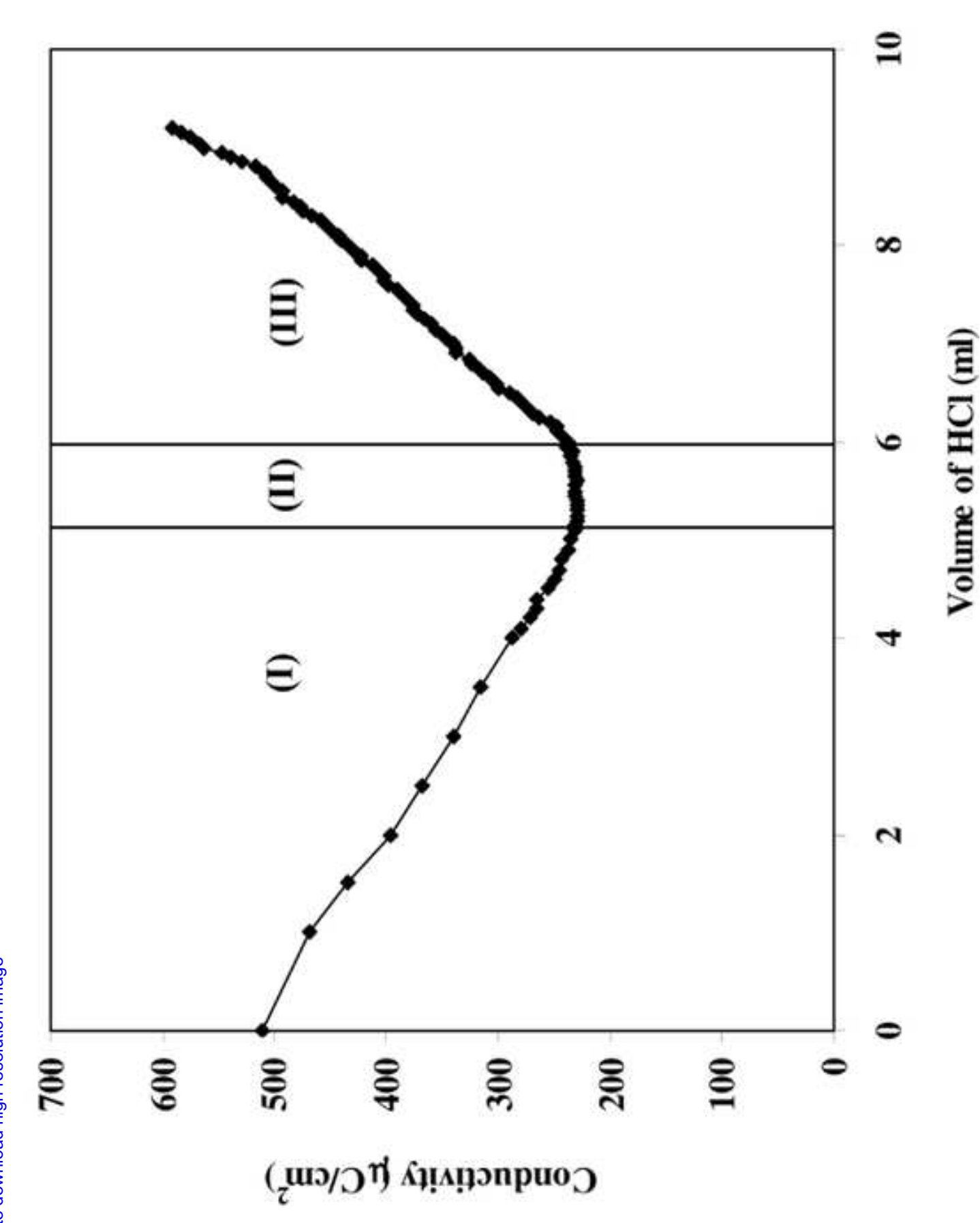


Figure 6
Click here to download high resolution image







# Professor Chulhee Kim Editor-in-Chief

Department of Polymer Science and Engineering, Inha University Incheon, Korea chk@inha.ac.kr

June 6, 2011

Dear Professor Chulhee Kim,

Attached please find the manuscript titled "Preparation of Superparamagnetic Polystyrene-based Nanoparticles Functionalised by Acrylic Acid" submitted for publication as a research article in Macromolecular research.

The manuscript aimed to reduce the steps used for preparing homogeneous and functionalised magnetic polymeric nanoparticle (MPNP) under mild condition. Magnetic nanoparticles (MNPs) coated with oleic acid (OA) were synthesised by coprecipitation technique. Then, they were incorporated into polystyrene/acrylic acid (PS/AA) or PS/divinyl benzene/AA (PS/DVB/AA) matrix by using miniemulsion polymerisation process without using magneto-template. The prepared MNP and MPNP were systematically characterised. The effects of OA and DVB on the final morphology of the prepared MPNP were considered. Results confirmed that the combination of the removal of the excess OA and the addition of DVB was the key role to produce the homogeneous distribution of MNP in the polymer matrix without pure polymer particle formation. The PS/DVB/AA-MNP (53% of magnetic content) was superparamagnetic and, thus, appropriate for biomedical applications after suitable surface modification.

The work described in the manuscript is original and has never been submitted for publication or presented elsewhere. The manuscript has been prepared according to the instructions for authors. It is believed that the work described in the manuscript would highly benefit the scientific community due to its usefulness and wide application. We sincerely hope that the manuscript will be favorably considered for publication.

Yours sincerely,

Duangporn Polpanich
Dr.
Corresponding Author
National Nanotechnology Center
National Science and Technology Development Agency
111 Thailand Science Park
Pathumthani
Thailand 12120

Tel 66 2 564 7100 ext. 6564 Fax 66 2 564 6981

#### "turn-on" chemosensor selective based dansylsalicylaldehyde Schiff base for Cu2+ ion detection

Srung Smanmoo,\*a Weerachai Nasomphan and Pramuan Tangboriboonrat

Received (in XXX, XXX) Xth XXXXXXXXX 200X, Accepted Xth XXXXXXXX 200X

5 First published on the web Xth XXXXXXXX 200X

DOI: 10.1039/b000000x

A novel "turn-on" fluorescence chemosensor based on dansvl Schiff base derivative (1) has been simply prepared for the detection of Cu2+ ion. 1 exhibited a remarkable blue shift of 10 emission upon the addition of Cu<sup>2+</sup> ion in CH<sub>3</sub>CN/H<sub>2</sub>O.

Molecular recognition of heavy metals is one of the active research areas in supramolecular chemistry. Of transition metal ions, Cu<sup>2+</sup> ion is one of the important metals both in physiological 15 and environmental systems. It involves various enzymatic processes as a cofactor. However, high concentration of Cu<sup>2+</sup> ion leads to cytoxicity and many diseases, e.g. Wilson, leukemia, and dyslexia. ref Cu<sup>2+</sup> ion is known for the correlation to Alzheimer's

Over the past decade, the development of selective Cu<sup>2+</sup> ion fluorescence chemosensor receives much research attention. However, these sensors are usually cross-selective with other metal ions, e.g.  $Hg^{2+}$ ,  $Ag^{+}$  and  $Pb^{2+}$  ions.<sup>2</sup> Besides, the sensors exhibit an "off-type" mode in which their fluorescence intensities 25 are quenched by either i) an energy or electron transfer<sup>3</sup> or ii) an enhancement of spin-orbit coupling.4 The disadvantages of fluorescence quenching are due to high signal output and the differentiation of spectra of similar complexes with time-resolved fluorometry.5 For the issue of sensitivity, a chemosensor whose 30 fluorescence emission maximum is enhanced or changed upon the complex with metal ions is highly desired. Cu<sup>2+</sup> ion induced fluorescence enhancement (a "turn-on" type) chemosensors have been reported, However, those sensors require complicated synthetic manipulations and some of them are completely 35 dissolved in organic solvents.6

In recent years, several dansyl-based chemosensors have been developed for the sensitive and selective detection of various metal ions. Dansyl moiety is popularly chosen as an intramolecular charge transfer (ICT) fluorophore due to its highly 40 sensitive fluorescence response to the surrounding environment. In a polar solvent (e.g. water), dansyl fluorophore shows weak fluorescence emission while strong fluorescence and a blue shift of emission are observed in nonpolar solvents.

The design of metal induced fluorescence enhancement 45 chemosensor needs serious consideration. In general, an "ontype" chemosensor requires a minimized fluorescence quenching process while the corresponding process is in the minimization at the metal-bound state.<sup>5</sup> We have deliberately designed a simple yet highly selective chemosensor based on a dansyl Schiff base 50 for Cu<sup>2+</sup> ion. Imine and 2-hydroxyl groups serve not only as donors for the good coordination to Cu<sup>2+</sup> ion, but they also facilitate and maximize the contact between the dansyl fluorophore and a bound Cu<sup>2+</sup> ion. The intramolecular corporation of dansyl and salicylaldehyde unit is intended in such 55 that the binding of Cu<sup>2+</sup> ion with 1 induces photophysical changes of the system. To the best of our knowledge, among few "turnon" fluorescence chemosensors for Cu2+ ion, none of the dansylsalicylaldehyde Schiff base sensors has been ever reported.

1 was simply prepared in one step from the reaction between 60 2-hydroxybenzaldehyde and dansyl hydrazine in distilled water (Scheme 1). After the reaction mixture was left stirring under nitrogen atmosphere for 24 hours, crude dansyl receptor 1 was obtained and crystallized from ethyl acetate/hexane to afford pure 1 in 92% yield. The structure of 1 was confirmed by 'H NMR, 65 13C NMR and HRMS (ESI†). The imine group present in 1 is known as an active functional group which shows a strong affinity towards the transition metals.<sup>8</sup> This is due to the special characteristic of the imine group in providing geometric and cavity control to the metal ion complex. Consequently, the 70 lipophilicity, selectivity and sensitivity are enhanced. 9 The presence of dansyl sulfonamide proton (C=N-NH) in 1 is proposed for the responsibility in stabilizing the cationic adduct resulting from the complex between 1 and Cu<sup>2+</sup> ion.<sup>10</sup>

Scheme 1 Synthesis of 1

The photophysical property of 1 was investigated in CH<sub>3</sub>CN. The emission spectra of 1, when excited at 350 nm, displayed the 85 maximum at 547 nm which is the characteristic emission of dansyl chromophore. 11 As previously described, the fluorophore of Cu2+ ion sensors is generally quenched due to the paramagnetic effect via an energy or electron transfer process. 12 However, upon the addition of Cu<sup>2+</sup> ion, 1 exhibited a blue shift 90 (hypsochromic shift) of the emission maximum to 479.5 nm with fluorescence enhancement (Fig. 1a). The new blue shift of emission at 479 nm was made possible by the coordination of Cu<sup>2+</sup> ion by 1. The blue shift of 1 was evident by the emission

color changing from yellow to blue (Fig. 1b). In the presence of other transition metal ions including physiological metal ions  $(Mn^{2+}, Cd^{2+}, Zn^{2+}, Ag^+, Ni^{2+}, Pb^{2+}, Co^{2+}, Fe^{2+})$ , the fluorescence emission of 1 exerted no change. The addition of  $Hg^{2+}$  ion 5 resulted in a slight blue shift in 1's emission (to 534 nm) with fluorescence quenching. After the addition of  $Fe^{3+}$  ion, there was no hypsochromic shift of 1's fluorescence emission. However, a substantial decreasing of fluorescence intensity was observed.

The efficiency of a blue shift of 1's emission in the presence of  $\operatorname{Cu}^{2+}$  ion was confirmed by the fluorescence intensity ratio  $(F_{479nm}/F_{537.5nm})$  where  $F_{479nm}$  and  $F_{537.5nm}$  are the fluorescence intensities of 1 with respect to the wavelength at 479 nm and 537.5 nm. It was shown that 1 exhibited remarkable selectivity in response to  $\operatorname{Cu}^{2+}$  ion, while other transition metal ions displayed no response (ESI†).

Next, the quantitative data of 1 was obtained. 1 was titrated against various concentrations of  $Cu^{2+}$  ion. When it was observed that increasing in concentrations of  $Cu^{2+}$  ion resulted in a blue shift of 1's emission with a slight enhancement. The blue shift could be noticed when 1 equiv of  $Cu^{2+}$  ion was added. Continuing addition of  $Cu^{2+}$  ion gradually increased the fluorescence intensity of 1. After the addition of  $25 \times 10^{-5}$  M  $Cu^{2+}$  ion, the fluorescence intensity of 1 reached the maxima and exhibited no significance in fluorescence enhancement (Fig. 2).

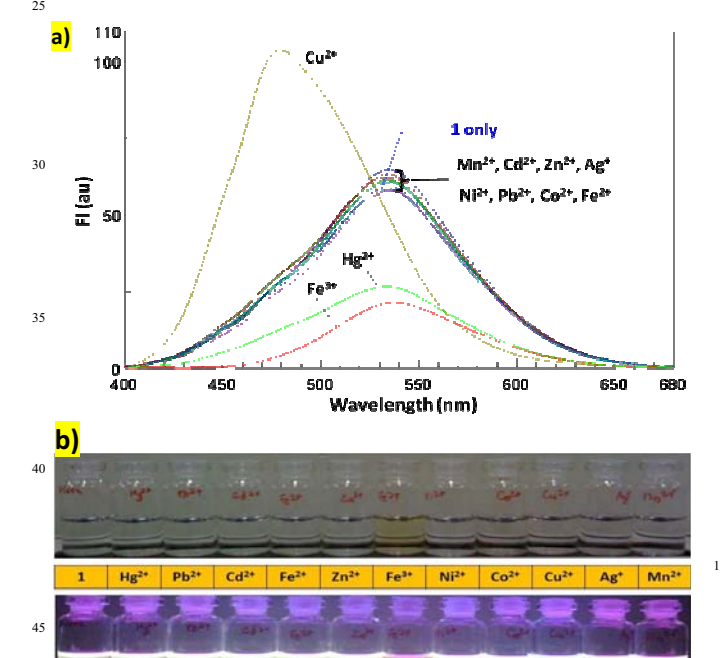


**Fig. 1** Fluorescence emission spectra of **1** in the presence of so various transition metal ions. [**1**] =  $2.5 \times 10^{-5}$  M, [ion] =  $25 \times 10^{-5}$  M, CH<sub>3</sub>CN/H<sub>2</sub>O (1:1, v/v). Excitation wavelength was 365 nm.

It is documented that some fluorescence dyes once aggregated result in either a bathochromic (J-type) or ss hypsochromic (H-type) shift of the emission band. Comparing to our case, the blue shift of 1 upon the addition of Cu<sup>2+</sup> ion is proposed based on an ICT process.

An attempt to determine the binding ratio between 1 and  $\text{Cu}^{2+}$  ion by mass spectroscopic technique was unsuccessful.

Therefore, the binding analysis by the method of continuous variations (Job's plot) which indicated the binding ratio between 1 and  $\text{Cu}^{2+}$  ion at 1:1 (ESI†). The association constant,  $K_{assoc}$  was estimated by a nonlinear curve fitting of the fluorescence titration data of 1 and found at  $1.68 \times 10^{-7} \text{ M}^{-1}$  which demonstrated the strong affinity between 1 and  $\text{Cu}^{2+}$  ion (ESI†). 14

The metal competing experiment was accomplished. This could provide the information on the selectivity of **1** in the presence of Cu<sup>2+</sup> with other co-existing metal ions. Results from Fig. 3 indicated that the hypsochromic shift of **1** by Cu<sup>2+</sup> ion was not influenced by the addition of other transition metal ions.

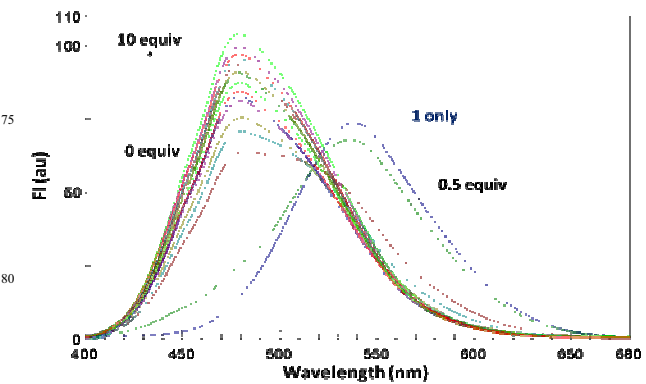


Fig. 2 Fluorescence titration of 1 with increasing concentrations  $^{85}$  of  $\text{Cu}^{2^+}$  ion.

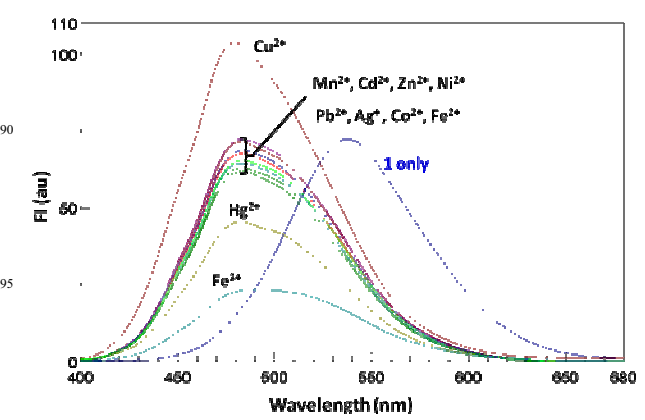


Fig. 3 Fluorescence emission spectra of 1 ( $2.5 \times 10^{-5}$  M) and 1 in the presence of respective metal ions (10 equiv) in responses of 1 containing Cu<sup>2+</sup> ion to different metal ions in CH<sub>3</sub>CN/H<sub>2</sub>O (1:1, v/v). Excitation wavelength was 366 nm.

In order to get a better insight into the coordination between 1 and  $Cu^{2+}$  ion,  $^1H$  NMR experiment was conducted (Fig. 4).  $^1H$  NMR spectra clearly indicated the coordination of  $Cu^{2+}$  ion since the proton on salicylaldehyde shifted upfield ( $\Delta\delta=0.10$  ppm) and broadened upon the addition of 1 equiv  $Cu^{2+}$  ion. The proton from dansyl moiety was shifted downfield ( $\Delta\delta=0.12$  ppm) due to the  $Cu^{2+}$  ion coordination which caused the decrease in electron density of dansyl unit. The proposed coordination of  $Cu^{2+}$  ion by 1 is shown in the optimized geometry (Fig. 5).

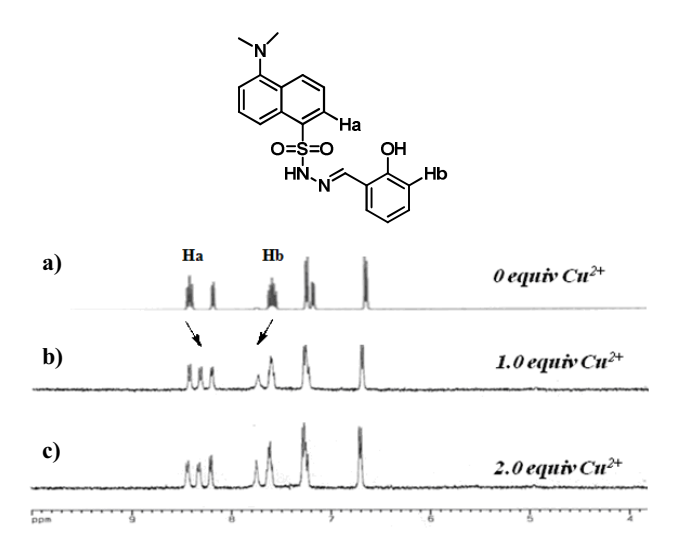
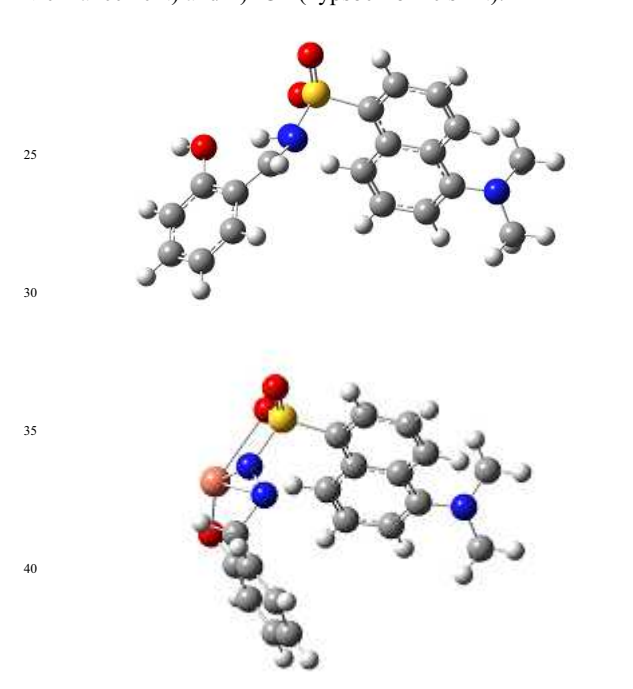


Fig. 4 Partial <sup>1</sup>H NMR spectra of 1 measured in DMSO-d6/D<sub>2</sub>O 5(1/1, v/v): (a) without  $Cu^{2+}$  ion and with (b) 1 equiv  $Cu^{2+}$  ion, (c) 2 equiv Cu<sup>2+</sup> ion.

The fluorescence enhancement of 1 upon the addition of Cu<sup>2+</sup> ion could be explained via the radiationless pathway from the  $n\pi^*$ 10 state of the emission from imine lone-pair electrons. The photoinduced electron transfer (PET) channel is operated which suppresses the fluorescence emission of 1.15 In the presence of Cu<sup>2+</sup> ion, the bound Cu<sup>2+</sup>·1 complex interferes with the PET pathway resulted from imine lone-pair electrons. This would raise 15 the energy state of  $n\pi^*$  while the  $\pi\pi^*$  state of emission from dansyl fluorophore is minimized.<sup>16</sup> While the hypsochromic shift of emission is on the basis of ICT process. Therefore, the fluorescence responses of 1 towards Cu2+ ion operates via two channels which are the combination of i) PET (fluorescence 20 enhancement) and ii) ICT (hypsochromic shift). 17



45 Fig. 5 Optimized geometries of 1 and 1·Cu<sup>2+</sup> ion complex.

In summary, a novel fluorescence "turn-on" chemosensor (1) is simply prepared and evaluated for its fluorescence response towards Cu<sup>2+</sup> ion. 1 has been deliberately designed based on a 50 combination of PET and ICT processes. The "suppressed" PET mechanism offers 1 with fluorescence enhancement upon binding to Cu<sup>2+</sup> ion while the ICT process facilitates 1 with a blue shift of emission. Since 1 is quite soluble in an aqueous environment, this could offer 1 as a potential chemosensor for Cu<sup>2+</sup> ion for the 55 practical use. 1 is currently integrated into a hydrophilic polymeric template as a new polymeric sensor for a 100 % aqueous utility.

The Thailand Research Fund/Commission on Higher 60 Education's research grant to S.S. and P.T. (RTA5180003) and the Development and Promotion of Science and Technology Talents Project's scholarship to W.N. are gratefully acknowledged. We are also grateful to the partial support from National Center for Genetic Engineering and Biotechnology 65 (BIOTEC).

#### Notes and references

<sup>a</sup>Bioresources Research Unit, National Center for Genetic Engineering and Biotechnology (BIOTEC), 113 Thailand Science Park, Phaholyothin Road, Klong Luang, Pathumthani 12120 Thailand, Fax: 662 564 6632:

70 Tel: 662 564 6700 ext 3560; E-mail: srung.sma@biotec.or.th

<sup>b</sup>Department of Chemistry, Faculty of Science, Mahidol University, Rama 6 Road, Phyathai, Bangkok 10400 Thailand. Fax: 662 354 7151; Tel: 662 201 5135; E-mail: scptb@mahidol.ac.th. (P.T.) and weerachai na@hotmail.com (W.N.)

75 † Electronic Supplementary Information (ESI) available: Synthesis of 1; Fluorescence spectra of 1. See DOI: 10.1039/b000000x/

- (a) L. Hesse, D. Beher, C. L. Masters and G. Multhaup, FEBS Lett., 1994, 349, 109-116; (b) G. Multhaup, A. Schlick-supp, L Hess, D. Beher, T. Ruppert, C. L. Masters and K. Beyreuther, Science 1996, 271, 1406-1409; (c) C. J. Maynard, A. I. Bush, C. L. Masters, R. Cappai and Q.-X. Li, Int. J. Exp. Path. 2005, 86, 147-159; (d) E. Breslow, J. Biol. Chem., 1964, 239, 3252-3259; (e) A. Zgirski and E. Frieden, J. Inorg. Biochem., 1990, 39, 137-148; (f) C. K. Luk, Biochemistry 1971, 10, 2838-2843; (g) Z. L. Harris and J. D. Gitlin, Am. J. Clin. Nutr., 1996, 63, 836S-841S.
- (a) Z. Xu, J. Yoon and D. R. Spring, Chem. Commun., 2010, 46, 2563-2565; (b) W.-C. Lin, C.-Y. Wu, Z.-H. Liu, C.-Y. Lin and Y.-P. Yen, Talanta, 2010, 81, 1209-1215.
- (a) M. B. Gholivand, P. Niroomandi, A. Yari and M. Joshagani, Anal. Chem. Acta, 2005, 538, 225-231; (b) R. K. Mahajan, T. P. S. Walia and T. S. Lobana, Anal. Sci., 2006, 22, 389-392; (c) A. Mokhir, A. Kiel, D. P. Herten and R. Kraemer, Inorg. Chem. 2005, 44, 5661-5666.
- D.S. McClure, J. Chem. Phys., 1952, 20, 682-686.

100

105

- (a) K. Rurack, U. Resch-Genger and W. Rettig, J. Photochem. Photobiol. A. Chem., 1998, 118, 143-149; (b) R. Martinez, F. Zapata, A. Caballero, A. Espinosa, A. Tarraga and P. Molina, Org. Lett., 2006, 8, 3235-3238.
- (a) G.-K. Li, Z.-X. Xu, C.-F. Chen and Z.-T. Huang, Chem. Commun., 2008, 1774-1776; (b) T. Abalos, D. Jimenez, R. Martines-Manez, J. V. Ros-Lis, S. Royo, F. Sancenon, J. Soto, A. M. Costero, S. Gil and M. Parra, Tetrahedron Lett., 2009, 50, 3885-3888
- (a) A. Ueno, S. Minato, I. Suzuki, M. Fukushima, M. Ohkubo, T. Osa, F. Hamada and K. Murai, Chem. Lett., 1990, 605-608; (b) Y. Wang, T. Ikeda, A. Ueno and F. Toda, Chem. Lett., 1992, 863-866; (c) F. Hamada, Y. Kondo, R. Ito, I. Suzuki, T. Osa and A. Ueno, J. Incl. Phenom., 1993, 15, 273-279; (d) Y. Wang, T.

- Ikeda, A. Ueno and F. Toda, *Bull. Chem. Soc. Jpn.*, 1994, **67**, 1598-1607; (e) M. Nakamura, T. Ikeda, A. Nakamura, H. Ikeda, A. Ueno and F. Toda, *Chem. Lett.*, 1995, 343-344; (f) M. Nakamura, A. Ikeda, N. Ise, T. Ikeda, H. Ikeda, F. Toda and A. Ueno, *J. Chem. Soc.*, *Chem. Commun.*, 1995, 721-722.
- (a) N. Aksuner, E. Henden, I. Yilmaz and A. Cukurovali, *Dyes Pigments*, 2009, 83, 211-217;
   (b) H. Chen, Y. Wu, Y. Cheng, H. Yang, F. Li and P. Yang, *Inorg. Chem. Commun.*, 2007, 10, 1413-1415;
   (c) C. Sousa, P. Gameiro, C. Freire and B. Castro, *Polyhedron*, 2004, 23, 1401-1408.
- 9 O. Oter, K. Ertekin, R. Kihncarslan, M. Ulusoy and B. Cetinkaya, *Dyes Pigments*, 2007, **74**, 730-735.
- 10 Y. M. Chung, B. Raman, D.-S. Kim and K. H. Ahn, *Chem. Commun.*, 2006, 186-188.
- 11 (a) N. A. O'Connor, S. T. Sakata, H. Zhu and K. J. Shea, *Org. Lett.*, 2006, **8**, 1581-1584; (b) M. H. Lee, H. J. Kim, S. Yoon, N. Park and J. S. Kim, *Org. Lett.*, 2008, **10**, 213-216.
  - 12 Y. Zheng, J. Orbulescu, X. Ji, F. M. Andreopoulos, S. M. Pham and R. M. Leblanc, J. Am. Chem. Soc., 2003, 125, 2680-2686.
- (a) K. K. Rohatgi and G. S. Singhal, J. Phys. Chem., 1966, 70, 1695-1701; (b) J. E. Selwyn and J. I. Steinfeld, J. Phys. Chem., 1972, 76, 762-774; (c) R. W. Chambers, T. Kajiwara and D. R. Kearns, J. Phys. Chem., 1974, 74, 380-387; (d) U. Rösch, S. Yao, R. Wortmann and F. Würtner, Angew. Chem. Int. Ed., 2006, 45, 7026-7030.
  - 14 J. Gonzàlez-Jimènez, G. Frutos and I. Cayre, Biochem. Pharmacol. 1992, 44, 824-826.
  - 15 S. J. Qu, Z.-H. Lin, C.-Y. Duan, H.-T. Zhang, and Z.-P. Bai, Chem. Commun., 2006, 4392-4394.
- 16 P.-J. Jiang, L. –Z. Chen, J. Lin, Q. Liu, J. Ding, X. Gao and Z.-J. Guo, Chem. Commun., 2002, 1424-1425.
  - 17 Z. Xu, G.-H. Kim, S. J. Han, M. J. Jou, C. Lee, I. Shin and J. Yoon, *Tetrahedron*, 2009, 65, 2307-2312.

Pyrazolidine luminol as a selective colorimetric receptor for  $\operatorname{Cu}^{2^+}$  in an aqueous environment

Weerachai Nasomphan<sup>a,b</sup>, Pramuan Tangboriboonrat<sup>b</sup> and Srung Smanmoo<sup>a</sup>\*

<sup>a</sup>Bioresources Research Unit, National Center for Genetic Engineering and Biotechnology (BIOTEC), 113 Thailand Science Park, Phaholyothin Road, Klong Luang, Pathumthani 12120 Thailand

<sup>b</sup>Department of Chemistry, Faculty of Science, Mahidol University, Rama 6 Road, Phyathai, Bangkok 10400

Thailand

**ABSTRACT** 

Pyrazolidine luminol (PL) was prepared as a selective colorimetric receptor for  $Cu^{2+}$  ion. PL exhibits good selectivity and sensitivity towards  $Cu^{2+}$  over other metal cations, e.g.  $Cr^{3+}$ ,  $Al^{3+}$ ,  $Pd^{2+}$ ,  $Ni^{2+}$ ,  $Ce^{4+}$ ,  $Sn^{2+}$ ,  $Mn^{2+}$ ,  $Co^{2+}$ ,  $Fe^{2+}$ ,  $Fe^{3+}$ ,  $Mo^{2+}$ , and  $Ag^{+}$  ions. The colorimetric change of PL was easily observed by naked eyes in which the color of PL changed from pale yellow to dark green. The detection limit for PL was determined to be  $3.75 \times 10^{-4}$  M with the binding ratio between PL and  $Cu^{2+}$  of 2:1. PL was immobilized on a silica gel plate and employed for the detection of  $Cu^{2+}$  ion in an aqueous environment with good detection limit.

Keywords: Colorimetric receptor, Luminol derivatives, Copper (II) sensor

Corresponding author. Tel.: +662 564 6700 ext 3560; Fax +662 564 6632

E-mail address: srung.sma@biotec.or.th

#### 1. Introduction

The design of the colorimetric receptor with high selectivity and sensitivity has gained chemists' attention because the detection of analyte could simply be achieved via naked eyes [1-3]. A number of colorimetric receptors play significant roles in sensing biological analytes and metal cations [4,5]. In the field of environmental sciences, colorimetric receptors have been employed for the determination of contaminated heavy metals in natural resources [6,7].

In general, the design of colorimetric receptor is based on the careful selection of an ionophore (the analyte binding unit) and a chromophore (the signaling part). The recognition of analytes at the binding unit is achieved by various modes of interactions, e.g., hydrogen-bonding, electrostatic interaction, metal-ligand coordination and Van der Waals interaction [7-9]. Upon binding of analytes to the ionophore, the communication between the binding moiety and the chromophore is initiated to alter the photophysical property of the receptor. The measurement of the physical change of chemosensors normally relies on spectroscopic methods which sometime involve complicated sample preparation and analysis [10,11]. Therefore, the development of a portable chemosensor kit with low cost of sampling and sensitive detection is desirable.

Luminol and its derivatives are well known chemiluminescence (CL) reagents due to their high quantum yields [12]. CL emission of luminol is initiated by reacting luminol with appropriate oxidizing agents in the basic condition [13]. Recently, luminol derivative has been used as a CL sensor for metal cations [14]. The incorporation of a crown ether moiety into the luminol structure offers a CL receptor which confers the binding mode to metal cations. Upon binding to metal cations, the signal transmission between the receptor (crown ether) and the chromophore is established.

In this paper, we have synthesized a new chromogenic receptor, pyrazolidine luminol (PL). The luminol scaffold was used as the chromophore of the receptor, while the presence of the 5-membered ring of PL served as the binding unit to the metal cation. Among metal cations, PL exhibited good selectivity towards Cu<sup>2+</sup> ion and showed the colorimetric change upon the addition of Cu<sup>2+</sup> ion. This offers PL as a selective receptor for the detection of Cu<sup>2+</sup> ion by the colorimetric mean.

#### 2. Experimental

#### 2.1. Materials and instrumentations

The stock solution of the corresponding PL was prepared in DMF with the concentration of  $500~\mu M$ . The metal complexes used in this study were as followed: cobalt (II) chloride, chromium (III) chloride, copper (II) chloride, nickel (II) chloride, palladium (II) chloride, manganese (II) chloride and disodium molybdate (VI), iron (II) chloride, iron (III) chloride, aluminium (III) chloride, silver (I) chloride, tin (II) chloride and cerium (IV) sulfate. Metal complexes were obtained from Aldrich or Acros and used without further purification. Solvents were used as a HPLC grade. Other chemicals used were supplied from Aldrich as analytical grade and used without further purification. MilliQ water was used throughout unless other stated. The concentration of stock solution of metal cations was 10~mM.

The reactions were monitored by thin-layer chromatography (TLC) on a commercial silica coated plates with a particle size of 60 Å. Developed plates were visualized by UV lamp (254 nm). Column chromatography was performed using 0.063 – 0.20 nm silica gel. Fluorescence measurements were carried out using a FP-6300 spectrofluorometer (JASCO) equipped with a xenon lamp source and a 1.0-cm quartz cell, and the scan speed was 600 nm min<sup>-1</sup>. Absorption spectra were recorded by a Shimadzu-240 UV-vis spectrophotometer using a 1.0-cm quartz cell. <sup>1</sup>H spectrum was recorded on Bruker DPX 400 MHz spectrometer in CDCl<sub>3</sub> using TMS as the internal standard. CDCl<sub>3</sub> (77.0 ppm) were used as the internal reference for <sup>13</sup>C NMR. Mass spectra were recorded on Bruker Esquire and Finnigan MAT INCOS 50 mass spectrometers. The fluorimetric images were taken after the membrane exposed under the UV lamp (λ = 366 nm).

## 2.2 Preparation and characterization of pyrazolidine luminol (PL)

The preparation of PL was achieved in 2 steps as followed. In a flame dried round bottom flask, a solution of luminol (1 g, 5.64 mmol) in methanol (5 mL) was added sodium methoxide (0.91 g, 16.9 mmol) and the reaction was brought to reflux for 3 hrs. After the reaction was cooled down to room temperature, methanol was completely removed under vacuum before the obtained yellow solid was re-dissolved in ethanol followed by the addition of epichlorohydrin (2.21 mL, 28.2 mmol) under the N<sub>2</sub>

atmosphere and left stirring at room temperature for 4 days. The crude product was recrystallised in water before the desired PL was obtained as a white solid; 70%; mp. 215 °C; IR  $v_{max}$  (KBr) 1406, 1591, 1619, 3443 cm<sup>-1</sup>; ESMS; Calculated for  $C_{11}H_{11}N_3O_3$  [M<sup>+</sup>] = 233.080; measured mass [M<sup>+</sup>+Na] = 256.0697; <sup>1</sup>H NMR (DMSO-*d*6):  $\delta$  3.95-4.04 (m, 2H, C*H*2), 4.11 (dd, *J* = 11.8 Hz, 2H, C*H*2), 4.58 (m, 1H, C*H*OH), 5.76 (br, 1H, O*H*), 6.30 (br, 2H, N*H*2), 6.98 (dd, 1H, *J* = 2.36 Hz and 8.55 Hz, 1H, Ar*H*), 7.22 (s, 1H, Ar*H*), 7.81 (d, 1H, *J* = 8.56 Hz, Ar*H*); <sup>13</sup>C NMR (DMSO-*d*6): 54.5 (*C*H<sub>2</sub>), 54.8 (*C*H<sub>2</sub>), 65.0 (*C*H), 108.0 (Ar*C*H), 117.08 (Ar*C*H), 118.5 (Ar*C*H), 128.2 (Ar*C*H), 131.2 (Ar*C*H), 153.3 (Ar*C*H), 154.4 (NH*C*=O), 154.8 (NH*C*=O).

#### 3. Results and discussion

#### 3.1. Synthesis of pyrazolidine luminol

On the course of optimization for PL synthesis, the condition described in scheme 1 provided the best yield hence it was employed in the study throughout. The synthesis of PL was achieved in 2 steps as already mentioned. Spectroscopic data of PL agreed well with the structure shown. PL is designed as a chromogenic receptor where the luminol moiety acts as a chromophore. The 5-membered ring with the hydroxyl group is used as a chelating unit for metal cations.

**Scheme 1.** Synthetic procedure for PL. Reaction conditions: (i) NaOMe, MeOH, 80 °C, 3 hrs; (ii) epichlorohydrin, ethanol, RT, 4 days.

#### 3.2. Chemiluminescence (CL) profile of PL comparing to luminol

It is known that the chemical manipulation of the luminol's phthalhydrazide ring generally leads to the loss of its CL property [15]. Therefore, the CL emission of PL was investigated and compared with luminol. Previously, we have optimized the condition for the CL emission of luminol employing Fe<sup>3+</sup> catalysis [13(a)]. Therefore, the corresponding condition was used for the CL emission of PL. CL emitting reagents (CH<sub>3</sub>CN, TPA, and FeCl<sub>3</sub>) were used to initiate the CL emission of both luminol and PL. It was shown in Fig. S2 (see supplementary material) that the introduction of a 5-membered ring into the PL structure retained its CL property. Therefore, this offers PL as a newly synthesized CL reagent.

#### 3.3. Selectivity of PL towards metal ions

The selectivity of PL over other metal cations was investigated. Various cations were added into the PL solution and the color change of the solution was observed by naked eyes in the optimized solvent (DMF:H<sub>2</sub>O). In the presence of other metal cations (e.g. Fe<sup>2+</sup>, Fe<sup>3+</sup> and Mn<sup>2+</sup> ions), no significant colorimetric change of PL solution was observed. It was interesting to note that in the presence of Cu<sup>2+</sup> ion, the color of PL solution significantly changed from pale yellow to dark green (Fig. 1). The change was not observed when the same molar equiv of Cu<sup>2+</sup> ion was added into luminol solution (see supplementary material, Fig. S3), hence the presence of hydroxyl group in PL is crucial for this interaction. The colorimetric change of PL solution upon the addition of Cu<sup>2+</sup> ion indicated the interaction between PL and Cu<sup>2+</sup> ion which is believed that the observed effect proceed via the intramolecular charge transfer (ICT) process. The ICT mechanism of PL is originated from the binding to Cu<sup>2+</sup> ion which subsequently triggers the ICT from the receptor (the 5-membered ring moiety) to the chromophore.

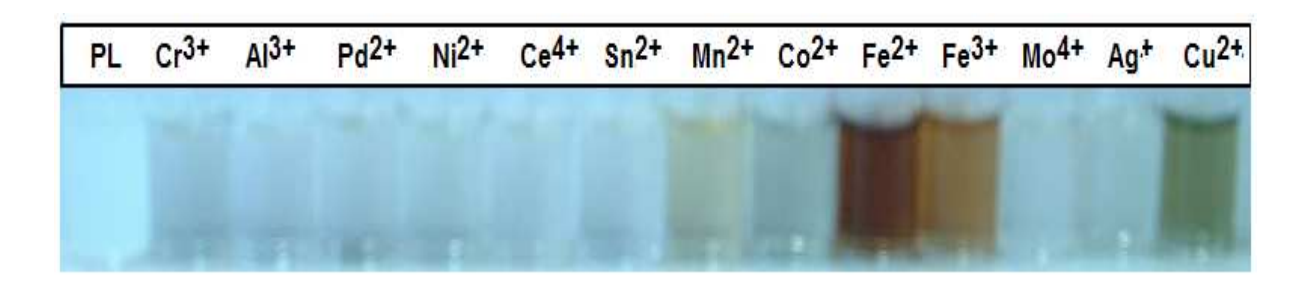


**Fig. 1.** Pictures of PL upon the addition of various metal cations in DMF:H<sub>2</sub>O (9:1; v/v). [PL] =  $4.5 \times 10^{-4}$  M, [metal cations] =  $1 \times 10^{-3}$  M.

#### 3.4. UV-vis spectra of PL upon the addition of various metal cations

The ground state absorption of PL was recorded in DMF: $H_2O$  (9:1; v/v). It was clearly shown that in the absence and presence of other metal cations, the absorption spectra indicated three absorption maxima at 305, 350 and 375 nm. In the presence of  $Cu^{2+}$  ion, there was a new absorption observed at 425 nm (Fig. 2) which is a CT band. The colorimetric change of PL solution upon the addition of  $Cu^{2+}$  ion corresponded to the occurring of the new absorption at 425 nm. Since no absorption at 425 nm in the presence of other metal cations, the absorption at 425 nm indicated the characteristic interaction between PL and  $Cu^{2+}$  ion.

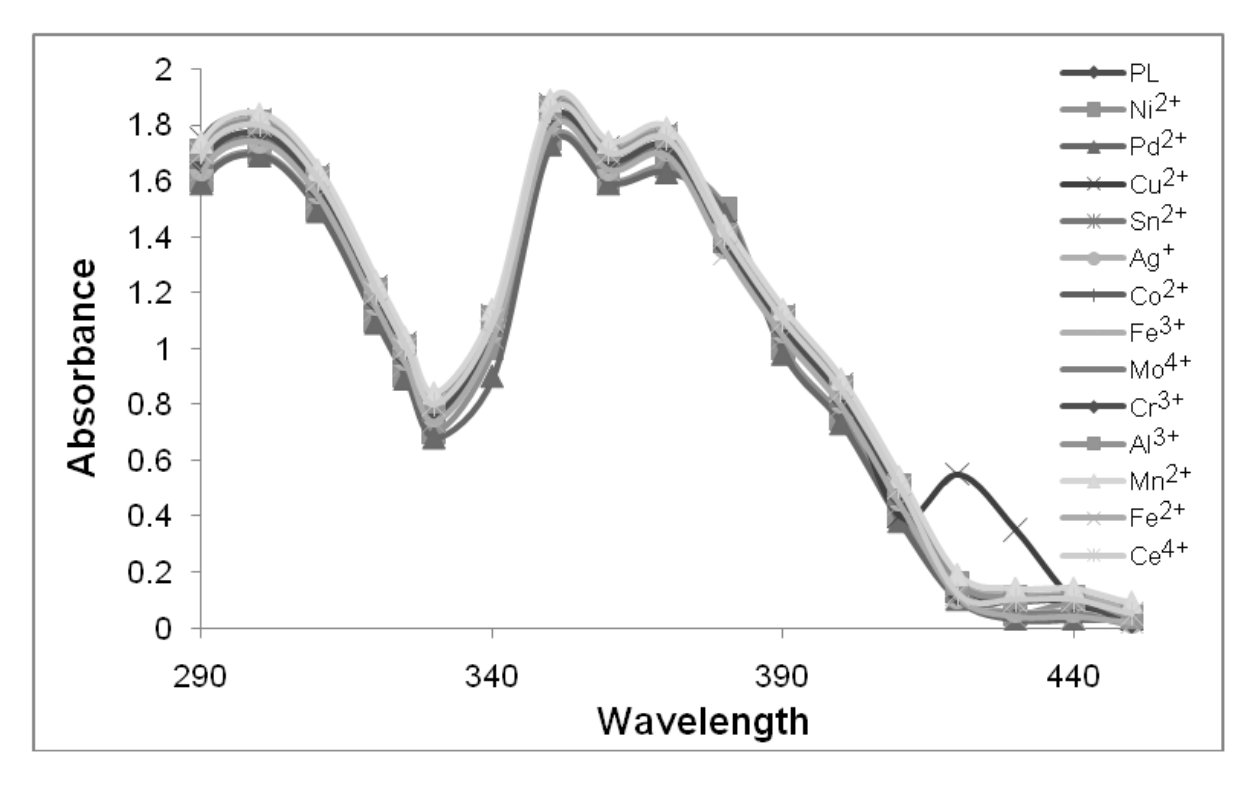


**Fig. 2.** UV-vis titration spectra of PL in the presence of various metal cations. [PL] =  $4.5 \times 10^{-4}$  M, [metal cations] =  $1 \times 10^{-3}$  M.

#### 3.5. Ratiometric response of PL upon the addition of various metal cations

The change in the absorption of PL in the presence of metal cations was demonstrated with respect to two absorptions at 350 and 425 nm. The absorbance ratio at 350 and 425 nm indicates the good selectivity of PL towards metal cations. It was clearly shown that the change in the corresponding absorbance ratio (A425/350) of PL upon the addition of  $Cu^{2+}$  ion was more pronounced than other metal cations (Fig. 3). In the presence of other metal cations, the A425/350 absorbance ratio did not significantly change. This shows that PL is highly selective in its response to  $Cu^{2+}$  ion in comparison to other metal cations.

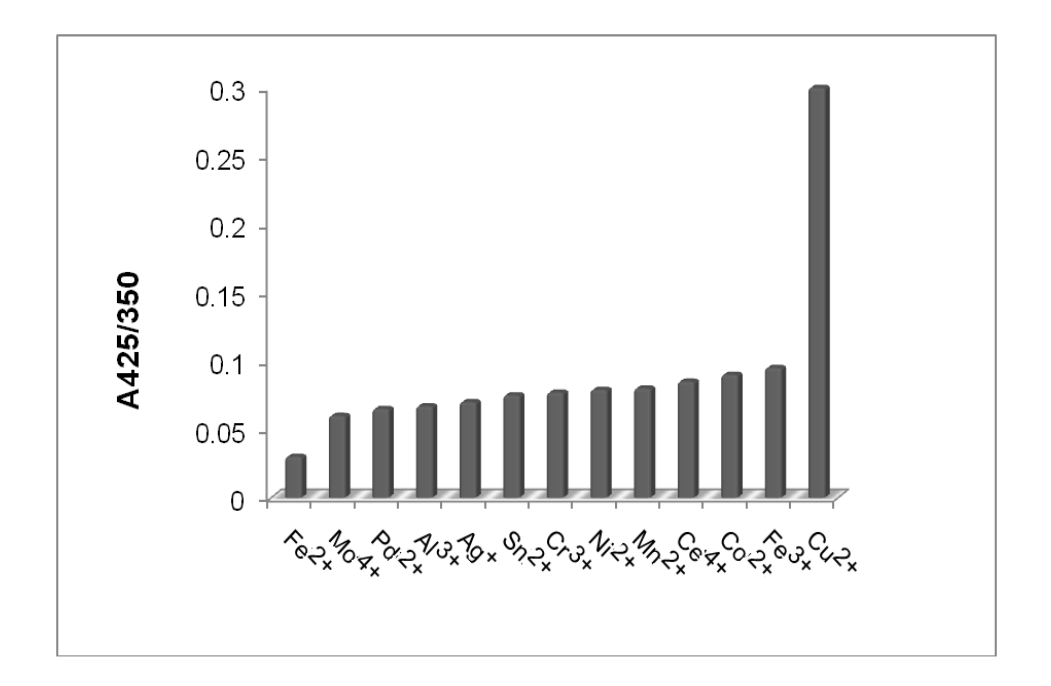


**Fig. 3.** Ratiometric response of PL towards different metal cations. [PL] =  $4.5 \times 10^{-4}$  M. [metal cations] =  $1 \times 10^{-3}$  M.

# 3.6. UV-vis titrations of PL with various concentrations of $Cu^{2+}$ ion

It is clear that the absorption of PL is highly affected by  $Cu^{2+}$  ion. The change in the absorption spectra of PL in DMF: $H_2O$  in the presence of various concentrations of  $Cu^{2+}$  was investigated. Fig. 4 represented the CT band (absorption at 425 nm) which selectively responded to  $Cu^{2+}$  ion. Increasing concentrations of  $Cu^{2+}$  ion resulted in the progressive incline of the absorption maxima at 425 nm, which was thought to be due to the interaction of the hydroxyl group participating in the ICT process.

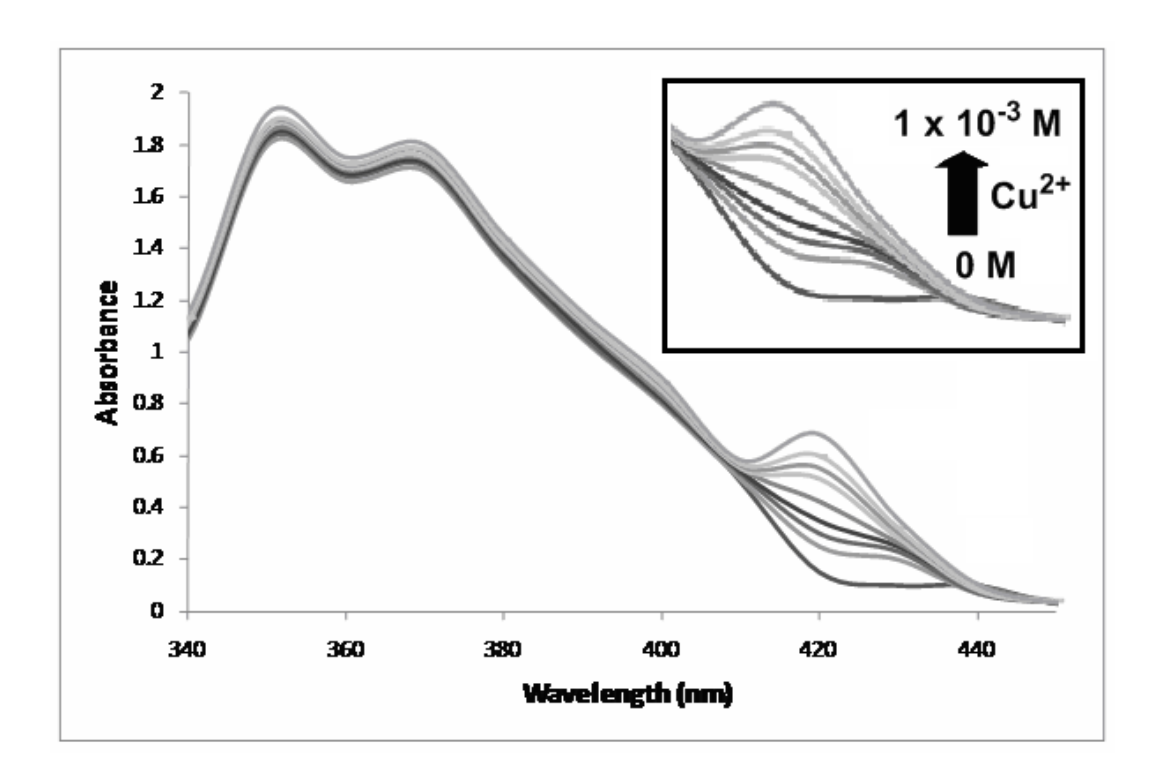


**Fig. 4.** UV-vis titration spectra of PL  $(4.5 \times 10^{-4} \text{ M})$  in the presence of increasing concentration of Cu<sup>2+</sup> ion in DMF:H<sub>2</sub>O (9:1; v:v).

# 3.7. Colorimetric response of PL upon the addition of various concentrations of $Cu^{2+}$ ion

Next, the colorimetric change of PL was observed in the presence of various concentrations of  $Cu^{2+}$  ion. It was noticed that the color of PL solution gradually developed more intense green color upon increasing concentration of  $Cu^{2+}$  ion (Fig. 5). From the naked eye detection, the clear cut for the color change of PL solution was observed when  $3.75 \times 10^{-4}$  M of  $Cu^{2+}$  ion was added into the PL solution. Further increasing concentration of  $Cu^{2+}$  ion resulted in a more intense green color. Therefore, the detection limit for the liquid-phase colorimetric detection of  $Cu^{2+}$  ion employing PL was  $3.75 \times 10^{-4}$  M.

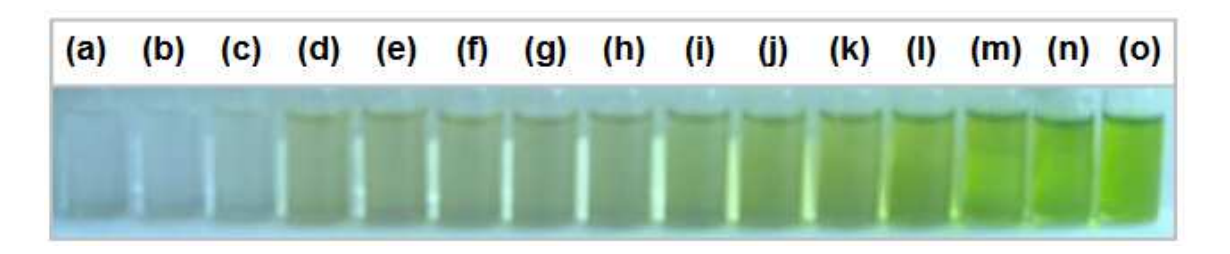


**Fig. 5.** Pictures of color changes of PL upon increasing concentrations of  $Cu^{2+}$  ions in DMF:H<sub>2</sub>O (9:1; v/v). PL with  $Cu^{2+}$  ion (a) 0 M (b) 1 × 10<sup>-5</sup> M (c) 1 × 10<sup>-4</sup> M (d) 3.75 × 10<sup>-4</sup> M (e) 7.5 × 10<sup>-4</sup> M (f) 1× 10<sup>-3</sup> M (g) 1.5 × 10<sup>-3</sup> M (h) 3 × 10<sup>-3</sup> M (i) 6 × 10<sup>-3</sup> M (j) 1 × 10<sup>-2</sup> M (k) 1.2 × 10<sup>-2</sup> M (l) 2.4 × 10<sup>-2</sup> M (m) 4.8 × 10<sup>-2</sup> M (n) 7 × 10<sup>-2</sup> M (o) 1× 10<sup>-1</sup> M. [PL] = 4.5 × 10<sup>-4</sup> M.

# 3.8. Mass spectroscopic spectra of PL with the addition of $Cu^{2+}$ ion

In order to investigate the stoichiometric binding ratio between PL and  $Cu^{2+}$  ion, ESI-MS was used for the investigation. Various stoichiometric binding ratios between PL and  $Cu^{2+}$  ion were employed and subjected to the mass spectroscopic analysis. Of binding ratios, the solution containing 2:1 molar equiv between PL and  $Cu^{2+}$  ion showed the peak at m/z = 528.54 corresponded to the complex between PL and  $Cu^{2+}$  ion at 2:1 (Fig. 6).

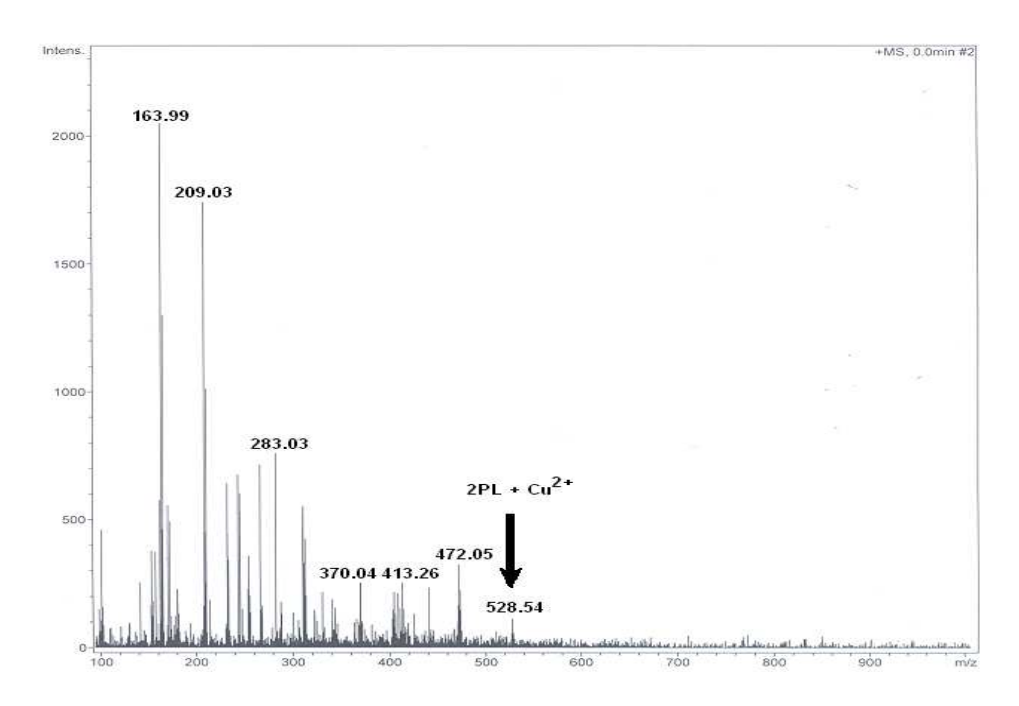


**Fig. 6.** Mass spectroscopic analysis of PL and  $Cu^{2+}$  ion in DMF:H<sub>2</sub>O (9:1; v/v). The binding ratio between PL and  $Cu^{2+}$  ion was indicated as the black arrow (PL: $Cu^{2+}$  ion = 2:1).

# 3.9. Proposed complex between PL and Cu<sup>2+</sup> ion

From the mass spectroscopic data and the computational modeling, the proposed binding complex between PL and Cu<sup>2+</sup> ion is shown in Fig. 7. It was believed that the binding mode between PL and Cu<sup>2+</sup> ion is through the coordination of Cu<sup>2+</sup> ion by two moles of PL. The

coordination of Cu<sup>2+</sup> ion by PL is a C2 symmetry which is assisted via the chelation from the hydroxyl group present in the 5-membered ring of PL and the carbonyl group. The coordination of Cu<sup>2+</sup> from the other PL adopts the same mode of binding with the opposite orientation to obtain the tetragonal complex between PL and Cu<sup>2+</sup> ion. From computer modeling, the hydroxyl group of the 5-membered ring adopts the puckered conformation which facilitates the binding between Cu<sup>2+</sup> ion, hydroxyl and carbonyl groups. This result demonstrates the importance of the 5-membered ring present in PL and could explain the lack of selectivity of luminol towards Cu<sup>2+</sup> ion.

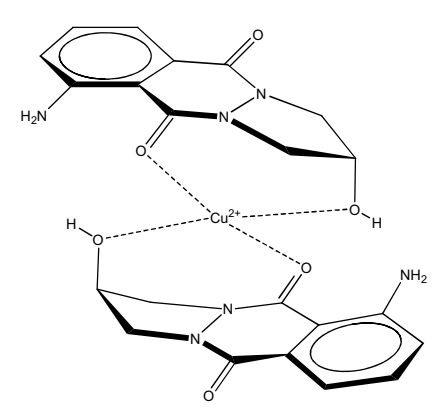


**Fig. 7.** MM2 energy-optimized complex between PL and  $Cu^{2+}$  ion at the binding ratio between PL and  $Cu^{2+}$  ion of 2:1.

#### 3.10. Preliminary application of PL chemosensor kit

In order to develop PL as a chemosensor kit, a silica plate was immobilized with PL. The immobilizing process was achieved by immersing a silica plate into PL solution before drying under vacuum. It was clearly shown that the immobilized plate with PL exhibited the characteristic pale yellow. After the immersion into  $Cu^{2+}$  ion solution, PL immobilized plate showed a colorimetric change from pale yellow to green which clearly observed by naked eyes (Fig. 8). PL immobilized plate was employed for the detection of  $Cu^{2+}$  ion in an aqueous environment and found that the detection limit for  $Cu^{2+}$  ion was as low as  $0.4 \times 10^{-3}$  M. Therefore, this chemosensor kit has a potential to further develop as the portable detection kit for  $Cu^{2+}$  ion with the lower detection limit and will be employed as an analytical device in environmental science.

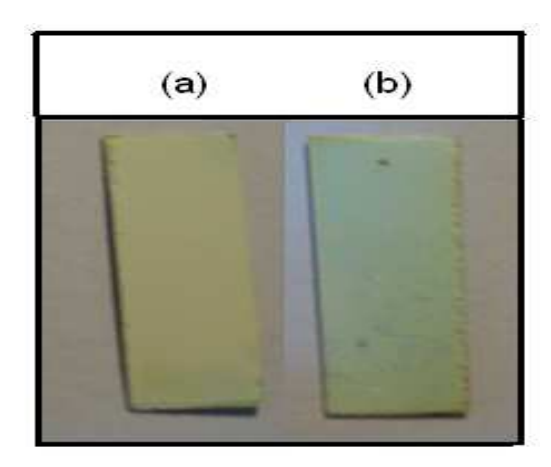


**Fig. 8.** Pictures of silica plates: (a) the PL immobilized silica plate. (b) the PL immobilized silica plate after immersion into the  $0.4 \times 10^{-3}$  M of Cu<sup>2+</sup> ion solution.

#### 4. Conclusion

We herein demonstrate a new colorimetric receptor based on the luminol scaffold, pyrazolidine luminol (PL). Its colorimetric change is clearly observed by naked eyes with selective response to Cu<sup>2+</sup> ion. The color of PL solution changed from pale yellow to dark green upon the addition of Cu<sup>2+</sup> ion. The detection limit of PL solution towards Cu<sup>2+</sup> ion was 10<sup>-4</sup> M. The binding ratio between PL and Cu<sup>2+</sup> ion was determined by mass spectrometry and found to be 2:1. To the best of our knowledge, this is the first colorimetric receptor for Cu<sup>2+</sup> ion based on PL. For the application, PL was immobilized on a silica plate and used for the detection of Cu<sup>2+</sup> ion in an aqueous environment. The improvement of the PL sensitive chemosensor kit could facilitate applications in biological and environmental sciences.

## Acknowledgements

The Thailand Research Fund (TRF)/Commission on Higher Education (CHE)'s research grant to S.S. and P.T. and the Development and Promotion of Science and Technology Talents Project's scholarship to W.N. are gratefully acknowledged. We are also grateful to the partial support from National Center for Genetic Engineering and Biotechnology (BIOTEC).

#### Appendix A. Supplementary data

Supplementary information associated with this article can be found, in the online version, at doi:XXXX

#### References

- [1] S. R. Rickett, D. Douglas, Sensor. Actuat. B-Chem. 135 (2008), 46. (b) H. Jiang, Y. Wang, Q. Ye, G. Zou, W. Su, Q. Zhang, Sensor. Actuat. B-Chem. in press.
- [2] H. Li, Z. Cui, C. Han, Sensor. Actuat. B-Chem. (2009), in press. (b) J. Li, H. Lin, H. Lin, J. Photoch. Photobio. B 97 (2009), 18.
- [3] (a) Y.-J. Kim, H. Kwak, S. J. Lee, J. S. Lee, H. J. Kwon, S. H. Nam, K. Lee, C. Kim, Tetrahedron 62 (2006), 9635. (b) Y. Egawa, R. Gotoh, S. Niina, J.-I. Anzai, Bioorg. Med. Chem. Lett. 60 (2007), 11133.
- [4] D. Zhang, M. Zhang, Z. Liu, M. Yu, F. Li, T. Yi, C. Huang, Tetrahedron Lett. 47 (2006), 7093. (b) D. Prabhakaran, H. Nanjo, H. Matsunaga, Anal. Chim. Acta 601 (2007), 108. (c) S. Shao, Y. Guo, L. He, S. Jiang, X. Yu, Tetrahedron Lett. 44 (2003), 2175.
- [5] (a) I. Grabchev, P. Bosch, M. McKenna, D. Staneva, J. Photoch. Photobio. A 201 (2009), 75 (b) P. Kaur, S. Kaur, A. Mahajan, K. Singh, Inorg. Chem. Commun. 11 (2008), 626.
- [6] (a) H. Yang, Z. Zhou, F. Li, T. Yi, C. Huang, Inorg. Chem. Commun. 10 (2007), 1136.(b) P. Buhlmann, E. Pretsch, E. Bakker, Chem. Rev. 98 (1998), 1593.
- [7] (a) M. H. Keefe, K. H. Benkstein, J. T. Hupp, Coord. Chem. Rev. 205 (2000), 201. (b) F. Wang, Y. Xu, B. X. Ye, M. P. Song, Y. J. Wu, Inorg. Chem. Commun. 9 (2006), 797.
- [8] (a) L. A. Baumes, M. B. Sogo, P. Montes-Navajas, A. Corma, H. Garcia, Tetrahedron Letters 50 (2009), 7001. (b) S. Chah, M. R. Hammond, R. N. Zare, Chem. Biol. 12 (2005), 323. (c) D. Saravanakumar, N. Sengottuvelan, M. Kandaswamy, P. G. Aravindan, D. Velmurugan, Tetrahedron Lett. 46 (2005), 7255.
- [9] (a) D. Saravanakumar, S. Devaraj, S. Iyyampillai, K. Mohandoss, M. Kandaswamy, Tetrahedron Lett. 49 (2008), 127. (b) Y. Wan, W. Niu, W. J. Behof, Y. Wang, P. Boyle, C. B. Gorman, Tetrahedron 65 (2009), 4293. (c) P. Montes-Navajas, L. A. Baumes, A. Corma, H. Garcia, Tetrahedron Lett. 50 (2009), 2301.

- [10] (a) D. A. Jose, D. K. Kumar, B. Ganguly, A. Das, Tetrahedron Lett. 46 (2005), 5343.
  (b) Z. Yuan, T. W. Hanks, Polymer 49 (2008), 5023. (c) K. Liu, L. He, X. He, Y. Guo, S. Shao, S. Jiang, Tetrahedron Lett. 48 (2007), 4275. (d) A. Mitra, B. Ramanujam, C. P. Rao, Tetrahedron Lett. 50 (2009), 776.
- [11] (a) S. Chaure, D. Paul, P. Vadagma, A. K. Ray, J. Hard. Mater. in press. (b) D. Delmarre, R. Méallet, C. Bied-Charreton, R. B. Pansu, J. Photoch. Photobio. A 124 (1999), 23. (c) M. P. McCurdie, L. A. Belfiore, Polymer 40 (1999), 2889. (d) F. Capitelli, F. Colao, M. R. Provenzano, R. Fantoni, G. Brunetti, N. Senesi, Geoderma 106 (2002), 45.
- [12] (a) H. Yoshida, R. Nakao, H. Nohta, M. Yamaguchi, Dyes Pigments 47 (2000), 239. (b)M. Nakazono, T. Hino, K. Zaitsu, J. Photoch. Photobio. A 186 (2007), 99.
- [13] (a) C. Smanmoo, M. Yamasuji, T. Sagawa, T. Shibata, T. Kabashima, D.-Q. Yuan, K. Fujita, M. Kai, Talanta 77 (2009), 1761. (b) H. Chen, F. Gao, R. He, D. Cui, J. Colloid Interf. Sci. 315 (2007), 158.
- [14] H. Okamoto, M. Kimura, Method. Enzymol. (2004), 183.
- [15] H. R. Schroeder, F. M. Yeager, Anal. Chem. 50 (1978), 1114.

#### **Biographies**

**Weerachai Nasomphan** is working towards his M.Sc. degree in functionalized polymer at Mahidol University and BIOTEC.

**Pramuan Tangboriboonrat** obtained Ph.D. in chemistry from Université de Haute Alsace, France. She is currently professor in polymer chemistry at Mahidol University. Her research work has been focused on colloidal chemistry.

**Srung Smanmoo** received his Ph.D. in organic chemistry from the University of Sheffield, UK. He is now working as a researcher at bioresources unit, National Center for Genetic Engineering and Biotechnology (BIOTEC). His research interest mainly focuses on the development of new molecular sensing systems.

### **Polymer Composites**



# Physical properties of maleated sulfur prevulcanized natural rubber-g- cellulose fiber

| Journal:                      | Polymer Composites   |
|-------------------------------|--|
| Manuscript ID:                | PC-11-0402   |
| Wiley - Manuscript type:      | Research Article   |
| Date Submitted by the Author: | 22-Jun-2011  |
| Complete List of Authors:     | Riyajan, Sa-Ad; Prince of Songkla University, Material Science and Technology<br>Intharit, Isara<br>Tangboriboonrat, Pramuan |
| Keywords:                     | cellulose, composite   |
|                               |  |

SCHOLARONE™ Manuscripts

# Physical properties of maleated sulfur prevulcanized natural rubber-g- cellulose fiber

Sa-Ad Riyajan<sup>1</sup>\*, Isara Intharit<sup>1</sup> and Pramuan Tangboriboonrat<sup>2</sup>

<sup>1</sup>Department of Materials Science and Technology and Natural Product Center and, Faculty of Science,

Prince of Songkla University, Songkhla 90112 Thailand

<sup>2</sup>Department of Chemistry, Faculty of Science, Mahidol University, Bangkok 10400 Thailand

\*Corresponding author: saadriyajan@hotmail.com

Phone/Fax 660-074288398

#### **ABSTRACT**

The maleated sulfur prevulcanized natural rubber grafted cellulose (M-SPNR-g-cellulose) was prepared from SPNR latex and cellulose fiber of corn leaves by using benzoyl peroxide and potassium persulfate as thermal initiators. The chemical structure of the M-SPNR-g-cellulose was confirmed by ATR-FTIR and solid state <sup>13</sup>C-NMR. The swelling ratio of M-SPNR-g-cellulose film decreased as a function of cellulose and maleic anhydride contents. Their modulus and hardness dramatically increased with increasing cellulose content. However, the tensile strength and elongation at break decreased when compared to the unmodified SPNR. The M-SPNR-g-cellulose exhibited good thermal resistance at 90°C. The well dispersed cellulose fibers in rubber matrix was confirmed by SEM and optical microscopy. The composite film had antibacterial activity and could be easily degraded when buried in moist soil.

**KEYWORDS**, Natural rubber; Maleic anhydride; Cellulose; Chemical modification;

Latex; Biopolymer

#### INTRODUCTION

The biodegradable materials, e.g., cellulose, natural rubber (NR) and starch, are used to replace the synthetic polymers due to the environmental friendly reason. Moreover, cellulose, the most abundant natural polymer, can be obtained from the 'waste' agricultural by-product, e.g., sugar beet pulp, eucalyptus kraft pulp, palm and rice husk [1-4]. Before utilization, cellulose must be treated with acid and base to remove the non-cellulose, e.g., fatty acid, wax and hemicellulose [5,6]. However, the drawbacks of the treated cellulose, i.e., high moisture absorption and high fungi attack, still exist.

In order to solve these problems, several chemical modifications, i.e., etherification, esterification, oxidization, crosslinking and graft copolymerization, through hydroxyl groups of cellulose have been carried out [7-11]. Besides reducing the moisture absorption of cellulose, these modifications enhance the adhesion between hydrophilic and hydrophobic materials. Although the cellulose grafted with polymers, e.g., polyacrylonitrile, butyl acrylate, polystyrene, β-cyclodextrin and renewable polymeric matrices, were studied, the grafting between NR and cellulose has not yet been reported [12-16]. The previous works concerned only the blend of acid treated cellulose with NR. It was found that their modulus increased depending on cellulose content due to hydroxyl group and 1,4 glycoside linkage in cellulose. However, the poor adhesion between both materials caused the slight decrease of the tensile strength and elongation at break of the blend [17-20]. The better adhesion between cellulose and NR was obtained from using cellulose grafted with allyl acrylate and allyl methacrylate [17]. The stress/strain measurement and dynamic mechanical analysis of NR/allyl acrylate and allyl methacrylate grafted cellulose composites were, therefore, improved. The modification of cellulose from banana

fiber by maleic anhydride (MA) for its use as a coupling agent was also investigated [22]. Results showed that the mechanical properties of the maleated cellulose blended with polyethylene were enhanced due to the better compatibility [22].

In this present work, MA reacted with sulfur prevulcanized natural rubber (SPNR) latex producing maleated (M) SPNR which was grafted with cellulose fiber from corn leaves. The value-added agricultural 'waste' by-product was the main goal of this study. Effects of MA and cellulose contents on the physical properties, i.e., swelling ratio in toluene, tensile strength, elongation at break and hardness, of the M-SPNR-g-cellulose film were investigated. Their antibacterial activity, thermal properties, morphology and biodegradability in soil of the composite film were also studied.

### **EXPERIMENTAL**

#### **Materials**

High ammonia (HA) NR having 60% dry rubber content (DRC) was supplied by Chalong Latex Industry Co., Ltd (Songkhla, Thailand). Poly(vinyl alcohol) with 89% hydrolysis and vulcanizing agents, i.e., sulfur,) Zinc diethyl dithiocarbamate (ZDEC and Zinc oxide (ZnO), were purchased from Sonal Company (Songkhla, Thailand). Sodium dodecyl sulphate (SDS) was supplied from Fluka (Seelze, Germany). Maleic anhydride (MA) was supplied by Fluka (Seelze, Germany). Benzoyl peroxide (BPO) was purchased from Merck Schuchardt OHG (Seelze, Germany). Butylated hydroxytoluene (BHT) or 2,6-bis(1,1-dimethylethyl)-4-methylphenol was purchased from Kitpiboon Chemical Ltd. (Bangkok, Thailand). Teric 16, a non-ionic surfactant, was purchased from Lucky Four Company (Bangkok, Thailand). Potassium persulfate was supplied from Rankem analytical company (New delhi, India). Hydrogen

peroxide and perchloric acid were purchased from Solvay Peroxythai Ltd. (Bangkok, Thailand and Guangdong, China).

In order to prepare cellulose fiber, the corn leave was consecutively immersed in 10% NaOH for 24 h in H<sub>2</sub>O<sub>2</sub> solution for 24 h and in perchloric acid for 36 h. After being washed with water until reaching neutral pH, the cellulose was dried at 80°C.

## Preparation of M-SPNR-g-cellulose

First, 6%wt MA was dissolved in 10% Teric 16 aqueous solution while BHT was dissolved in toluene (2 mL). Both MA solution (10 mL) and 1.5% BHT solution (2 mL) and 1% w/w BPO were then added into SPNR latex having 30% DRC (50 mL). Then, PVA (3 g) and SDS (3 g) dissolved in distilled water (100 mL) at 80°C for 1 h were added into the mixture. 10% w/v Cellulose fiber dispersed in water (0, 5, 10, 20, 30, 50 or 100% w/w with respect to dried weight of SPNR) was then mixed at 80°C for 3 h by using a homogenizer. At the same time, the 1% w/w K<sub>2</sub>S<sub>2</sub>O<sub>8</sub> was added in the mixture. The M-SPNR-g-cellulose obtained was finally poured into a glass container to form a sheet with 0.5 mm in thickness after drying at ambient temperature and then at 80°C for 6 h. The sample was kept at room temperature for overnight before characterisation.

## Characterizations of M-SPNR-g-cellulose

The M-SPNR-g-cellulose was characterised by using attenuated total reflection-Fourier Transform Infrared spectrophotometer (ATR-FTIR) (Equinox 55; Bruker) for 100 times of scan. CP/MAS solid-state <sup>13</sup>C-NMR spectrometer (Chemagnetics CMX100) was operated under a static field strength of 2.3 T (100 mHz, 1H) at 20±1°C. The contact time for CP was 1 ms with a proton 90° pulse of 5.5 μs and decoupling power of 75 kHz. The MAS speed was 3 kHz and the delay time 4after acquisition of the FID signal was 4 s. The chemical shifts were calibrated by using an external hexamethyl benzene standard methyl resonance at 17.3 ppm with 1600 scans. In order to study of thermal properties, thermogravimetric analysis (TGA) was performed (TGA7; Perkin Elmer). Each sample (5–6 mg) was analysed under N<sub>2</sub> with a flow rate of 45 mL/min. The temperature was varied from 50 to 850°C at a heating rate of 10°C/min.

For the morphological study, the sample was fractured under liquid nitrogen and then coated with platinum (12 Pa vacuum) before being investigated under scanning electron microscope (SEM; JMS-5800 LV, JEOL) at an accelerating voltage of 6 kV. The photograph image of the M-SPNR-g-cellulose was analyzed by optical microscopy (OM, Primo Star company, Carl Zeiss.). The tensile strength (elongation at the break) and modulus of the sample were measured according to ASTM D412-98a and JIS K6251 using the tensile tester (Strograph E-L; Toyoseiki) at a crosshead speed of 500 mm/min with a load cell of 100 and 500 N, respectively. Its tear strength was also determined according to ISO 34-1. For the study of heat aging resistance, the tensile retention value considering the respective initial tensile strength was investigated after ageing the sample in a circulating air chamber at 90°C for a week. The aged specimen was left at room temperature for at least 24 h before testing. The hardness of the vulcanizate was determined from a Shore A type durometer by using the method adopted from ISO 48. For the examination of biodegradation, the specimen (3 cm ×3 cm) was buried under soil (100 g) at 5 cm from top soil (Hat Yai, Province of Songkhla, Thailand) while water was added every week for 3 months. Every month, the sample was carefully taken out, washed with distilled water and dried at 45°C for 2 days before being weighed.

Bacterial strain including *E. coli* ATCC25922, was used in this experiment as representative pathogenic bacteria of medical importance. All bacterial strains were cultured routinely on tryptic soy agar (TSA, Difco, France) and incubated at 35 °C for 24 h. The isolated colonies were suspended in Mueller Hinton broth (MHB, Difco, France) and then incubated for 16 h.

### **RESULTS AND DISCUSSION**

## FTIR and solid state <sup>13</sup>C-NMR analysis

The possible mechanism of grafting M-SPNR with cellulose by using BPO and  $K_2S_2O_8$  is presented in Fig. 1. Free radicals from BPO attacked carbon-carbon double bonds of MA which then reacted with carbon-carbon double bonds of SPNR molecules activated by  $K_2S_2O_8$  leading to the M-SPNR formation. When the M-SPNR reacted with cellulose fiber, the M-SPNR-g-cellulose was generated. In addition, the crosslink between M-SPNR and cellulose might occur through MA bridging.

| <br>                           |                   |         |               |          |
|--------------------------------|-------------------|---------|---------------|----------|
|                                | Figure 1          | Q.      | 2             |          |
| The chemical structure of M-SF | PNR-g-cellulose v | vas cor | nfirmed by A' | ΓR-FTIR. |

Fig. 2 shows the ATR-FTIR spectra (4000–500 cm<sup>-1</sup>) of cellulose, SPNR, M-SPNR and M-SPNR-g-cellulose.

Figure 2

-----

A broad band from 3100 to 3500 cm<sup>-1</sup> in the spectrum of cellulose was assigned to OH stretching and the peaks at 896, 1046, 1382 and 2926 represented C-H deformation, C-O-C from β-1,4–glycosidic, OH bending and C-H stretching, respectively [22]. In the spectrum of SPNR, C-H and strong asymmetrical methylene group vibrations were respectively observed near 2950 and 2853 cm<sup>-1</sup> while carboncarbon double bond was observed at 1664 cm<sup>-1</sup> [27]. The band at 1076 cm<sup>-1</sup> mainly attributed to the symmetric C-S-C group stretching vibrations in the two C-S bonds also appeared. During vulcanization, the addition of sulfur broke the double bond between two carbon atoms and then sulfur atoms bridged two polymer chains, i.e., crosslink between polymer chains was formed. In the case of M-SPNR, the absence of unreacted MA was identified by the disappearance of the characteristic band at 698 cm<sup>-1</sup> (C=C bond) of MA [2]. It should be stated that the absorption bands of unreacted MA were in the same region than those of the grafted anhydride [2,4]. The presence of grafted anhydride on SPNR molecules was confirmed by a broad and intense characteristic band at 1780-1784 cm<sup>-1</sup> and a weak absorption band at 1854 cm<sup>-1</sup> assigned to symmetric (strong) and asymmetric (weak) C=O stretching vibrations of succinic anhydride rings, respectively [28]. The grafted MA was also deduced from the absorbance ratio of FTIR peaks at 1780-1784 cm<sup>-1</sup> and 1854 cm<sup>-1</sup> to 835 cm<sup>-1</sup> (-C-H stretch on cis C=C bonds of cis-1,4-polyisoprene). The weak band at 3045 cm<sup>-1</sup> was attributed to an intramolecular hydrogen stretching bond from the maleate conformation. After chemical modification of M-SPNR with cellulose, the new functional group occurred. It was expected to be the carboxylic group (see Fig. 1) corresponding to the bands at 2530 cm<sup>-1</sup> due to the unsaturation and 1734-1724 and 1282-1164 cm<sup>-1</sup> assigned to C=O. The appearance of a new band at 821 cm<sup>-1</sup> in the M-SPNR-g-cellulose spectrum was attributed to out of plane deformation of carboxylic group. The absence of any band at 1850 and 1780 cm<sup>-1</sup> also confirmed the absence of non-reacted MA. The band at 776 and 1235 cm<sup>-1</sup> represented C–H and COOH plus out of plane hydroxyl bending.

The <sup>13</sup>C-NMR spectra of the cellulose, SPNR, M-SPNR and M-SPNR-g-cellulose are shown in Fig. 3.

\_\_\_\_\_

## Figure 3

\_\_\_\_\_

For cellulose fiber, the peaks at 60-70 ppm correlated to C6 of primary alcohol group whereas those of C2, C3 and C5 appeared at 70-81 ppm. In addition, the signals at 81-93 and 102-108 ppm related, respectively, to C4 and C1, anomeric carbon as the center of a hemiketal group [29]. The appearance of three singlet peaks at 23, 26 and 32 ppm in SPNR spectrum were assigned to methyl carbon and two methylene carbons. The two peaks at 125 and 134 ppm corresponded to olefinic carbons of SPNR. After modification of SPNR with MA, the new band of carboxyl group of M-SPNR was observed at 190 ppm. The signals at 64.8 and 72 ppm referred to hydroxyl group of M-SPNR-g-cellulose. In addition, those at 40, 44, 50 and 58 ppm represented hydroxyl group of SPNR-g-cellulose. It was explained that the carbon atom beared primary hydroxyl which involved intramolecular hydrogen bonds with the hydroxyl, and intermolecular bonds with the hydroxyl in the adjacent chains. The C-O-C of β-1,4–glycosidic bond in cellulose was observed at 103 ppm. The chemical shift of SPNR molecule at 14.4, 29.7, 129.9 ppm referred to -CH<sub>3</sub>, -CH<sub>2</sub>, and -CH, respectively. The success of the reaction was confirmed by the signal at 192 ppm relating to carbonyl groups. However, the signals were overlapped and expected to show both ester and carboxylic groups. This upfield shifted signal was mainly due to

the conjugated system of the two different isomers. The  $\alpha,\beta$ -unsaturated carbons of the modifier would shift the signal to 126 and 136 ppm [23].

## Mechanical properties

The values of tensile strength of the M-SPNR-g-cellulose sheets at various cellulose contents are illustrated in Fig. 4. The tensile strength of the samples having 5, 10, 30, 50, 70 and 100% w/w of natural cellulose were 13.8, 13.5, 13.2, 12.8, 10.5 and 9.5 MPa, respectively, while that of the SPNR was 18 MPa. The lower tensile strength of the M-SPNR-g-cellulose could be explained that the incorporated cellulose retarded the stress induced crystalline of SPNR molecule.

\_\_\_\_\_

## Figure 4

\_\_\_\_\_

Fig. 5 shows that the tear strength of M-SPNR-g-cellulose with 50% of cellulose was 32 N/mm whereas that of NR was 55 N/mm. The lower tear strength of M-SPNR-g-cellulose was observed comparing to pristine SPNR due to reduction of crystalline of SPNR molecule after chemical modification.

## Figure 5

-----

The percent elongation at break of SPNR-g-cellulose was in the range 470–350 while that of SPNR sheet was 560 as shown in Fig. 6. The elongation at break which decreased as a function of cellulose content might be attributed to the change in the hardness of SPNR sheets after grafting with cellulose. Fig.7 shows the influence of cellulose content on the hardness (Shore A) of the M-SPNR-g-cellulose sheets.

| <br>     |
|----------|
| Figure 6 |
| <br>     |
| Figure 7 |
|          |

It was found that the hardness of SPNR was 36 Shore A, whereas that of the SPNR-g-cellulose was ~50 Shore A. The results indicated the change of chemical structure of SPNR after addition of cellulose. Besides grafting of MA on SPNR or cellulose, the hard sample might be caused from the crosslinked rubber chains through MA bridging [27].

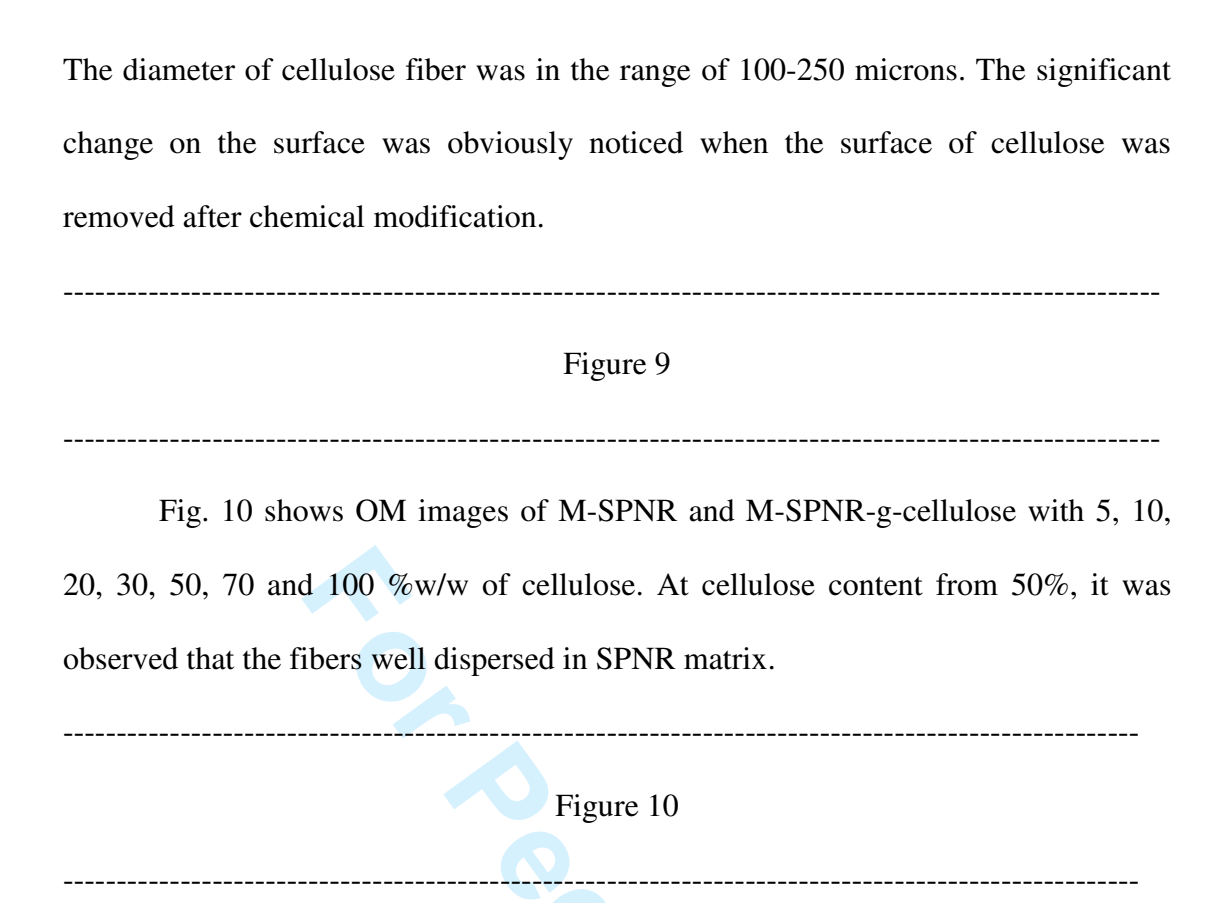
The modulus of the SPNR was also enhanced after grafting with cellulose as shown in Fig. 8. The increase in modulus with adding 10, 20 or 30% of cellulose was due to the hard cellulose. However, the 50 or 100% of cellulose resulted in a decrease of the modulus. The values of 100% modulus of SPNR and of M-SPNR-g-cellulose with 50% of cellulose were 1.1 and 1.3 MPa, respectively. This result agreed well with that of the hardness in Fig.7.

# Figure 8

\_\_\_\_\_

## **Morphology**

SEM image of cellulose fiber at magnification of 150 times is shown in Fig. 9. It was observed that the surface of untreated cellulose fiber was almost free of trenches.



SEM micrographs of the fracture surfaces of SPNR and M-SPNR-g-cellulose are shown in Fig. 11. The cellulose fibers homogeneously distributed in the SPNR matrix were observed in all samples. At cellulose content <50%, the adhesion between SPNR and cellulose seemed to be good. However, at > 50% of cellulose, the adhesion between M-SPNR and cellulose was poor as observed from void in the M-SPNR-g-cellulose [26]. It was explained that the higher amount of cellulose fiber caused the greater surface area of the fiber while the surface of SPNR was fixed. The imbalance between the surface area of M-SPNR and cellulose fiber was responsible for the void formation.

\_\_\_\_\_

Figure 11

-----

Antibacterial analysis

As shown in Fig. 12, both M-SPNR-g-cellulose and SPNR suppressed pathogenic growth. The antibacterial activity, investigated by measuring diameter of the clear zone, of the composite was significantly greater than that of SPNR possibly due to the carboxylic group which was a new functional group of the M-SPNR-g-cellulose. As previously reported, phenolic hydroxyl groups in poly(styrene-alt-maleic anhydride)-4-aminophenol conjugate was responsible for its antibacterial activity [30] although the bactericidal mechanism has not yet known. Therefore, it was assumed that both hydroxyl and carboxylic groups of the M-SPNR-g-cellulose contributed to its antibacterial activity.

\_\_\_\_\_

Figure 12

\_\_\_\_\_

## Thermal properties

TGA thermograms of the cellulose, SPNR, M-SPNR and M-SPNR-g-cellulose are shown in Fig. 13. It was observed that thermal decomposition of SPNR started at ~380 °C followed by two major losses of weight during the main volatilization and pyrolysis which were essentially completed by ~550°C. The onset degradation temperature at 265°C of the M-SPNR-g-cellulose containing 10, 25 and 50 wt% cellulose fibers was slightly lower than that of M-SPNR. When compared to SPNR, the M-SPNR-g-cellulose rapidly degraded at ~100°C due to the high thermal degradation of cellulose. The weight loss from 195 to 292°C in the TGA curve of M-SPNR-g-cellulose corresponded to water evaporation whereas that from 292 to 350°C related to the main chain of cellulose. With raising temperature to 350-400°C, the main M-SPNR molecules degraded. The weight loss at >400°C confirmed the grafting between M-SPNR and cellulose [23]. The onset degradation temperature of

cellulose at ~170°C indicated that cellulose was more sensitive to thermal degradation than rubber. Starting from ~390°C, both M-SPNR and M-SPNR-g-cellulose followed almost the same thermal degradation behavior. However, the amorphous (hemicellulose) region in cellulose fiber was easier to be degraded than that of the crystalline part [31]. It was previously reported that the mass loss stages for cellulose and hemicellulose shift towards high temperature from 330 to 430°C and from 225 to 400°C, respectively. From the more visible degradation of hemicellulose, it might be deduced that the thermal degradation of M-SPNR-g-cellulose was faster than that of SPNR due to hemicellulose.

\_\_\_\_\_

# Figure 13

------

## Biodegradation

The reduction of weight of M-SPNR-g-cellulose degraded in soil was investigated. Results in Fig. 14 show that the biodegradation of M-SPNR-g-cellulose dramatically increased with increasing the cellulose contents. It was believed that cellulose was greatly degraded by bacteria and fungi in soil activated by moisture and heat. In the case of SPNR, the sulfur bridges and high molecular weight (~10<sup>6</sup>) of *cis*-1,4-polyisoprene were responsible for the more difficult biodegradation [18]. The previous work reported that NR can be slowly degraded in nature by specific microorganisms. The high rate of degradation of M-SPNR-g-cellulose within 1 month and nearly constant after that was due to the low amount of cellulose in the composite.

Figure 14

\_\_\_\_\_

#### CONCLUSIONS

The M-SPNR-g-cellulose was successfully prepared. Its structure was proved by the appearance of a new band at 821 cm<sup>-1</sup>, in ATR-FTIR spectrum, attributing to the out of plane deformation of carboxyl group. Solid state NMR revealed the signal at 192 ppm related to carbonyl groups. At high cellulose content (over 50 phr), their tensile strength decreased from 18 MPa to range 8-14 depending on cellulose content due to the morphological change of the M-SPNR-g-cellulose film. Its optimum tensile strength of 11 MPa was found. The lowest swelling ratio of M-SPNR-g-cellulose in toluene at 50% cellulose was due to the hydrophilicity of cellulose. At this cellulose content, no phase separation was observed under SEM and OM. Both hydroxyl and carboxylic groups of the M-SPNR-g-cellulose were responsible for the antibacterial activity of the composite film. The thermal degradation and biodegradability of M-SPNR-g-cellulose were faster when compared to SPNR.

## **ACKNOLEDMENT**

Research grant (RTA5180003) from The Thailand Research Fund (TRF)/the Commission on Higher Education (CHE) to P.T. is gratefully acknowledged.

## **ABBREVIATIONS**

| ATR-FTIR | Attenuated   | total | reflection-Fourier | Transform | Infrared |
|----------|--------------|-------|--------------------|-----------|----------|
|          | spectrophoto | meter |                    |           |          |
| DDO      | D 1          | • 1   |                    |           |          |

BPO Benzoyl peroxide

BHT Butylated hydroxytoluene

DRC Dry Rubber Content

HA High ammonia

MA Maleic anhydride

M-SPNR-g-cellulose Maleated sulfur prevulcanized natural rubber grafted cellulose

SDS Sodium dodecyl sulphate

SEM Scanning Electron Microscope

TGA Thermogravimetric analysis

ZDEC Zinc diethyl dithiocarbamate

### **REFERENCES**

- 1. Z.Peng, L.X. Kong, S.D. Li, Y. Chen, M.F. Huang, Ind. Crop. Prod. 67, 3130 (2007).
- 2. H. Kang, P. Weiland, Bioresource Technol. 43,107 (1993).
- 3. M.C. Silva, O.R. Lopes, L.J. Colodette, A.O. Porto, J. Rieumont, D. Chaussy, M.N. Belgacem, G.G. Silva, Characterization of three non-product materials from a bleached eucalyptus kraft pulp mill, in view of valorising them as a source of cellulose fibres, Ind. Crop. Prod. 27 (2008): 288-295.
- 4. B. Jiang, L. Hu, C. Gao, J Shen, Acta. Biomater. 2, 9 (2006).
- 5.M.F.M. Zain, M.N. Islam, F. Mahmud, M. Jamil, Constr. Build. Mater. 25, 798 (2011)
- 6. J. Araki, M. Wada, S. Kuga, T. Okano, Colloid Surface A 142, 75 (1998)
- 7. F. Yaşar, H. Toğrul, N. Arslan, Food Eng. 81, (2007) 187-199.
- 8. A. Biswas, G. Selling, M.A.K.K. Woods, L.T. Willett, C.M. Buchanan, Carbohyd. Polym. 68, 5585 (2007).
- 9. Z. Ma, S. Ramakrishna, J. Membrane Sci. 319 (2008) 23-28.

10. I. Muhamad, L.S. Fen, N. Hui, N.A. Mustapha, Carbohyd Polym 83, 1207 (2011)

- 11.E. Khouly E, A.S. Kenawy, E. Safaan, A.A. Takahashi, Y. Hafiz, Y.A. Sonomoto, K.T. Zendo, Carbohyd. Polym. 83, 346 (2011).
- 12. X.M. Li, S. Chanklin, W. Zheng, A.H. Xiao, Carbohyd. Polym. 83 512 (2011).
- 13. N. Nishioka, M. Funakoshi, K. Inamoto, M. Uno, A. Ueda, J. Appl. Polym. Sci. 118, 2482 (2010).
- S. Benhadi, M. Ragoubi, J.-P. Joly, S. Molina, B. George, N. Brosse, B. George,
   N. Brosse, J. Incl. Phenom. Macro. 48, 1 (2010) .
- 15 B. Thielemans, W. Dufresne, A. Chaussy, D.M.N. Belgacem, Compos. Sci. Technol. 68, 3193 (2008).
- 16. F. Per, S. Bengt, Brit. Polym. J. 22 (1990) 147-153.
- 17. A. Bendahou, Y. Habibi, H. Kaddami, A. Dufresne, J. Biobased. Mater. Bio. 3,81(2009).
- 18. J. Bras, L.M. Hassan, C. Bruzesse, AE. Hassan, A. Nahla El-Wakil, A. Dufresn, Ind. Crop. Prod. 32, 627 (2010).
- 19. A. Bendahou, H. Kaddami, A. Dufresne, Eur .Polym. J. 46 609 (2010).
- 20. D. Pasquini, D.M.E. Teixeira, A.D.S.A. Curvelo, M.N. Belgacem, A. Dufresne, Ind. Crop. Prod. 32, 486 (2010).
- 21. M.H. Gabr, M.A. Elrahman, K. Okubo, T. Fujii, Compos. Part A-Appl . 41,1263 2010 (2010).
- 22. W. Zhanga, X. Zhanga, M. Lianga, C. Lu, Compos. Sci. Technol. 68, 2479 (2008).
- 23. D. Deroueta, P. Intharapata, Q.N. Trana, nF. Gohiera, C. Nakason, Eur. Polym. J. 45, 820 (2009).

- 24. K. Shirahama, S. Sato, M. Niino, N. Takisawa, Colloids Surfaces A 112, 233 (1994).
- 25. A.I. Khalf, D.E.E.I, Nashar, N.A. Maziad, Mater. Design 31, 2592 (2010).
- 26. A.F. Martins, J.C.M. Suarez, L.L.Y. Visconte, J. Mater. Sci. 38, 2415 (2003).
- 27. M. Yoshizawa, E.Marwanta, H. Ohno, Polymer 41, 9049 (2000).
- 28. H. Ismail, A. Rusli, A.A. Rashid, Polym. Test. 24, 856-862 (2005).
- 29. J.F. Kadla; R.D. Gilbert, Chem Technol 34, 197 (2000).
- 30. J.H. Jeong, Y.S. Byoun, Y.S. Lee, React. Funct. Polym. 50, 257 (2002).
- 31. D.K. Shen, S. Gu, A.V. Bridgwater, Carbohyd. Polym. 82, 39 (2010).

## Figure caption

- FIG.1 Possible mechanism of grafting M-SPNR with cellulose initiated by BPO and  $K_2S_2O_8$
- FIG.2 ATR-FTIR spectra of cellulose, SPNR, M-SPNR and M-SPNR-g-cellulose
- FIG.3 <sup>13</sup>C-NMR spectra of cellulose, SPNR, M-SPNR and M-SPNR-g-cellulose
- FIG. 4 Tensile strength of SPNR and M-SPNR-g-cellulose having various cellulose contents
- FIG. 5 Tear strength of SPNR and M-SPNR-g-cellulose having various cellulose contents
- FIG. 6 Elongation at break of SPNR and M-SPNR-g-cellulose having various cellulose contents
- FIG.7 Hardness of SPNR and M-SPNR-g-cellulose having various cellulose contents
- FIG.8 Modulus of SPNR and M-SPNR-g-cellulose having various cellulose content
- FIG.9 SEM image of cellulose fiber from corn leaves
- FIG.10 OM images of SPNR and M-SPNR-g-cellulose having various cellulose contents
- FIG. 11 SEM images of SPNR and M-SPNR-g-cellulose having various cellulose contents

- FIG. 12 Antibacterial of SPNR and M-SPNR-g-cellulose (50% cellulose)
- FIG.13 TGA of cellulose, SPNR, M-SPNR and M-SPNR-g-cellulose
- FIG.14 Biodegradation in soil of M-SPNR-g-cellulose having various cellulose contents



203x256mm (300 x 300 DPI)

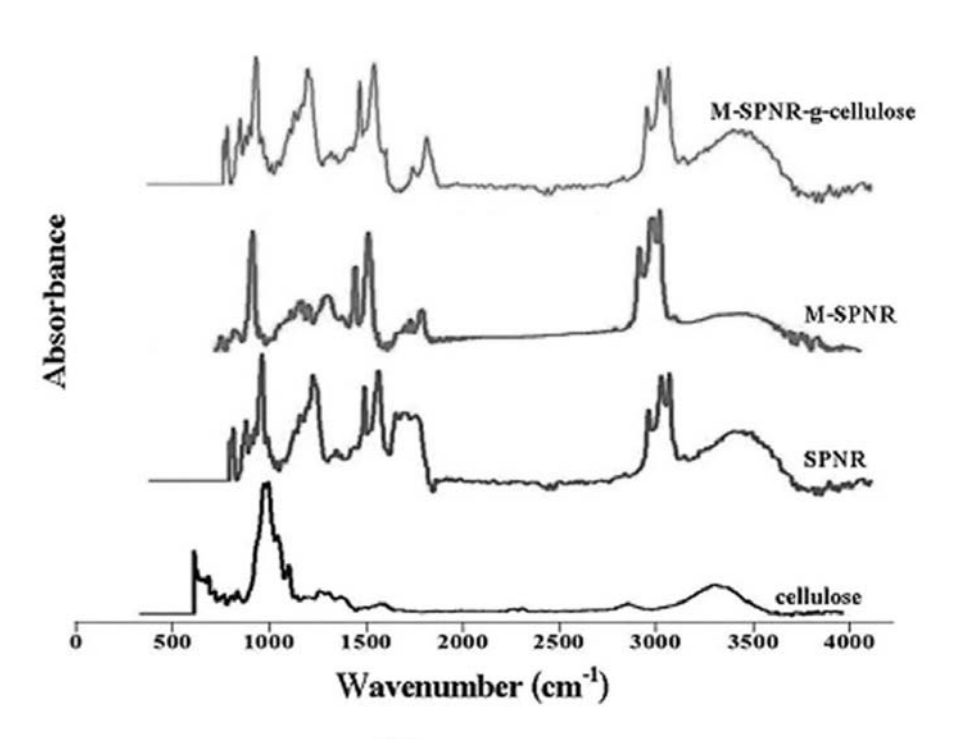
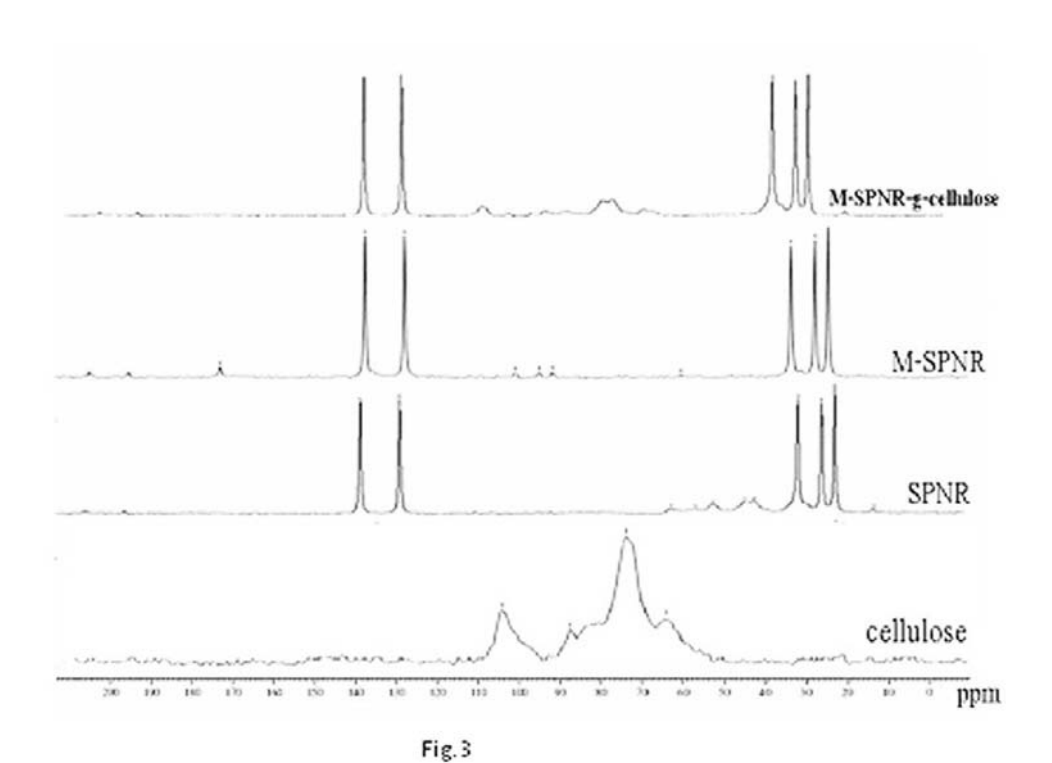
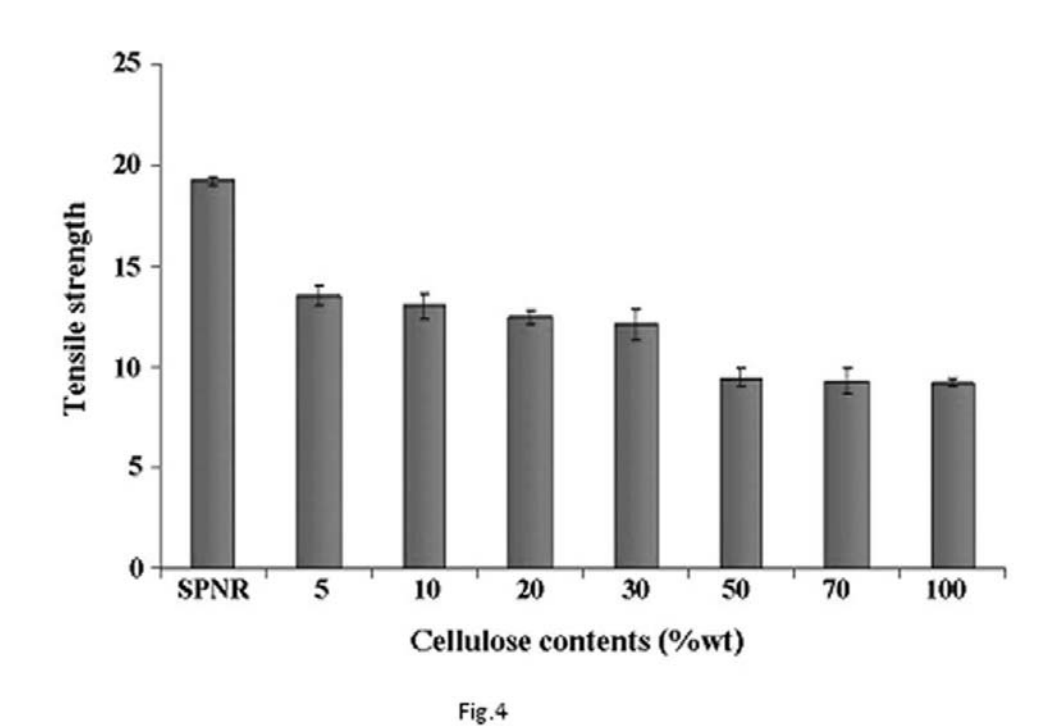


Fig.2

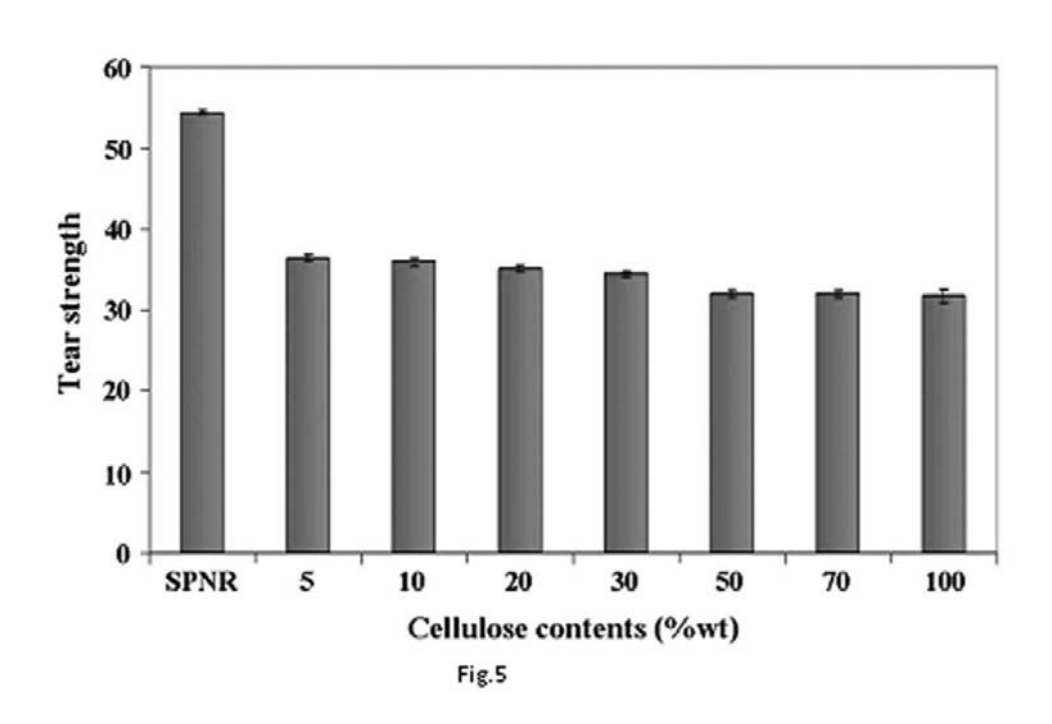
122x96mm (300 x 300 DPI)



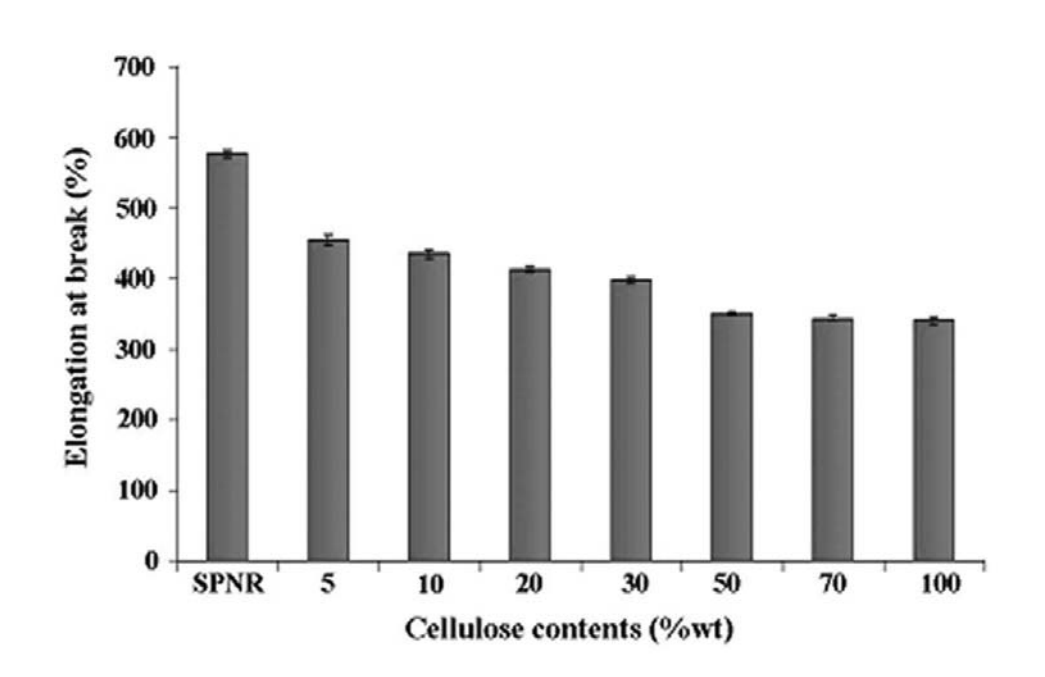
113x88mm (300 x 300 DPI)



109x81mm (300 x 300 DPI)

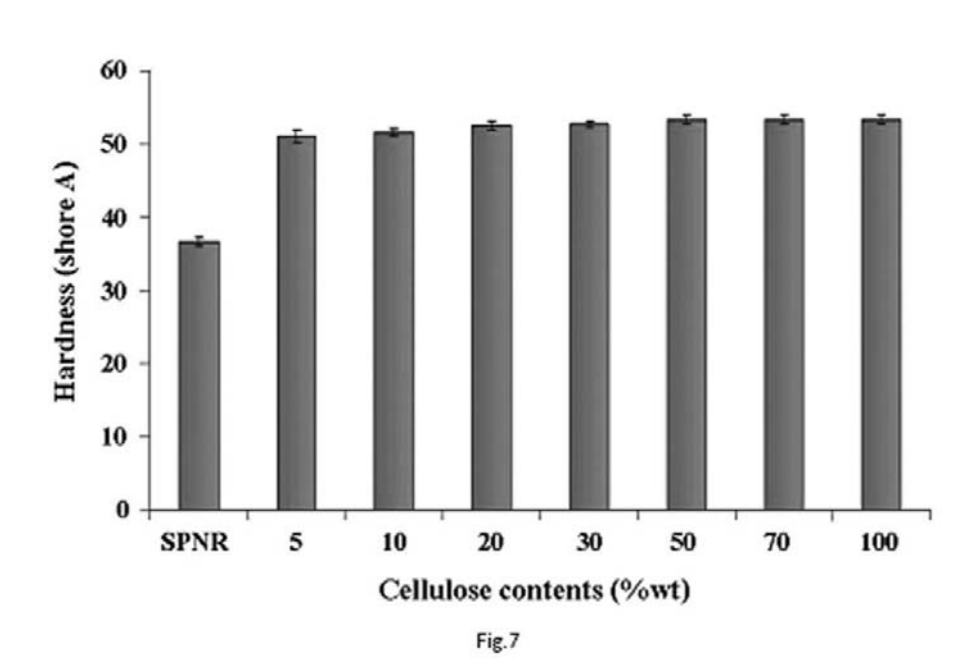


103x73mm (300 x 300 DPI)

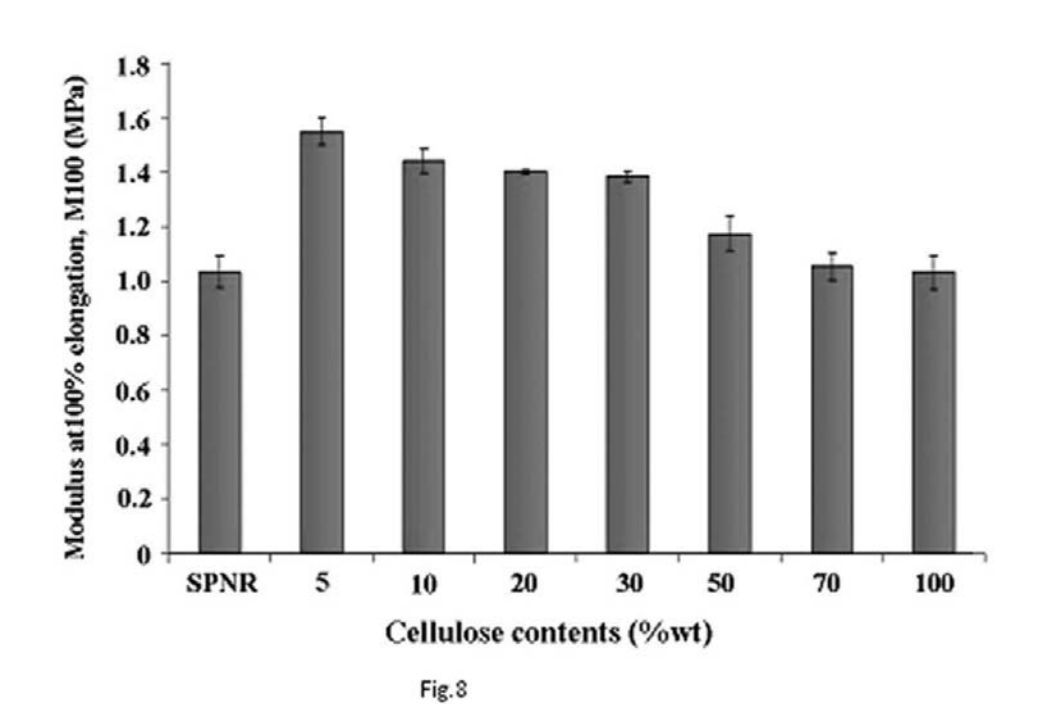


107x78mm (300 x 300 DPI)

Fig.6



102x66mm (300 x 300 DPI)



106x77mm (300 x 300 DPI)

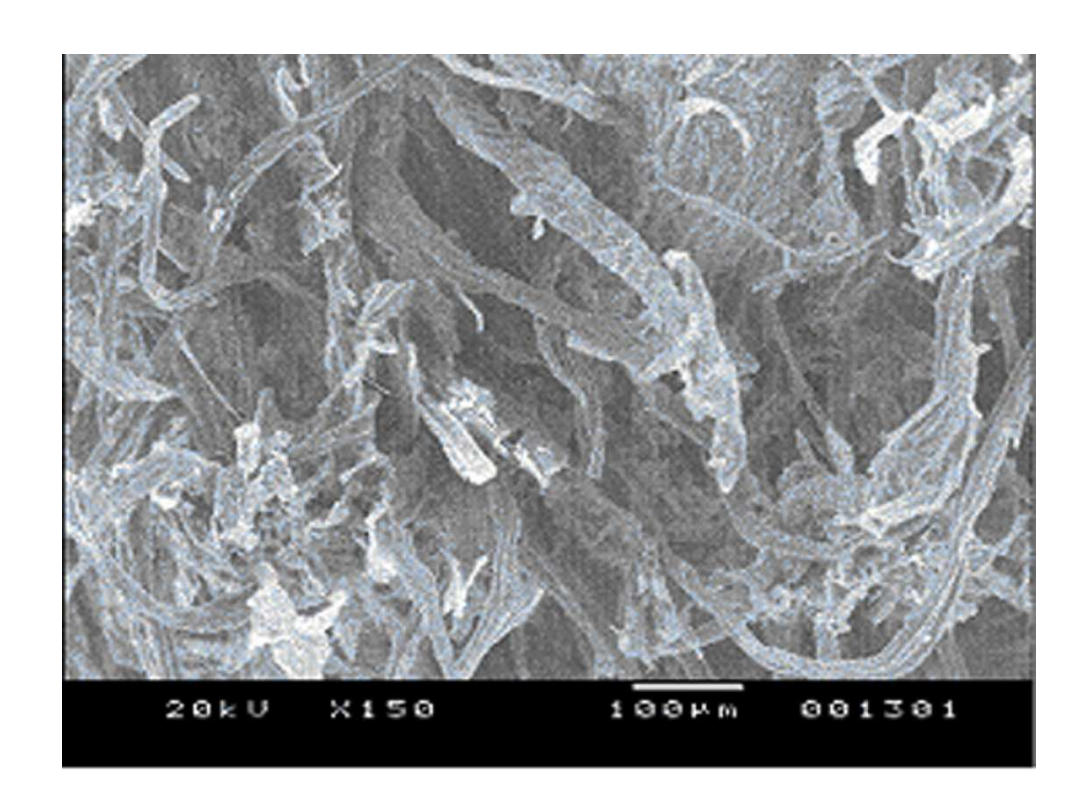


Fig.9

93x85mm (300 x 300 DPI)



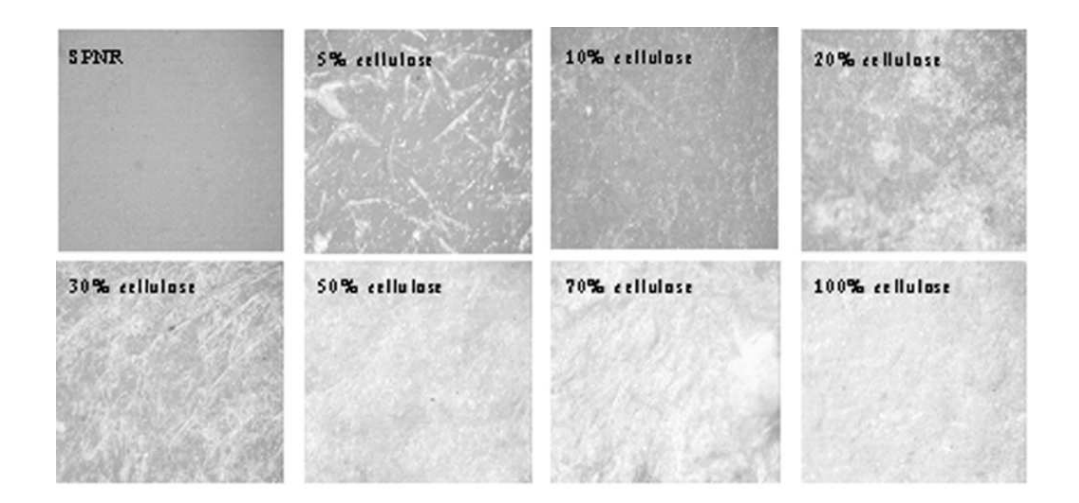


Fig. 10

86x50mm (300 x 300 DPI)

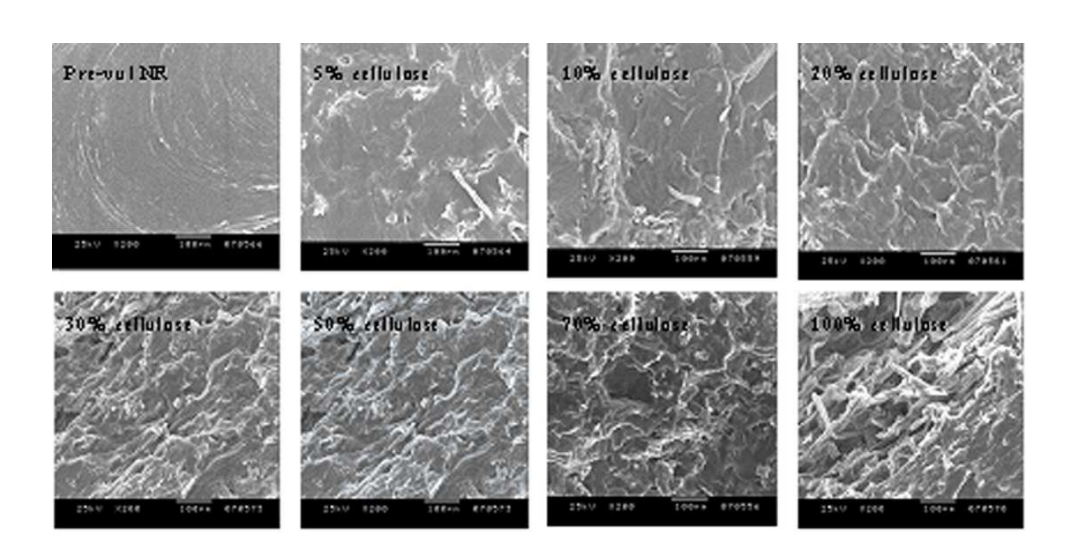
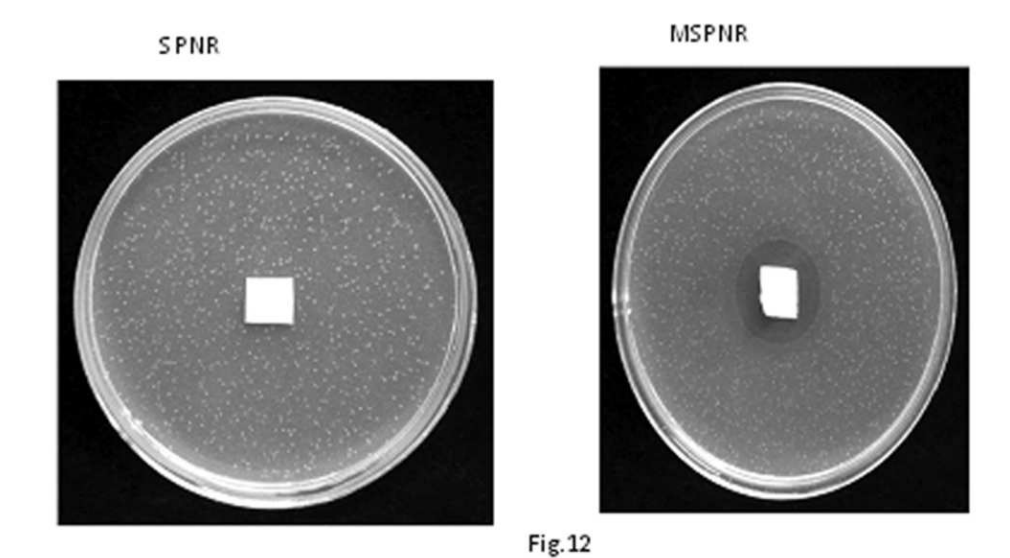
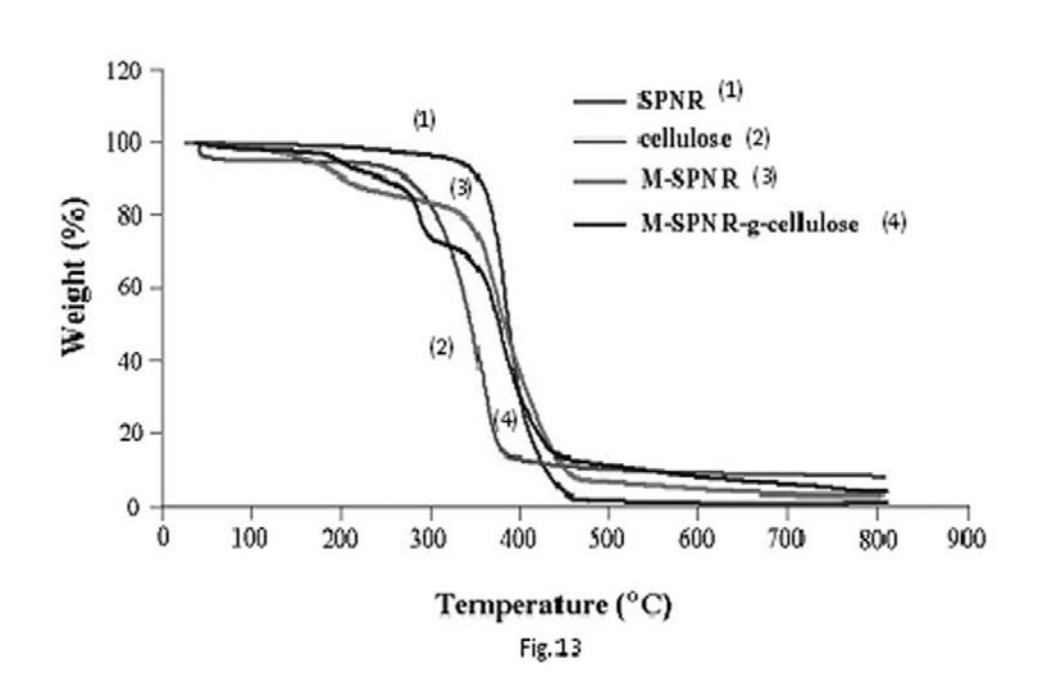


Fig. 11

93x58mm (300 x 300 DPI)



86x51mm (300 x 300 DPI)



99x65mm (300 x 300 DPI)

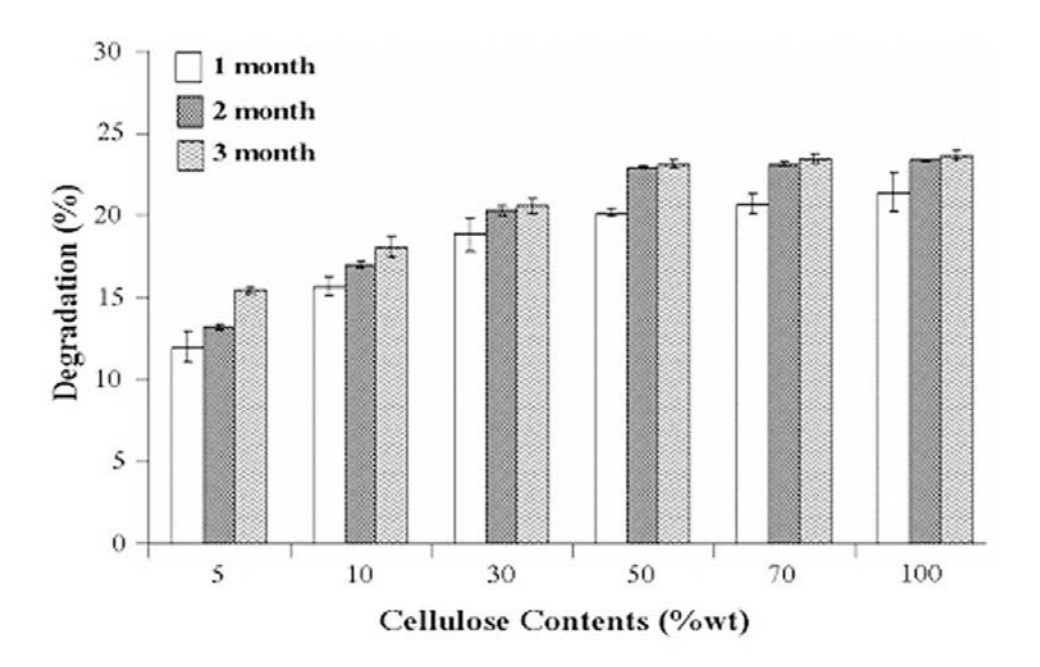


Fig.14

110x81mm (300 x 300 DPI)

### Elsevier Editorial System(tm) for Industrial Crops and Products Manuscript Draft

Manuscript Number: INDCRO-D-11-00618

Title: Physical properties of polymer composite: natural rubber glove waste/polystyrene foam

waste/cellulose

Article Type: Original Research Paper

Keywords: Natural rubber; Glove; Polystyrene; Waste; Cellulose; Chemical modification

Corresponding Author: Dr. saad riyajan, Ph.D

Corresponding Author's Institution: Prince of Songkla University

First Author: saad riyajan, Ph.D

Order of Authors: saad riyajan, Ph.D; Isara Intharit; Pramuan Tangboriboonrat

Abstract: The polymer composite was prepared from the wastes of natural rubber glove (NRG) and polystyrene foam (PSF) blended with cellulose from sugar cane leave via the laminate method. The NRG and PSF were firstly dispersed in toluene under continuous stirring. Then, maleic anhydride (MA) was added into the mixture. Effects of blend ratio and of MA content (0.5-15% w/w) on physical properties of the polymer composite were investigated. The toluene resistance of the polymer blend was improved after adding MA and cellulose. The highest toluene resistance was achieved when using 12% cellulose. The chemical reactions of MA with polymer blend and with composite were confirmed by ATR-FTIR. The hardness of the polymer blend and composite increased as a function of PSF. In addition, their impact strength increased with increasing NRG and cellulose contents.

Suggested Reviewers: Leonardo Simon PhD.
Department of Chemical Engineering, University of Waterloo lsimon@uwaterloo.ca
He is expert in polymer characterization.

Der-Jang Liaw

Department of Chemical Engineering , National Taiwan University of Science and Technology chem@mail.ntust.edu.tw
He is expert in polymer characterization.

Seiichi Kawahara

Prof., Department of Materials Science and Technology, Nagaoka University of Technology kawahara@chem.nagaokaut.ac.jp He is expert in polymer characterization.

Sabu Thomas School of Chemical Sciences, Mahatma Gandhi University sabuthom@vsnl.com He is expert in naturar rubber.



Polymer Science Program, Faculty of Science Prince of Songkla Univeristy, Thailand.
Tel./Fax 66-74-446925
e-mail: saadriyajan@hotmail.com

July 29, 2011

Dear Editorial Committee Industrial Crops and Products

I am pleased to send our manuscript entitled "Physical Properties of Polymer Composite:

Natural Rubber Glove Waste/Polystyrene Foam Waste/Cellulose

" in Industrial Crops and Products

To the best of our knowledge, this is the first study of its kind showing since the NRG waste was blended with PSF waste by using maleic anhydride (MA) as a crosslinker. As reported in the previous work concerning NR/ butadiene (BR)/ Ethylene Propylene Diene Monomer (EPDM) blend, it was expected that the addition of MA would improve the properties of NRG/PSF blend (Zhang et al., 2010). Effects of polymer blend ratio, MA and cellulose contents on the properties, i.e., tensile strength, hardness and tear strength, of polymer composite were investigated. Theirs chemical structure and morphology were studied by using attenuated total reflection-Fourier Transform Infrared spectrophotometer (ATR-FTIR) and scanning electron microscope (SEM), respectively. Toluene resistance of the polymer composite was also determined..Please you consider to publish in Industrial Crops and Products

Sincerely Yours,

(Asst. Prof.Dr. Sa-Ad Riyajan)

Carbohydate polymer

# Preparation and physical properties of natural rubber glove waste and polymer styrene foam waste

Dear Editor,

Thank you for your useful comments and suggestions on the language and structure of our manuscript.

We have modified the manuscript accordingly, and detailed corrections are listed below point by point:

1) In its current state, the level of English throughout your manuscript does not meet the journal's required standard. Authors have the responsibility to present their papers in good English which can be understood by the journal's readership without difficulty.

We have revised the WHOLE manuscript carefully and tried to avoid any grammar or syntax error. In addition, we have asked several colleagues who are skilled authors of English language papers to check the English. We believe that the language is now acceptable for the review process.

2) Please note that your abstract (250 words) has exceeded the maximum length of 150 words for research articles in this journal.

The abstract has been revised and its word count is now 149.

3) Figures should be cited in sequential order in the main text. In your manuscript, Fig. 6 is provided but not cited. Please check and revise accordingly.

Now all figures are provided and cited in sequence in the main text.

4) A cover letter should include the following statement: the manuscript has not been previously published, is not currently submitted for review to any other journal, and will not be submitted elsewhere before a decision is made by this journal. This is not seen in your cover letter.

The required information is now included in the cover letter.

5) The manuscript, including references, figure captions and tables, should be typewritten in uniform lettering and sizing, and with double spacing throughout.

We now have used uniform lettering and sizing throughout the manuscript, with double spacing.

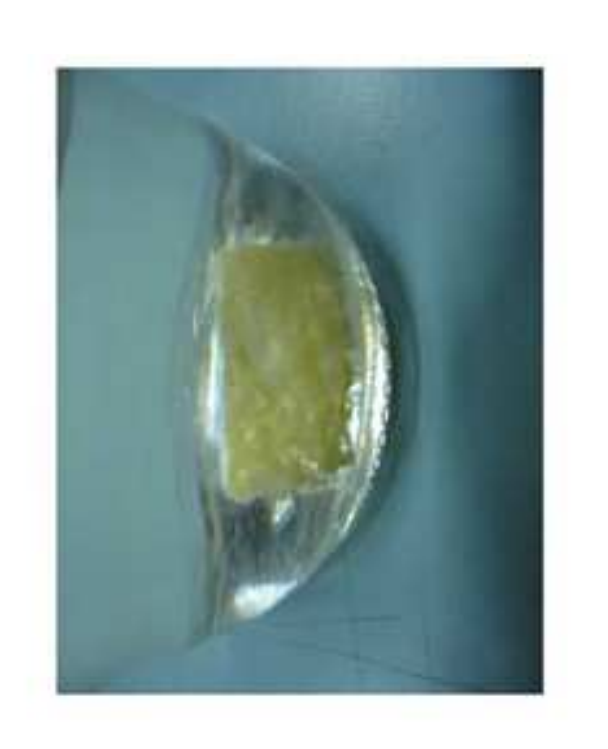
6) Please note that the reference style must conform strictly to the journal's Guide for Authors. To specify one problem in the reference list provided, journal names are not abbreviated and page span not provided.

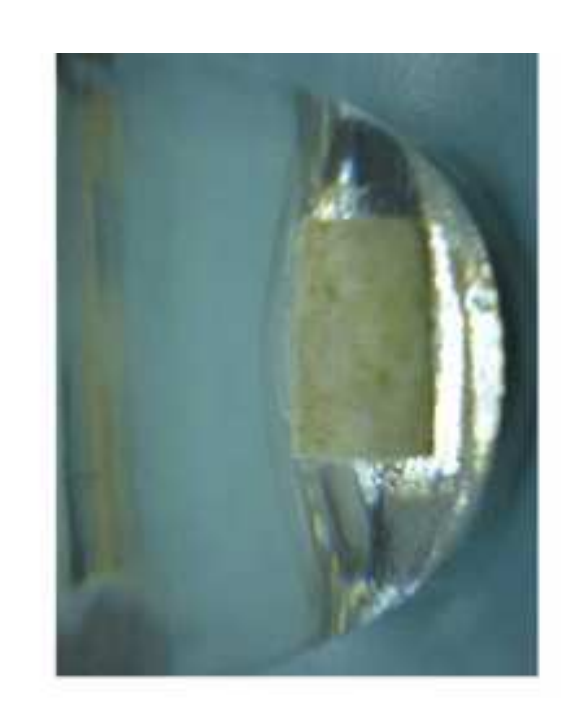
We have checked all the references and formatted them strictly according to the Guide for Authors. Especially, journal names have been abbreviated and page span provided. The manuscript has been resubmitted to your journal. We look forward to your positive response. Sincerely,

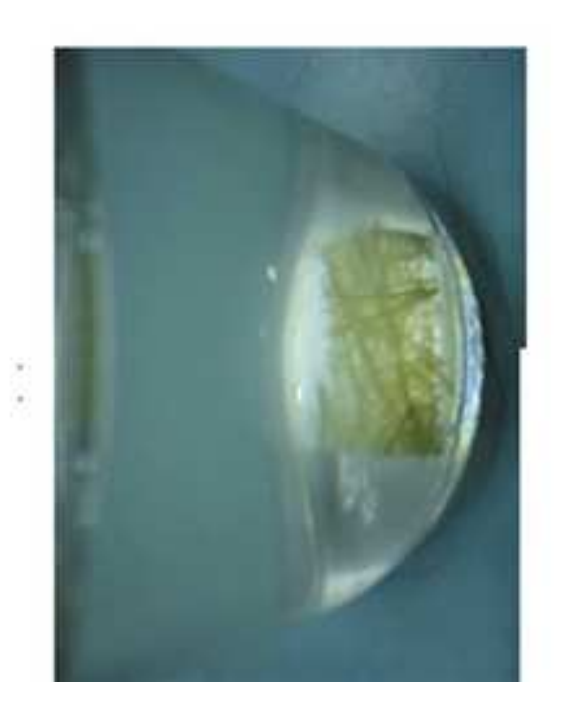
Assist. Prof. Dr. Sa-Ad Riyajan

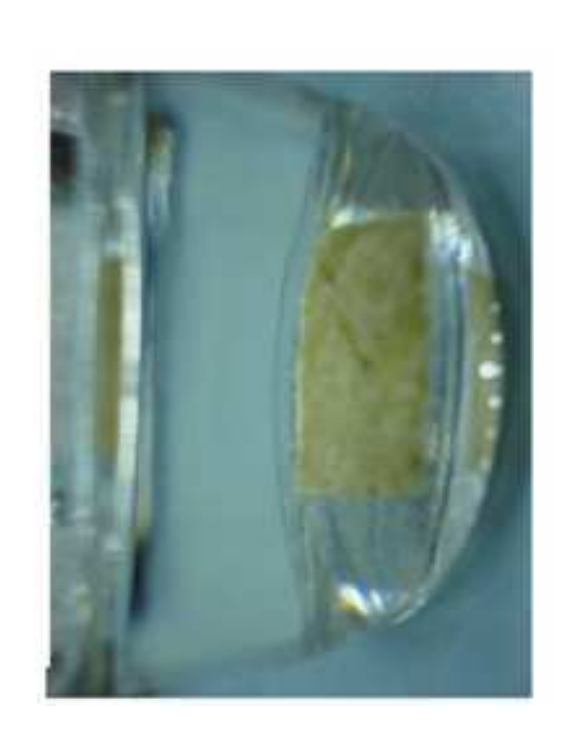
Saad R\_











## Highlights

We described the influence of cellulose on properties of NR glove/PS foam blend. ▶ The toluene resistance and mechanical properties was improved by cellulose ▶ It is the first polymer blend was obtained from waste from NR and PS foam. ▶ The advantage of this system is environment friendly.

Physical properties of polymer composite: 6 natural rubber glove waste/polystyrene foam waste/cellulose Sa-Ad Riyajan<sup>1</sup>\*, Isara Intharit <sup>1</sup>, Pramuan Tangboriboonrat<sup>2</sup> <sup>1</sup>Department of Materials Science and Technology, Faculty of Science, Prince of Songkla University, Songkhla 90112, Thailand 23 <sup>2</sup>Department of Chemistry, Faculty of Science, Mahidol University, Rama 6 Road, Bangkok 10400, Thailand \*Corresponding author: <a href="mailto:saadriyajan@hotmail.com">saadriyajan@hotmail.com</a> Phone/Fax 660-074288398 **ABSTRACT** The polymer composite was prepared from the wastes of natural rubber glove (NRG) and polystyrene foam (PSF) blended with cellulose from sugar cane leave via the laminate method. The NRG and PSF were firstly dispersed in toluene under continuous stirring. Then, maleic anhydride (MA) was added into the mixture. Effects of blend ratio and of MA content (0.5-15% w/w) on physical properties of the polymer composite were investigated. The toluene resistance of the polymer blend was improved after adding MA and cellulose. The highest toluene resistance was achieved when using 12% cellulose. The chemical reactions of MA with polymer blend and with composite were confirmed by ATR-FTIR. The hardness of 

the polymer blend and composite increased as a function of PSF. In addition, their impact strength increased with increasing NRG and cellulose contents.

Keywords: Natural rubber, Glove, Polystyrene, Waste, Cellulose, Chemical modification

## 1.Introduction

At present, the demand of natural rubber glove (NRG) exponentially increases due to the health awareness. After its use, NRG is generally left as garbage which is difficult to biodegrade since polyisoprene chains of NR are crosslinked either by sulfur (Riyajan et al., 2003; Hall et al., 2009) or peroxide system. The problem of NRG waste disposal is, therefore, growing as a direct result of rapid industrialization and population growth. Especially, the infectious waste from hospital and other toxic hazardous waste might cause serious environmental problem and great health risk to public. For example, the diseases like diarrhea, leptospirosis, typhoid and cholera can be transmitted through the mismanagement of waste. Moreover, the public increasingly concerns over the handling of medical waste because of the recent acquired immune deficiency syndrome (AIDS) dilemma, severe acute respiratory syndrome (SARS) epidemic, Avian influenza and those posed by other communicable diseases such as hepatitis B.

Susceptibility of NR products towards a microbial attack is a well known phenomenon (Hall et al., 2009). The environment authority agency such as The World Health Organization (WHO) uses the landfilling or incineration (WHO, 2000) and pyrolysis process (Deng et al., 2008; Conrardy et al. 2010) to reduce the rubber waste (Hall et al., 2009). Without catalyst, the pyrolysis oil from the rubber waste consisted mainly of limonene and oligomers of polyisoprene. The presence of the Y-zeolite catalyst in the pyrolysis of rubber caused an increase in the yield of hydrocarbon gases similar to the degradation of polystyrene (PS) (Berekaa et al., 2000). The destruction of NRG waste by molten salt oxidation produced

 $CO_2$ ,  $N_2$  and water (Hsu et al., 2000). In this case, the chemical composition of the degraded glove, analyzed by thermogravimetric analysis (TGA) under  $N_2$ , played a fundamental role in pyrolytic behavior.

In parallel, the NRG waste can be reused in several applications such as mat and massive tire as well as most of the constituent parts of both passenger and truck tire (Rajan et al., 2006). In addition, the rubber waste was blended with virgin synthetic rubber and NR to improve the polymer processing. However, the blend of NRG waste with polystyrene foam (PSF) waste was not found in literature. The reports concerned only about the use of PSF waste in polymeric flocculants (Wiesław et al., 2007), ion adsorption (Long et al., 2010), polymer mortar panels (Bhutta et al., 2011) and electrolyte (Bajdur et al., 2002). The polymeric flocculant, i.e., poly(styrene sulphonate) acid, was obtained from PSF waste and virgin PS during the sulphonation process using H<sub>2</sub>SO<sub>4</sub> as sulphonating agent and Ag<sub>2</sub>SO<sub>4</sub> as catalyst. The effectiveness of the flocculation depended on the number of sulphonic groups per monomer unit and its molecular weight. In addition, PSF waste blended with poly(methyl methacrylate) and reinforced with steel fiber was applied in polymer mortar panels (PMPs) (Bhutta et al., 2011). Due to their high ductile and load-bearing capacity, PMPs could replace a commercial polymer-impregnated mortar panel in practical applications.

In this present work, the NRG waste was blended with PSF waste by using maleic anhydride (MA) as a crosslinker. As reported in the previous work concerning NR/ butadiene (BR)/ Ethylene Propylene Diene Monomer (EPDM) blend, it was expected that the addition of MA would improve the properties of NRG/PSF blend (Zhang et al., 2010). The NRG waste was masticated by a two-roll mill and dispersed in toluene. The NRG dispersion was mixed with PSF and MA dissolved in toluene under continuous stirring. After drying at ambient temperature, the NRG/PSF blend was laminated with cellulose from sugar cane leave by using a compression molding. Effects of polymer blend ratio, MA and cellulose

contents on the properties, i.e., tensile strength, hardness and tear strength, of polymer composite were investigated. Theirs chemical structure and morphology were studied by using attenuated total reflection-Fourier Transform Infrared spectrophotometer (ATR-FTIR) and scanning electron microscope (SEM), respectively. Toluene resistance of the polymer composite was also determined.

## 2. Experimental

#### 2.1 Materials

PSF waste was received from a local company in Songkhla province, Thailand. Poly(vinyl alcohol), MA and benzoyl peroxide (BPO) were purchased from Sonal Company (Songkhla, Thailand), Fluka (Schnelldorf, Germany) and Merck Schuchardt OHG (Seelze, Germany), respectively. Hydrogen peroxide and perchloric acid were purchased from Solvay Peroxythai Ltd. (Bangkok, Thailand and Guangdong, China) while sodium hydroxide was supplied from Lab Scan Analytical Science (Bangkok, Thailand)

In the preparation of cellulose fiber, sugar cane leaves were immersed in 10% NaOH solution for 24 h and then washed with water until reaching neutral pH. The wet cellulose was cast on a glass plate and dried at ambient temperature for 3 days and, subsequently, at 50°C for 24 h. The diameter of dried cellulose fiber was determined under an optical microscopy (OM; Primo Star company, Carl Zeiss).

## 2.2 Preparation of polymer composite

NRG waste from Sri Trang Company (Songkhla, Thailand) was masticated by using two-roll mill (Charoenchaikarnchange; Bangkok, Thailand) at 30-32°C for 30 min. The masticated NRG was immersed in toluene for 2 days at ambient temperature and then stirred for 5 h. After stirring with a mechanical stirrer for 1 h, the size and size distribution of the NRG suspended in toluene was measured by a Laser Particle Size Analyzer (LPSA; Beckman Coulter LS 230).

The NRG suspension with various contents was blended with 10% w/v of PSF in toluene at room temperature by using a homogenizer (PL Trading internation Co. Ltd; Bangkok, Thailand). 0.5% BPO, 5% glycerol and different MA concentrations were added into the blend under stirring. In order to form a sheet of 0.45 mm in thickness, the mixture was poured into a glass plate  $(10\times10\times0.5 \text{ cm}^3)$  at ambient temperature. The cellulose sheet was placed between two NRG/PSF sheets. After heating at 80°C for 6 h, the dried polymer composite compressed by compression molding (Charoenchaikarnchange; was Bangkok, Thailand) at 150°C for 10 h and was kept at ambient temperature overnight. Under a hot-press, the sample was preheated at 150°C for 6 min and then compressed for 4 min before being cooled under 3 MPa at 30°C for 4 min.

## 2.3 Characterizations and testing of polymer composite

The chemical structure of polymer composite was investigated by using ATR-FTIR (Equinox 55; Bruker) for 100 times of scan. Its gel content was determined by immersing a known weight of specimen (2.5 cm x 2.5 cm x 0.5 mm) in toluene at 32°C for 5 days. The sample was then dried at 50°C for 24 h and weighed until a constant weight was obtained. The degree of gel content was calculated from equation (1):

51 123 Gel content = 
$$(W_2 - W_1) / W_1$$
....(1)

56 125

where  $W_1$  is the original weight of the sample and  $W_2$  is the weight of dried residual sample.